Author:
Wilson, J. C

Title:
A study of particulate foams

A STUDY OF PARTICULATE FOAMS

by

JUNE CLARE WILSON

A thesis submitted in fulfilment of the requirements for the degree of Doctor of Philosophy at the University of Bristol

Department of Physical Chemistry
University of Bristol

May 1980


Pears
COPYRIGHT
PEARS

MEMORANDUM

The work described in this dissertation was carried out in the Department of Physical Chemistry at the University of Bristol under the supervision of Professor R.H. Ottewill between October 1976 and December 1978. The work is original except where reference is made in the text.
No part of this work has been submitted for another degree at this or any other university.

J. Clare Wilson

ACKNOWLEDGEMENTS

I wish to express my gratitude to Professor R.H. Ottewill for his help and guidance throughout this research project.

Additionally I would like to take this opportunity to thank Dr. R. Bee, Unilever Food Division, for his help in identifying the problem, initially, and in the numerous hours of discussion we consequently had as to the direction and meaning of my research. Also I am grateful to Unilever Food Division for the financial assistance they have given me.

I would also like to thank Dr. J.W. Goodwin, Mr. J.W. Dimery and Mr. P.G. Rogers for their assistance with the practical problems that arose.

Finally I thank my typist, Mrs. Frost, for the wonderful job she has done, and my many friends who have helped me through the last three and half years.

ABSTRACT

This research project investigated particle-fluid interactions at the air-water interface, thus enabling the important factors involved in the formation of particle stabilised foams to be understood. It was hoped that this would lead to an understanding of the behaviour of aerated milk products which are stabilised by milk fat globules.

Experiments were devised to simulate the properties of the globules at the interface, in particular their wetting and dewetting behaviour, and to determine the structure of foam films formed in particulate systems.

For this purpose a model system, polystyrene latex particles having diameters in the range 1 - 4 μm, was used. The following conclusions were reached.

Polystyrene particles will not foam when suspended in water alone. Particulate foams were only formed when the system approached the conditions required for bulk coagulation. Two foaming systems have been isolated; one where instability of the bulk phase was the result of increased ionic strength and the other was the result of specific adsorption of ions.

The structure of the foam film has been postulated as a bilayer of latex particles, the particles in each monolayer being hexagonally close-packed. Within each monolayer the particles appear to be in positions of the primary minimum energy, whilst in the adjacent layers they are situated in positions of the secondary minimum. The monolayers have been found to be rigid and solid-like in character.

A particle size effect exists, latices having diameters of 1 μm were reluctant to foam. Following from this the calculated interaction energy and strength of the monolayer increased with particle size. The mixed particle size monolayers indicated the formation of a more liquid-expanded film illustrating the weakening of the monolayer due to the presence of smaller particles.

The contact angle data indicated an increase in contact angle to give angles greater than 90^{o} within the foaming regions for both foam systems studied.

Therefore the particles must acquire a hydrophobic nature to make it energetically favourable to be situated at the air/liquid interface as compared to the bulk. By so doing a latex stabilised foam was formed.

CONTENTS

CHAPTER 1

INTRODUCTION

1.1 General Introduction

The majority of foams encountered in everyday life consist of bubbles of gas dispersed within a liquid phase. The distribution of bubble sizes found in a liquid foam is usually large, ranging from those in the size range of colloidal particles, ca. 1 nm to 1 μm, to macroscopic bubbles which can be 1 mm or even 1 cm in dimension. The basic reason, however, why foams can be considered as colloidal systems is that the thickness of the liquid lamellae between the gas bubbles is within the size domain of colloidal systems and is stabilised by the same type of interactions which stabilise dispersions of lyophobic colloidal particles[1,2]. That is the drainage of the liquid film by capillary suction is resisted by a repulsive force acting in a direction normal to the surface of the liquid lamella.

As in all colloidal dispersions the foam has a very large surface area and since the surface tension of the liquid - air interface is finite it also has a large interfacial free energy. Thus in the thermodynamic sense the foam is not stable since it is not in the lowest free energy state, that is that having a minimum liquid - air interfacial area. It is basically a metastable system with a large kinetic energy barrier, owing to repulsive interaction in the liquid foam lamella, to transcend to reach the lowest energy state.

Pure liquids do not foam. A third component, a foam stabiliser, is required to assist the formation of the air cells and to prevent their rupture. This is similar to the emulsion stabiliser used in the formation of emulsions. The properties associated with foam stability closely resemble those required for emulsion stability. Several authors have treated these two systems synonymously in connection with their stability[1,2].

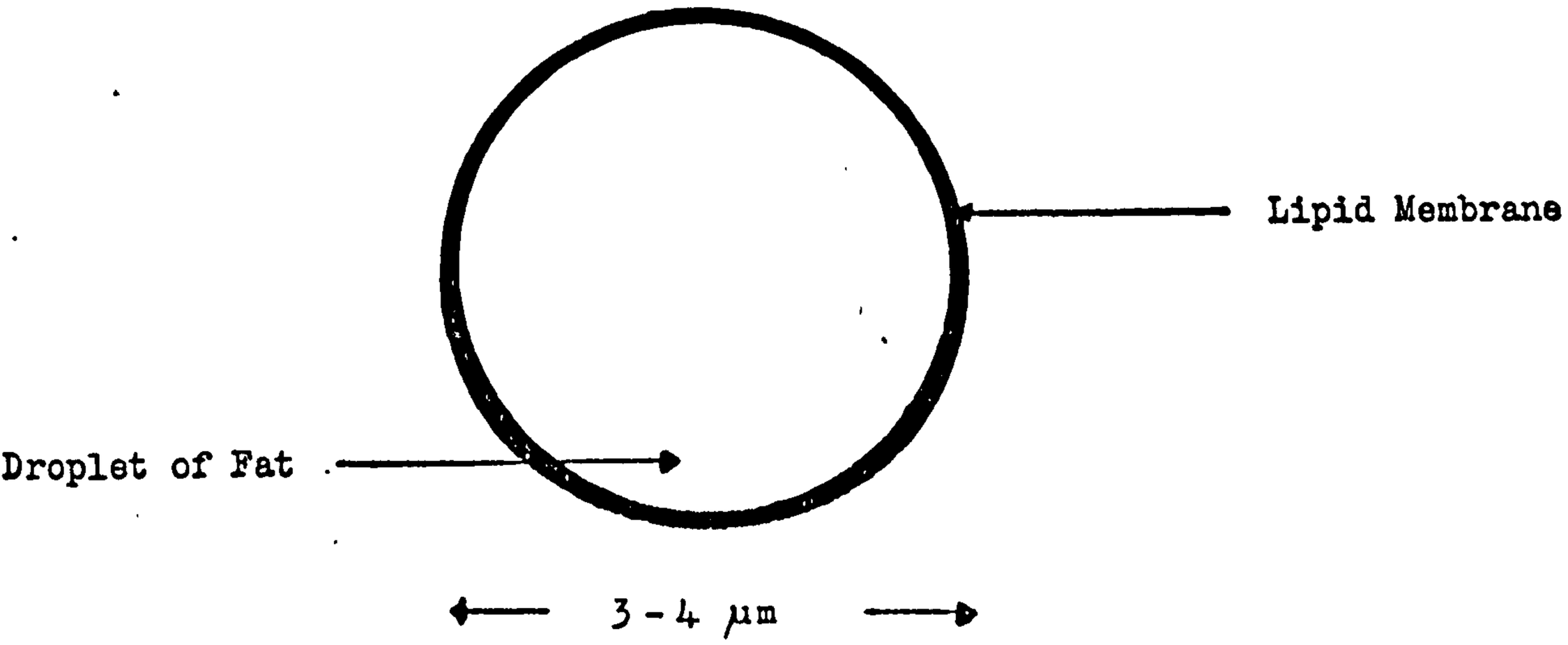

Figure 1/1 : Milk Fat Globule

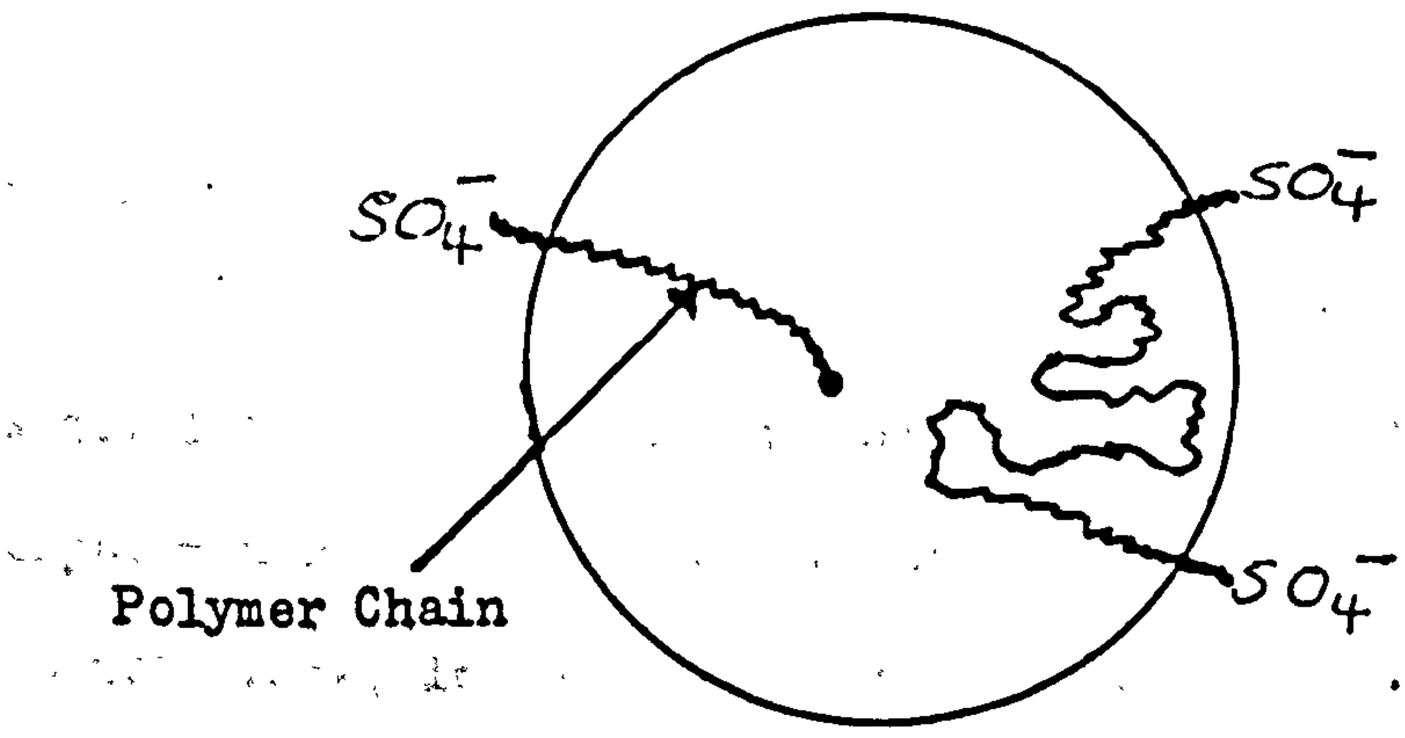

Figure 1/2 : Schematic Diagram of Polystyrene Latex Particle

In this research a particle stabilised foam has been investigated, in which the bubbles were stabilised by solid particles. Solid foams are important in flotation processes such as the flotation of coal, production of cellulose and the production of paper. In addition they are extremely important in food products, for example, in the conversion of fluid cream into whipped cream, a foam.

1.2 The Purpose of this Study

The aim of this research was to investigate particle-fluid interactions at the air-water interface in order to understand, at a basic level, the important factors involved in forming particle stabilised foams. It was hoped that having established the fundamental basis of stability this would lead to an understanding of the behaviour of aerated milk products, such as ice-cream, mousses and whipped cream. Here the air cell is stabilised by the milk fat globule. A stable foam cannot be formed unless there is sufficient fat to form a network enclosing the air cells.

The milk fat globule can be defined as a droplet of fat encased in a lipid membrane, figure 1/1. The average diameter of this globule is between 3 and 4 μm, that is a colloidal particle.

The inner core consists of esters of fatty acids. 150 different fatty acids have been isolated in milk. However only ten of these occur in amounts greater than one percent. The main protein in milk is β-caesin.

Several questions arose as to why these globules dewet at the air-water interface and why the air cells are stable once formed. Therefore experiments had to be devised to simulate the properties of the globules at an interface, in particular their wetting and dewetting behaviour, and to determine the structure of foam films formed in particulate systems.

1.3 The Model System

Food products themselves are very complicated systems; the proteins which stabilise the colloidal particles are deformable as are the fat globules themselves. The globules in the milk are polydispersed and their actual 'make-up' and size can depend on the seasons, the fodder and also the breed of cow. In order to simplify the system and hence reduce the number of experimental variables it was decided to use rigid particles of spherical geometry as a model system.

In previous work on polystyrene latex in this department, large latex particles, 4 μm diameter, were found to spontaneously foam during their preparation. These materials were used as the starting point for this research, since the average milk fat globule size is 3 to 4 μm in diameter.

Polystyrene latex particles proved to be a useful model system. The particles are spherical and with careful preparation it is possible to control the particle size. Also there is a wide range of particle sizes available from 50 nm to 4 μm. The particle surface charge arises from the ionic end groups on the polymer chain. These depend on the type of initiator.

If persulphate initiator is used the end groups are sulphate groups. These cause the charge on the particle to be negative, figure 1/2. The surface charge is positive if an initiator such as azo-bis-isobutyramidine hydrochloride is used. Zwitterionic latices have also been prepared. The different types of initiators available for emulsion polymerisation and the type of products obtained have been summarised recently[3].

Lastly, another advantage of polystyrene latex particles is that the volume fraction can be changed over a wide range of values and up to 0.1 can be achieved in preparation. Even higher values can be achieved by special techniques.

These large latex particles were used in order to simulate the more complex natural materials. However, the effect of particle size was also considered by investigating the properties of a range of latices of smaller size.

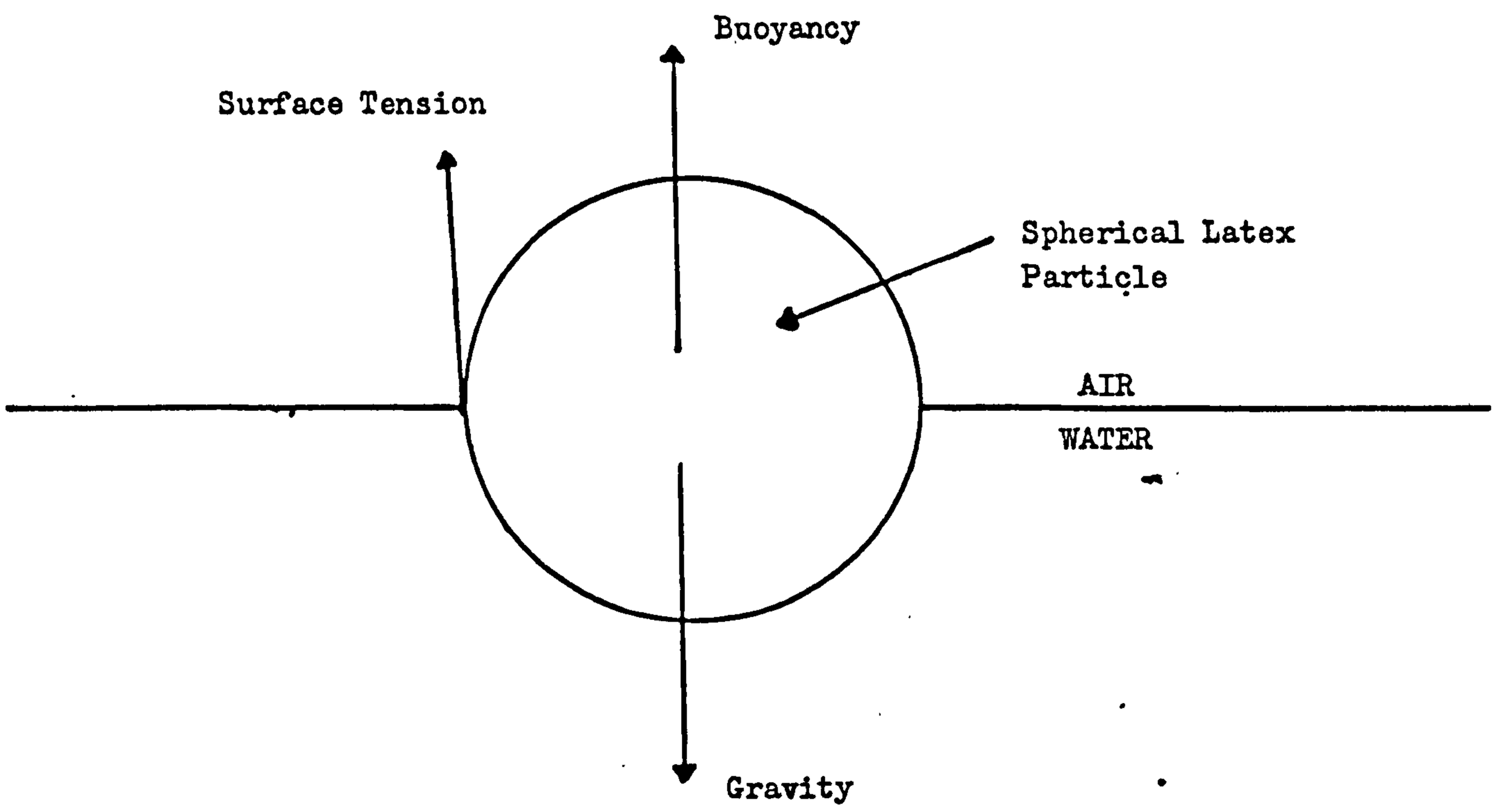

Figure 1/3 : Sphere resting at an Air/Water Interface

1.4 The Forces acting on a Sphere at an Air-Water Interface

The equilibrium position of a single sphere at an interface had to be investigated and particularly the dependence of the depth of immersion on contact angle, particle density and particle radius. Basically a sphere will reside at an interface if the buoyancy and the surface tension balance the force due to gravity, figure 1/3.

1.5 The Forces acting on a Latex Particle

There are two types of interaction forces, short and long range. The short range interactions involve chemical bonding of the molecules, dipole interactions, hydrophobic bonding and Born repulsion forces. Long range forces include van der Waals attraction and electrical double layer repulsion. The D.L.V.O. theory, for the stability of lyophobic sols, states that the total energy of interaction between two particles at any instant of time is the sum of the van der Waals' attractive and electric repulsion interaction energies[4,5].

1.5.1. London - van der Waals Attractive Energy

The total attractive energy between two molecules consists of three contributions: the Keesom energy which is a consequence of dripole-dipole interactions, V_K, the Debye energy for dipole-induced dipole interactions, V_D, and the London fluctuating dipole interaction energy, V_L. The dominant term is usually the London - van der Waals. Thus the total van der Waals interaction energy, V_{vdW}, can be written as

$$V_{vdW} = V_K + V_D + V_L$$

when $V_L >> V_K$ and also, $V_L >> V_D$

then $V_{vdW} \approx V_L$

where for two identical molecules

$$V_L = -\frac{3}{4} \frac{h \partial_o \alpha_o^2}{r^6}$$

where h is Planck's constant, ∂_o the dispersion frequency, α_o the static polarisability and r is the distance of separation of the molecules.

London - van der Waals energies are additive and therefore for condensed matter, for example solids or liquids, the energies of interaction can be summed over all the molecules in the system. Thus for two solid spheres of the same radius in a vacuum the relationships between the energy of attraction, V_A, and the distance of separation, H_o, takes the form,

$$V_A = -\frac{A}{12}\left[\frac{1}{x^2 + 2x} + \frac{1}{x^2 + 2x + 1} + 2 \ln \frac{x^2 + 2x}{x^2 + 2x + 1}\right] \quad \ldots (1)$$

where A is the Hamaker constant of the solid material and is given by

$$A = \pi^2 q^2 \lambda \quad \ldots (2)$$

with q as the number of atoms per cm^3 and λ is the London - van der Waals interaction constant.

$$\lambda = \frac{3}{4} h \partial_o \alpha_o^2 .$$

In equation (1) x is given by $H_o/2R$ where R is the radius of the spheres. For the condition that x is much less than unity equation (1) reduces to the approximate form

$$V_A = -\frac{A R}{12 H_o}$$

When the spheres are immersed in an aqueous medium, the Hamaker constant is modified by the presence of the fluid, and becomes equal to

$$A_{net} = (A_{pp}^{\frac{1}{2}} - A_{ww}^{\frac{1}{2}})^2$$

The new Hamaker constant, A_{net}, is defined by the Hamaker constants for the basic materials both of which can be calculated from equation (2).

1.5.2. <u>The Electrostatic Repulsive Interaction</u>

As mentioned previously, a polystyrene surface can acquire a charge from ionic groups on the surface formed in the polymerisation. As a consequence of these charges an electrical double layer exists at the polystyrene-solution interface. Therefore as two polystyrene surfaces

Figure 1/4 : A Potential Energy Curve for Latex JC

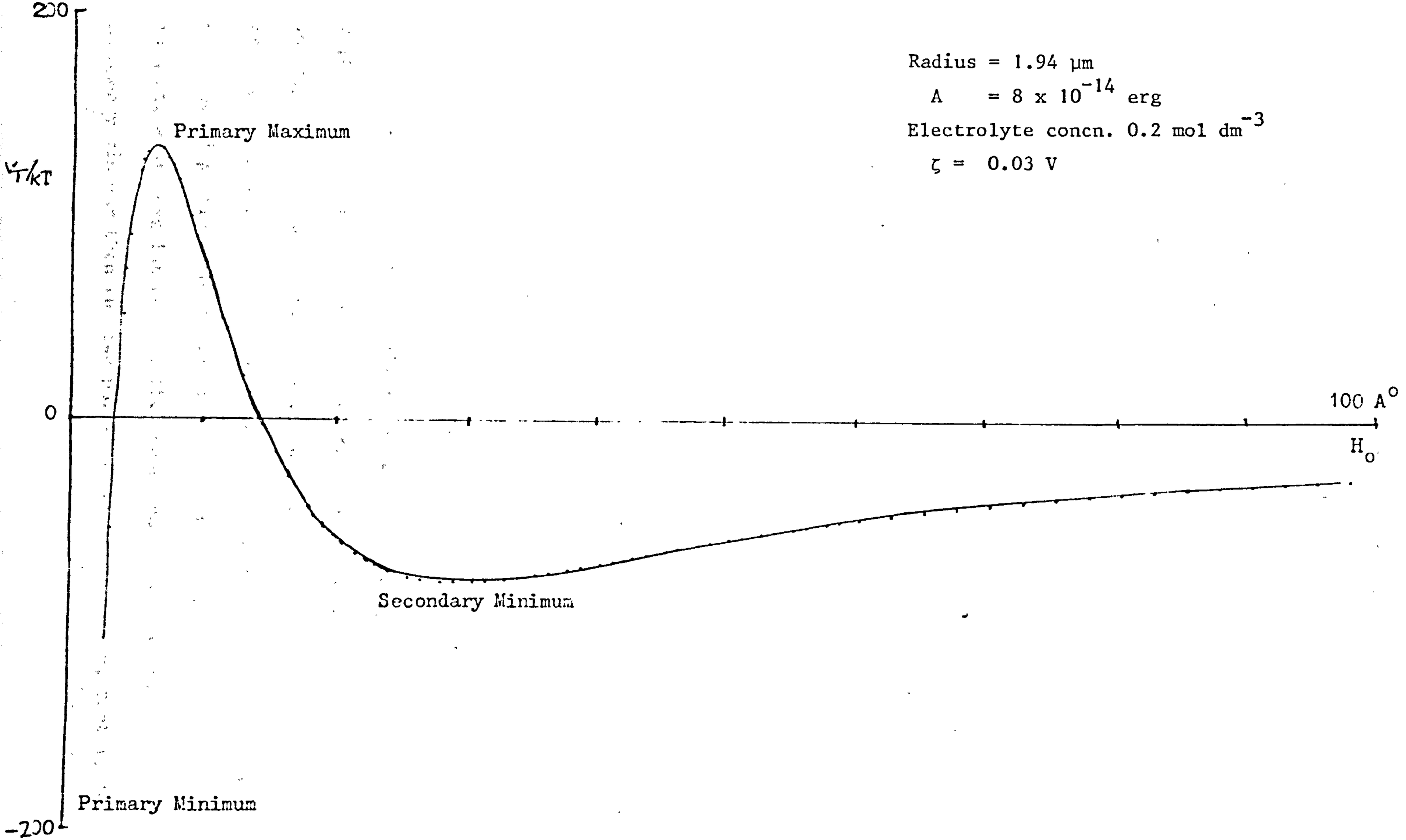

Radius = 1.94 μm

A = 8×10^{-14} erg

Electrolyte concn. 0.2 mol dm^{-3}

ζ = 0.03 V

approach, in a liquid, overlap of the electrical double layers occurs leading to a repulsive interaction. The repulsive interaction energy, V_R, for two spheres of radius, R, with their surfaces separated by a distance H_o is given by[5]

$$V_R = \frac{\varepsilon_r \, R \, \psi_o^2}{2} \ln \left[1 + \exp(-\kappa H_o)\right]$$

where ψ_o is the surface potential, $1/\kappa$ is the thickness of the double layer and ε_r is the relative permittivity of the liquid medium.

$$\kappa = \sqrt{\frac{8\pi \, n_o \, z^+ z^- \, e^2}{\varepsilon_r \, kT}}$$

where n_o is the concentration of ions at infinite separation in the liquid medium, $z^+ z^-$ the valency of the positive and negative ions, e the fundamental protonic charge, k the Boltzmann constant and T the absolute temperature.

1.5.3. The Total Energy of Interaction

As stated by Derjaguin and Landau[4] and Verwey and Overbeek[5], the total energy of the system, V_T, can be taken as the sum of the attractive, V_A and the repulsive, V_R, interaction energy terms. Hence this leads to an expression for the total energy of interaction, V_T, in the form,

$$V_T = V_R + V_A$$

$$= \frac{\varepsilon_r \, R \, \psi_o^2}{2} \ln \left[1 + \exp(- H_o) - \frac{A_{net} \, R}{12 \, H_o}\right]$$

An example showing how the potential energy, V_T, varies with the distance of separation, H_o, for two spheres of the same radius is shown in Figure 1/4. The second particle can either reside in the secondary or primary minimum. The primary minimum represents the closest approach of a second particle to the first, that is when the particles are in a state of coagulation. If the second particle lies in the secondary minimum then the two particles are flocculated, that is the

particles are separated by a finite distance but they are not free to move independently of each other. However this is a metstable state since there is a high energy barrier, the primary maximum to be overcome before they move into the unstable coagulated phase.

1.6 This Study

In this research, regions where a foam can be formed have been defined, thus enabling some predictions to be made of conditions which lead to foam formation. These foams were stabilised by polystyrene latex particles, 1 to 4 μm in diameter, having sulphate end groups. The foam bubbles were examined by both microscopic and laser techniques.

An attempt to relate the occurrence of the foam with the fundamental properties of the dispersion such as zeta-potential, surface tension and contact angle has been made. Examination of the surface properties of a film of polystyrene latex particles on sodium chloride solutions is also reported.

CHAPTER 2

LITERATURE SURVEY

2.1 Historical Review

Robert Boyle, as early as 1660-1672, studied the interference colours arising from a thin film of soap. He observed the apparent appearance of holes - more correctly termed black films - on the bubble's surface before rupture occurred. Newton reported black films of 'different shades'. It was not until the 19th century that more quantitative observations were made.

Plateau formulated laws of bubble geometry[7]. These have been translated and listed in a review by Ross[8]. The first law states that when three lamellae come together they meet at an edge; the angle each lamella makes with the others is 120^{o}. These junctions have been named Plateau borders. The second law states that four of these edges meet at a point, and at this point the angles are all equal to 109^{o}28'.

Sir William Hardy, as early as 1925, described the soap film around a bubble as being a layer of soap solution sandwiched between two adsorbed monolayers of solute[9]. Corkill et al. used a radioactive technique to prove the correctness of this model[10], and Laing has discussed the composition of soap films[11].

Bikermann in his review[12] defined a foam as a dispersion of a relatively large volume of gas in a small volume of liquid. The foam bubbles were polyhedral in shape. As a contrast to this a gas emulsion could be defined as a dispersion where the volume of liquid was greater than the volume of gas. Here the bubbles were spherical.

These two different states have also been defined by Manegold[13] and have been described by Ross[8]. A dispersion of spherical bubbles in the liquid phase, gas emulsion, has been designated kügelschaum, meaning sphere-foam; whereas an array of polyhedral bubbles were called polyederschaum, polyhedron-foam. Photographs of the two different systems

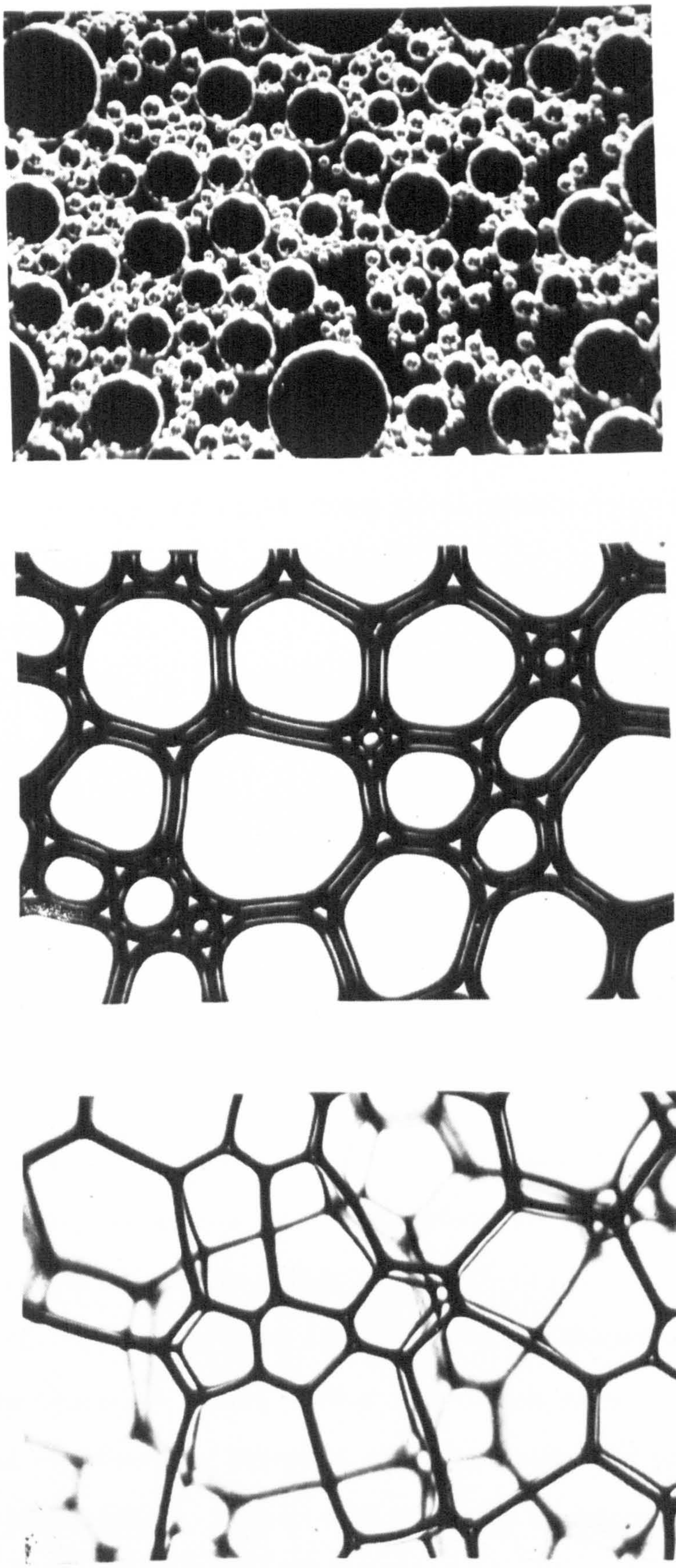

Figure 2/1: Different Types of Foams from Kitchener and Cooper[14]

are shown in figure 2/1.

Foams are fundamentally unstable systems in the thermodynamic sense. They have a large interfacial area and a high interfacial tension. This leads to a tendency for the interfacial area to decrease and by so doing restore the equilibrium state of lowest energy. Kitchener in his reviews on foams[14,15] has classified foams with respect to their metastable states.

Unstable foams break when the liquid drains from the foam. This leads to bubble coalescence which results in a decrease in the interfacial area. These correspond to kügelschaum foams which can be described as temporary dispersions of gas bubbles in liquid having no foam stability. The rate of collapse of these foams is inversely proportional to

(a) the bulk viscosity of the liquid,

(b) the bubble size,

and is independent of the surface tension of the liquid. If a second non-foaming solute, such as glycerol, is added then the rate of liquid drainage is decreased due to the increased viscosity of the liquid phase. This increases the foam stability. De Vries has demonstrated this form of foam stabilisation[16].

Metastable foams are those where the drainage of the liquid has become negligible. These foams can remain stable for a period as long as 2 - 3 years if they are protected from external disturbances.[17] These bubbles are polyhedral and so the foams correspond to polyederschaum. Their stability is due to loss of fluidity in the lamellae arising from surface plasticity of the films.

Solid foams have been classified by Kitchener and Cooper[14] as supercooled transient foams. They can either have a spherical or a polyhedral structure. Examples of these foams are polyurethane or expanded polystyrene. Their main property is their increased viscosity as the monomer used undergoes polymerisation.

Cellular foam is formed by blowing air through a horizontal plate in

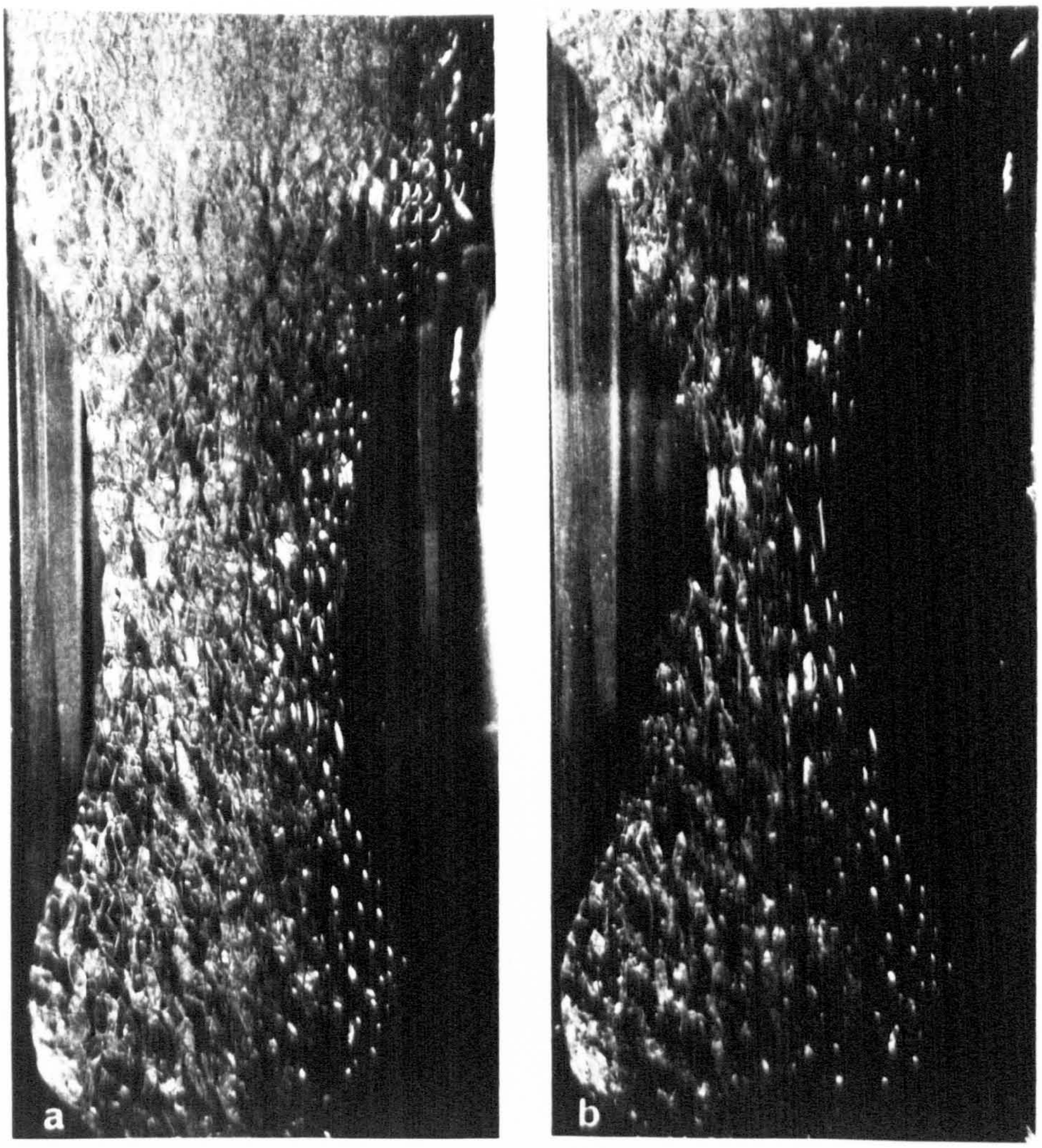

Figure 2/2: Biliquid Foams Sebba[20]

a column of liquid. Froths having uniform bubble size can be formed using this method[18]. Hartland and Barber[19] have derived a relationship for foam height to foam thickness for a cellular foam consisting of regular dodecahedral bubbles.

Sebba has formed biliquid foams. In these the gas cell has been replaced by a liquid. There are two different types of lamellae, one oil and the other water. They are formed by letting globules of water containing a suitable surfactant fall through an oil phase. Figure 2/2 shows photographs of these foams from the original paper[20].

Kruglyakov and Taube have studied the effect of dropping solid particles into a surfactant foam[21]. The solid phases they used in this investigation were finely dispersed silica, sulphite bleach cellulose and carbon black. They found the foam stability increased in the presence of the solid. This was due to the formation of a three-dimensional skeleton which increased the mechanical properties of the surfactant foam. The solid phase protected the soap lamellae. The increase in stability was found to depend on the size, shape and wettability of the solid particles. There was however a limit to the stabilising effect of the solid, too high a solid concentration was found to be detrimental to foam stability. The concentration of surfactant was also found to have an effect. At small concentrations of surfactant the solid phase increased the rate of film drainage and decreased the foam stability. However, at larger concentrations of surfactant the reverse effect occurred.

2.2 Foam Formation

The properties of a foaming system fall into two categories, those which affect the foaming ability of the system and those which stabilise the foam. In fact, a large amount of work has been carried out on the stability of foams but very little on their formation. However, research on foam prevention has considerably aided knowledge of the mechanism of their formation.

One criterion for foaming is that the foaming agent must be able to adsorb at the air/liquid interface to give a mechanically strong film. Ross in a series of papers[22-24] has shown that the action of one type of antifoaming agent is to spread on the interface by preferential adsorption thus causing desorption of the foaming agent. An example of this type of anti-foaming agent is polydimethylsiloxane. It spreads easily to form an interfacial film which has little lateral cohesion. By contrast most good foaming agents have considerable lateral cohesion, for example between the hydrocarbon chains of the surfactant molecules.

Burcik has discussed the importance of surface tension lowering with respect to foaming[25]. The foaming ability of a system should increase with decrease in surface tension.

A measure of foamability is the specific surface area produced in the foam formation process. Chang et al. defined specific surface area as the total surface area of the gas/liquid interface in 1 cm^3 of foam[26]. Clark and Blackman showed that the specific surface area could be obtained by observing the transmission of light through the foam[27].

Ross[8] considers that a more fundamental measure of foamability would be the increase in potential energy on foaming. This increase arises from three sources: the extension of the liquid surface, the compression of the gas and the hydrostatic potential of the fluid in the foam cells. To illustrate this idea Ross has suggested a model based on the isothermal expansion of a gas cell.

2.3 Foam Stability

The stability of foams has been found to depend on the strength and rheological properties of the thin films such that the distance between the adsorbed layer at the opposing interfaces is small compared to the bubble dimensions. Any extension of the surface increases the free energy of the interface. Therefore once a foam is formed the interfacial area starts to decrease until a metastable equilibrium is set up.

Gibbs[28] stated that there were two factors involved in the stability of any foam, film drainage and film strength. Bikermann has defined three processes occurring in all foams: redistribution of bubble size, thinning of the liquid film and film rupture[12]. These will be discussed below, but first the various methods of measuring foam stability will be considered.

2.3.1 Measurement of Foam Stability

A fundamental problem in dealing with foams is to devise experimentally a quantitative measurement of stability which is applicable to all systems. So far, this has not been achieved and is indeed very difficult owing to the complex nature of the stability, involving as it does both kinetic and thermodynamic parameters.

However several authors have reported measurements on the lifetime of foams[29-32] as a criterion of their stability. Although this appears to be a fundamental measure of foam stability, in practice a subjective decision has to be made as to when the foam has collapsed. This can be done by estimating when only a few small bubbles or a single bubble remain. Clearly this decision has to be taken by the experimentalist and will depend on the foam. Using this as a method of determining foam stability, Schütz[29] has found a relationship between foam lifetime and the molecular weight of the surfactant stabilising the foam. Also he has found that there is a maximum in foaming at a certain concentration of surfactant. This also can be related to the number of carbon atoms in the hydrocarbon chain[30]. Brady and Ross have designed a foameter to study foam stability at different temperatures[32]. They defined three lifetimes: the lifetime of liquid in a foam, the lifetime of gas in a foam and the lifetime of the foam.

The foam height and its decrease with time have been used by Foulk and Miller to measure foam stability[33]. Also Nash has found the critical micelle concentration from foam height measurements[34]. Brown et al.[35] used

foam volume as their measure of foam stability. However they considered that foam volume alone does not describe the changes undergone in the foam. A better parameter appeared to be the specific surface area of the foam.

Clark has defined an expansion factor which is the ratio of the gas volume in the foam to the volume of liquid. He determined this ratio from measurements of the electrical conductance of the foam[36].

Bikerman defined the lifetime of a cellular foam as the average foam volume divided by the volume of the air forced through a septum in a known time[37].

Barmore measured the amount of liquid draining from a weighed sample of foam as a function of time. The slower the rate of drainage the more stable was the foam[38].

A more theoretical parameter was proposed by Ross[8] to define foam stability, namely, the rate of dissipation of the potential energy acquired by the foam during formation. He considered that by determining the difference in potential energy between the bulk phase and the foam the foamability and foam stability could be described using the same parameter.

2.3.2 Bubble Size and its Distribution with Time

The most stable shape for a bubble is a sphere. However foams tend to be polydispersed, thus resulting in a pressure difference between bubbles of different sizes. The pressure inside a bubble is related to its curvature and is equal to $2\gamma/R'$ where R' is the bubble radius. Therefore a small bubble is at a higher pressure than a large bubble. Gas diffuses from the high to the low pressure region thus causing a small bubble to grow smaller and a large bubble to grow larger. This is called the Ostwald ripening effect. The photographs in a paper by Clark and Blackman illustrate this phenomenon[39]. Chang et al.[26] have also studied the process of Ostwald ripening experimentally, using a freezing technique to find the bubble size distribution. The average bubble size increased with time,

whereas the specific surface area decreased[39]. Clark and Blackman also studied other gases besides air in their researches.

There are two processes which cause decreases in interfacial area; one is the diffusion of gas from high pressure to low pressure regions, and the other is the coalescence of adjacent bubbles as the result of the collapse of the liquid lamellae in the foam.

The rate of diffusion of gas is determined by the pressure difference between adjacent bubbles and the permeability of the liquid film. De Vries derived a theoretical equation for the kinetics of foam destabilisation based on the total number of bubbles[40]. He made two assumptions, the first being that the bubble size distribution was given by the equation

$$F(R') = \frac{6\,\bar{\alpha}R'}{(1 + \bar{\alpha}R'^2)^4}$$

where $\bar{\alpha}$ is a parameter of the distribution function and R' is the radius of a bubble. Also he assumed that the deficiency of bubbles at the external surface compared with the number of bubbles in an arbitrary plane was independent of time. The slope of the curve of the number of bubbles against time was a function of the physical parameters of the foam. The latter were the permeability of the liquid, the surface tension, the initial mean square radius and the average thickness of the lamellae. He used a highly viscous liquid so there would be no appreciable drainage and no collapse of bubbles during the measurements. The decrease in interfacial area was therefore only due to the result of diffusion of the gas phase. However, the agreement of the experimental results with the diffusion theory was poor. Errors in the values arose from an incorrectly assigned theoretical bubble size distribution. Therefore no quantitative evaluation of foam stability with respect to transfer of gas could be made. In relation to this work it is worth noting that Brown et al. have made the observation that the diffusion of gas can be retarded by the presence of an adsorbed monolayer of surfactant[41].

De Vries[42] has also derived an equation to calculate the rate of coalescence of bubbles when the initial bubble size distribution is known. The assumptions that he made were that the rate of diffusion was smaller than the rate of dissolution and that the pressure difference between the two spherical bubbles, ΔP, could be described by the following equation :

$$\Delta P = 2\gamma\left(\frac{1}{R'} - \frac{1}{R''}\right)$$

where R' and R'' are the radii of the bubbles. He used viscous emulsions to decrease the rate of drainage in an attempt to find the rate of coalescence of the bubbles. The plot of the square of the bubble radius against time was linear. From the slope the average thickness of the film was obtained. The disappearance of bubbles was found by de Vries to depend on the surface tension, the permeability of the film and the film thickness.

2.3.3 Drainage of Thin Liquid Films

Several authors[43-45] have investigated the drainage of free liquid films and have attempted to develop models to describe the thinning process.

Jones et al.[46] defined three causes of drainage of the liquid from the film lamellae:

(a) the flow of liquid in the interior of the film due to gravity;

(b) the suction effect due to curvature at the periphery of the film, an effect which can exceed that of gravity;

(c) evaporation from the upper part of the film followed by condensation in the lower sections.

It was found that the film drained to a certain thickness and then, as a result of instability set up in the system by thermal or mechanical vibrations, the film spontaneously ruptured.

Miles et al.[47] have shown that the rate of drainage can be affected by the physical state of the adsorbed monolayer. Fast-draining films occurred with gaseous monolayers, while slow-draining ones corresponded to

condensed liquid monolayers. Sporek[48] also found that fast draining films had gaseous monolayers. Dashier and Mabis have proposed a model for drainage assuming close-packing of the hydrocarbon chains in the surface monolayer[49].

Mysels[50] defined two different types of drainage:

(1) The rigid film where drainage took place via a viscous liquid flow between the stationary adsorbed monolayers. For this type of flow the rate of drainage can be calculated if the bulk viscosity is known.

(2) Fast draining films which were a consequence of highly turbulent flow occurring in the film. The prediction of drainage rates proved unsuccessful.

Jones et al.[46] have commented that the major cause of drainage is capillary suction. Derjaguin et al. attempted to measure both the capillary pressure and the film thickness[51]. Since the capillary suction is proportional to the curvature of the bubble the rate of thinning depends on the bubble size distribution. Drainage can therefore occur through the Plateau borders[52]. Hence, drainage continues until the excess hydrostatic pressure is balanced by the normal forces acting in the film to give a metastable state.

This state is characterised by strict uniformity of film thickness. The thickness, however, is a function of the normal force, that is the disjoining pressure. This quantity was defined by Derjaguin[53,54] as the net result of the repulsive and attractive forces arising from the adsorbed monolayers. The forces which act normally within the film across the aqueous core are London - van der Waals attractive forces and electrostatic repulsive forces. Both depend on film thickness, and the electrostatic force also depends on the electrolyte concentration[55]. However there are systems where the electrical stability is not important, therefore this is not the only stabilising force.

Ivanov and Dimitrov postulated that the critical thickness did not

depend on surfactant concentration but that it was determined by the properties of the adsorbed layer[56]. They derived an equation for the rate of thinning. However this involved using the poor assumption that the surface viscosity, discussed in a following section, did not depend on the surfactant concentration or flow velocity.

Radeov et al. also attempted to describe the effect of surfactant concentration on the thinning process[57]. They derived two equations, one for high surfactant concentration and one for low concentration. They discussed the role of surface diffusion in foam stability and suggested that its importance increased as the film thickness decreased.

Miles et al.[58] have derived equations for the rate of flow of liquid through a foam and the rate of drainage in a vertical capillary. They found reasonable agreement with their experimental results.

Thompson has attempted to measure the drainage rates of foams having a high expansion factor[59]. He observed the movement of the interference fringes down a single foam film held in a frame. He defined a useful parameter as being the half drainage time which was the time for the first order coloured fringes or the black fringes to reach the centre of the film. The plot of the position of the interference fringe against time was found to be approximately exponential. However, to obtain the initial drainage rate the total liquid in the film at formation was required since the drainage was too rapid to extrapolate back to zero time.

2.3.4 Surface Viscosity

A historical review of surface viscosity has been reported by Scriven and Sternling[60]. Several authors have found that high surface viscosity of the liquid film correlates with high foam stability[35,61,62]. However high viscosity is desirable but not essential for high foam stability.

High surface viscosity also retards the drainage of the thin liquid film. It is dependent on the composition of the system as the foam additive must be neither too dilute nor too concentrated. An increase in

temperature also has an effect on the rate of drainage due to the resulting decrease in viscosity it produces[14,58].

Ideally the rheological properties of the thin liquid film should be plastic. Both Newtonian and plastic viscosity have been found to occur[35,63,64]. Shih and Lemlich have postulated a theory for film drainage based on interstitial Newtonian flow[65].

Joly[64] has studied the viscosity of various types of monolayers of proteins and polypeptides. He found the viscosity to be Newtonian but the monolayer formed a gel on compression to a certain surface pressure.

2.3.5 Film Rupture

The probability of film rupture defines the film stability. Rupture occurs when the thickness of the film locally decreases to molecular dimensions that are below the critical film thickness. Brady and Ross have derived a theory for film rupture assuming the rate of thinning for all the lamellae was the same and that rupture took place instantaneously after the critical thickness had been reached[32].

A more comprehensive theory was postulated by de Vries[66,67]. He studied single liquid films in frames using a high speed ciné camera. However the variation in film lifetime was longer than the total exposure. Therefore he used two techniques to induce rupture: an electrical discharge or a copper needle brought within 40 μm of the film, which was heated electrically. The hole formed remained circular as it expanded. The rate of increase in radius was found to be 3.55 m s^{-1}. Dupré has calculated the speed of expansion of a hole assuming that all the surface energy released was converted to give an increased kinetic energy to the liquid.

The equation

$$v = \left(\frac{4}{t'\rho}\right)^{\frac{1}{2}}$$

where v is the velocity, t' the thickness and ρ the density, was found to be essentially correct. However it follows that the rate of expansion of the

hole should be independent of the viscosity.

De Vries formulated an expression for the activation energy for film rupture[56]. For unstable films the black spots that appear in the thin film are a consequence of London-van der Waals forces. These are large enough to balance the double layer repulsion and surface forces. Likewise the rate of growth of these black spots depends on the value of the London-van der Waals force and the viscosity of the liquid. Rupture is preceded by very rapid growth of the total black area.

De Vries has also described a mechanism for the film rupture of stable films[67]. Here the surface area is smaller than before[66] and so the influence of both the London-van der Waals force and the double layer repulsion are negligible compared with the surface forces. The viscosity of the layer, which is higher than the bulk, tends to retard the rate of thinning.

The stabilising force acting in these thin films is due to the surface tension of the liquid and has been termed Gibbs elasticity. Several authors have explained its existence and its effect[14-16,46,55,60,67,69]. It can be defined by the equation

$$E = 2A\left(\frac{\partial \gamma}{\partial A}\right)_{tn_1 n_2}$$

where A is the area.

Any extension of the surface area increases the free energy. Since the free energy is a function of the surface tension the resistance to deformation depends on the interfacial tension. From the Gibbs adsorption equation

$$d\gamma = -\sum_i \Gamma_i d\mu_i$$

where Γ_i is the surface excess of species i and μ_i is the chemical potential of i, it can be seen that any increase in surface area will decrease the amount of solute per unit area causing the surface tension to rise. Solute is therefore desorbed from the interface and transferred to the bulk.

Corkill et al. used a radiotracer technique to show that there was an excess of solute in the aqueous film core compared with the bulk concentration. This counteracts further extension and so restores the initial equilibrium. However the rate of attainment of this initial equilibrium must be high since the film will collapse if the driving force is greater than the restoring force. The action of antifoaming agents is to cause an instantaneous decrease in surface tension.

Marangoni in 1865 also postulated a theory for surface elasticity. This was based on the setting up of a dynamic surface tension[14,15,56].

An extension of the Marangoni idea is the surface transport theory[14]. This involves the movement of the monolayers caused by a surface tension gradient in the interface thus causing the underlying liquid to be carried with the monolayer.

Local temperature differences will decrease the lifetime of the foam. De Vries reported[16] a demonstration by Plateau in 1875 on the effect on temperature. He showed that the warmth of a finger brought close to a large soap bubble caused a decrease in film thickness, that is he observed a colour change from yellow to green.

As previously stated, the liquid film thins to a critical thickness after which it undergoes spontaneous rupture. Ivanov et al.[71] have originated a theory for the relationship between the critical film thickness and rupture. Although they attempted to account for the energy of the thicker parts of the film lamellae, that is the Plateau borders, there was still a descrepancy between the theoretical and experimental values. However the theory gave a reasonable agreement with experimental data for low surfactant concentrations.

Barber and Hartland have studied the collapse of cellular foams[72]. Their model was based on the relationship of foam height to the thickness of the liquid film. They assumed dodecahedral bubbles and that a steady state was reached when the rate of rupture was equivalent to the rate of arrival

of bubbles at the coalescing interface. They observed films thinning below the critical thickness. The force causing film drainage was found to be inversely proportional to the radius of the Plateau border. The collapse time increased with increasing viscosity, initial foam height and bubble size but decreased with increasing density, surface tension and critical film thickness. The critical film thickness is therefore a function of the film drainage.

2.4 Solid Sphere at an Interface

The ease with which particles can be attached to bubbles and the strength of the adhesion of the particle are of prime importance in the flotation of minerals. Several authors have devised models to analyse the forces involved in particles floating at interfaces. All have concluded that the particle is in a state of metastable equilibrium and that three major forces are involved. These forces arise from the buoyancy, the surface tension and the hydrostatic pressure.

2.4.1 Maru et al. treatment

It was assumed in the model formulated by Maru et al. for a rigid sphere situated at a fluid-fluid interface that the electric and molecular forces could be neglected in comparison to the buoyancy and surface tension effect[73]. The contact area was assumed to be spherical and the thickness of the intermediate film with the interface was neglected. Also the shape of the contact area and the bulk interface were taken to be symmetrical about the vertical axis of symmetry. The portion of the surface AB, figure 2/3, was defined in their model as being a circular arc with centre N and radius r. The rest of the interface was planar. Finally the surface tension of the contact area was equated to the surface tension of the free interface. Similar assumptions to these are made in all the theories.

They also defined a dimensionless quantity, β,

$$\beta = \frac{R^2 \Delta \rho_{32} g}{\gamma_{32}}$$

Figure 2/3 : Solid Sphere at an Interface from Maru[73]

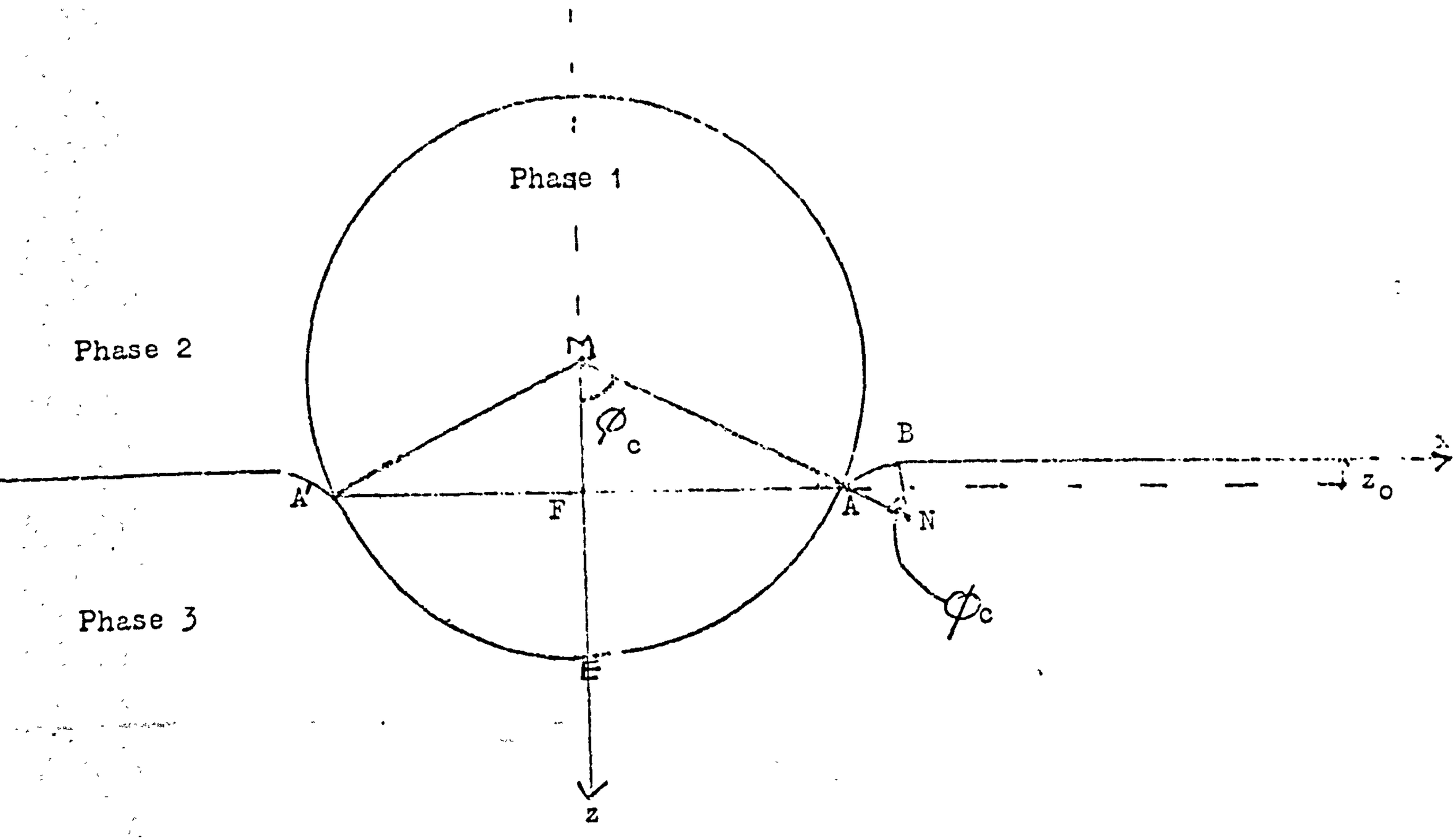

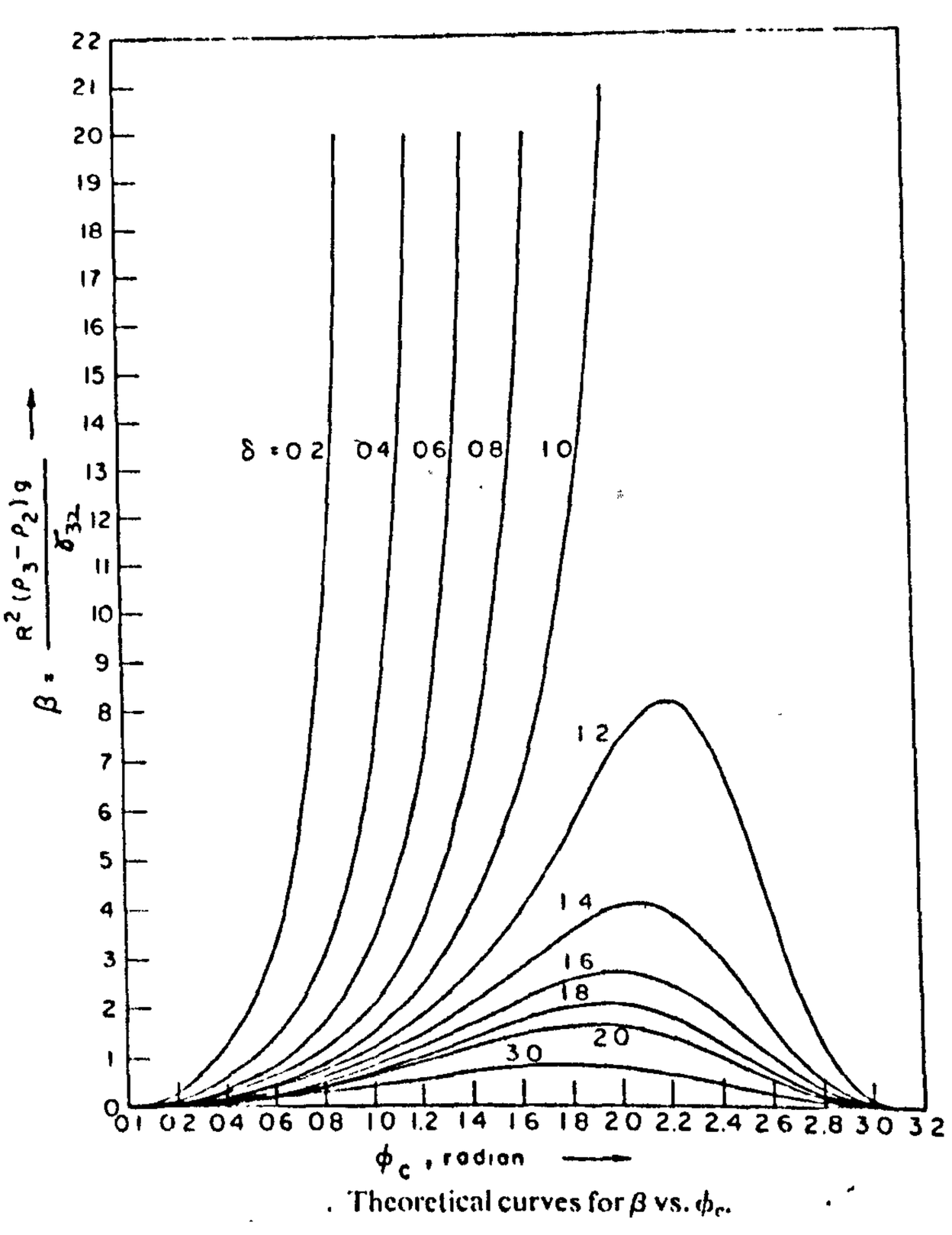

Figure 2/4: Theoretical curves for β vs ϕ_c from Maru[73]

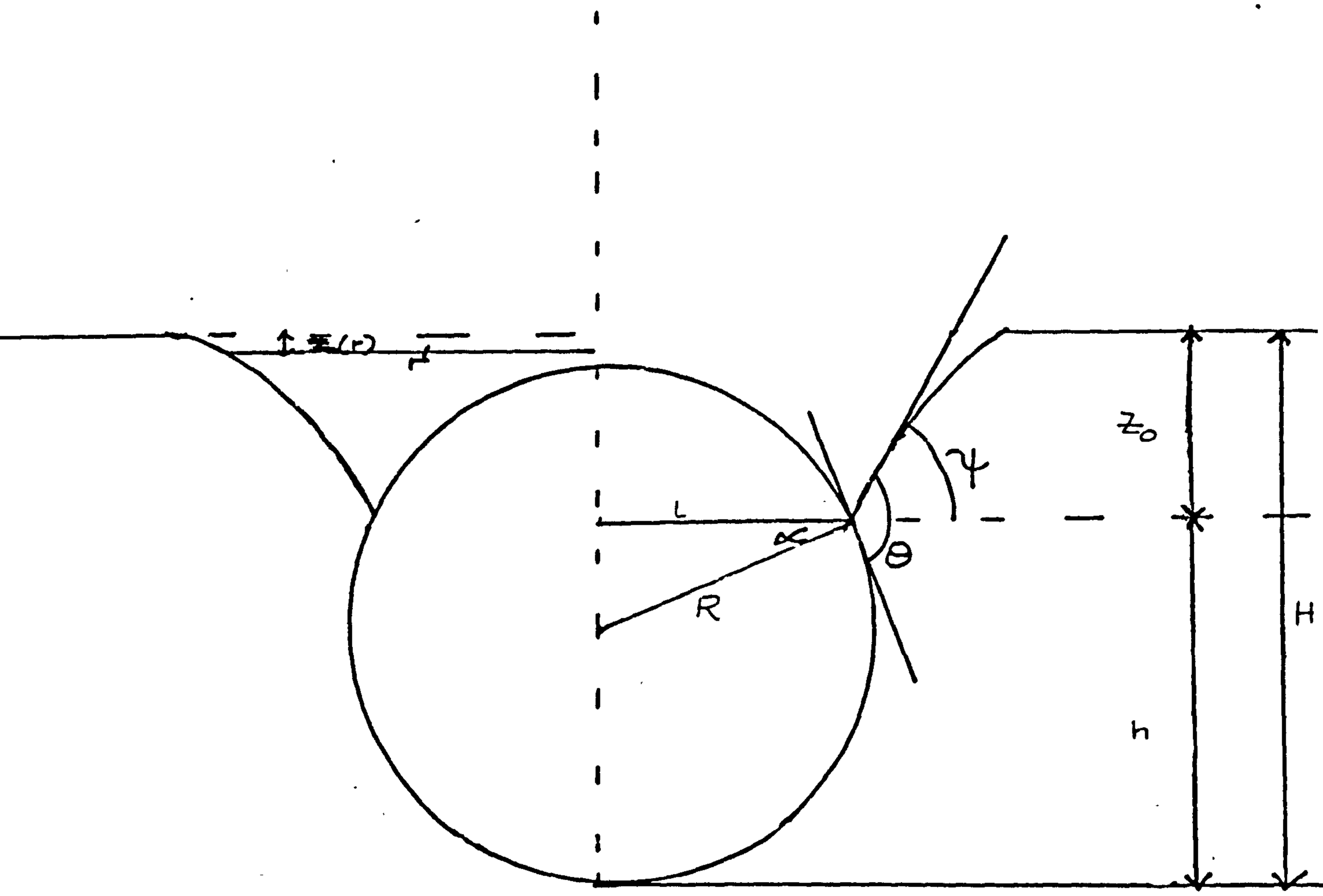

Figure 2/5 : Sphere at an Interface, from Torbin[74]

where R was the radius of the sphere, $\Delta\rho_{32}$ the difference in density between the exit phase, 2, and the entry phase, 3, γ_{32} was the interfacial tension and g acceleration due to gravity. Their plot of β against ϕ_c, the angle at the centre of the sphere, figure 2/3, is shown in figure 2/4. A parameter δ was also defined by the equation

$$\delta = \frac{\Delta\rho_{12}}{\Delta\rho_{32}}$$

where $\Delta\rho_{12}$ was the difference in density of the sphere and the exit phase. For values δ greater than one there was a maximum in the value of β. Maru et al. have defined two equilibria for β values less than this critical value. Since for each β there were now two values ϕ_c the lowest value corresponded to the metastable equilibrium. For spheres lying in this position, if they were displaced a small distance they would return to their equilibrium. The higher value of ϕ_c corresponded to the labile equilibrium if the sphere was now displaced it did not return to the equilibrium position. For $\delta \leqslant 1$ there was not a critical value for and so the spheres obtained equilibrium in all positions. They found good agreement with theory.

2.4.2 The treatment of Torbin et al.

Torbin et al. also discussed the equilibrium position of spherical particles at an air-water interface[74]. They made observations on mercury spheres on the surface of water, measuring the depth of immersion of the centre of gravity microscopically. The wetting perimeter and the contact angle between the liquid and the mercury drop were determined from the photographs. Figure 2/5 shows the model of the sphere resting at the interface. The position of the sphere is determined by the parameters α and z_o. At equilibrium the weight of the sphere is balanced by the surface tension and the hydrostatic force

$$W = f_\gamma + f_v$$

and

$$W = 4/3\,\pi R^3 \rho g$$

where R is the radius and ρ the density of the sphere. The vertical component of the surface tension, f_γ, can be defined as

$$f_\gamma = 2\pi r' \gamma \sin \psi$$

where r' is the radius of the contact area and γ is the surface tension. The vertical component of the hydrostatic pressure, f_v, can be equated to the relative weight of liquid.

To a first approximation the mercury drops are balanced mainly by the surface tension. From the equations postulated the maximum size of the floating drop can be determined. The theory gave agreement of the calculated values with the experimental values.

2.4.3 Fluid-Fluid Interfaces

A number of authors have proposed theories for a sphere at a fluid-fluid interface[73,75-80]. In all the theories the equilibrium involving the balance of the three forces, the weight of the particle, the vertical component of the surface tension and the vertical component of the hydrostatic pressure, is discussed.

Rapacchietta and Neumann have postulated that for a given system fluids can support a sphere of greater radius than the corresponding cylinder[76]. They subsequently found for contact angles greater than 90° that the critical radius was larger for a sphere than for a cylinder; the contrary is true for contact angles less than 90°.

Princen has published two papers describing the shape of a fluid drop at a liquid-liquid interface[82,83]. In one he discusses a model for the shape of a drop when the drop is the same fluid as the lower phase[82]. He found that the shape was a function of drop size, surface tension and density difference.

Hartland has studied the drainage of the film between a sphere and a liquid-liquid interface[77,78,84,85]. He compared the drainage of a sphere and a fluid drop[77]. The drainage film was found to be symmetrical

about the vertical axis of the sphere. For the drop the drainage was found to be unsymmetrical. The rate of drainage of a solid sphere was found to be slower than that of the drop. Hartland and Robinson, in their paper, list the authors who have studied the approach of a sphere to a fluid interface[78]. In this paper a similar theory to Maru et al.'s is postulated. They also found good agreement between theory and experiment.

In a later paper[84] Hartland has derived an equation for the variation in shape of the film with time. It was obtained by considering the effect of the pressure gradient due to the viscous flow and gravity on the deformable fluid-fluid interface. The profiles were independent of the direction of the motion of the sphere.

Hartland and Robinson[85] have found that rigid spheres of non-uniform density approaching a deformable liquid/liquid interface cause unsymmetrical drainage. Also the presence of surfactants was found to reduce the rate of drainage due to restriction of rotation of the sphere. Derjaguin et al.[81] have also studied the approach of rigid spheres to fluid-fluid interface.

2.4.4 Solid particles

Dukhin and Rulev[80] have studied the interaction between a sphere and a bubble. The interaction occurs when the distance between the surface of the particle and the bubble is less than or equal to the particle size. Nutt has studied the adhesion of solid particles to flat interfaces and bubbles[86]. The experimental results indicated that a force has to be overcome before the sphere can be detached from an interface. The strength of the adhesion was found to agree with the theory. As expected it increases with surface tension and with the contact angle. Derjaguin et al. have discussed the effect of particle size on the interaction of a spherical particle and a bubble[87].

Huh has studied the equilibrium of axi-symmetrical particles at a fluid interface[88,89]. In Huh's second paper[89] they extended the calculation

of the critical size of the sphere. Padday and Pitt[90] have also discussed the axi-symmetrical meniscus profile. It can be described by the height at a distance, z_o, from the axis of symmetry. However knowing the shape, size and density of the particle plus the contact angle, the shape of the meniscus profile can be obtained. Huh and Mason[89] gave a theory for the stability conditions and critical states of several spheroids. They have concluded that flotation can be improved if the shape of the sphere is changed to an oblate spheroid.

Detaching a sphere from an interface can be used to measure the interfacial tension. This has been demonstrated by Scheludko[91] and Huh[92]. This method can be used to measure simultaneously the interfacial tension, contact angle and difference between the density of the two phases[92]. However the radius and the height measurements need to be accurate.

2.5 Surface Coagulation

As observed by a number of authors, particularly Heller[93-99], a form of coagulation can occur when a colloidal system is stirred, shaken or has gas bubbled through it. Aggregation of the particles occurs at the interface and hence this form of aggregation is termed surface coagulation, or by some authors, for example Freundlich, as mechanical coagulation. This occurs usually before bulk in stability is reached. Ottewill has reviewed Heller's work in his specialist report[100].

Heller has reported Freundlich's work on surface coagulation[95]. He has found that the residual solid concentration decreased linearly, that is the rate increased with increasing agitation. Freundlich considered that this indicated a zero order reaction. He concluded that the coagulation occurred at the air/liquid interface. Stark's data also support this idea although he has explained that the effect is due to an increase in concentration near to the interface, thus causing the coagulation to be a second order reaction[101]. The order of the reaction reported does appear

to differ in the literature. Most of Heller's work was done on α-FeOH sols[95-99].

Heller and Roeder[94] have shown that the zeta-potential must also be critically low, less than 50 mV, before mechanical coagulation can take place. Roe and Brass illustrated that the effect of an increase in stabiliser concentration on the mobility of the colloidal particles was negligible in this system[102]. However, it did reduce the rate and degree of mechanical coagulation.

Heller and Peters have postulated a theory to explain mechanical and surface coagulation[95]. They have made the following assumptions :

(1) Coagulation proceeds exclusively in the liquid-air surface and is a bimolecular reaction.

(2) There is sufficient convection to exclude diffusion of particles to and from the surface as the rate determining step.

(3) The contribution of aggregates to the rate of coagulation is neglected.

(4) There exists a definite steady state for the distribution of primary colloidal particles between the bubble and the surface. This distribution is assumed to follow a Langmuir adsorption isotherm.

(5) The rate of adsorption is assumed to be large relative to the rate of mechanical surface renewal. Therefore the adsorption equilibrium is not affected.

The Langmuir isotherm can be written in the form

$$c/a = K_1 + K_2 c$$

where c is the concentration of the colloid in solution, a the surface concentration of colloid, mol cm^{-2}, and K_1 and K_2 are constants. The rate equation for a zero order reaction becomes

$$-\frac{dc}{dt} = k'\left(\frac{s}{V}\right) \qquad (1)$$

where t is time, k' the rate constant, s the surface area at constant rate

of renewal and V is the volume of the solution. For a second order reaction the following is obeyed

$$-\frac{dc}{dt} = k''\left(\frac{s}{V}\right) c^2 \qquad (2)$$

The reaction order depends on the colloidal particle concentration and the value of Langmuir constants K_1 and K_2.

The methods of coagulation used by Heller et al.[95] were the rotation of circular tubes, containing the colloid, and the passage of nitrogen bubbles through the system. The degree of coagulation was determined by centrifugation and analysis of the supernatant for ferrous ions.

They found that the colloidal systems which required large amounts of electrolyte for bulk coagulation were not susceptible to surface coagulation. Surface coagulation required a critically low solid stability. They proposed an explanation for the coagulation at the surface based on:

(1) Assymmetry of the double layer of a molecule in the surface.

(2) There is a lower dielectric constant in the surface. This affects the surface charge, thickness of the double layer and the value of the Debye-Hückel constant.

(3) There is an unequal distribution of electrolyte between the bulk and the surface.

(4) The rate of coagulation is affected by non-spherical particles which are preferentially orientated at the surface. Heller and Quinfe[151] have shown that the orientation of particles by an external field accelerates their aggregation.

In his second paper[96] Heller tested the above theoretical equation for coagulation caused by stirring. Peters and Heller[95] found equation (2) to be valid. Secondary and tertiary particles were found to have no significant effect on the mechanical coagulation except for in the final stages. The coagulation was found to be a second order rate process. The parameter defined in the first paper was found to depend on the rate of stirring, the geometry and the size of the vessel.

The system would on a theoretical basis coagulate in the bulk phase if the potential energy barrier was less than 15 kT. Here the kinetic energy was above this critical value. However the surface potential of the particle at the interface must be less than the potential of the particle in the bulk phase for the surface coagulation to occur[96].

They also found a strong increase in initial coagulation rate with temperature. This observation disagreed with the earlier observations of Freundlich[103].

In the third paper in the series Heller and DeLauder studied the promotion of mechanical coagulation by the addition of a destabilising electrolyte[97]. A system which was stable to both agitation and bubbling of a gas underwent mechanical coagulation on addition of potassium chloride.

They also found that an increase in temperature caused an increase in the rate of coagulation. This was attributed to desorption of stabiliser at the colloidal particle surface.

A fourth paper dealt with the prevention of surface coagulation in the presence of a surfactant[98]. Here they used nonionic surfactants. They found that the colloidal particles were stabilised by the nonelectrolyte. They postulated different types of stabilisation for the two systems they studied. For the polyethylene glycol the stabilisation was due to steric protection, whereas dodecyldimethylamine oxide competed with the particle for occupation at the air/water interface. This caused the concentration of the colloid to shift in favour of that in the bulk phase.

They found the addition of ionic surfactants to have a variable effect on the bulk stabilisation.

The final paper in this series was devoted to an attempt to determine the effect of the presence of a large area of solid-liquid interface in the system and also the effect that turbulence had on surface coagulation[99]. They found that the addition of quartz promoted coagulation. An experiment, where the air-liquid interface was excluded, was created to see if the

system would coagulate. It did, showing that the coagulation could occur at the solid-liquid interface. However in the presence of an air-water interface the dominant process occurred at that interface. From the experiments performed they could not determine the effect of turbulence on the stability of the colloidal dispersion.

As early as 1937 Heller studied the structure of aggregates formed from non-spherical particles[93]. He found that the aggregates formed were more regular than when coagulation occurred slowly. In this context Fair and Geminell have derived a mathematical model for coagulation[104]. They based it on the Smoluchowski equation for orthokinetic coagulation of spherical particles.

2.6 Cream and other food foams

The concentration of milk fat solids in cream is very high. Light whipping cream contains 30-36% milk fat, whereas heavy whipping cream can have any fat concentration between 36 and 80%.[105] The diameter of a milk fat globule is approximately 4 μm.[106] The depth of the cream layer and the rate of its formation depend on the size of the fat globule, composition of the milk, agitation of the milk and the temperature history of the sample.

Wang and Kinsella[1-7] have reviewed the work done on the foaming properties of proteins. The role of the protein was to lower the surface tension of the aqueous phase, facilitate spreading on the surface and permit the increase in surface area required for foaming. The protein spread to form an elastic membrane around the gas bubble.

This structural network formed was due to partial denaturing of the proteins during the spreading. There were three processes involved in the adsorption of the protein :

(a) Diffusion of the native globule molecules to the interface where they adsorbed.

(b) Surface denaturation.

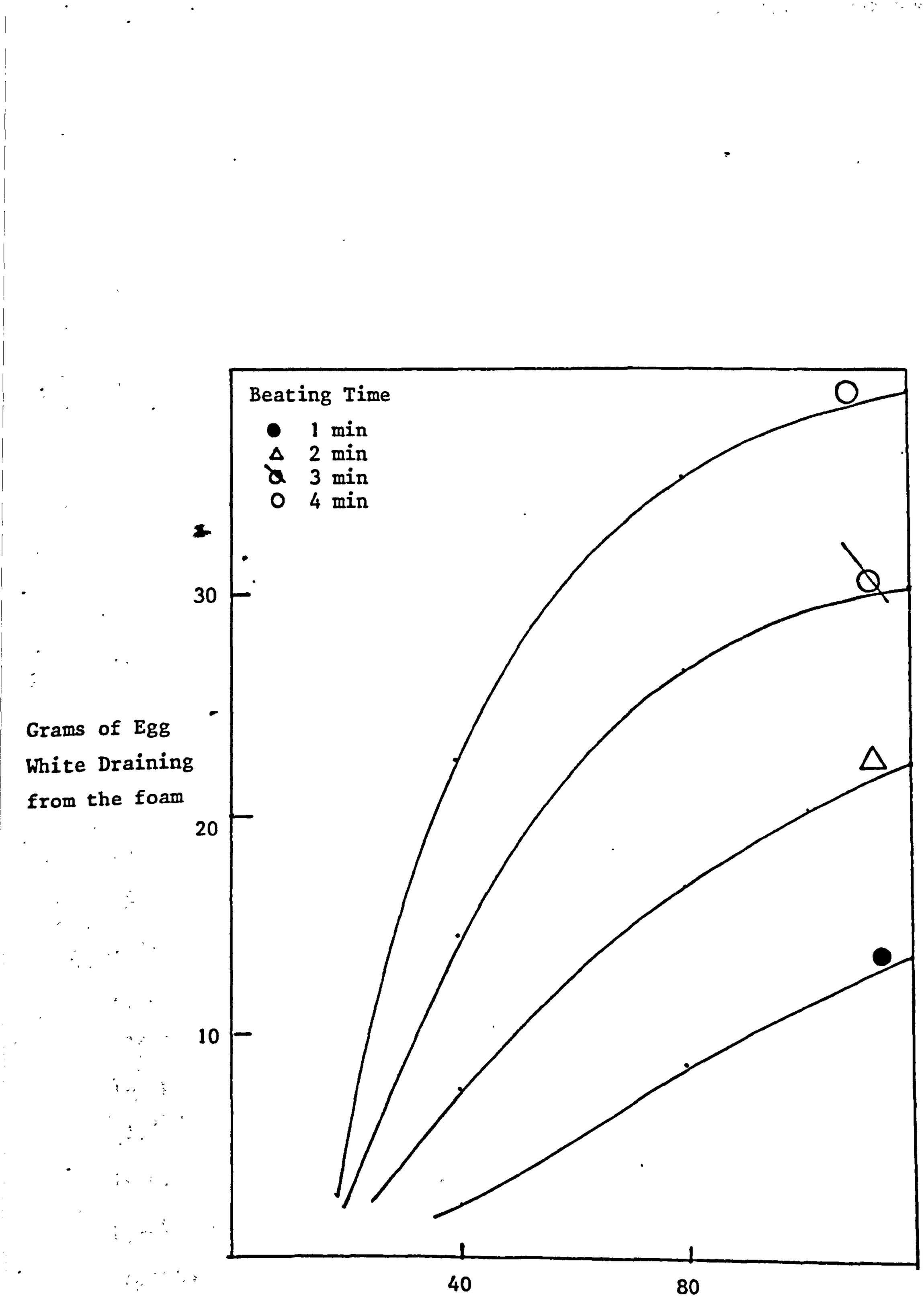

Figure 2/6: Barmore's Plot of Foam Drainage with Time

(c) Aggregation of the surface denaturated protein. This was detrimental to the foaming properties of the protein system.

In this section several different food foaming products will be reviewed. The basic principles are the same in all the protein systems. A fairly high concentration of the protein is required; there must be adequate amounts of soluble protein to provide surface films. For the whipping of soybean products the optimum concentration is between 7 and 8%.[108] The foaming properties of whey protein concentrate from milk were found to be inferior to the egg white protein and caesinate[109].

The effect of beating on the properties of these foams has been discussed by several authors[38,110,111]. The longer the beating the smaller were the bubbles and the more unstable was the foam. Barmore[38] has shown that the amount draining from the foam with time was greater the longer the egg whites were beaten, figure 2/6.

Preheating of the protein system has been found to enhance the whipping properties[38,108,109,111,112]. The optimum temperature for soybean products was 50°C [108], whereas for whey protein concentrate it was between 65 and 70°C.[109] Any heating at temperatures higher than this impaired the foaming properties[109]. However Barmore found no effect on the whipping properties of egg whites if the system was first preheated between 30 and 50°C. Higher temperatures did however cause decrease in the foam stability[38]. The preheating probably helped the denaturation of the protein. Richert et al.[109] found that temperatures higher than 70°C caused protein aggregation to occur particularly if the protein system was close to its isoelectric point. They found that the increase in the protein denaturation and aggregation caused a decrease in foam volume and hence foam stability.

Barmore[38] found a linear relationship between the viscosity of the system and the foam stability. Both viscosity and foam stability varied linearly with specific gravity of the foam. Cumper studied the coalescence of individual bubbles[113]. He found that the lifetimes of

bubbles depended on the surface viscosity. However the surface viscosity alone was not responsible for the stability of the foam. Richert et al.[109] also found correlations between surface viscosity and both protein denaturation and solubility.

Another area where research has been carried out is on the effect of pH on the foaming properties. Barmore found that the foam stability increased on the addition of the acid salt tartrate [38]. Several authors have found that the foam stability was minimum at the isoelectric point and increased to a maximum in a narrow pH region either side of the isoelectric point[107,108,111-113]. The viscosity of the system also increased in this narrow range around the isoelectric point[38].

The effect of table salt on the whipping of egg whites has been discussed by Sechler et al.[114] Within the flavour acceptibility range the foam stability decreased on addition of salt. However above this range they found an increase in foam stability, but this was still less than the system without added salt. The specific gravity of the foam was found to be constant with increase in salt concentration. However Monaghan-Watts found that the presence of salt improved the whipping ability of soybean products due to the chief protein being salt soluble[108]. Cumper found the surface rigidity decreased on addition of salt[113]. Peter and Bell found that calcium salts had no effect on the foaming properties of whey protein or egg-albumin. However they did find an increase in foam stability if the calcium ion was present in an alkaline medium. Tannic acid, saponin, sodium sulphite were all found to improve the foam stability[112].

The presence of lipoid substances was found to decrease the foam stability[115]. Leviton and Leighton postulated that this was due to the spreading of the lipoid at the interface. Several authors have found that the presence of yolk in egg whites foams caused foam instability[107,111,116].

CHAPTER 3

MATERIALS AND THEIR CHARACTERISATION

3.1 Materials

The water used for most of this research had been distilled once in an all Pyrex apparatus. For the electrophoretic, surface tension and contact angle measurements, fresh doubly distilled water was used.

Sodium chloride, B.D.H., was normally roasted at 700°C for twelve hours before use. This removed any organic impurities.

Other inorganic compounds used in the course of this research were magnesium sulphate, barium chloride and lanthanum nitrate. These were B.D.H. reagents. Sodium hydroxide, a B.D.H., concentrated volumetric standard ampoule was diluted with twice distilled water for the use in the conductometric titrations.

The cationic surfactant dodecyltrimethylammonium bromide, DTAB, was synthesised by P.G. Rogers from dodecyl bromide and trimethylamine. It was recrystallised from moist acetone. A pure sample of sodium dodecyl sulphate, SDS, was also obtained from P.G. Rogers.

3.1.1 Polystyrene Latices

The polystyrene latex, JC, was prepared by J.C. Files using a seeded emulsion polymerisation with persulphate initiation[117], using a 2 μm seed latex in the absence of surfactant. Particle size analysis of the electron micrographs of this sample showed that the number average diameter was 3.89 μm; the coefficient of variation on the diameter was 4.7%, figure 3/1.

Latex RB55 was supplied by Dr J.W. Goodwin. The particle size analysis gives the number average particle diameter as 1.02 μm.

The other latices used had been prepared by Dr Sunil Jayasuriya; the details appear in his Ph.D. thesis[118]. The particle diameters of the latices are summarised in Table I.

Figure 3/1 : Electron Micrograph of Latex JC

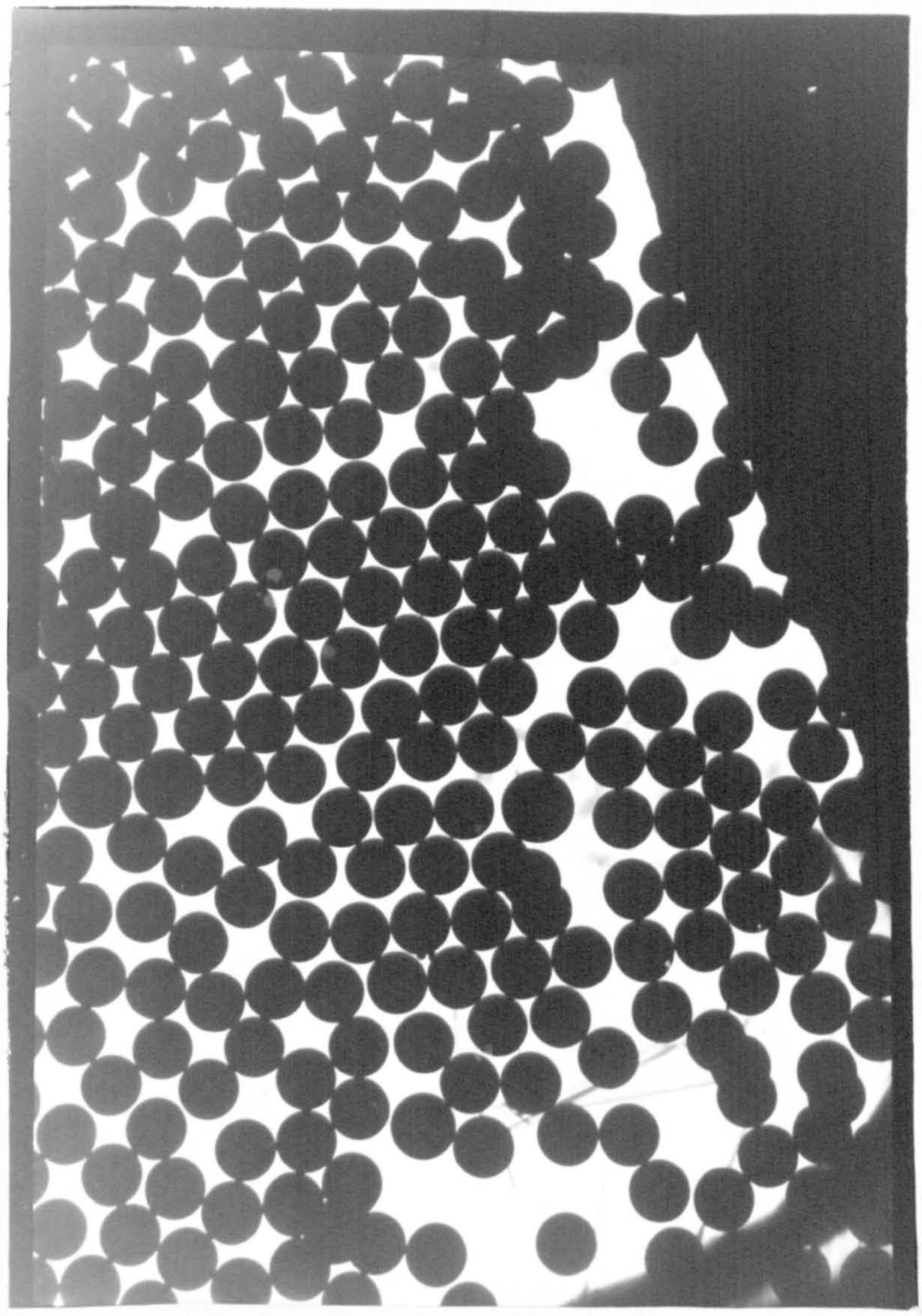

TABLE I

Latex	Number average radius / μm	Surface charge density / Cm^{-2}
RB55	0.57	0.039
S15	0.75	0.039 *
S17	0.78	0.061 *
S61	1.05	0.008 *
S65	1.09	0.072 *
S67	1.1	0.223
JC	1.94	0.059

* determined by Sunil Jayasuriya[118]

3.2 Characterisation of the Polystyrene Latices

Polystyrene latex particles prepared from persulphate initiation of the monomer, styrene, can be described as spherical balls of packed polymer chains which have sulphate end groups. Some of these end groups are situated at the surface of the latex while others are buried inside its core. It is the surface end groups which give the latex polymer its charge. This surface charge can be estimated by first converting the sulphate end groups to the acid form, either by dialysis or ion exchange resin, so that they can then be titrated with a base.

3.2.1 Method

The titration cell used was a flat-bottomed cylindrical cell surrounded by a thermostatted water jacket. The perspex lid had an opening for a Pye dip-type conductivity cell, type no. 7407. This consisted of two blacked platinum electrodes which were approximately 1 centimetre square and 0.5 centimetre apart. The platinum sheet was supported by a glass sheet to provide rigidity. Further openings in the lid provided for a nitrogen gas inlet and an outlet for an Agla micrometer syringe.

A nitrogen stream was used to flush out any carbon dioxide in the

Figure 3/2

Conductometric Titration of Sunil 67 against 0·05 M Sodium Hydroxide

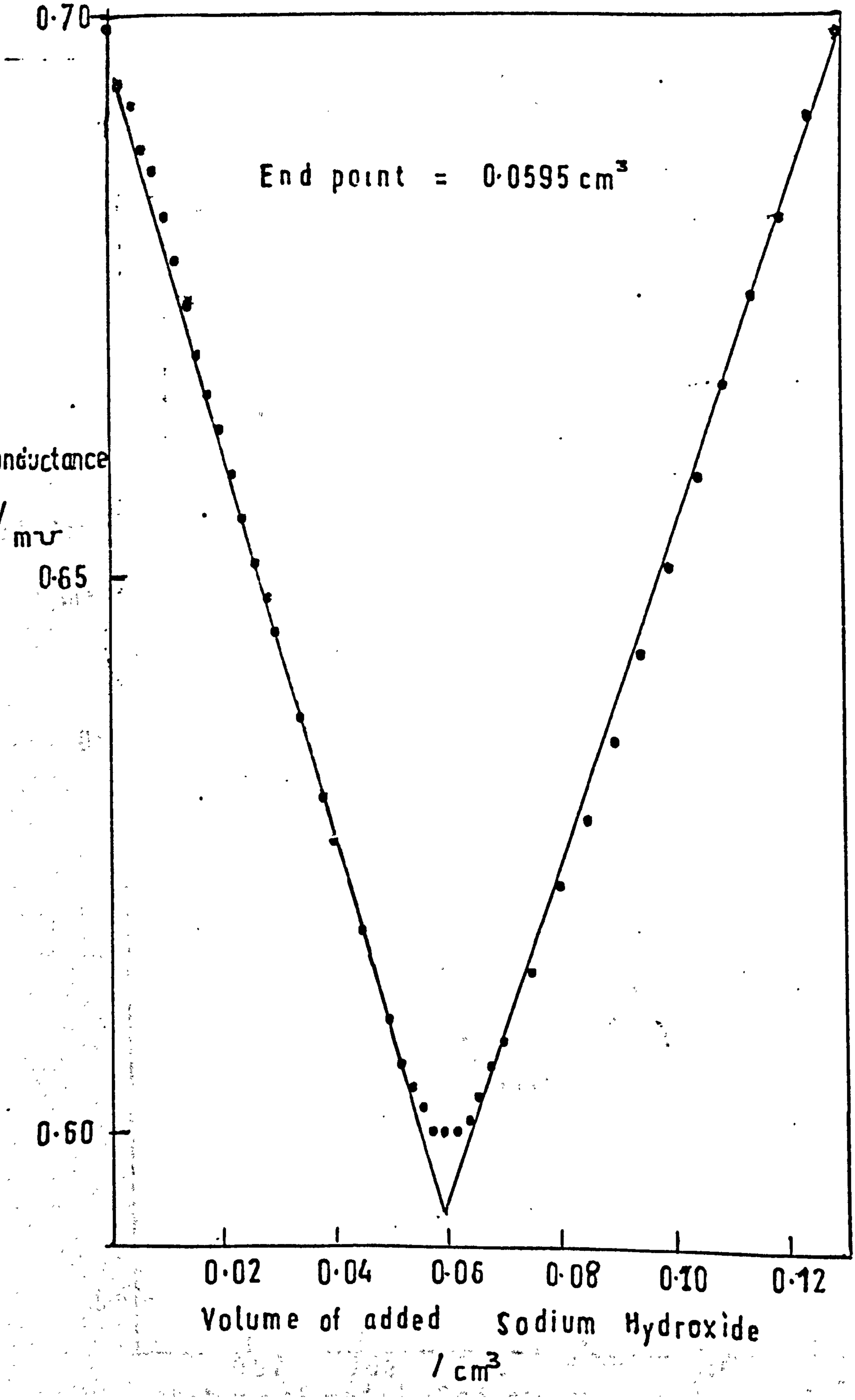

Figure 3/3

Conductometric Titration of RB 55 against 0·05 M Sodium Hydroxide

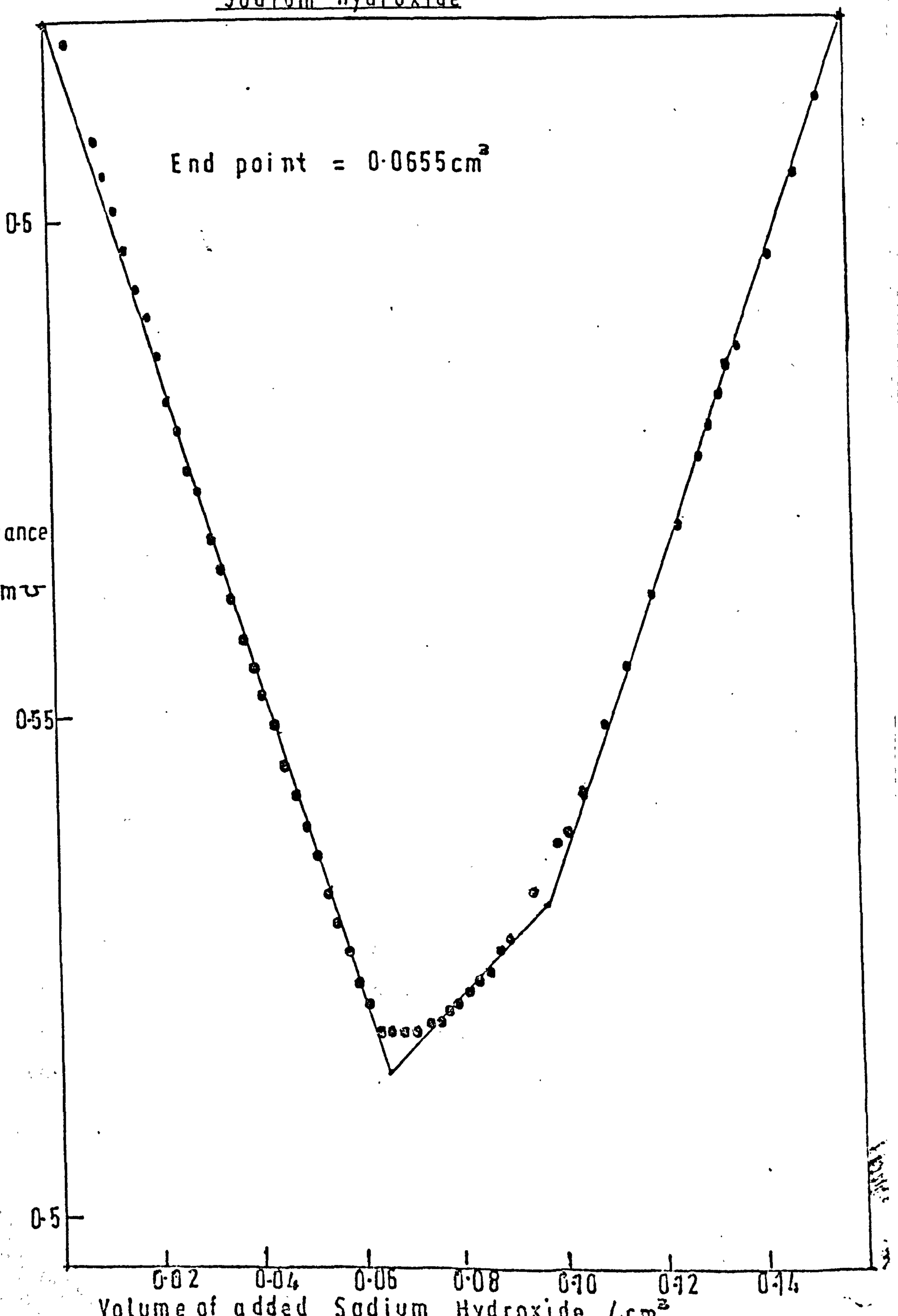

suspension before the titration. Before entering the titration cell the gas had already passed through 5 mol dm^{-3} sodium hydroxide, to remove carbon dioxide, 5 mol dm^{-3} sulphuric acid to remove any alkaline impurity, and finally through distilled water over ion exchange resin which removed any alkaline or acidic splashings.

The latex suspension, 20 cm^3, was pipetted into the cell. To this was added 5 cm^3 of 5×10^{-3} mol dm^{-3} sodium chloride; this was added to prevent any double layer shielding of the surface charge when approaching the end point. The suspension was then stirred with a magnetic follower. The titration was commenced after the nitrogen had bubbled through the mixture for two hours. This was continued throughout the titration.

The sodium hydroxide, 0.05 mol dm^{-3}, was added in 0.002 cm^3 steps using an Agla micrometer syringe. After each incremental addition of sodium hydroxide the suspension was stirred for two minutes. The conductance of the mixture was determined using a Wayne-Kerr Bridge, type B224, the stirrer being stopped for the actual measurements.

The weight of the latex suspended in the titration mixture was measured gravimetrically.

3.2.2 Results

Figure 3/2 shows the titration curve for latex S67. This shows typically strong acid behaviour, indicative of the original surface sulphate groups.

After a latex has been standing in dialysis tubing for any length of time there is the possibility of picking up carboxyl groups from the cellulose; Yates et al.[119]. This results in some weak acid behaviour masking the true acid end-point. This is the case for RB55, figure 3/3.

3.2.3 Calculation of Surface Charge Density

The volume fraction of latex in the titrated suspension was determined gravimetrically from the dried latex weight in a known volume of suspension. From this the total weight, m_L, of latex neutralised by sodium hydroxide was calculated. Given that the density of polystyrene latex is 1.057×10^3 kg/m^3 then the total surface area of the latex, A_L, can be found from

$$A_L = \frac{3 m_L}{1.057 \times 10^3 R}$$

where R = the radius of the latex particle.

The total charge, C_L, titrated against 0.05 mol dm^{-3} sodium hydroxide can also be determined

$$C_L = c M L e$$

where c = volume of sodium hydroxide added at end point

M = molarity of sodium hydroxide = 0.05 mol dm^{-3}

L = Avogadro's Number = 6.023×10^{23} mol^{-1}

Then the surface charge density is the total charge of the system divided by the total surface area of the latex particles; the surface area was available from the electron microscope size determination.

The surface charge densities of the latices are given in Table I.

Latex S67 appears to have an extremely high surface charge density that is 0.22 C m^{-2} which consequently converts to give the area occupied per charge to be 0.72 nm^2. Previous recorded values for the sulphate group on the surface of a polystyrene particle usually lie in the range 2-4 nm^2 [152]. This area per charge is of the same order as adsorbed surfactant groups on the latex surface, for DTAB the area per charge was found to be 0.56 nm^2 [150].

CHAPTER 4

STUDIES ON LATEX FOAMS

4.1 Foam Tests

Several different parameters have been described in the literature, as a means of defining foam stability. These have been extensively reviewed in chapter 2, section 2.3.1. In the current research, the regions in which foams were formed were determined, by measuring the rate of collapse of air cells in the foam; the latter were generated by shaking the latex. The foam lifetime was defined as the time from the last shake of the latex up to the time when three or fewer bubbles remained visible on the surface.

In parallel with these measurements, observations were also made on the properties of the bulk phase. In fact, it was determined whether the latex particles in the bulk phase remained dispersed as single particles or coagulated under the conditions that the foams were formed.

These measurements enabled the salt concentrations at which the onset of foam formation was observed, for various systems, to be compared with those at which coagulation occurred.

4.1.1 Experimental

The foam test was carried out by shaking 5 cm^3 of the concentrated latex with 5 cm^3 of the salt or surfactant solution under test. These dispersions were mechanically shaken, thirty times, in stoppered measuring cylinders (25 cm^3) at room temperature, namely $20^\circ \pm 3^\circ C$.

Immediately after the 5 cm^3 of the salt solution had been pipetted into the latex, the cylinder was stoppered and shaken. The number of shakes chosen, that is thirty, was arbitrary but was found to give good mixing and reasonably reproducible results.

Observations, such as the quality of foam and its lifetime, were recorded for a series of latices covering the particle diameter range, 1 μm

to 4 μm. The sodium chloride used covered the electrolyte concentration range, in the latex, from 0.05 to 0.5 mol dm^{-3}.

Additional foam tests were performed for latices in 2:2, 2:1 and 3:1 electrolytes as well as in the presence of the surfactants, DTAB and SDS. The effect of pH on the foaming properties of a polystyrene latex was also investigated.

4.2 Results

4.2.1 Dilute Latex Systems

For the latex JC several foam tests were carried out on diluted latex systems covering the concentration range from 0.01 to 6% w/v. It was very difficult to interpret the results since for these dilute latex systems it was impossible to distinguish between the different foam types.

Generally as the latex was diluted the ability of the latex to foam decreased. When the latex was diluted 500 x from the original 6% dispersion, no foam was observed even at the strongest sodium chloride concentration 0.45 mol dm^{-3}.

The rate of bulk coagulation depends on the number of particles in the dispersions. Therefore for the diluted suspensions no observable coagulation occurred within the time of the experiment, since the number concentration of the particles was only of the order of 10^7 per cm^3.

It appeared that the ability of the latex to foam also depended on the number of particles in the system. At too dilute a latex concentration there were insufficient particles to cover the air cells formed on shaking, so the bubbles formed were unstable and quickly burst. The best latex foams were formed at a high latex concentration, 6% w/v, and high salt concentration 0.1 to 0.4 mol dm^{-3}.

Therefore for the rest of foam tests concentrated latex systems were used as clear distinctions of the different foam types could then be made.

4.2.2 Terminology for categorising Foams

The terminology used to describe the state of the foam was related directly to the collapse time as defined in the following way.

No foam	the bubbles, if formed, collapsed within two seconds of the final shake
Slight foam	the bubbles formed collapsed within three minutes
Good foam	a definite volume of foam was observed and this was stable for five minutes
Very good foam	the foam was stable overnight and had a high ratio of foam volume to dispersion volume remaining after eighteen hours

The photographs shown in figure 4/1 illustrate examples of these foams for latex JC in the presence of sodium chloride solutions. All the photographs in this chapter were taken 24 hours after the latex suspension was shaken.

Although the above terms are subjective, it was found after a large number of experiments that the experimenter could achieve a fairly clear and consistent appreciation of the foam type.

4.2.3 Foam Tests with Sodium Chloride

The foams formed were solid foams where the latex particles covered the air cell with a 'solid' closely-packed layer. The foam had a 'dry' solid appearance. After the foam had collapsed the polystyrene particle film remained at the air/liquid interface. The bubble size was a random quantity; wide ranges of bubble sizes, micro, ca. 1 μm, to macro, ca. 2 cm diameter were found to occur in the same foam system.

Figures 4/2 - 4/8 show the regions of electrolyte concentration in which foams were formed for different latices studied. The volume concentrations of the latices used in the experiments are listed in Table I.

It is interesting to compare the bulk latex instability with the foam type produced. The large, 3.89 μm, latex JC produced a very good foam before coagulation had occurred, while the latices S61 and S67, with diameters of 2.10 and 2.20 μm respectively, formed a very good foam even

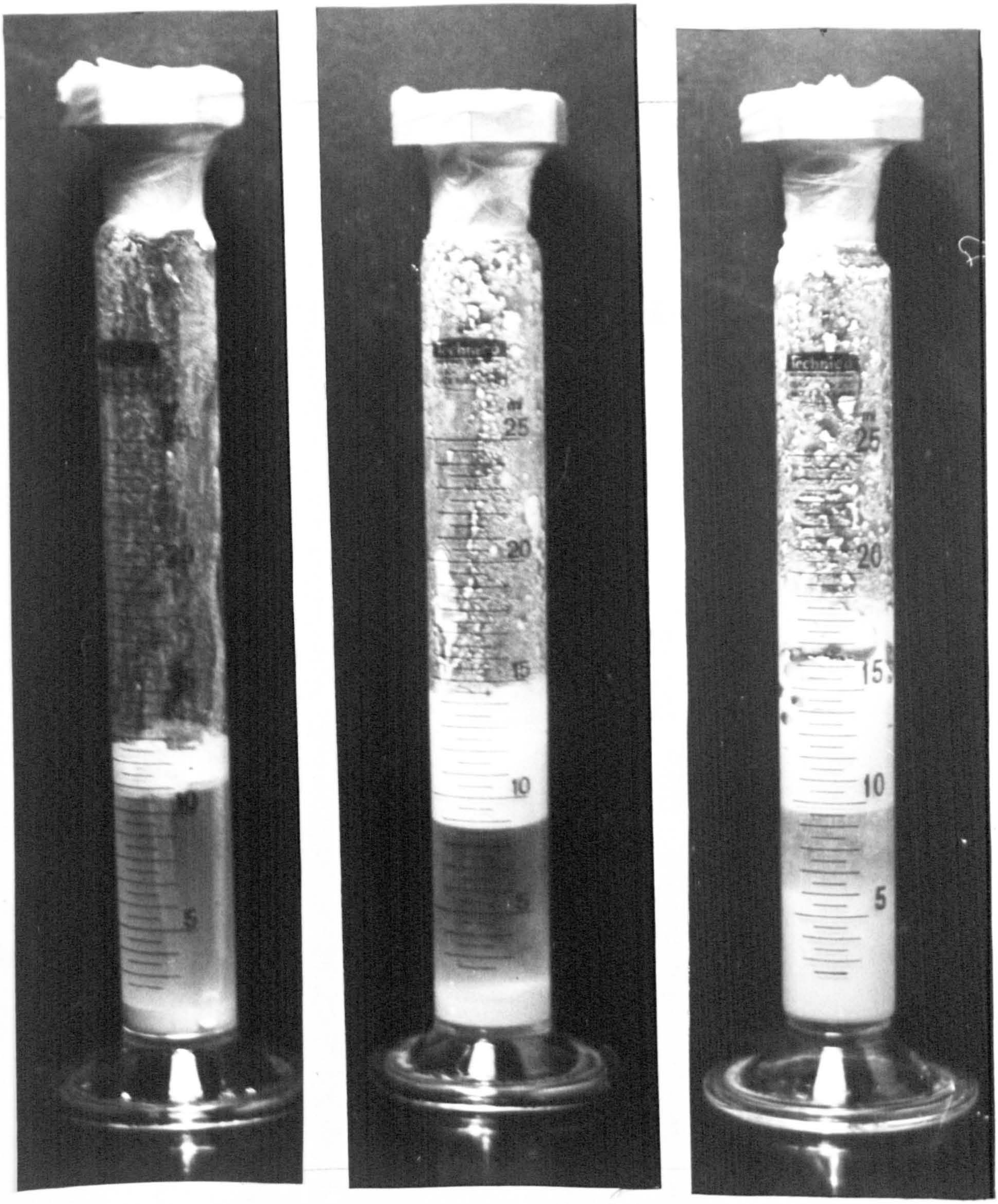

0.05 mol dm^{-3}
Slight foam

0.2 mol dm^{-3}
Good foam

0.3 mol dm^{-3}
Very good foam

Figure 4/1 : Latex JC in Sodium Chloride Solutions

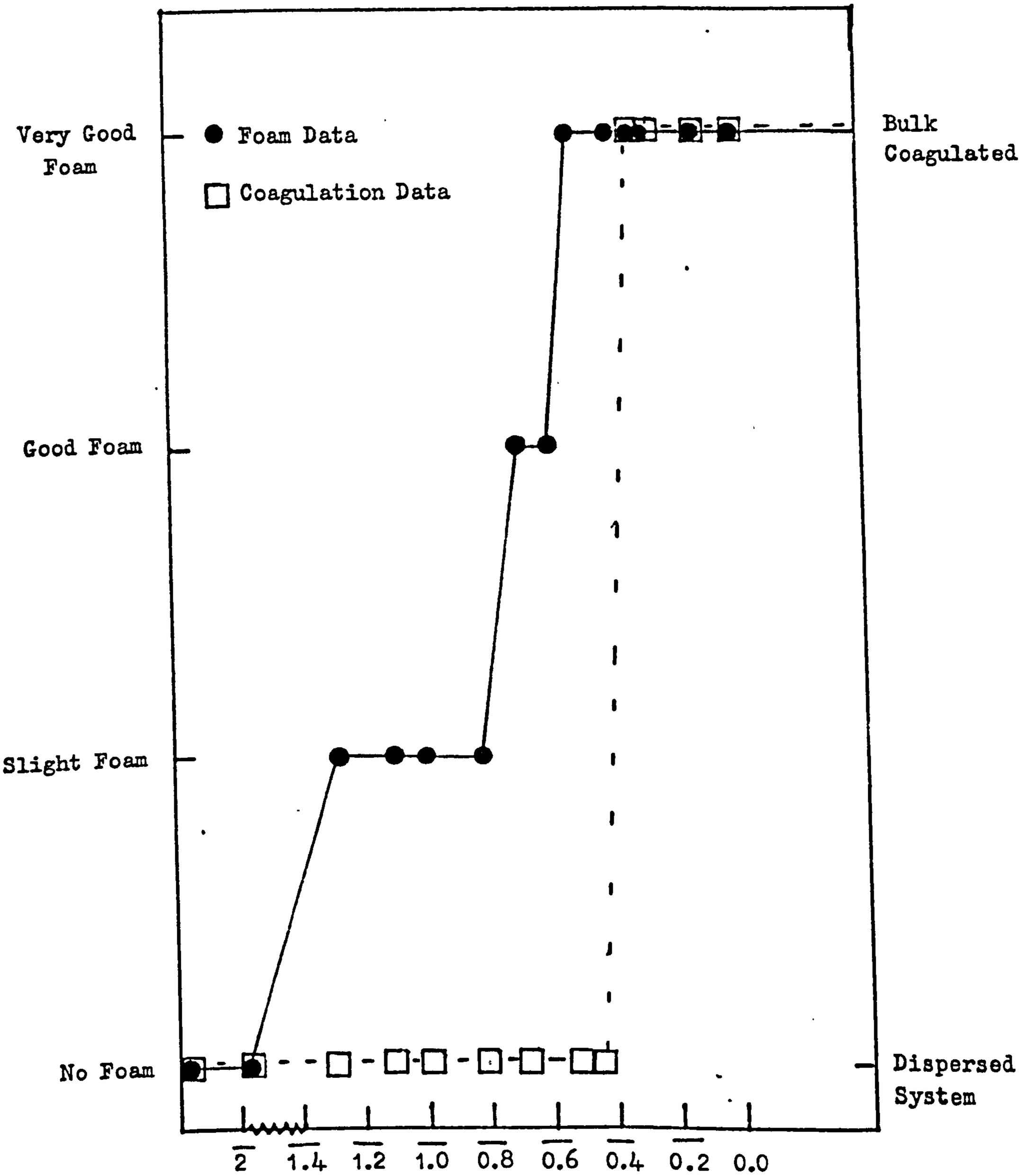

Figure 4/2 : Foam Data for Latex JC, diameter 3.89 μm, surface charge density 0.059 C m^{-2}, latex concentration 6.7% .

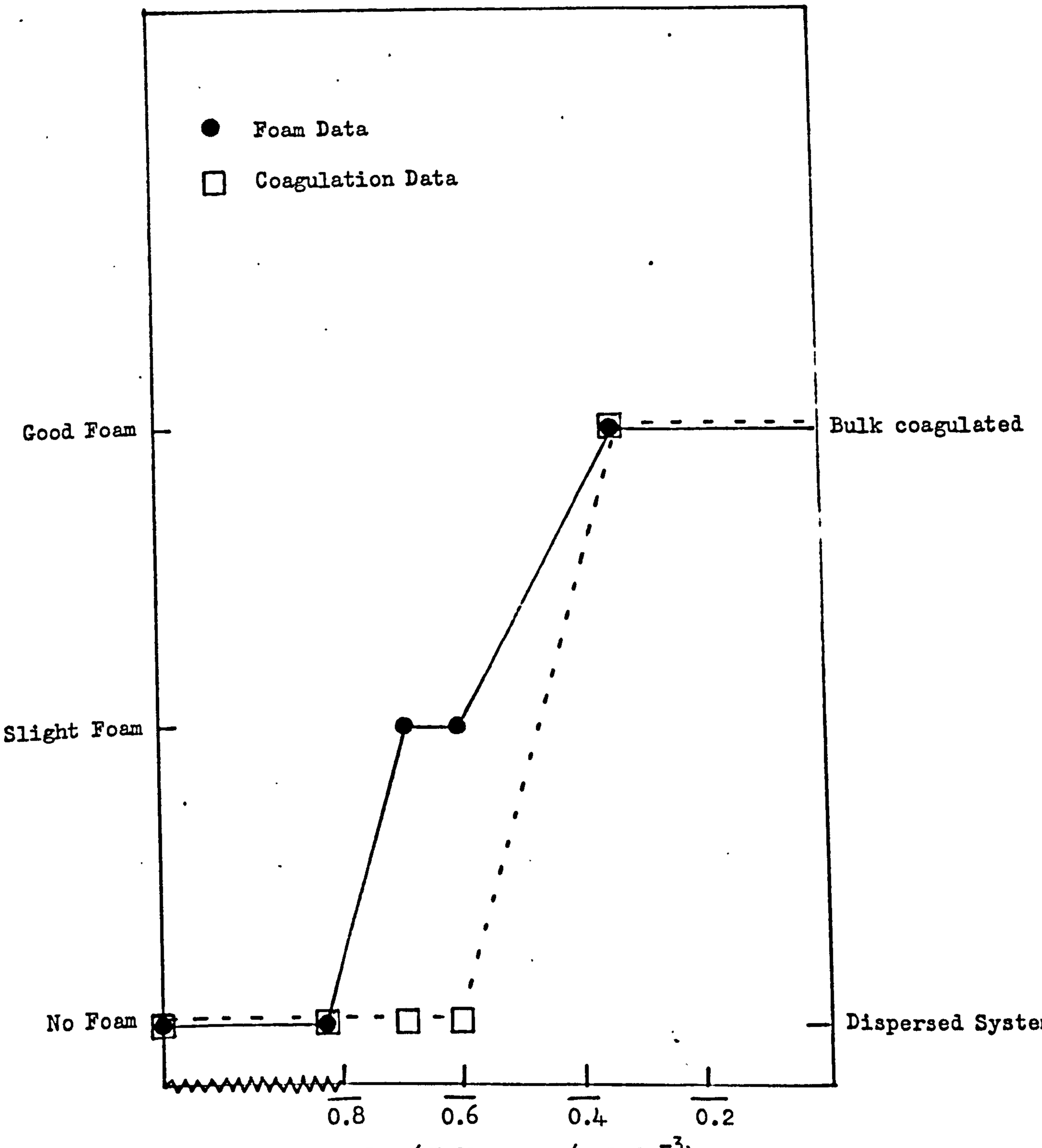

Figure 4/3 : Foam Data for Latex S67, diameter 2.2 μm, surface charge density 0.223 C m^{-2}, latex concentration 6.0%.

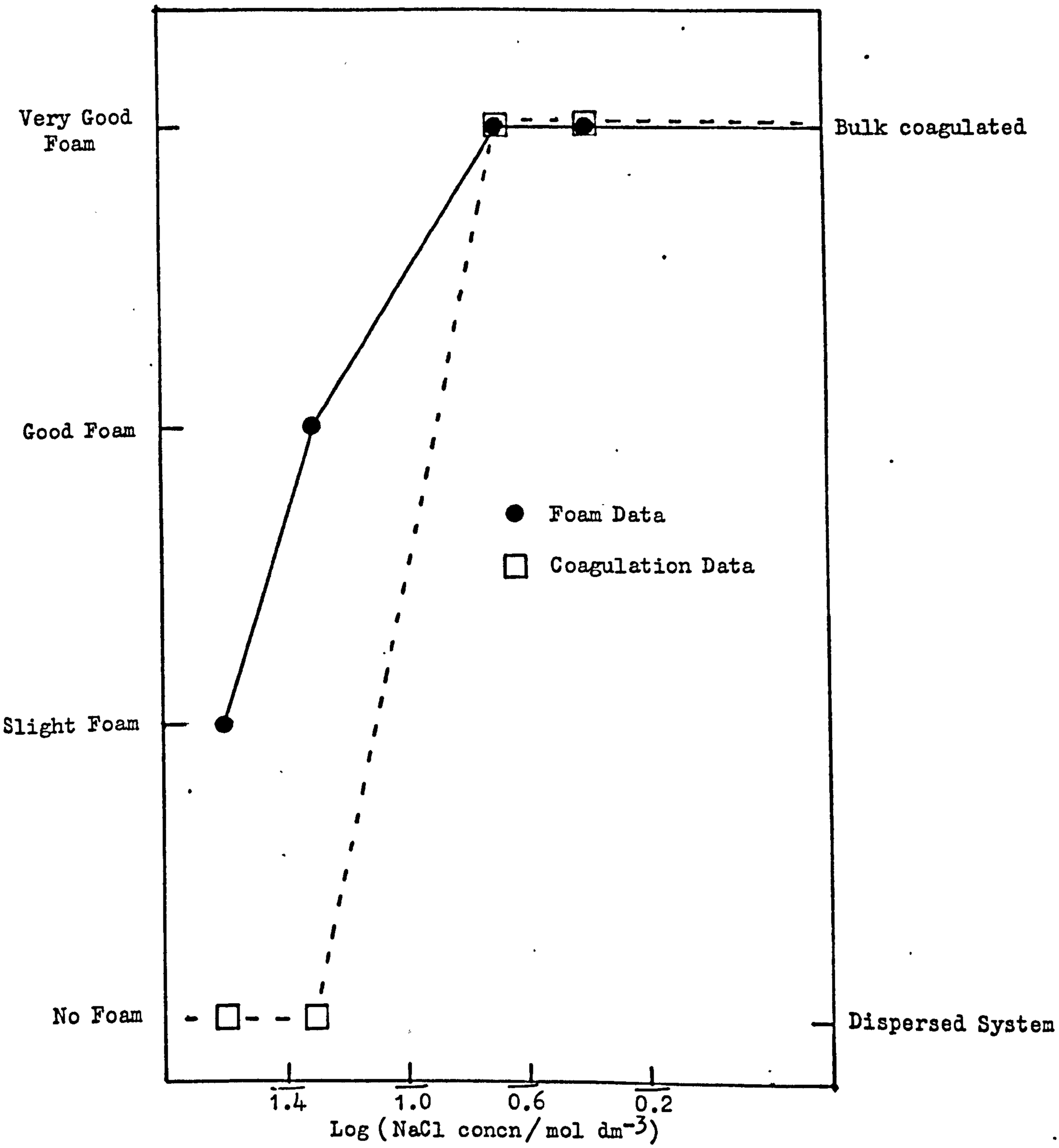

Figure 4/4 : Foam Data for Latex S61, diameter 2.1 μm, surface charge density 0.008 C m^{-2}, latex concentration 1.8%.

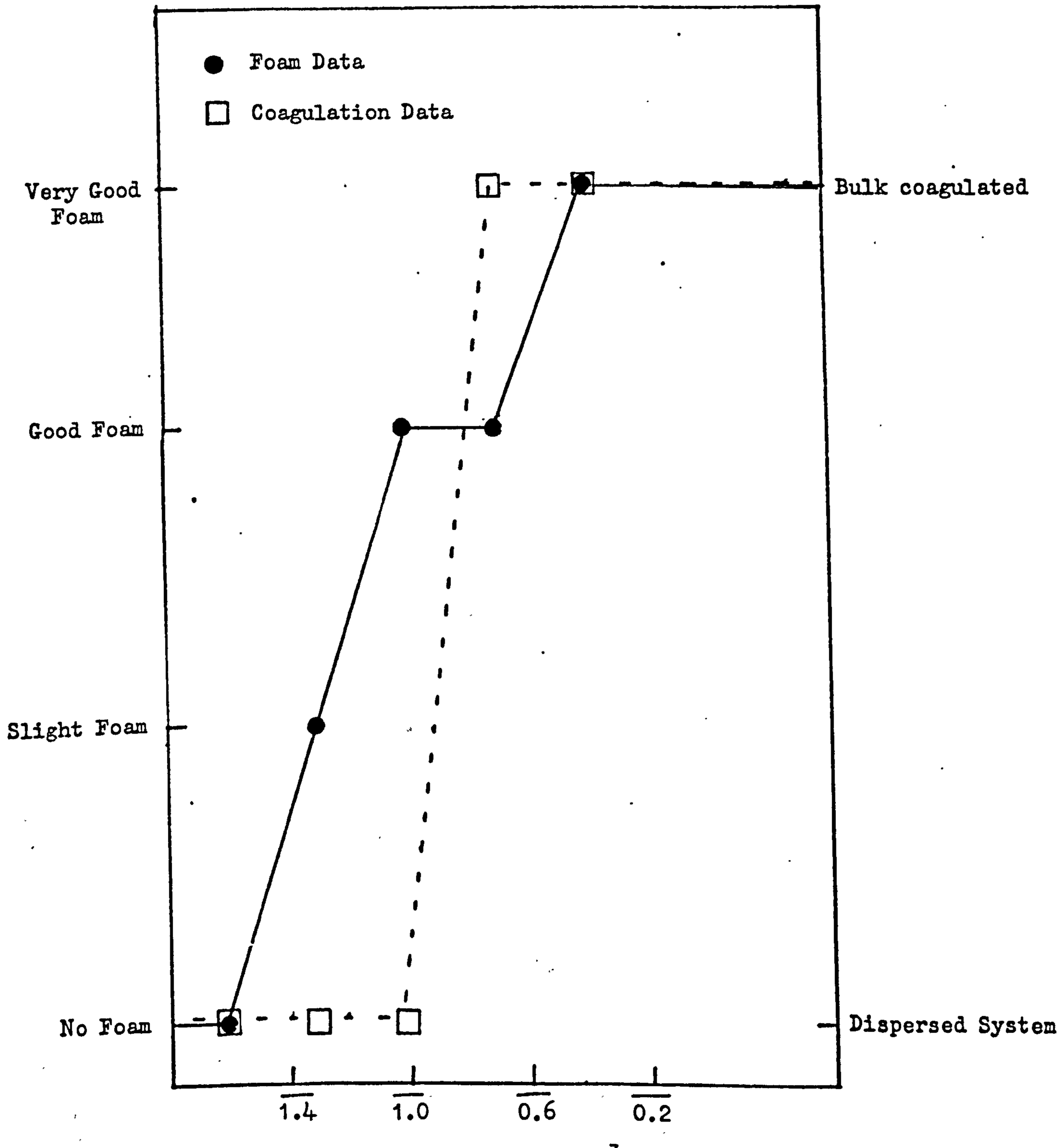

Figure 4/5 : Foam Data for Latex S65, diameter 2.18 μm, surface charge density 0.072 C m^{-2}, latex concentration 0.9 %.

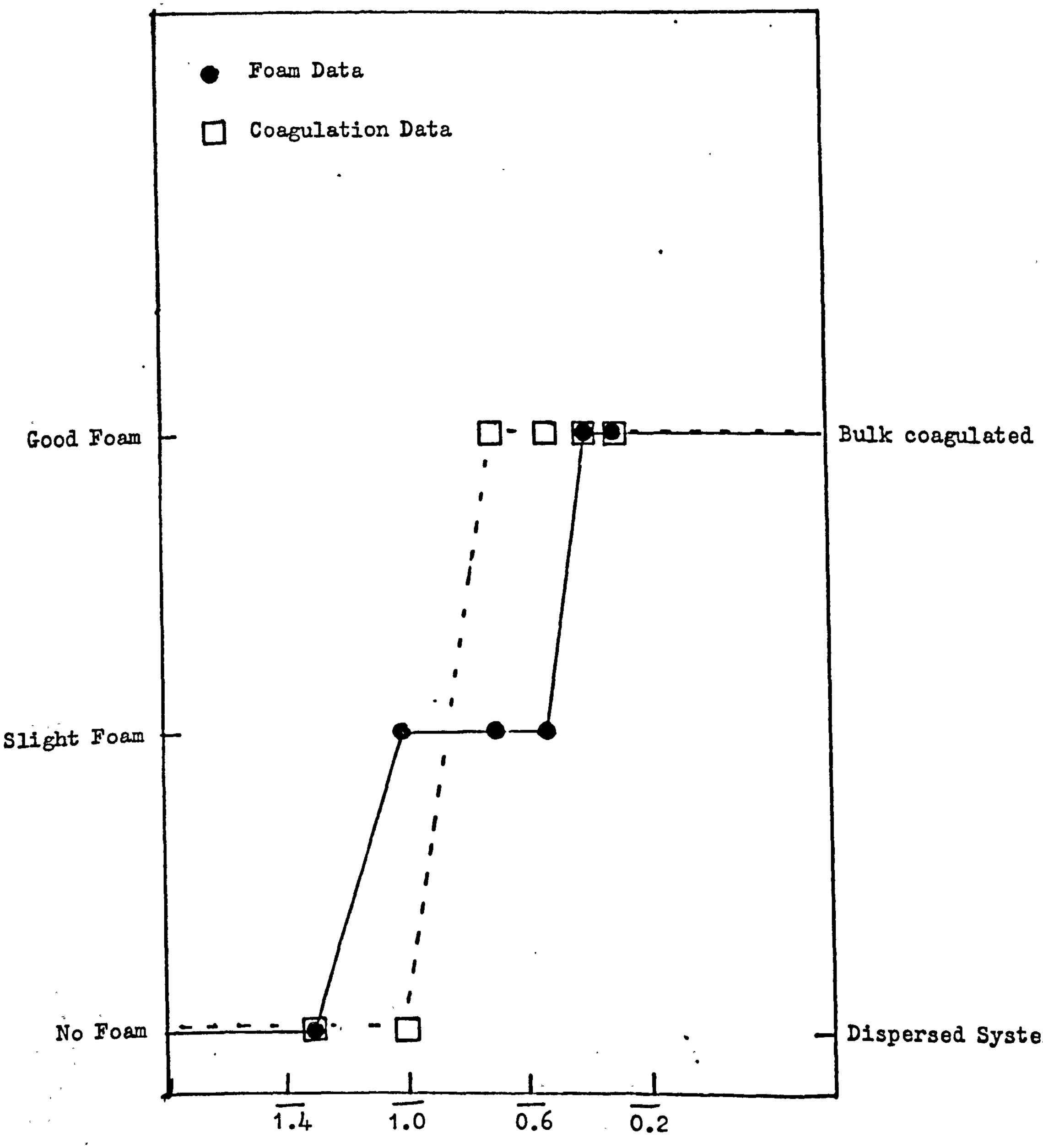

Figure 4/6 : Foam Data for Latex S17, diameter 1.56 μm, surface charge density 0.061 C m^{-2}, latex concentration 0.3%.

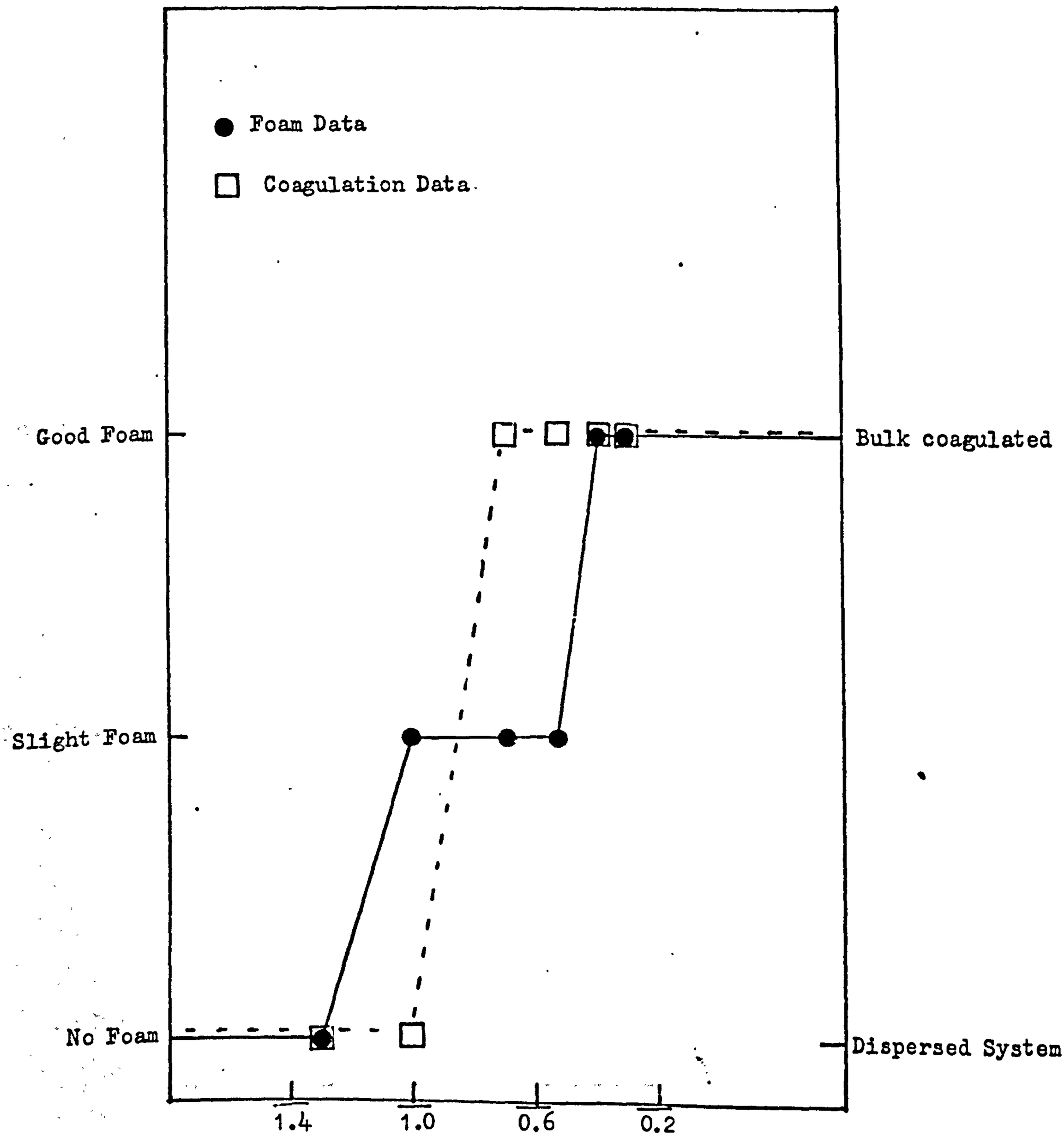

Figure 4/7: Foam Data for Latex S15, diameter 1.5 μm, surface charge density 0.039 C m^{-2}, latex concentration 0.2%.

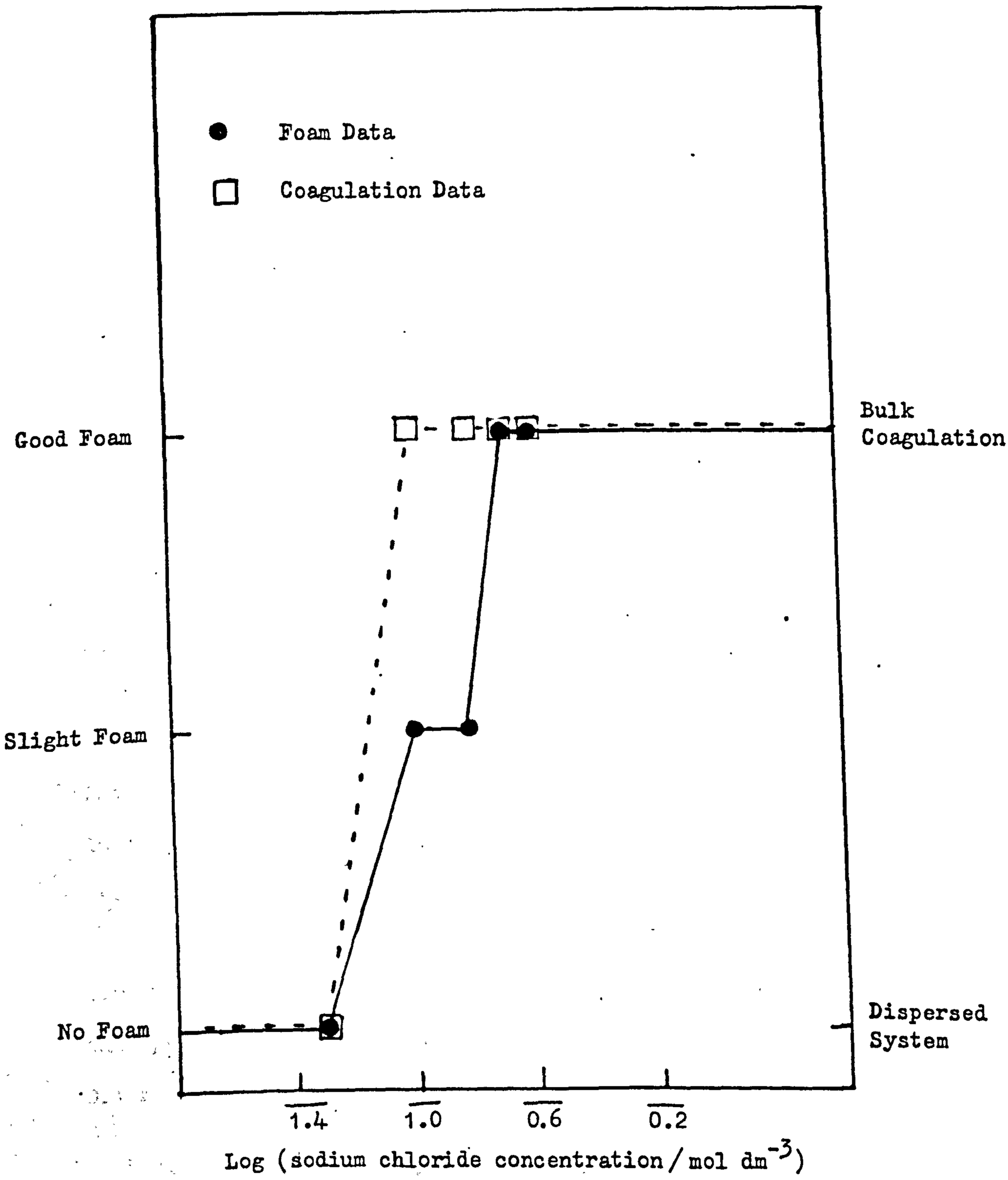

Figure 4/8: Foam data for Latex RB55, diameter 1.02 μm, surface charge density 0.039 (m^{-2}), latex concentration 0.2%.

after coagulation had occurred in the bulk phase.

TABLE I

Latex	Diameter/μm	Latex concn.% g/100 cm^3	Very good foam before coagn.	Very good foam on coagn.	Very good foam after coagn.
JC	3.89	6.70	✓		
S61	2.10	1.83		✓	
S67	2.20	6.00		✓	
S65	2.20	0.93			✓
S17	1.56	0.27			✓
S15	1.50	0.17			✓
RB55	1.02	0.20	Does not form a very good foam		

Latices S17 and S15, diameters 1.56 and 1.50 μm respectively, exhibited very similar foaming behaviour. Both formed a good foam after bulk coagulation had occurred, see Table I.

The smallest latex studied, RB55, diameter 1.02 μm, did not form a foam at all, even to a slight extent, until after coagulation had occurred in the bulk phase. Sutherland and Wark have previously reported the reluctance of particles having diameters of 1 μm to foam[120].

It can be concluded therefore that the foaming properties of polystyrene latices are particle size dependent, and moreover that a foam was only produced when the sodium chloride concentration was higher than 0.1 mol dm^{-3}.

4.2.4 Foam Tests on Latex JC with other Electrolytes

The electrolytes studied were magnesium sulphate, barium chloride and lanthanum nitrate. The foaming behaviour of latex JC, diameter 3.89 μm, in the presence of the various salts is summarised in figures 4/9 - 4/14. The volume concentration of the latex was 7% w/v in all cases.

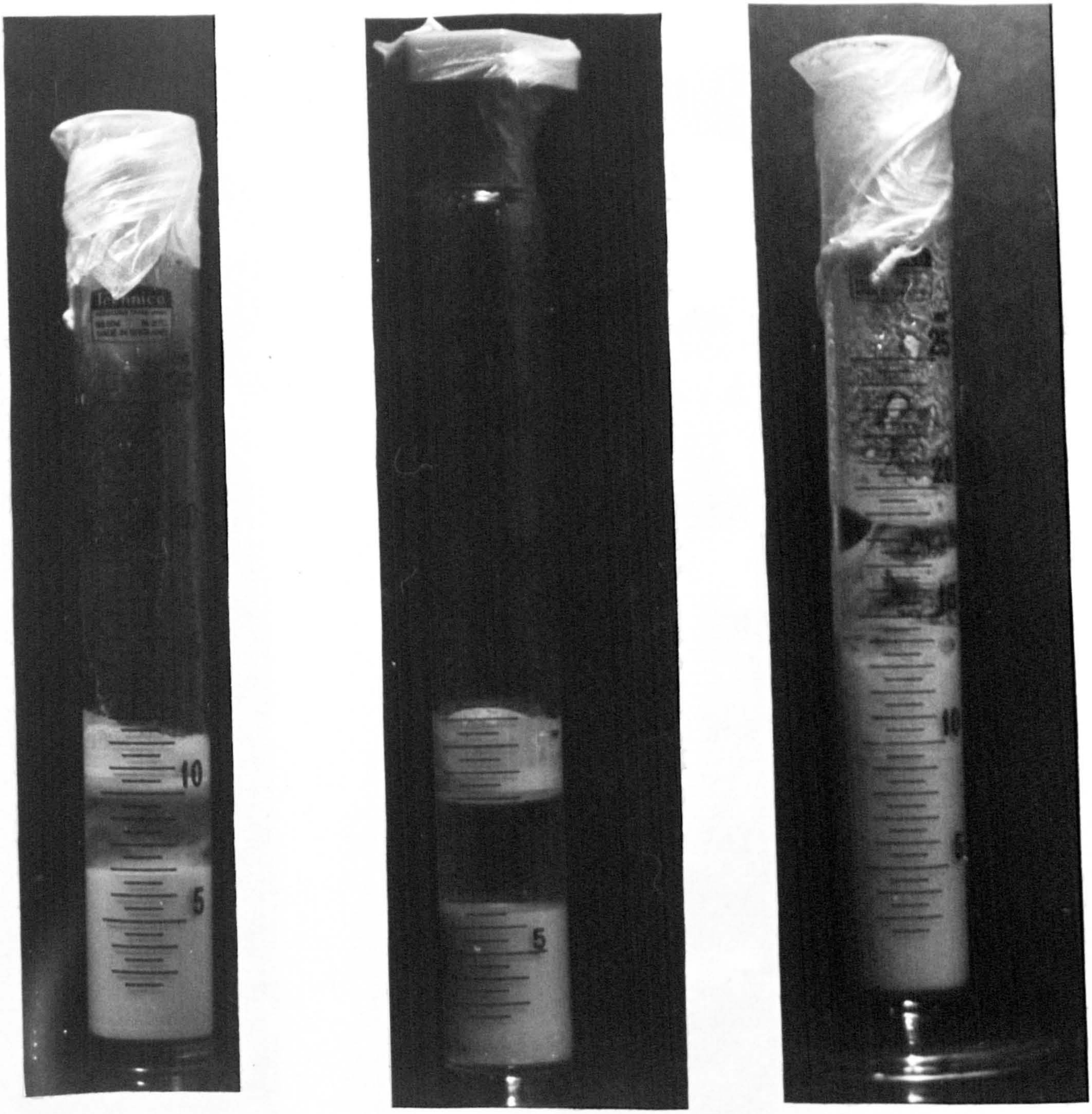

3×10^{-4} mol dm^{-3} Slight foam

1.5×10^{-3} mol dm^{-3} Good foam

5×10^{-2} mol dm^{-3} Very good foam

Figure 4/9: Latex JC in Magnesium Sulphate Solutions

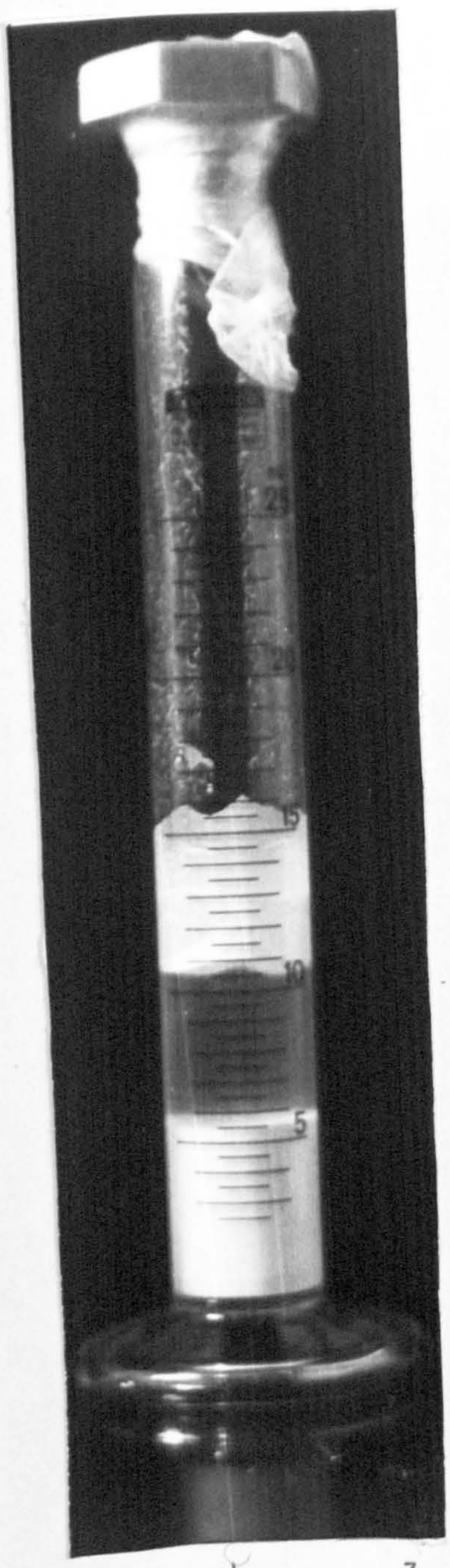

5×10^{-4} mol dm^{-3}

Good foam

0.05 mol dm^{-3}

Very good foam

Figure 4/10 : Latex JC in Barium Chloride Solutions

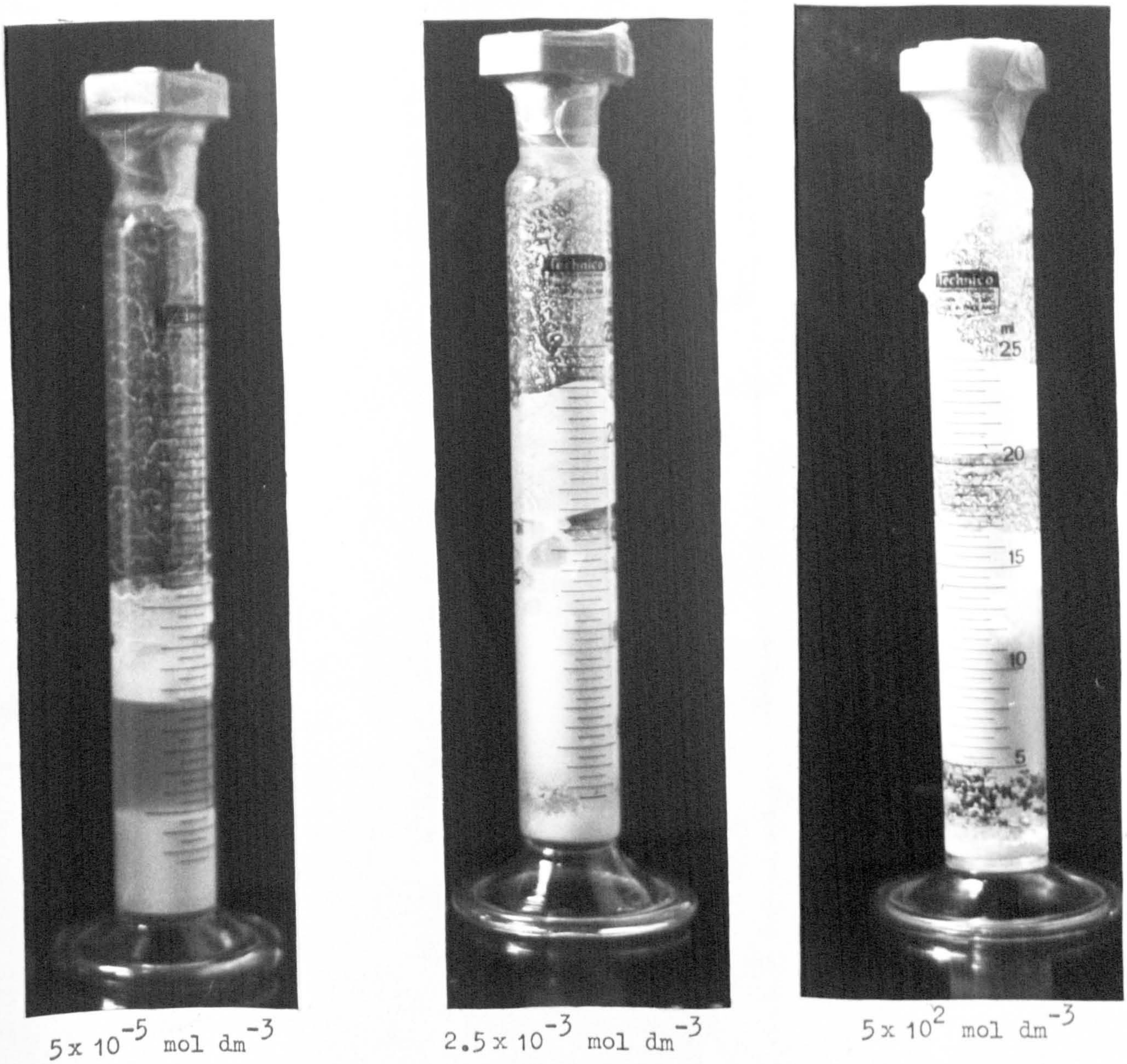

5×10^{-5} mol dm^{-3} — Slight foam

2.5×10^{-3} mol dm^{-3} — Good foam

5×10^{2} mol dm^{-3} — Very good foam

Figure 4/11 : Latex JC in Lanthanium Nitrate Solutions

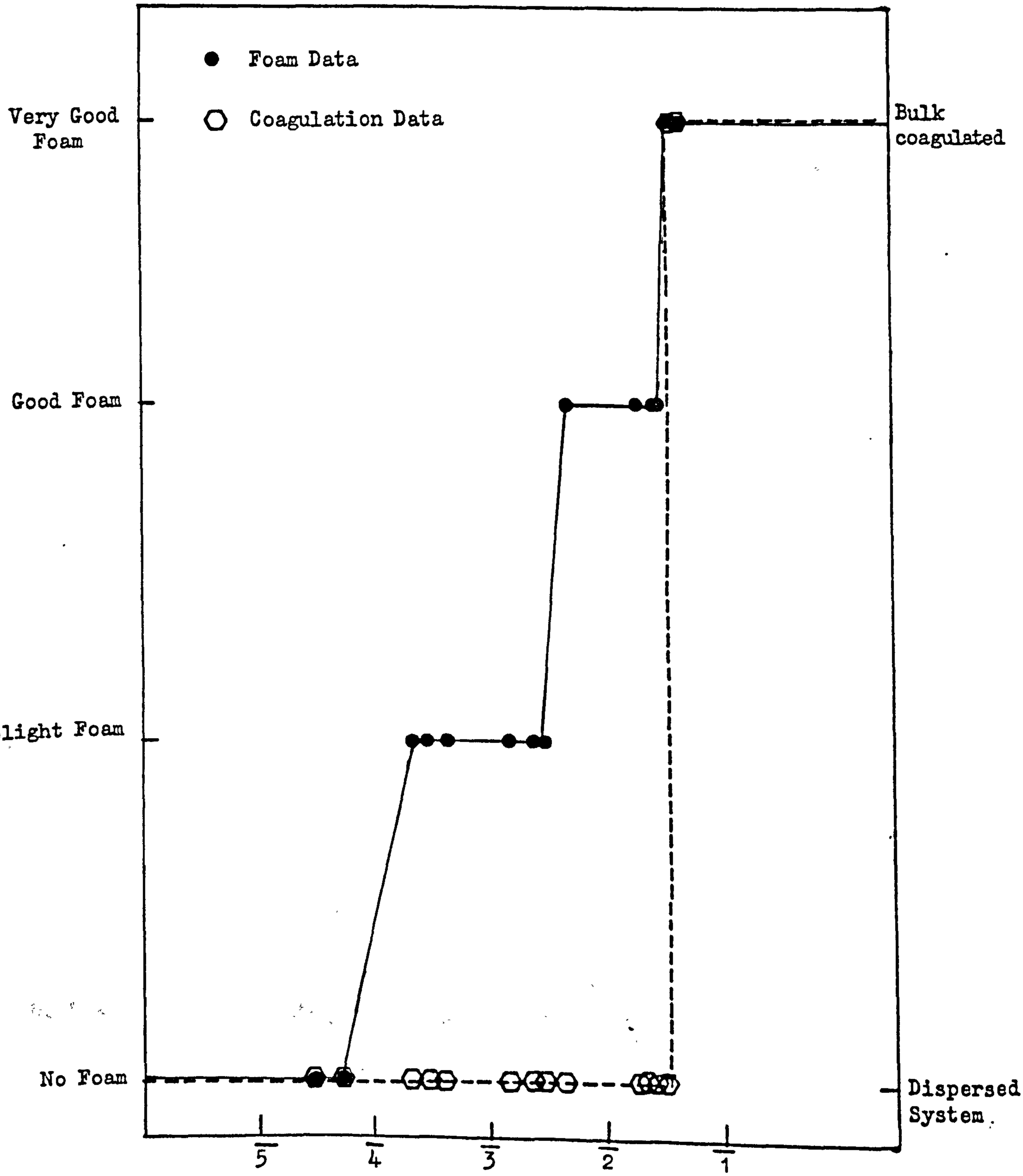

Figure 4/12 : Foam Data for Latex JC, diameter 3.89 μm, surface charge density 0.059 C m^{-2}, latex concentration 7%.

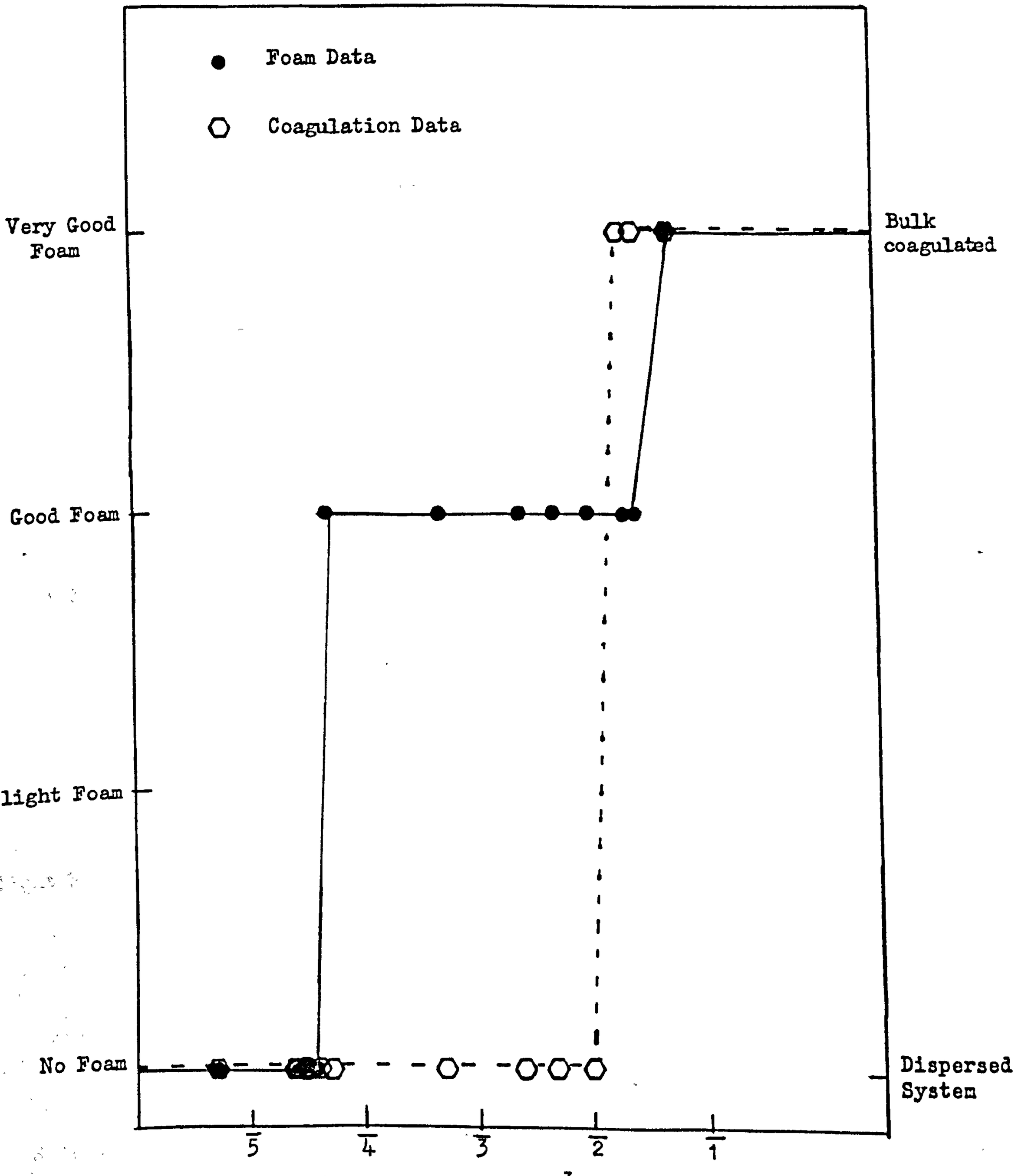

Figure 4/13 : Foam Data for Latex JC, diameter 3.89 μm, surface charge density 0.059 C m^{-2}, latex concentration 7%.

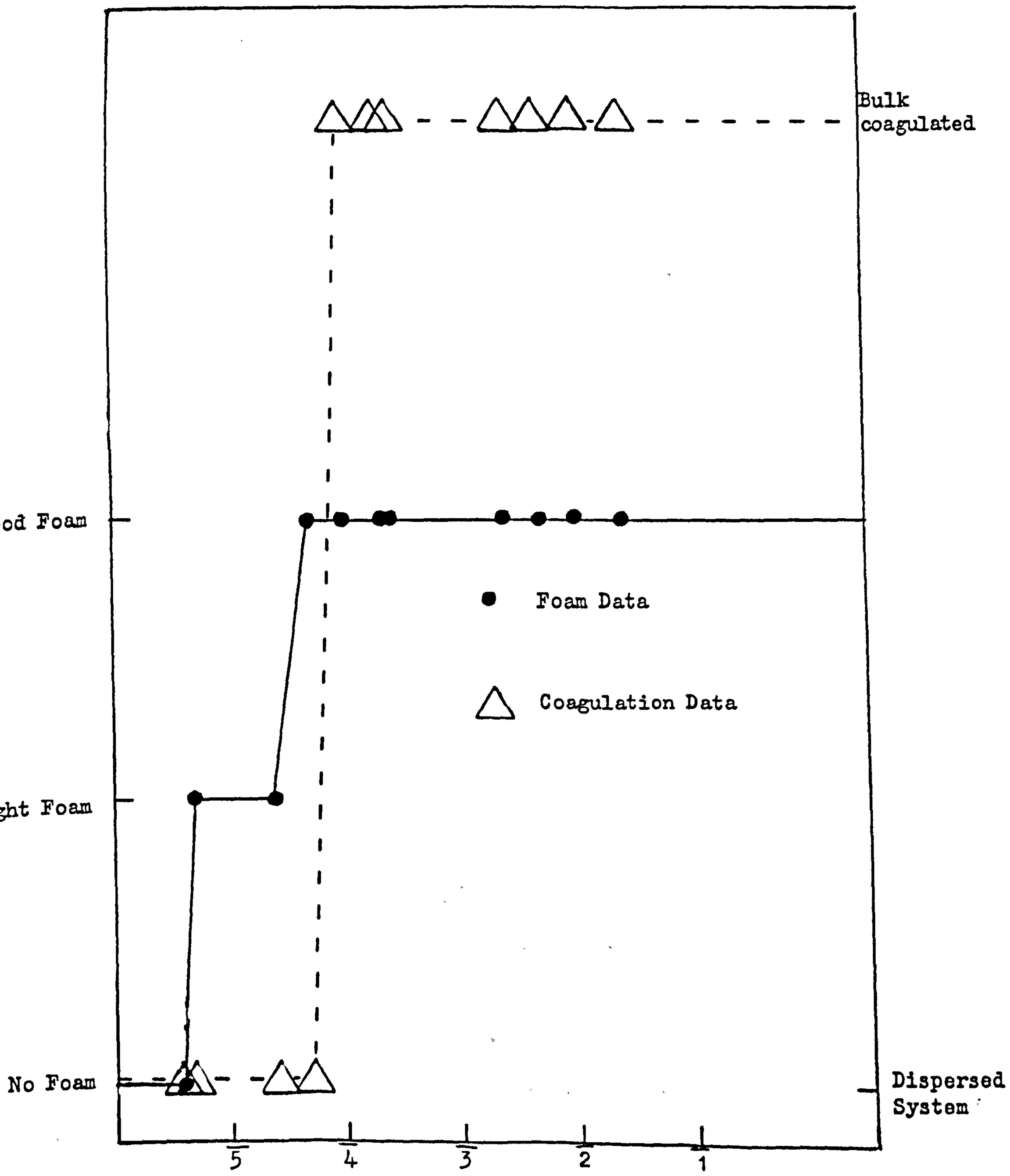

Figure 4/14: Foam Data for Latex JC, diameter 3.89 μm, surface charge density 0.059 C m^{-2}, latex concentration 7%.

TABLE II

Latex	Electrolyte	Stable foam before coagn.	Stable foam on coagn.	Stable foam after coagn.
JC	$BaCl_2$			✓
JC	$MgSO_4$		✓	
JC	$La(NO_3)_3$	✓		
JC	pH		✓	

As with sodium chloride, latex JC formed a stable foam with barium chloride before bulk coagulation had taken place. However a very good foam was formed after bulk coagulation, Table II. With lanthanum nitrate only a slight foam was formed before bulk coagulation, whereas with magnesium sulphate a good foam was formed before bulk instability occurred. As in the case of barium chloride, magnesium sulphate produced a very good foam which was produced on the point of bulk coagulation.

It would appear that with the higher valency electrolytes, for example, 2:1 and 3:1, the foam formed was not as good as that formed with a 1:1 electrolyte, for example sodium chloride, as judged by both foam volume and collapse time.

4.2.5 Effect of pH on Foaming Properties of Latex JC

Figure 4/16 summarises the foaming properties of latex JC with change in pH.

The pH was changed by adding drops of concentrated nitric acid followed immediately by shaking the suspension thirty times. The pH of the resulting suspension was determined on a calibrated Pye Unicam digital pH meter PW 9409. The pH of the latex in water was found to be 9.4.

A good foam was formed at pH 3.2 and a very good foam at pH 0.7 where bulk coagulation had taken place.

It can be seen that in a strongly acidic environment polystyrene

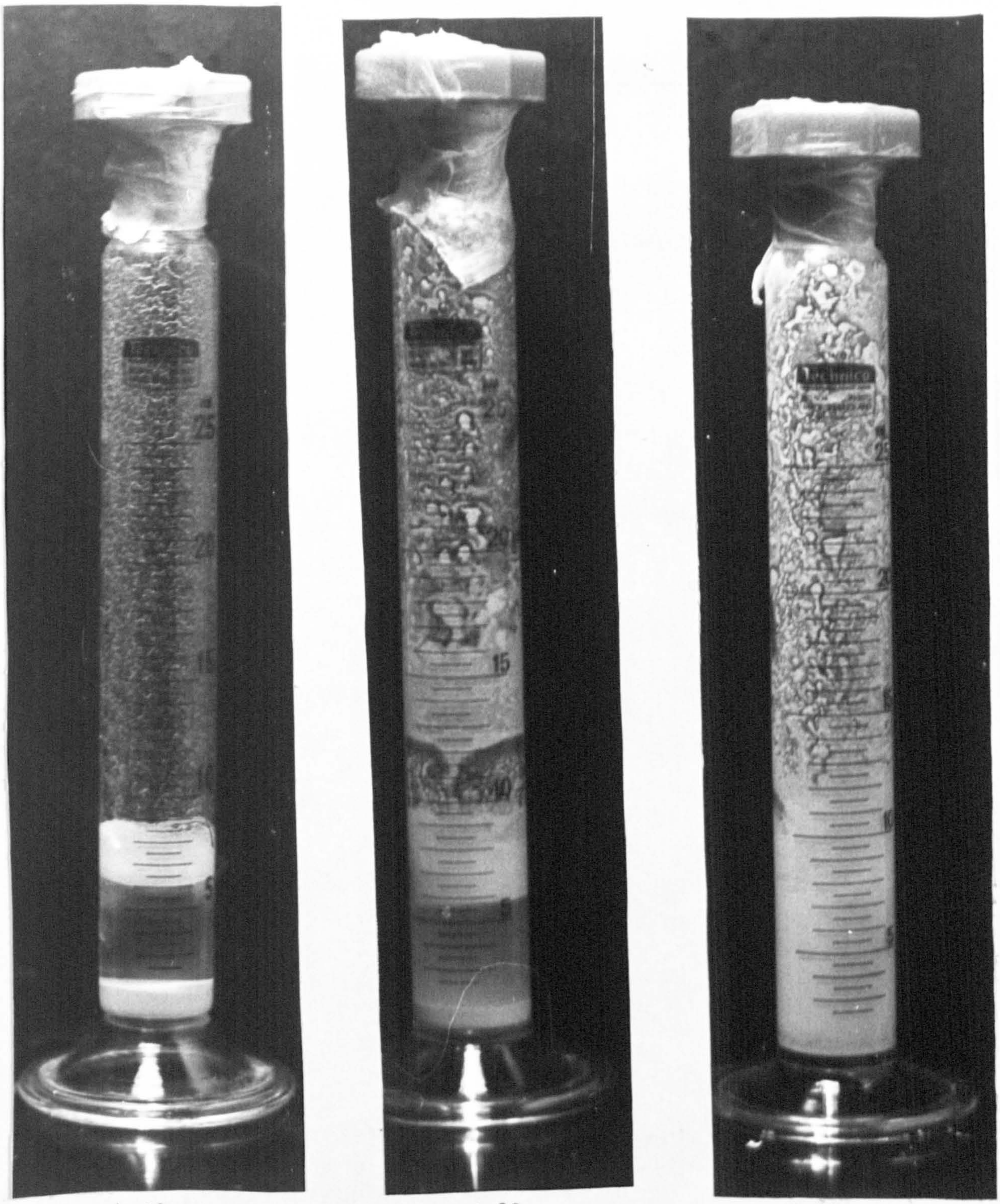

4.10	1.29	0.70
Slight foam	Good foam	Very good foam

Figure 4/15 : Latex JC at different pH

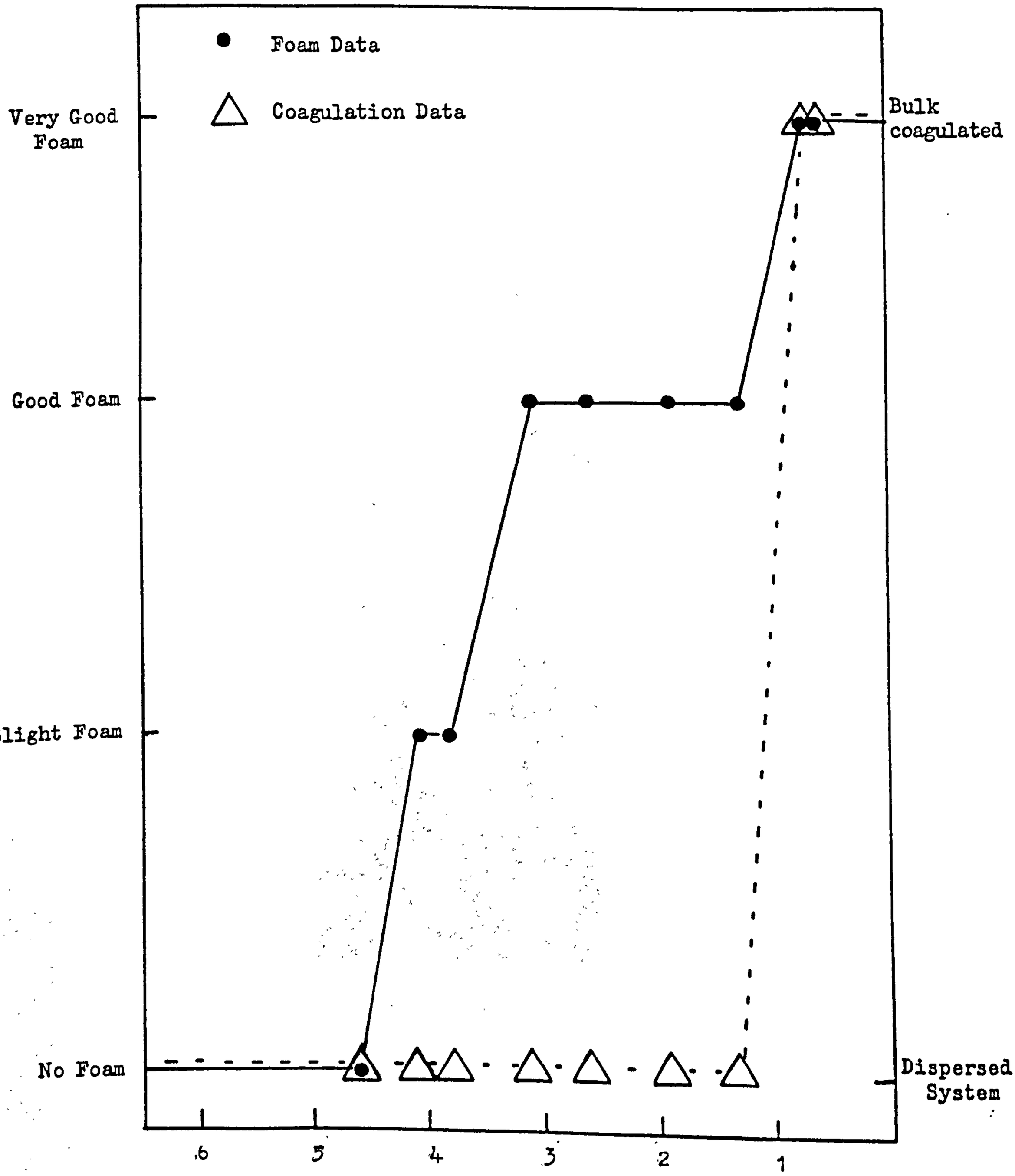

Figure 4/16 : Foam Data for Latex JC, diameter 3.89 μm, surface charge density 0.059 C m^{-2}, latex concentration 7 %.

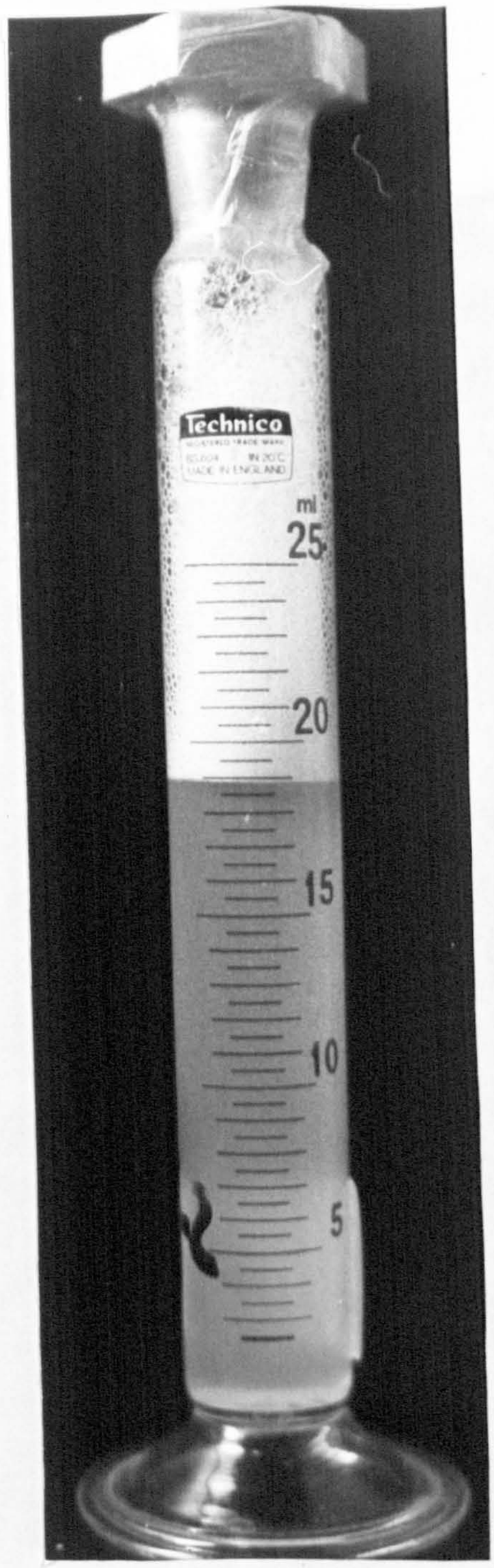

Latex JC diluted to 0.06% in 1.8×10^{-3} mol dm^{-3}
SDS Surfactant Foam

Figure 4/17: Latex JC with Sodium Dodecyl Sulphate

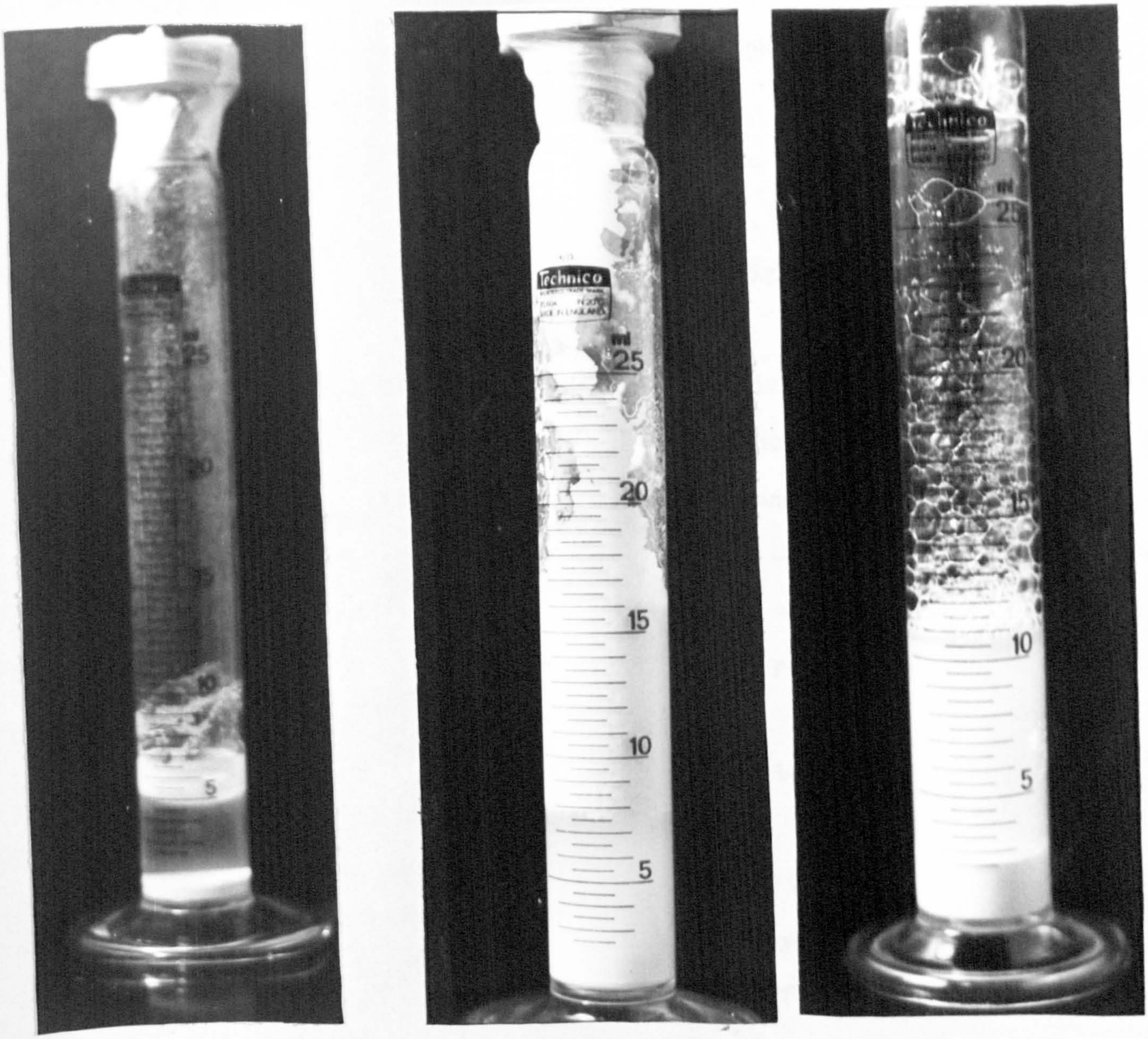

1.5×10^{-5} mol dm^{-3}
No foam

5×10^{-4} mol dm^{-3}
Very good Latex foam

5×10^{-2} mol dm^{-3}
Surfactant foam

Figure 4/18 : Latex JC with Dodecyl Trimethyl ammonium bromide

latex, diameter ca. 4 μm, will foam. Here again the foaming region corresponds to a region where bulk instability of the latex particles is being approached.

4.2.6 Foam Tests with Surfactants

Two surfactants were used, sodium dodecyl sulphate, SDS, and dodecyltrimethyl ammonium bromide, DTAB.

For the anionic surfactant, SDS, no latex foam was formed, only the surfactant foam, which had a wet 'liquid' appearance, see photograph, figure 4/17. This was observed at concentrations higher than the critical micelle concentration which is 8.2×10^{-3} mol dm^{-3}.

SDS is not specifically adsorbed on the negatively charged latex particle. It can be adsorbed, however, to form a monolayer with the hydrophobic tails oriented towards the surface. Consequently this means that the particle becomes more hydrophilic in nature and so can be more easily wetted. Hence, the contact angle is lowered and can approach zero degrees, thus leading to unfavourable conditions for particle stabilised foam formation, see chapter 9.

For the cationic surfactant DTAB, the foaming behaviour for a range of latex sizes is shown in figures 4/18 - 4/25.

It can be observed from figure 4/19 that latex JC, ca. 4 μm diameter, goes from a non-foaming situation, particles with a hydrophilic surface, to a very good, solid latex foam, where the particle surface becomes hydrophobic in nature, to a liquid surfactant foam where the latex surface then becomes hydrophilic and the particles are dispersed in the bulk phase. In the latex foaming region bulk coagulation occurs. Photographs of the various foams are shown in figure 4/18.

The latex foam appeared to have a wetter appearance; after a few shakes it was very difficult to shake the suspension due to the large volume of foam formed. The walls of the measuring cylinder were noticeably 'cleaner' than in a similar test with salt. That is, no dry clumps of

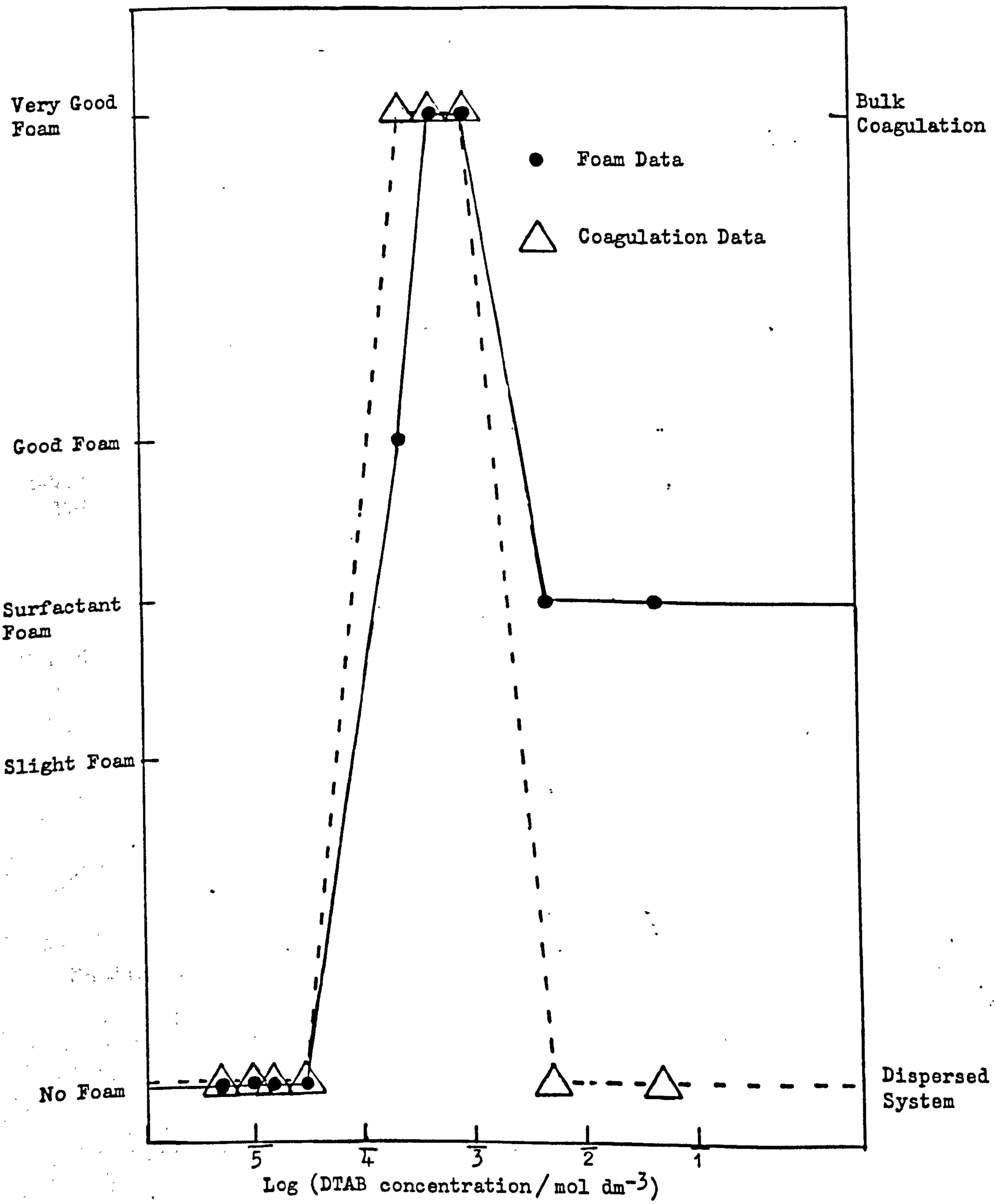

Figure 4/19: Foam data for Latex JC, diameter 3.89 μm, surface charge density 0.059 cm^{-2}, latex concentration 7%.

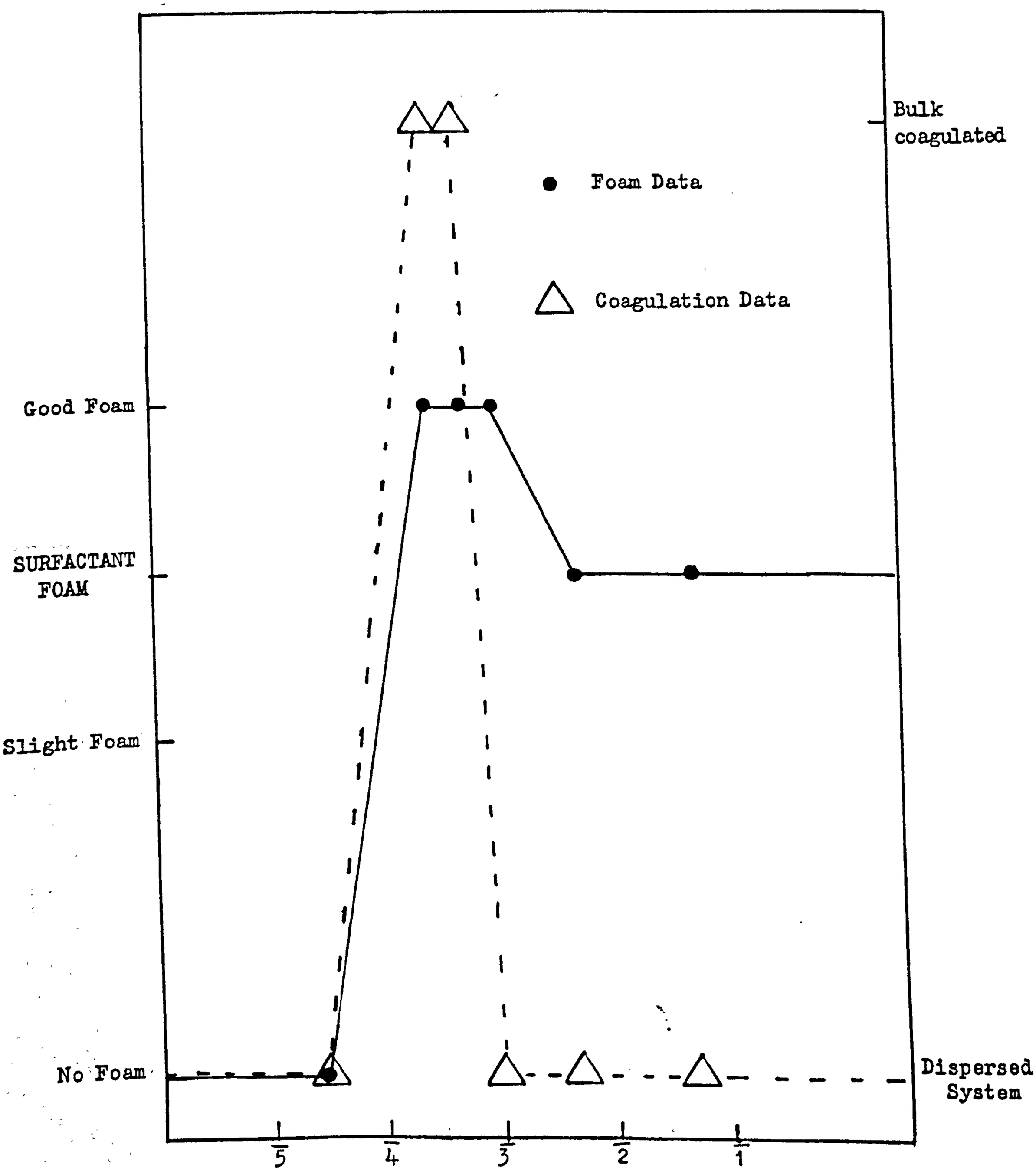

Figure 4/20 : Foam Data for Latex S67, diameter 2.2 μm, surface charge density 0.253 C m^{-2}, latex concentration 6.0 %.

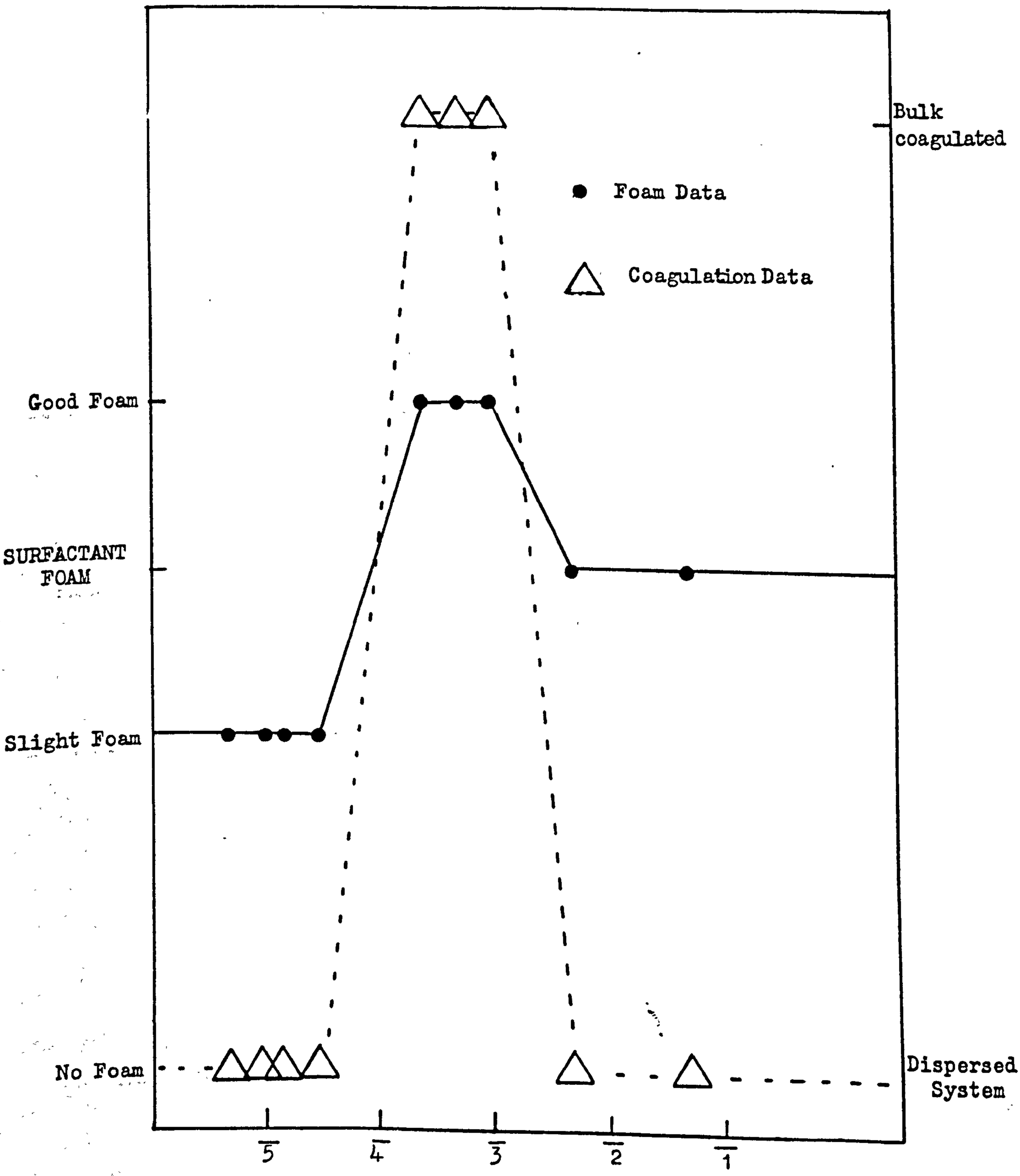

Figure 4/21 : Foam Data for Latex S61, diameter 2.1 μm, surface charge density 0.008 C m^{-2}, latex concentration 1.8 %.

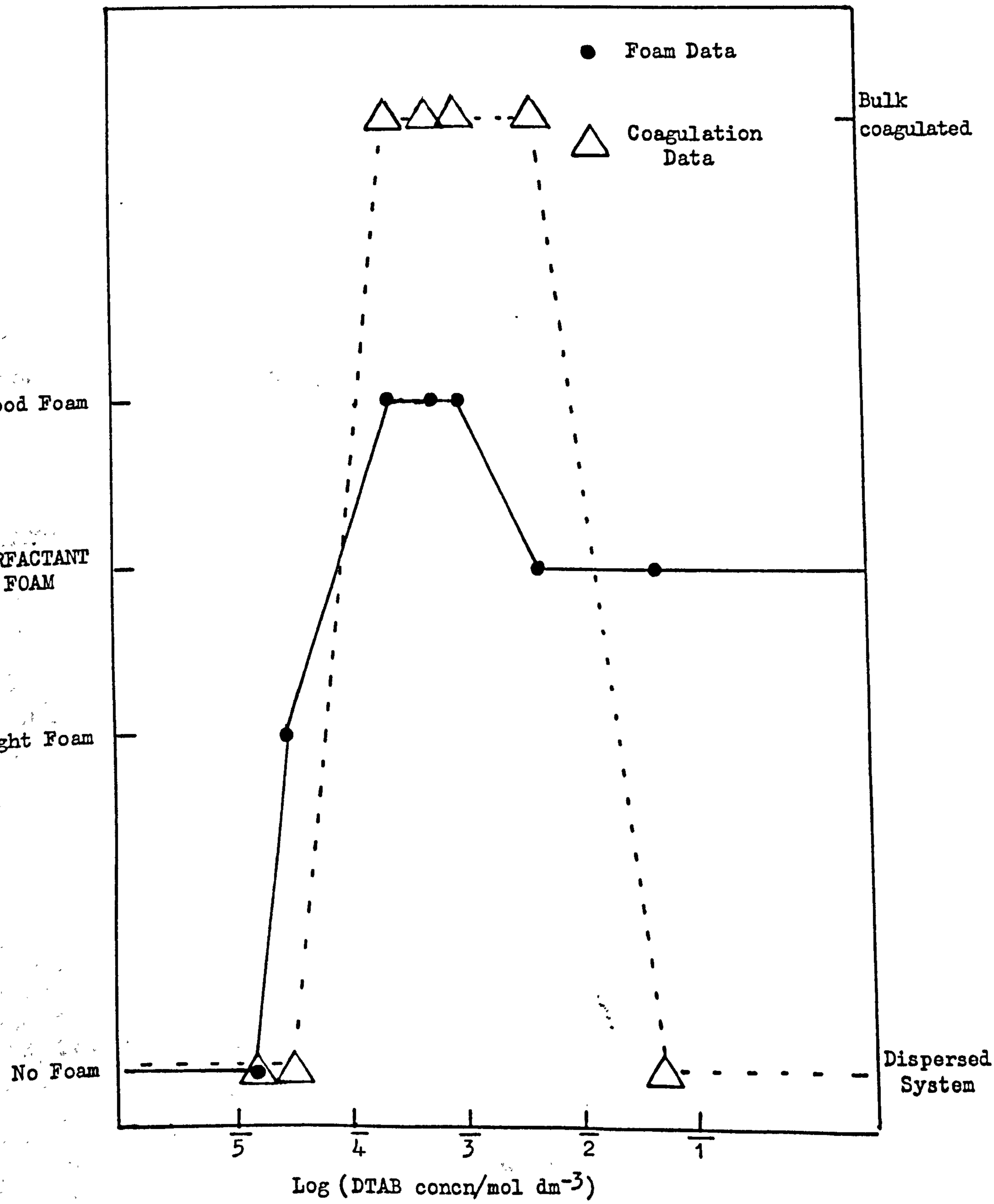

Figure 4/22 : Foam Data for Latex S65, diameter 2.18 μm, surface charge density 0.072 C m^{-2}, latex concentration 0.93 %.

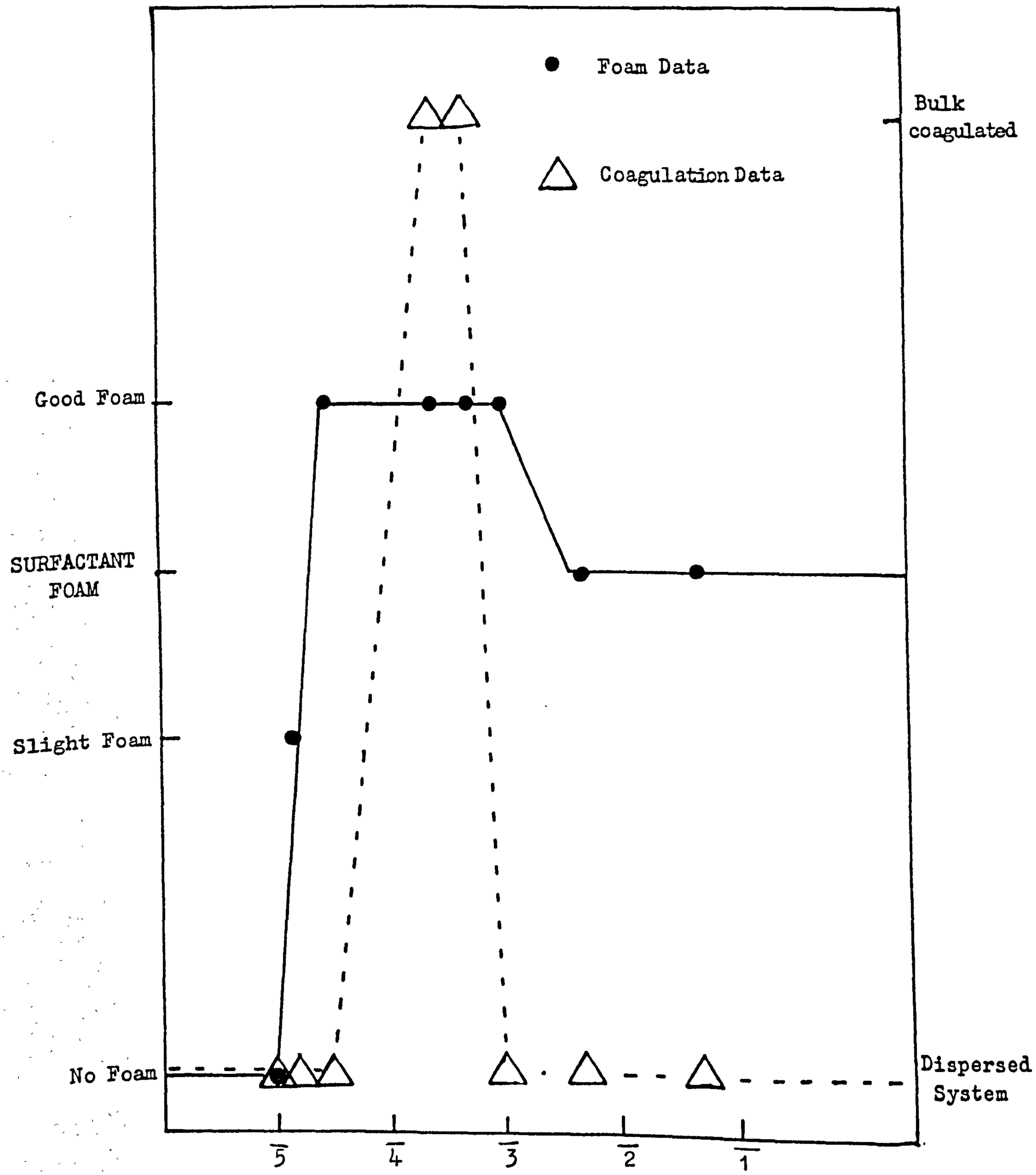

Figure 4/23 : Foam Data for Latex S17, diameter 1.56 μm, surface charge density 0.061 C m^{-2}, latex concemtration 0.27%.

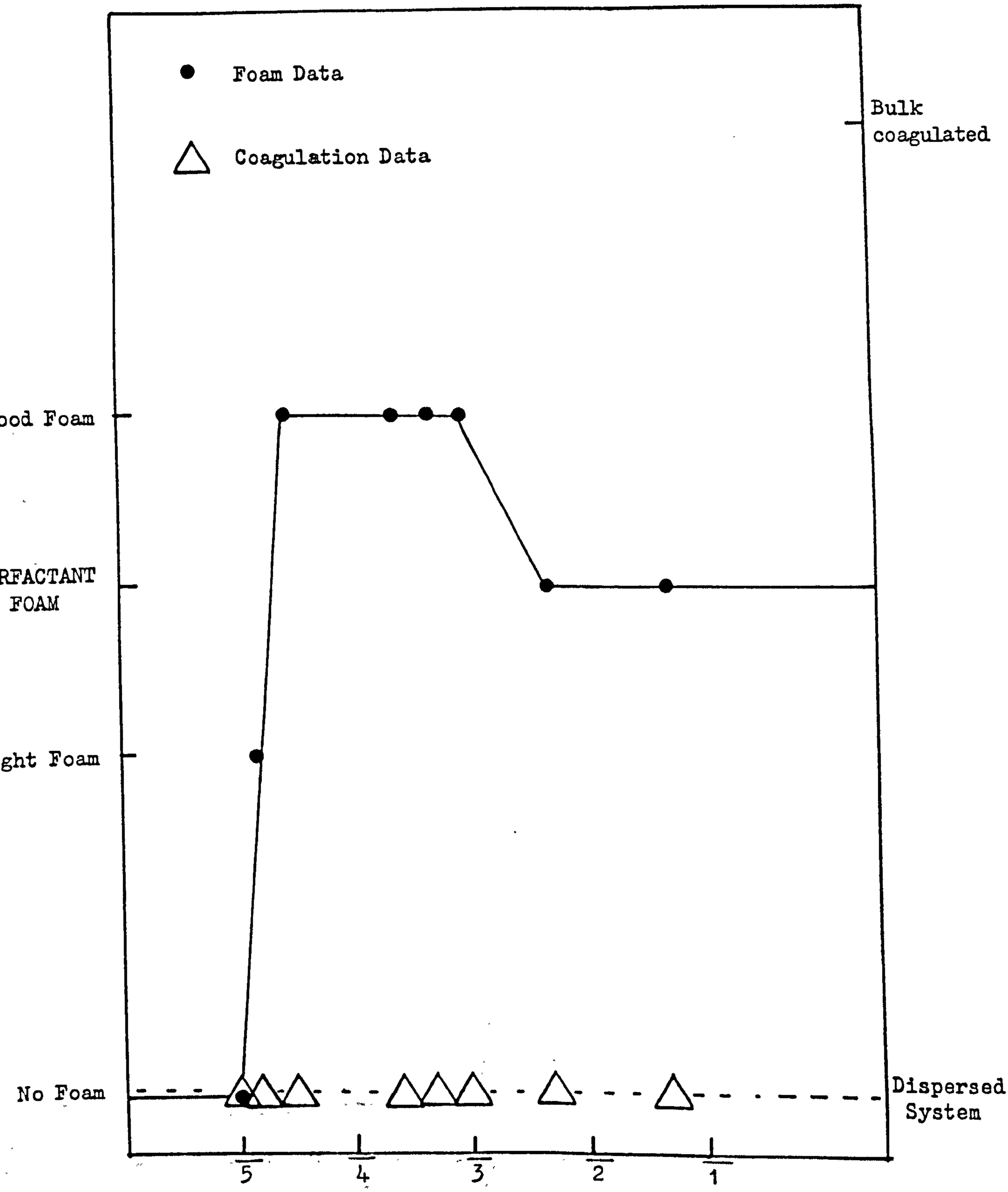

Figure 4/24 : Foam Data for Latex S15, diameter 1.5 μm, surface charge density 0.039 C m^{-2}, latex concentration 0.17 %.

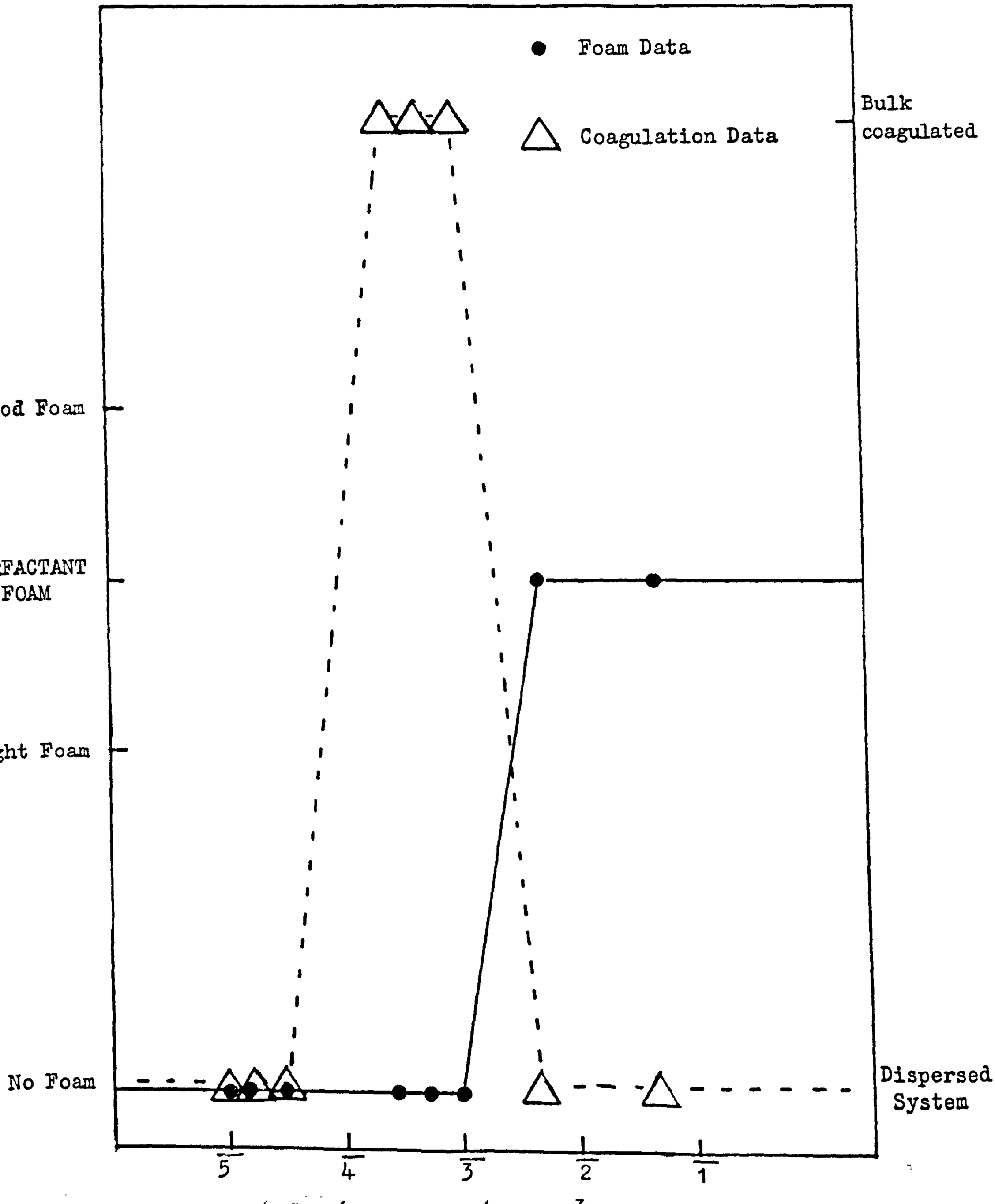

Figure 4/25 : Foam Data for Latex RB55, diameter 1.02 μm, surface charge density 0.039 C m^{-2}, latex concentration 0.2 %.

polystyrene latex particles were clinging to the sides of the vessel as with the latex/salt foams.

Similar behaviour was found for the latex S61, ca. 2 μm diameter. The other 2 μm diameter latices showed slightly different behaviour. For S65, a surfactant foam was observed whilst the bulk phase was still coagulated; whereas for S67 a good foam was formed although the bulk latex had redispersed in 5×10^{-3} mol dm^{-3} DTAB.

For S17, diameter 1.6 μm, a good foam was formed on both sides of the coagulation region; whereas for S15, 1.5 μm diameter, no bulk coagulation was observed. This was probably due to the low latex concentration of the suspension used. The volume concentration for S15 and S17 were 0.17 and 0.27% respectively.

For latex RB55, ca. diameter 1 μm, no latex foam was observed although the bulk suspension did coagulate. Here again the ease of foam formation appeared to depend on the size of the latex particle.

4.3 Calculations resulting from the Foam Tests

4.3.1 Comparison of the sodium chloride concentration where a foam is first observed with the concentration where bulk coagulation occurs

As a means of presenting the results, the sodium chloride concentration at which a foam was first observed can be denoted by F, and the concentration at which the bulk latex phase coagulated by C; the latter quantity is often referred to in the literature as the critical coagulation concentration. Table III lists these quantities for the latices studied.

From the figures presented earlier in this chapter it can be seen that F is, for the larger particles examined, smaller than C. However, as the particle size was decreased towards 1 μm it was found that F and C became almost identical. In order to examine the effect of particle size one quantity (C - F) was plotted against particle diameter as shown in figure 4/26, for the systems examined in sodium chloride solutions. This showed a

Figure 4/26

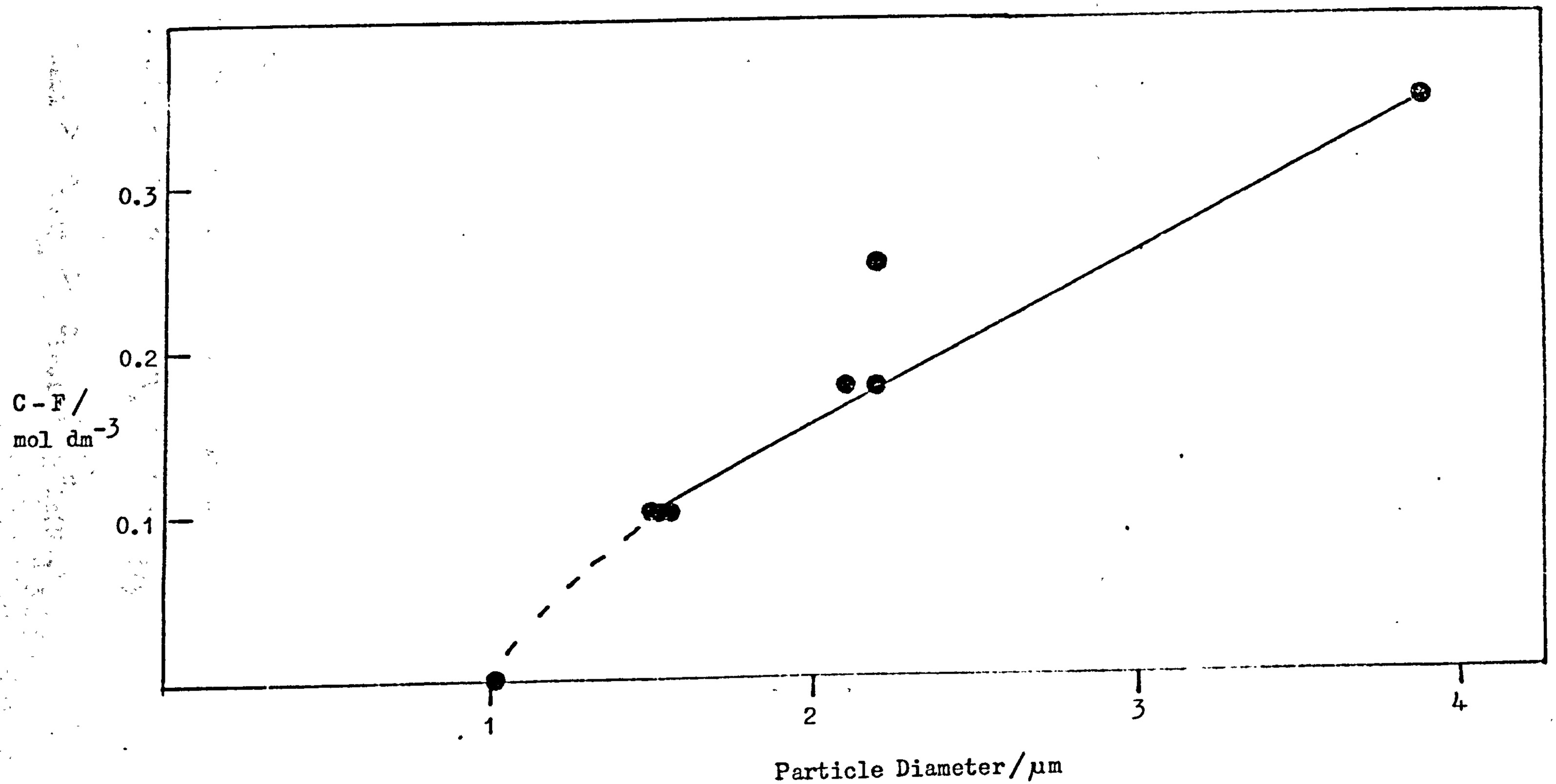

TABLE III

Latex	Particle diameter/μm	F/mol dm^{-3}	C/mol dm^{-3}	C - F/mol dm^{-3}
RB55	1.02	0.1	0.1	0
S17	1.56	0.1	0.2	0.1
S15	1.50	0.1	0.2	0.1
S67	2.20	0.2	0.45	0.25
S61	2.10	0.025	0.2	0.175
S65	2.20	0.025	0.2	0.175
JC	3.89	0.075	0.425	0.35

definite increase in (C - F) with increase in particle diameter. The curve apparently crosses the axis, that is (C - F) = 0, at a particle diameter of 1 μm. A tentative interpretation of these data is that provided (C - F) is positive then the latex will foam before coagulation occurs. When (C - F) is zero the latex foams at the same sodium chloride concentration as instability occurs in the bulk phase. It becomes apparent from this curve that for particle diameters less than 1 μm the system will coagulate before foaming can occur.

It should be noted that one point falls off the drawn curve. This was for latex S67 which had a substantially higher surface charge density than the others examined. Consequently it required a higher electrolyte concentration to achieve bulk coagulation.

If the same two quantities, F and C, are examined for the latex JC in electrolytes other than sodium chloride, an interesting fact emerges. Table IV lists these quantities and it can be seen that for both F and C the following order of electrolyte effects exists :

$$F_{NaCl} > F_{MgSO_4} > F_{BaCl_2} > F_{La(NO_3)_3}$$

and

$$C_{NaCl} > C_{MgSO_4} > C_{BaCl_2} > C_{La(NO_3)_3}$$

TABLE IV

Latex	Electrolyte	F/mol dm^{-3}	C/mol dm^{-3}
JC	NaCl	0.075	0.425
JC	$BaCl_2$	5×10^{-5}	2×10^{-2}
JC	$La(NO_3)_3$	5×10^{-6}	1×10^{-4}
JC	$MgSO_4$	2.24×10^{-4}	3.5×10^{-2}

The parameter C, the critical coagulation concentration, reflects the effect of the counterion, that is its valency, as described by the Schulze-Hardy rule[2]. According to the D.L.V.O. theory for interaction between flat plates, the critical coagulation concentration is given by the expression

$$C = \frac{8 \times 10^{-22} \Gamma^4}{A_{net}^2 z_o^6}$$

where C is expressed in mol dm^{-3} in water at 25°C, A_{net} is the composite Hamaker constant, and z_o is the valency of the counterion.

$$\Gamma = \frac{(\exp(z_o e \psi_o / 2kT - 1)}{(\exp(z_o e \psi_o / 2kT + 1)}$$

For high surface potentials, that is $z_o e \psi_o / 2kT > 6$, Γ tends to unity and hence

$$C = \frac{8 \times 10^{22}}{A_{net}^2 z_o^6}$$

The ratio $C_{1:1} : C_{2:2} : C_{3:3}$ electrolytes becomes

100 : 1.56 : 0.137

For a potential of 50 mV the ratio is

100 : 8.39 : 1.44

It should be noted that for the data in Table IV the ratio for NaCl : $BaCl_2$ is 100 : 4.71 which would be in accord with some specific

adsorption of the barium ions to the sulphate groups on the latex surface.

For a 3:3 electrolyte and a potential of 50 mV the $C_{1:1} : C_{3:3}$ expected is 100 : 1.44. The value observed for $La(NO_3)_3$ was 100 times lower; which would be consistent with adsorption of the lanthanum ion in the hydrolysed state. Unfortunately this cannot be confirmed as the pH was not measured.

The critical foaming concentration, F, shows a similar order to that found for the bulk coagulation data. However it would appear to be more pronounced, suggesting stronger specific ion effects in the foam than those occurring in the bulk phase.

4.3.2 Comparison between the surface charge density of the polystyrene particle and its foaming properties

Table V compares the surface charge density of the various sized latex systems with the sodium chloride concentration at which a foam was observed.

TABLE V

Latex	Particle diameter/μm	F/mol dm^{-3}	Surface charge density/C m^{-2}
JC	3.89	0.075	0.059
S67	2.20	0.2	0.223
S61	2.10	0.025	0.008
S65	2.20	0.025	0.072
S17	1.56	0.1	0.061
S15	1.50	0.1	0.039
RB55	1.02	0.1	0.039

Latices JC, S65 and S17 all have surface charge densities close to each other, yet the foaming salt concentrations vary by a factor of 4. A larger discrepancy is found for latices S61 and S65 which both form a slight foam at 0.025 mol dm^{-3} sodium chloride but whose surface charge densities are 0.008 and 0.072 $C m^{-2}$ respectively. Although both latices

S15 and RB55, having a surface charge density of 0.039 C m^{-2}, have a foaming salt concentration of 0.1 mol dm^{-3} there does not appear to be a correlation between the surface charge and the foaming properties. However it should be noted that the latex with the largest surface charge density, S67, did require the largest salt concentration to foam.

It would appear that there is a strong correlation between particle size and foaming; the larger the latex particle the lower the sodium chloride concentration at which the latex foamed. However this itself is not completely clear since latices S61 and S65, ca. 2 μm diameter, foam at a sodium chloride concentration less than that required for the larger latex JC; whereas S67, ca. 2 μm diameter, requires a higher salt concentration than the smallest latex examined, RB55. This could suggest that particle size and surface charge density are interdependent variables which determine the foaming properties of polystyrene latex particles.

4.3.3 Calculation of the concentration of DTAB required to neutralise the surface charge on polystyrene latex particle

It could be anticipated that there should be a correlation between the concentration of DTAB required to produce reversal of surface charge on the polystyrene particle and the point where the latex foams.

If we have a latex suspension, containing particles of radius R, and surface charge density, $\bar{\sigma}$, then the molarity of DTAB required to neutralise the suspension, C_c, can be calculated, assuming that it is all adsorbed on the latex surface, by the following expression

$$C_c = \frac{4\pi R^2 \bar{\sigma} N_o \times 1000}{e \times 10^4 L}$$

This is the minimum amount of DTAB required to neutralise the surface charge on the latex surface and not the equilibrium concentration of DTAB after adsorption; the latter is fully discussed by Connor and Ottewill[150]. Therefore the actual initial concentration of DTAB required to produce a latex foam, C_1, should be larger than this. From Table VI

it can be seen that this is indeed the case.

TABLE VI

Latex	C_c/mol dm^{-3}	C_1/mol dm^{-3}
JC	7.2×10^{-5}	2.1×10^{-4}
S67	1.3×10^{-4}	2.5×10^{-4}
S61	4.4×10^{-6}	5.0×10^{-6}
S65	2.0×10^{-5}	2.8×10^{-5}
S17	6.9×10^{-6}	1.5×10^{-5}
S15	3.0×10^{-6}	1.5×10^{-5}
RB55	1.1×10^{-4}	No latex foam

It is interesting that for a given size range the concentration of DTAB required to give a good foam is constant. The ratio of these concentrations is approximately 18:9:1 for latex diameters approximately 2.6:1.5:1. There is a dependence on the foaming properties of polystyrene latex suspended in DTAB solutions.

4.4 Conclusions

Polystyrene latex particles with a diameter greater than 1 μm in concentrated sodium chloride solutions, greater than 0.1 mol dm^{-3}, will form foams. The foam stability depends on the latex particle size; latex particles smaller than 1 μm will not foam. The latex concentration must be high too, 1 - 6% w/v, for a very stable foam, that is for the foam to remain stable for longer than a week, to be formed.

The foaming of the largest latex, JC, diameter 3.89 μm, has also been investigated in other electrolytes than sodium chloride. For this latex the ease of foaming when suspended in the following electrolytes increased in the order $La(NO_3)_3$, $BaCl_2$, $MgSO_4$, NaCl.

The high electrolyte concentration causes the extension in space of the electrical double layer around the surface to decrease, thus reducing

the electrostatic repulsion forces and so enabling the latex particles to approach each other more closely than in dilute salt solution. Close approach of the particles is essential if they are to form a close-packed layer around the air cell.

The close approach is also helped by an acidic environment where again the repulsion of the surface charges is reduced by the formation of acid groups. The foam tests carried out at various pH values confirmed this hypothesis.

In the cationic surfactant solutions another mechanism for reducing the repulsion due to the surface charges arises. At low DTAB concentration only small amounts of the cationic surfactant ions are adsorbed, so that the particle charge remains negative and the particles are strongly repelled. However, since the surfactant molecules are adsorbed at the negative charges, eventually a neutral, hydrophobic outer shell is created. Around the DTAB concentration value where this adsorbed state occurs the latex particles should foam due to the reduced repulsion between them. As the DTAB concentration is increased more extensive adsorption of the surfactant occurs and the particles acquire a positively charged outer shell of surfactant ions, so that the electrostatic repulsion increases. This caused the concentration of latex to shift in favour of that in the bulk phase.

Also, for the surfactant system as for the salt system a dependence on latex particle size was found. The 1 μm latex did not form a latex foam. However, latices with diameters of 1.5 μm and above formed solid latex foams. Also within a given size range, for example 2 μm diameter particles, the concentration of DTAB required to produce a good foam was the same regardless of the surface charge density of the latex.

CHAPTER 5

THE STRUCTURE OF THE FOAM

5.1 Description of the Foam

5.1.1 Introduction

In his review on foams and free liquid films Kitchener discussed the classification of foams[15]. However, it is probably more helpful in the present context not to bracket foams into distinct types but to describe the foam itself.

The foam produced by shaking polystyrene latex under the appropriate foaming conditions is particle stabilised. Here the bubbles have a 'solid' appearance and are very stable compared with liquid surfactant foams. The bubbles appear to be mainly spherical although liquid bridges joining two or three bubbles are also seen. The bubbles observed here varied in size from microbubbles to bubbles having diameters of the order of 2 cm.

5.1.2 Optical Observations

The bubbles are coated with a latex film. For the small particles, 1.5 μm diameter, interference colours can be seen as the film drains. This indicates the regularity of the packing of the polystyrene latex particles on the bubbles' surfaces.

The close-packing of the solid particles can be seen from the micrographs of the bubbles produced from latex JC, 3.89 μm diameter in sodium chloride solutions, figures 5/1 - 5/6.

These were taken using a camera attached to an optical microscope. The film used was Ilford Pan F which is a slow film with a speed of ASA 50. It was developed using an ultra fine grain developer, Promicrol. The total magnification, including photographic magnification, was calibrated from photographs of a Carl Zeiss, $5 + \frac{100}{100}$ mm, grid; its value was 340 x. Examples of these micrographs can be seen in figures 5/1 - 5/4.

Very good, hexagonally close-packed arrays of polystyrene particles

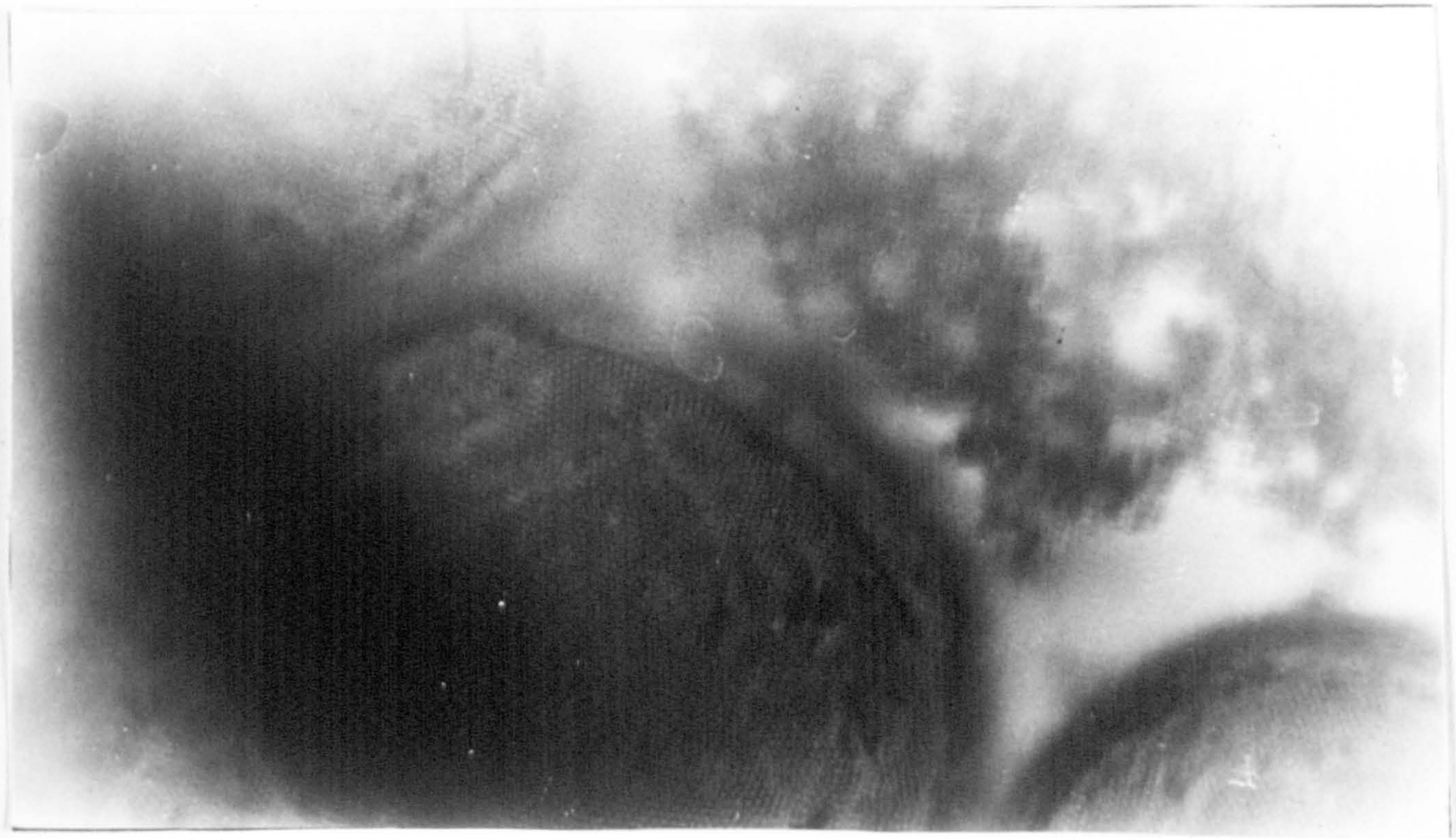

Latex JC in 0.45 mol dm^{-3} Sodium Chloride

Figure 5/1 : Bubble Micrograph

Latex JC in 0.45 mol dm^{-3} Sodium Chloride

Figure 5/2: Bubble Micrograph

Latex JC in 0.45 mol dm^{-3} Sodium Chloride

Figure 5/3 : Bubble Micrograph

Latex JC in 0.3 mol dm^{-3} Sodium Chloride

Figure 5/4 : Bubble Micrograph

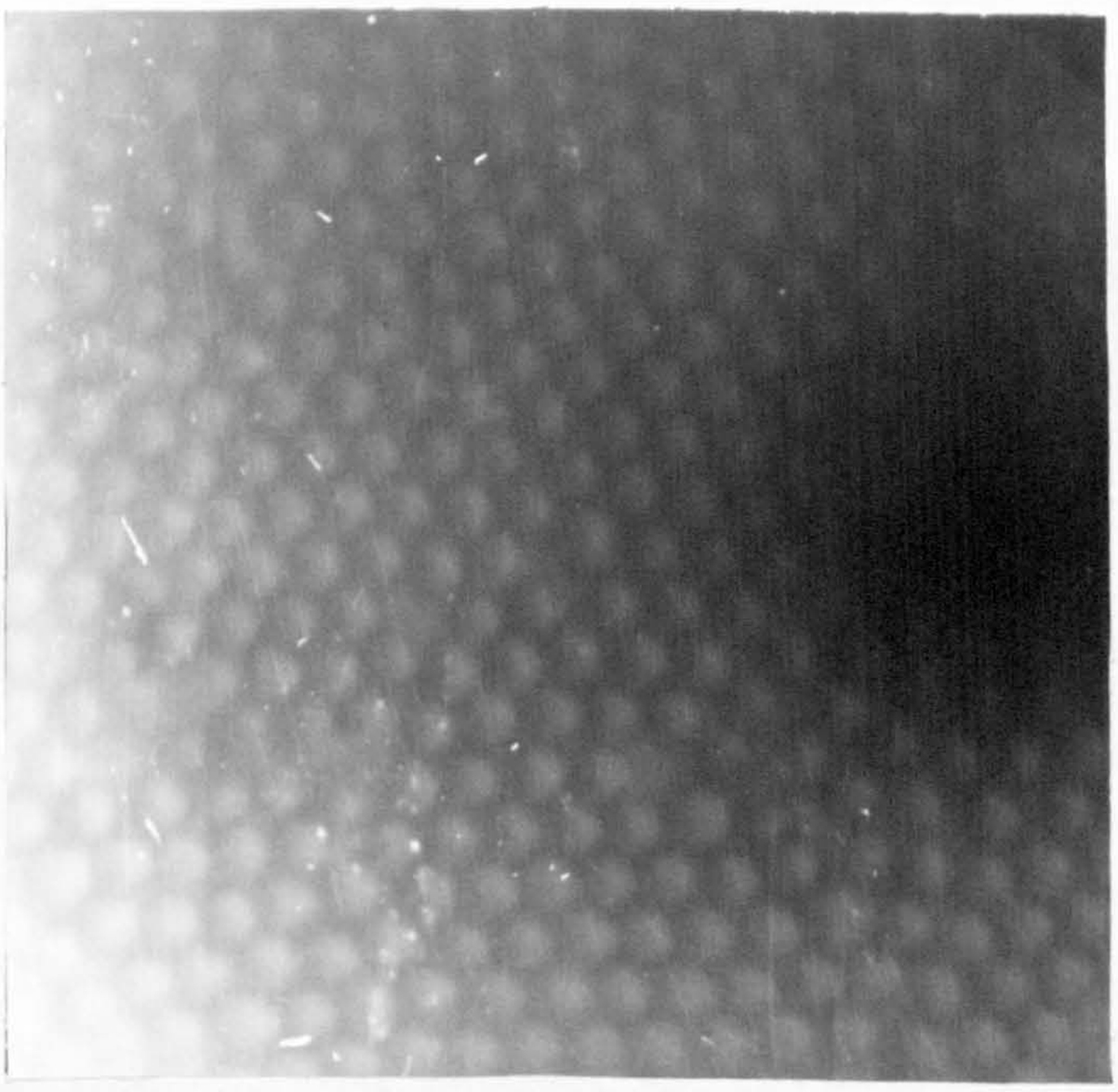

Latex JC in 0.1 mol dm^{-3} Sodium Chloride

Figure 5/5 : Bubble Micrograph

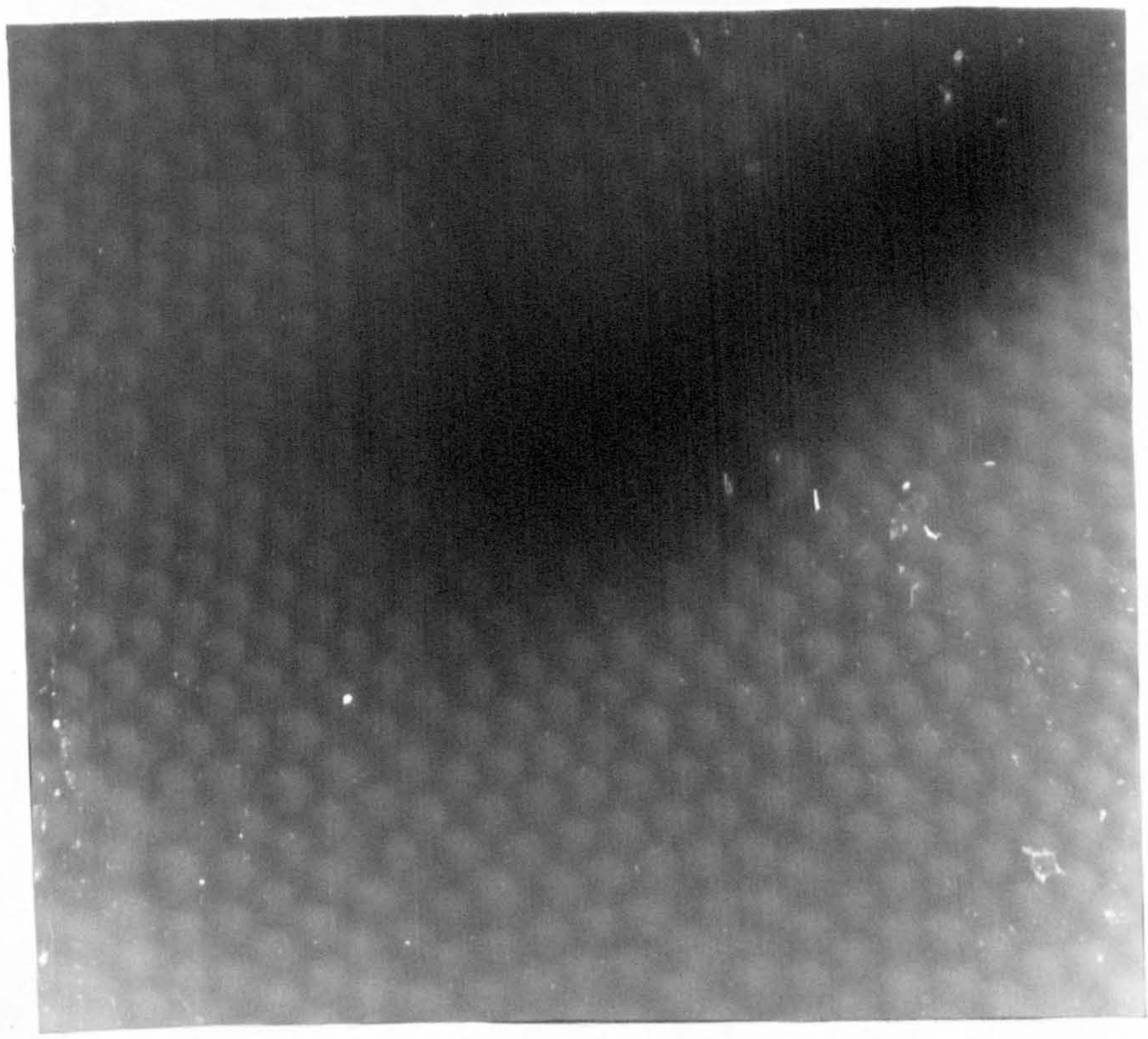

Latex JC in 0.45 mol dm^{-3} Sodium Chloride

Figure 5/6 : Bubble Micrograph

Figure 5/7

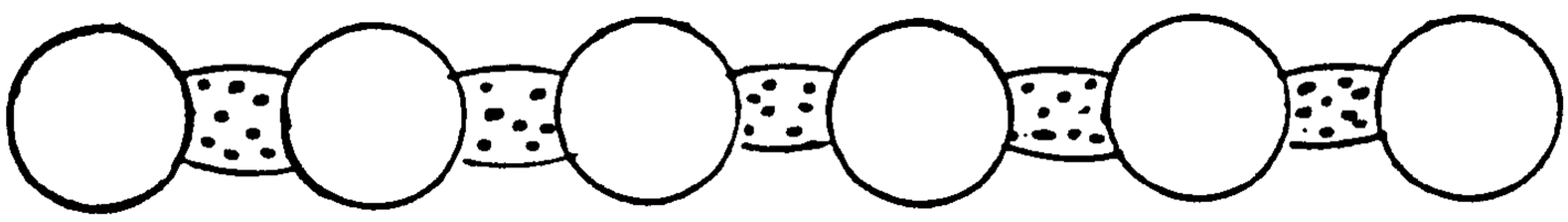

Monolayer

Bilayer

Figure 5/8

Bubbler for Diffraction Studies

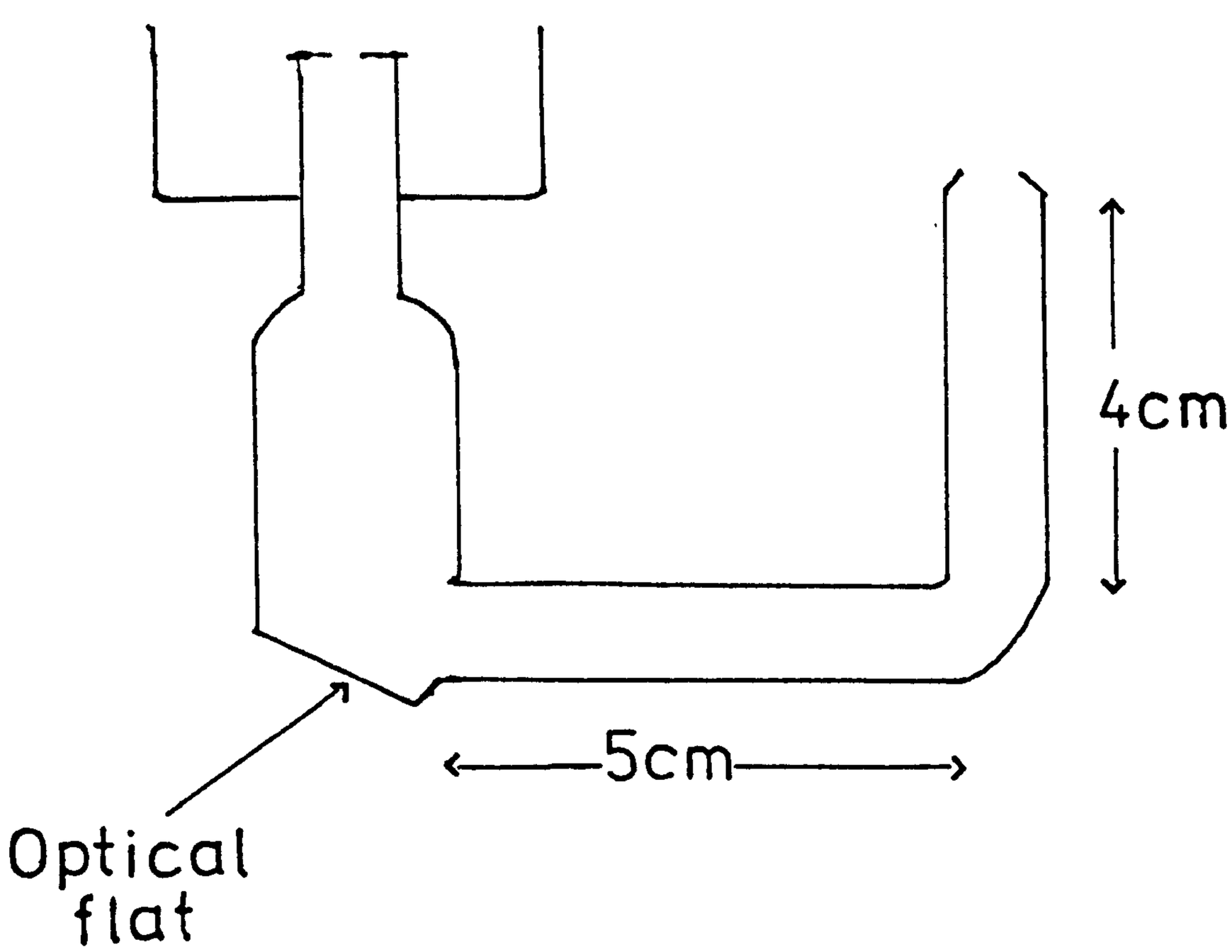

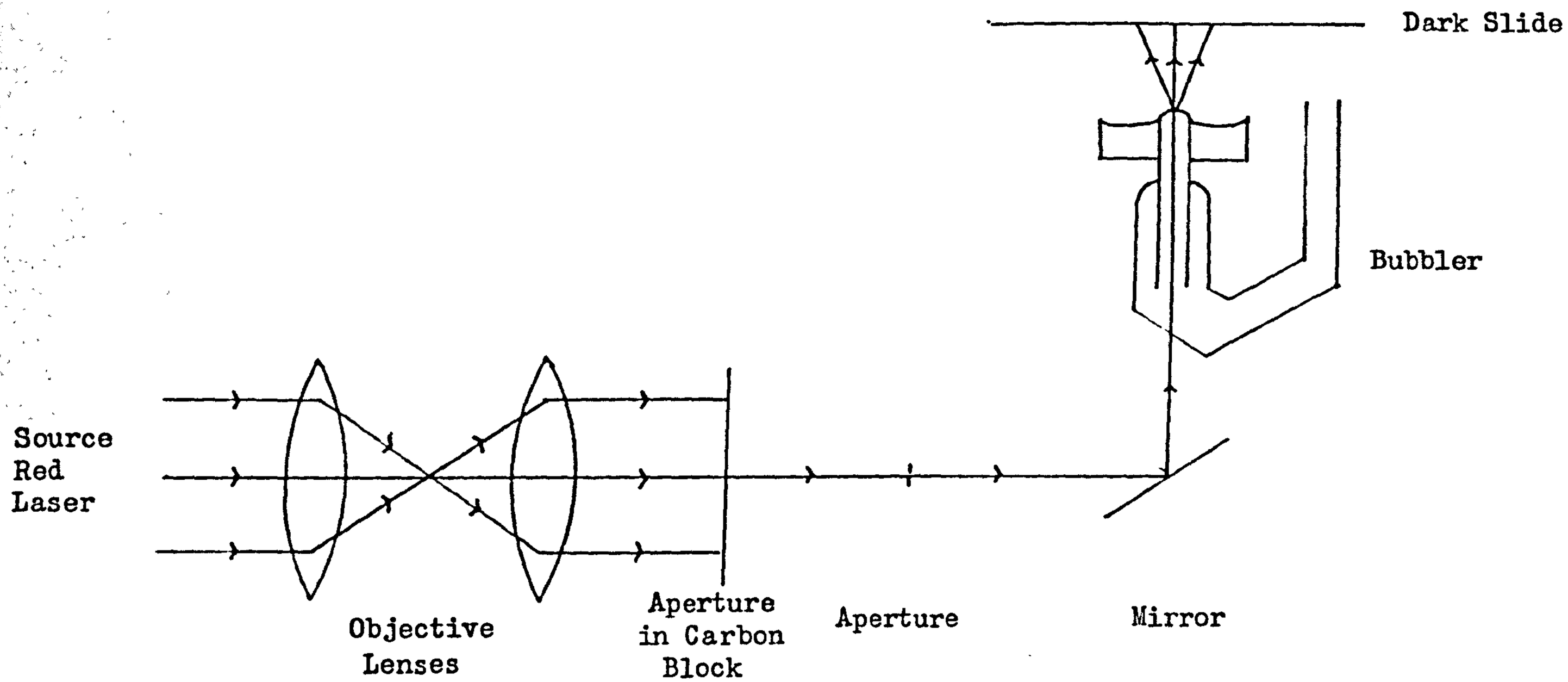

Figure 5/9 : The Optical Bench for Bubble Diffraction

can be seen on the bubble surface, figure 5/1, and in some cases this ordering is continued in the surrounding film, figure 5/4. These are photographs of foam in a measuring cylinder which was in the vertical plane.

Additional photographs were taken of a single bubble formed in the surface of a latex in salt solution, figures 5/5 and 5/6. Here a Watson Microsystem 700 microscope was used and the magnification was 400 x. These gave a clear picture of the regularity of the packing of the polystyrene particles on the bubble surface. Grain boundaries can be seen with the odd larger particle distorting the array, figures 5/5 and 5/6.

5.2 Structure of the Film

5.2.1 Introduction

One of the questions posed by the above micrographs is whether the latex film is a monolayer or a bilayer, figure 5/7. The latter seems the more likely structure from considerations such as forces between the particles and the flexibility of the structure.

As the ordering of the polystyrene particles in the film appeared to be so good it was decided to investigate the diffraction of a laser beam by the latex film. Hopefully it would clarify the structure of the film, that is whether it was a monolayer or a bilayer.

5.2.2 Experimental

The latex used was latex JC, diameter 3.89 μm. The bubbler described in figure 5/8 was used for this work. The optical bench arrangement is illustrated in figure 5/9; the laser was a 2 mW Spectra Physics Helium-Neon red laser. The film used was an experimental red sensitive film kindly supplied by Dr J. Lewis of Messrs Ilford Ltd. Using this film exposures as short as $1/125^{th}$ of a second could be used. The developer used was ID 13 which caused less fogging than the ordinary Universal developer.

Diffraction patterns from latex dried down on glass microscope slides

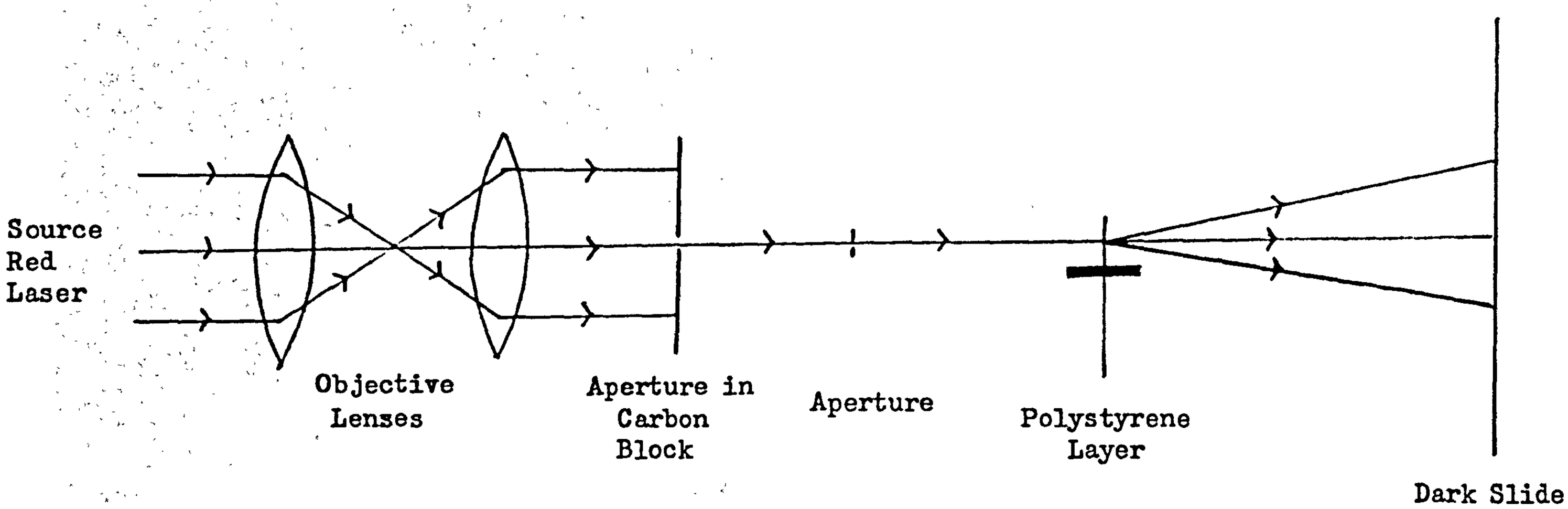

Figure 5/10 : The Optical Bench for Layer Diffraction

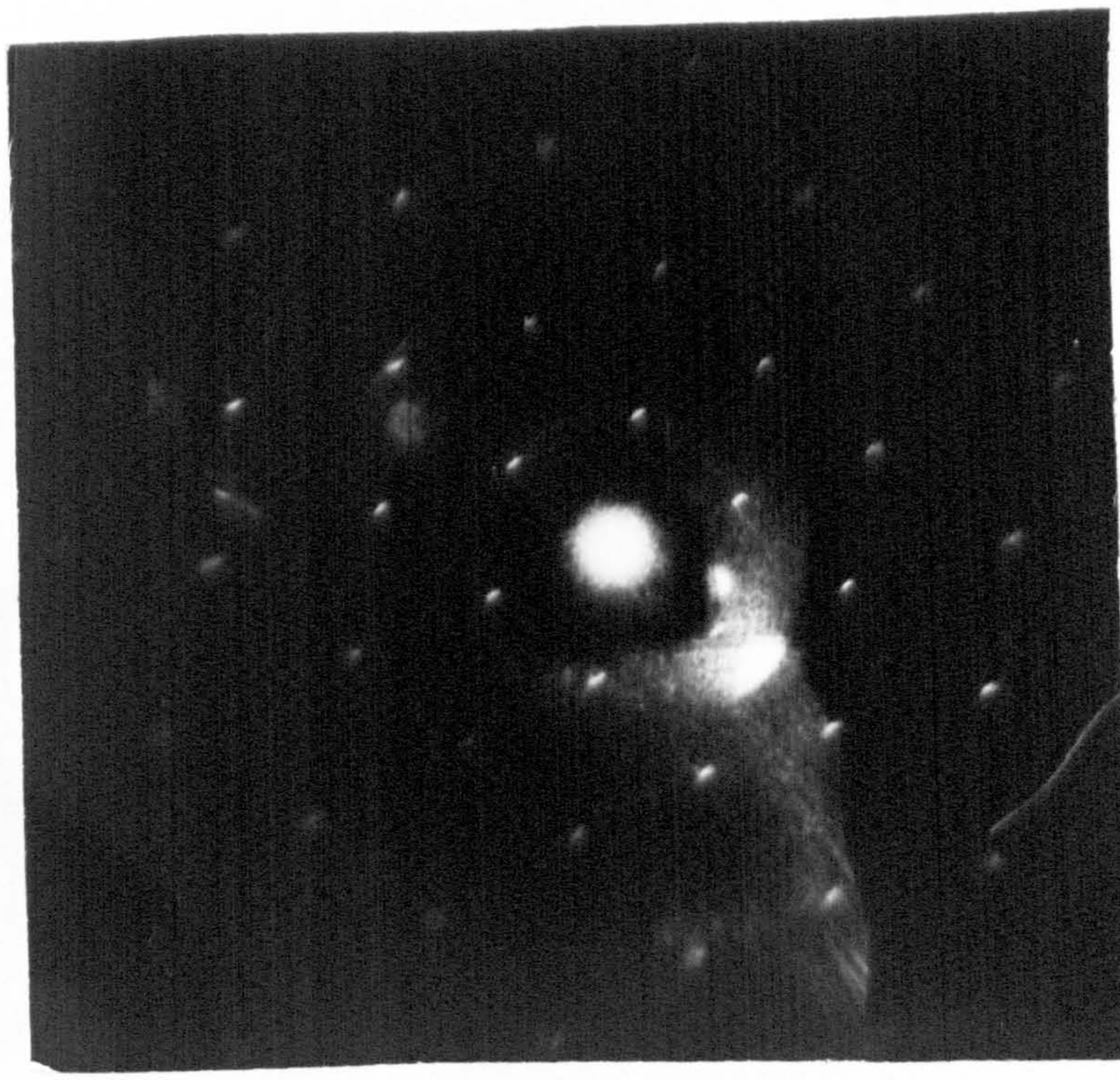

Figure 5/11 : Monolayer of Latex JC

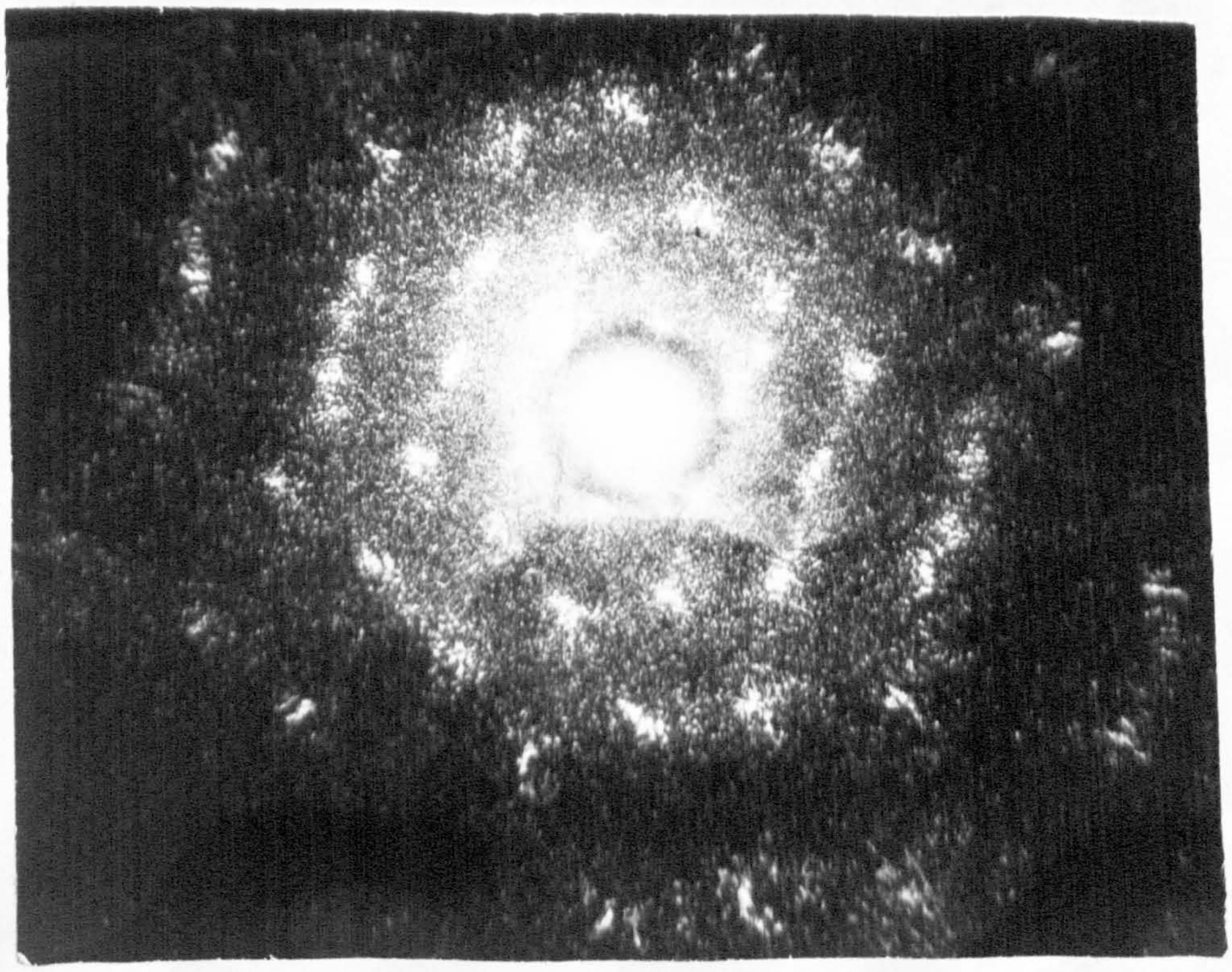

Figure 5/12 : Two Layers of Latex JC touching

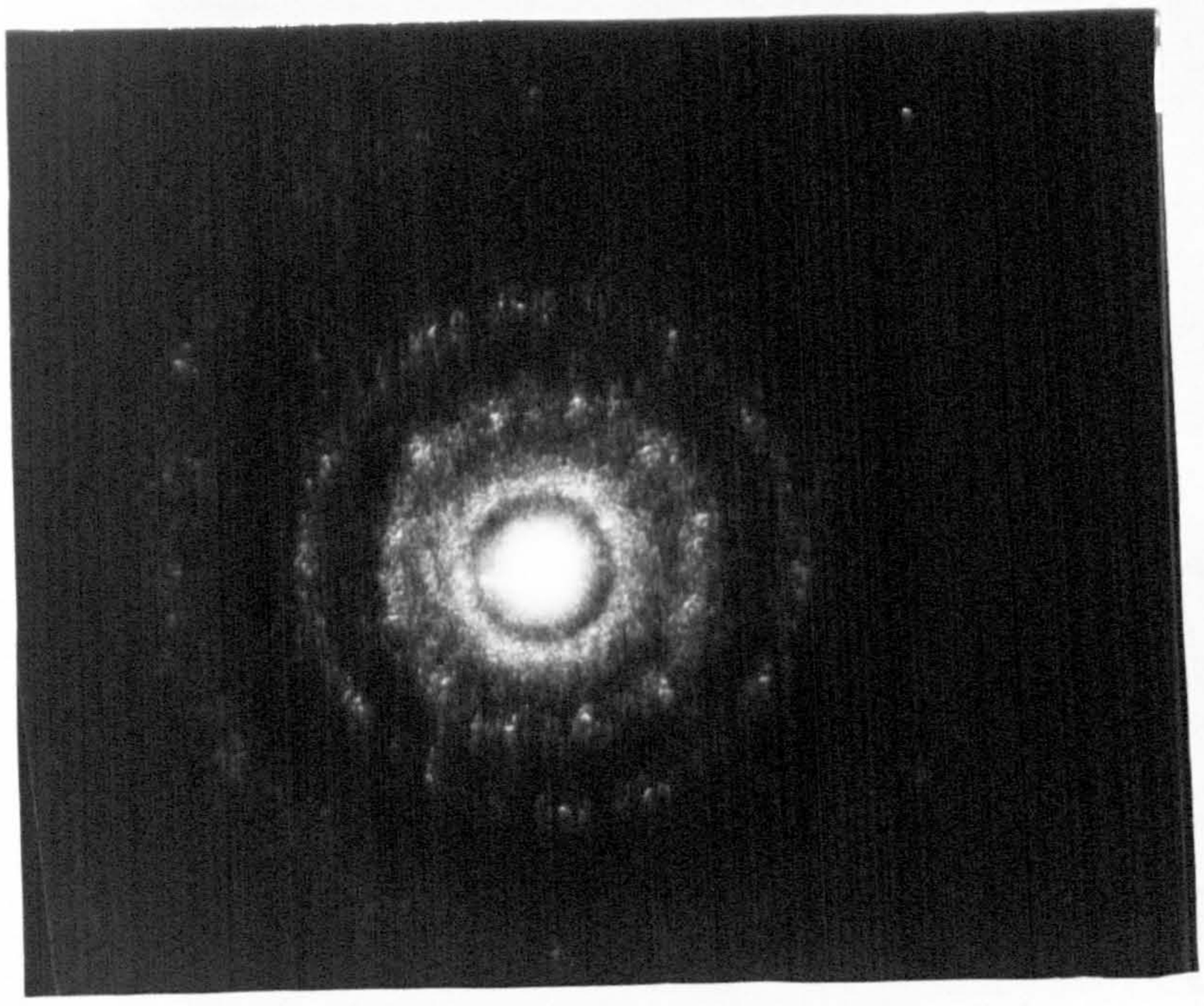

Figure 5/13 : Two Layers of Latex JC touching

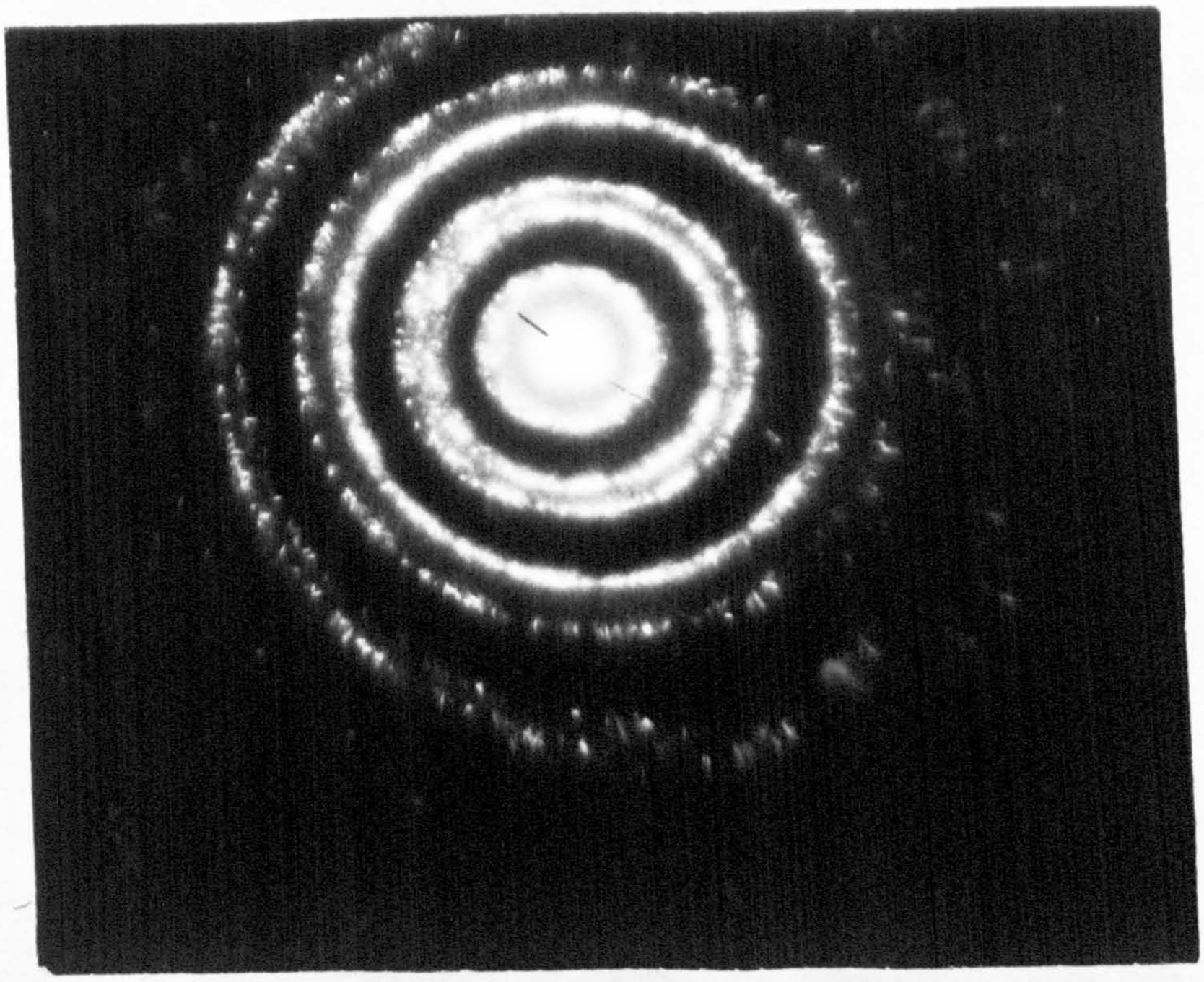

Figure 5/14 : Bubble Diffraction for Latex JC in 0.1 mol dm^{-3} Sodium Chloride

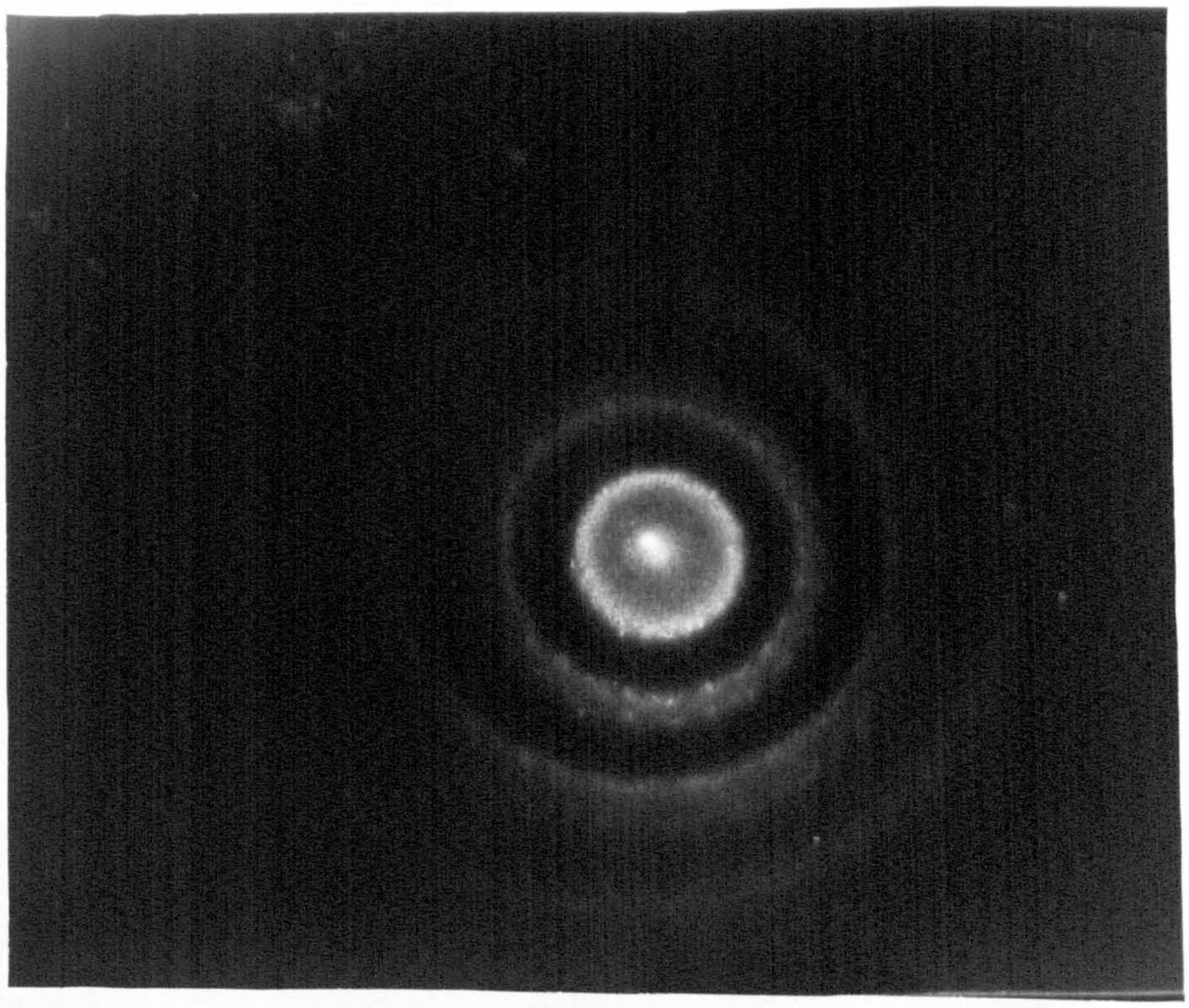

Figure 5/15 : Bubble Diffraction for Latex JC in 0.25 mol dm^{-3} Sodium Chloride

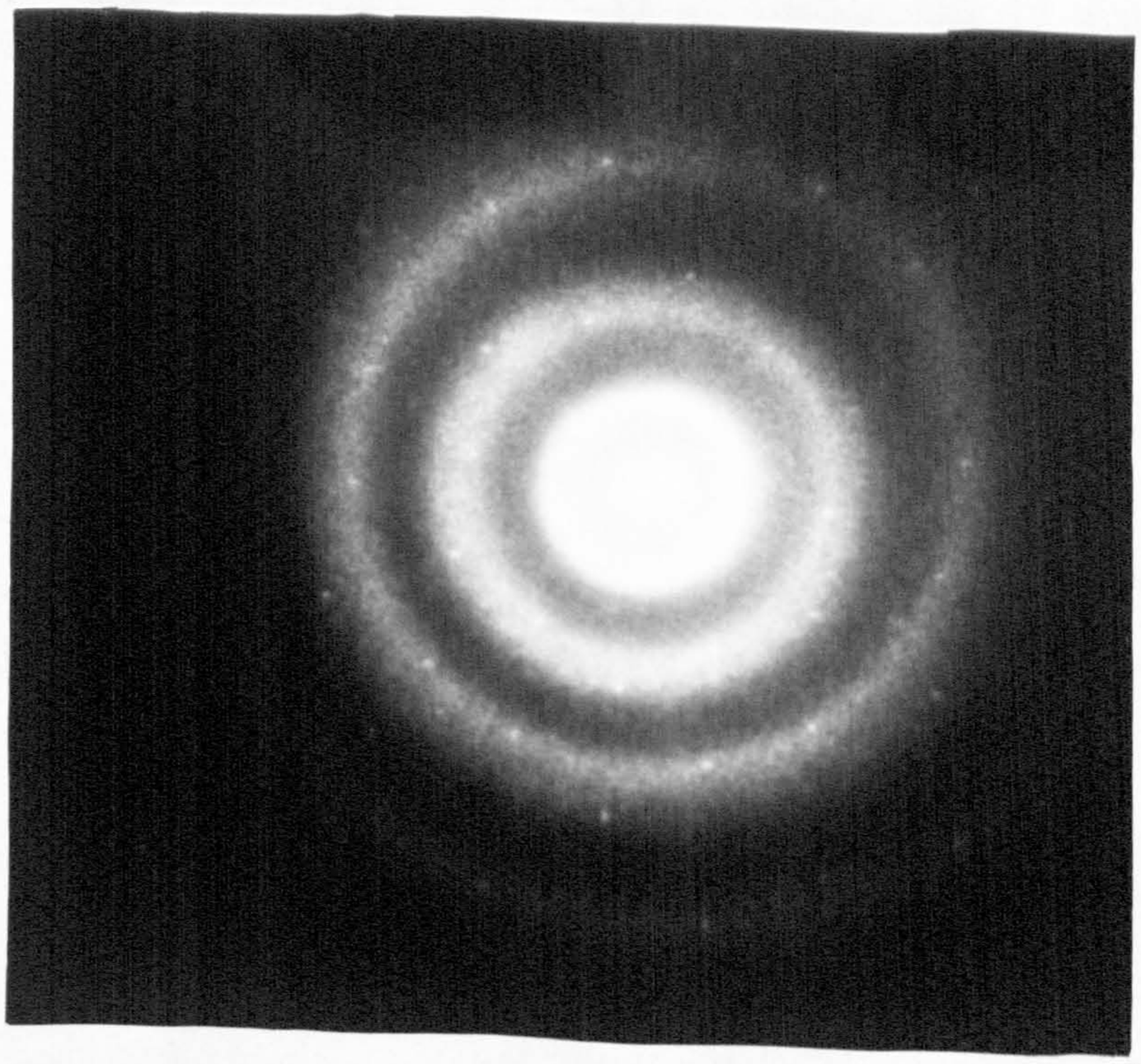

Figure 5/16 : Bubble Diffraction for Latex JC in 0.25 mol dm^{-3} Sodium Chloride

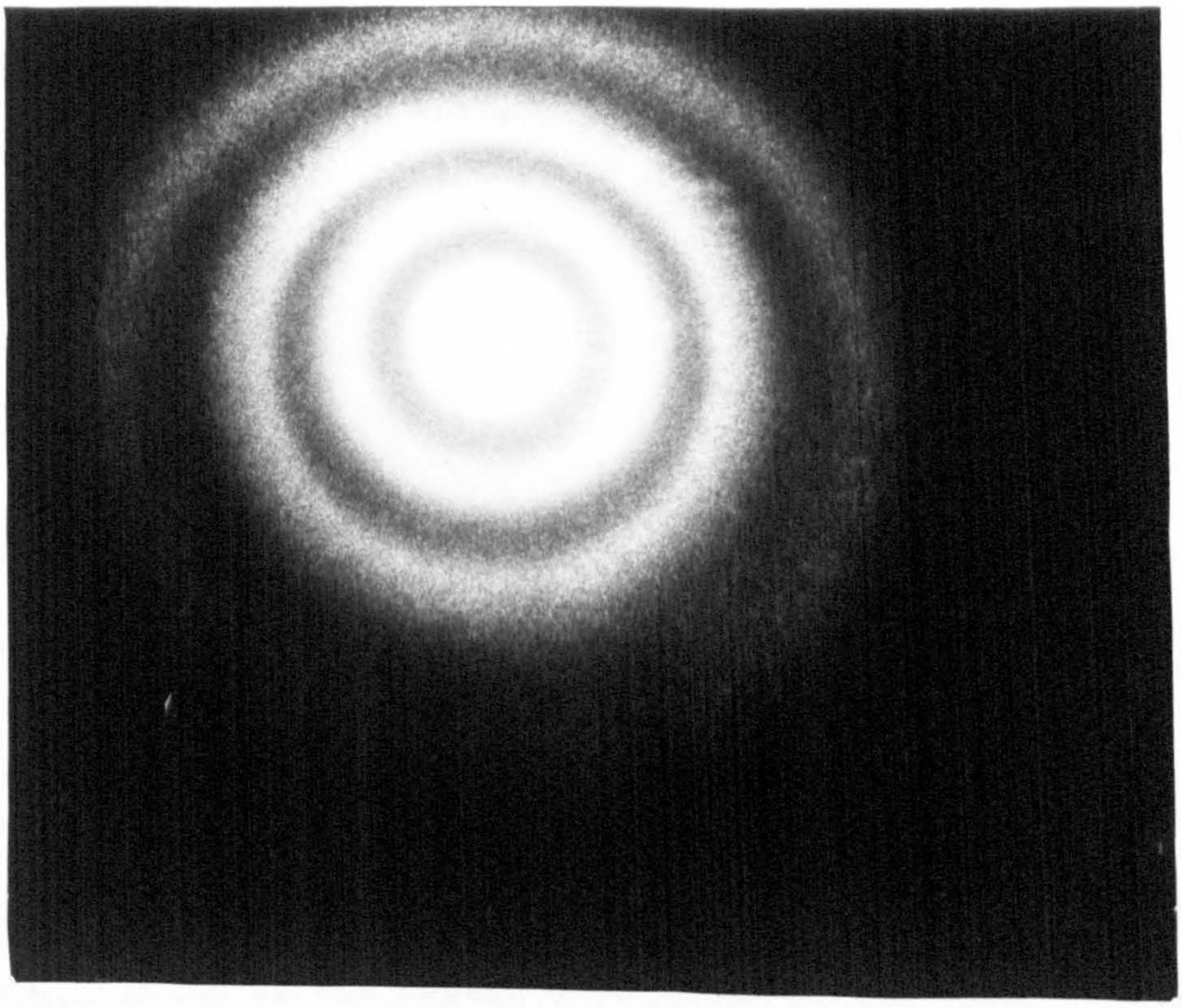

Figure 5/17 : Bubble Diffraction for Latex JC in 0.1 mol dm^{-3} Sodium Chloride

using a latex concentration of 0.13% were also photographed. Figure 5/10 shows the optical bench arrangement used for this type of diffraction examination.

5.2.3 Results

(a) Layer diffraction

Photographs of the diffraction pattern are shown in figures 5/11 - 5/13. A single layer of polystyrene particles, diameter 3.89 μm, gives a hexagonal spot pattern. Analysis of these patterns shows that the particles are hexagonally close-packed in the film[121].

If a second layer is placed close to the first, the crystal spot pattern of a single layer broadens to give the powder ring array for two layers, figures 5/12 and 5/13; the radius of the rings being equivalent to the radius of the circles joining the spots.

(b) Bubble diffraction

The diffraction patterns varied considerably in the widths of the diffraction rings, probably due to vibrations occurring in the system. The area on the surface of the bubble through which the laser beam passes needs to be regular in its packing for a distinct diffraction pattern to result. Any distortion due to a random large particle will broaden the rings. Figures 5/14 - 5/17 are examples of the patterns obtained.

Figure 5/14 shows a very clear ring pattern where the rings consist of diffuse diffraction spots, that is a spot with a halo of secondary diffraction spots situated around it. Figure 5/15 also shows this splitting of rings into spotty areas.

In figure 5/16 a crystal spot pattern can be seen on top of the random ring array.

Finally, figure 5/17 shows the broadening of the bands.

The ring patterns could be due to thermal vibrations of the particles, broadening the crystal array obtained from the dried layer of polystyrene particles. However, as will be shown in the next chapter, the particles

form a very rigid film and so vibrations should be heavily damped.

In some cases sharp rings were observed, figure 5/14. A more likely explanation is that there are two layers of particles, one on each side of liquid film.

5.2.4 Calculations on the Diffraction Patterns

(a) Layer diffraction

Figure 5/18 shows a schematic description of the diffraction occurring from layers of polystyrene latex particles.

For the case of diffraction through a single layer, obeying Bragg's diffraction law, the following equation can be derived :

$$n\lambda = d_{hk} (\sin i + \sin d) \quad ^{122}$$

where n is a positive or negative integer, λ the wavelength of the light, for a red laser this is 632.8 nm, i the angle of incidence, d the angle of diffraction, and d_{hk} is a parameter describing the layer. For a two-dimensional lattice

$$d_{hk} = D \left[\frac{3}{4(h^2 + k^2 - hk)}\right]^{\frac{1}{2}}$$

where h and k are the Miller Indices and D is the interparticular spacing of the particles in the layer. For this system of 4 μm particles which are assumed to be hexagonally close packed this quantity, D, is equal to 3.49 μm.

Diffraction through a single layer of polystyrene, with the laser beam normal to the surface, this becomes

$$\frac{\lambda}{d_{hk}} = -\sin\theta \qquad (1)$$

assuming n is unity. If the diffracted beam then passes through a second layer which diffracts it through an angle ϕ , then the following equation is obeyed:

$$\frac{\lambda}{d'_{hk}} = \sin\theta - \sin(\theta + \phi) \qquad (2)$$

where d'_{hk} is the parameter describing the second layer.

Also the principal beam from the first layer, this is the beam which passes through the first layer without being diffracted, can be diffracted by the second layer. Then

$$\frac{\lambda}{d'_{hk}} = -\sin\theta \qquad (3)$$

Now if the distance between the layers is l and the distance between the second layer and the photographic film, the camera length, is L then

$$-\sin\theta = \frac{R_1}{\sqrt{R_1^2 + L^2}} \qquad (4)$$

where R_1 is the radius of the innermost ring. Combining equations (3) and (4)

$$\frac{\lambda}{d'_{hk}} = \frac{R_1}{\sqrt{R_1^2 + L^2}}$$

assuming $h^2 + k^2 - hk = 1$. Then

$$d'_{hk} = 3.02\ \mu m$$

Table I shows a comparison of R_1 with the radius of the first ring obtained from the diffraction patterns.

The next ring in the diffraction pattern should correspond to diffraction through two layers having the same layer parameter d_{hk}.

Let $d_{hk} = d'_{hk} = 3.02\ \mu m$.

Equating equations (2) and (3)

$$2\sin\theta = \sin(\theta+\phi)$$

and from equation (1)

$$\theta = -12.09^\circ$$

and $$\theta + \phi = -24.09^\circ$$

But $$\tan(\theta+\phi) = \frac{R_2}{L}$$

This band is displaced from the centre of the diffraction pattern by distance r, due to diffraction of the beam through the first layer.

Likewise $$\tan\theta = \frac{r}{l}$$

TABLE I

Photo No.	R_1/cm	Radius Ring 1/cm	% Difference
36	0.343	0.425	24
37	0.343	0.4	17
39	0.450	0.525	17
40	0.429	0.475	11
41	0.407	0.5	23
42	0.386	0.525	36

TABLE II

Photo No.	$R_2 + r$/cm	Radius Ring 2/cm	% Difference
36	0.759	0.825	13
37	0.749	0.7	6
39	0.98	1.0	2
40	0.966	0.9	7
41	0.898	0.925	8
42	0.895	0.925	3

TABLE III

Photo No.	$R_3 + r$/cm	Radius Ring3/cm	% Difference
36	1.135	1.225	8
37	1.125	1.1	2
39	1.473	1.5	2
40	1.435	1.425	0.7
41	1.344	1.45	8
42	1.317	1.35	2.5

Table II shows the calculated radius, $R_2 + r$ and radius of the second band from the diffraction pattern.

The next band must correspond to diffraction through two layers having different layer parameter, d_{hk}.

Now $d_{hk} \neq d'_{hk}$

Let d_{hk} correspond to $h^2 + k^2 - hk = 1$ and d'_{hk} correspond to $h^2 + k^2 - hk = 1.73$. Then d_{hk} is 3.02 μm and d'_{hk} is 1.75 μm. For diffraction through the first layer

$$\frac{\lambda}{d_{hk}} = - \sin\theta$$

and $\theta = - 12.09^\circ$ (as above).

Equation (2) becomes

$$\frac{\lambda}{d'_{hk}} = \sin\theta - \sin(\theta+\phi)$$

Hence $\theta + \phi$ is $- 38.84^\circ$.

Now $\tan(\theta + \phi) = \frac{R_3}{L}$

and $R_3 + r$ is the distance of the band from the centre of the pattern. Table III shows the theoretical and experimental values for the third band in the diffraction pattern.

All radii of the diffraction rings were measured from traces produced on a densitometer for both the layer and bubble diffraction.

(b) Bubble diffraction

Since the patterns observed are rings and not the single crystal spot array obtained from a single layer, it suggested that the bubble was surrounded by a bilayer of particles. If this is the case it would be interesting to calculate the interparticle distances in the bilayer using the above argument used for layer diffraction.

The radius of the second ring, $R_2 + r$ can be described in terms of the camera length L and the interlayer distance, l.

$$R_2 + r = \tan(\theta + \phi) L + \tan\theta l \qquad (5)$$

assuming hexagonally close packed array of particles and that $d_{nk} = d'_{nk}$.

Then $\theta = -12.09^\circ$

and $\theta + \phi = -24.09^\circ$

Table IV shows the calculated interlayer distance for the diffraction patterns obtained.

As negative interlayer distances are found this indicates a large experimental error. As $L \gg l$ and $\theta + \phi > \theta$ then equation (5) becomes

$$R_2 + r \approx \tan(\theta + \phi) L$$

However l is of the order of 1 μm, whereas L is of the order of 2 cm. The interlayer distance, l, lies within the experimental error in measuring the camera length L. Hence the interlayer distance cannot be successfully calculated by this technique.

TABLE IV

Photo No.	Sodium chloride concn/mol dm^{-3}	Interlayer distance/m
8	0.45	5.9×10^{-6}
19	0.25	-6.9×10^{-3}
21	0.25	-8.1×10^{-3}
22	0.25	-9.3×10^{-3}
23	0.1	1.1×10^{-3}
25	0.1	-6.8×10^{-3}
26	0.1	-2.1×10^{-3}

5.2.5 Conclusions

A model for layer diffraction has been formulated and fairly good agreement found between theory and the experimental system. However, due to the inadequacies in the measurement of the camera length the interlayer distance for the bubble diffraction cannot be calculated.

For a completely ordered and matched orientated bilayer two sets of diffraction spots would be seen. However, one set of spots embedded in a diffraction ring was observed. This was probably a consequence of patches of order within the layer causing some miss-match between the orientation of the two layers.

The mere fact that diffraction rings are seen and not single crystal spots strongly suggests that there is a bilayer of polystyrene latex particles separated by a liquid film surrounding each bubble.

CHAPTER 6

SURFACE FORCES ACTING IN THE LATEX FILM

6.1 Surface Pressure

6.1.1 Introduction

The surface tension of a pure liquid, γ, can be defined as the free energy per unit area of the surface. The units of surface tension are mN m^{-1}. When a small amount of an insoluble material is placed at a liquid-air interface it frequently spreads to give a monolayer of molecules in equilibrium with the liquid substrate. If an excess of material is added this will give a bulk phase at the interface in equilibrium with the spread monolayer.

Franklin in 1774 observed the calming effect of oil spread on the surface of the pond at Clapham Common. Rayleigh in 1890 [123] showed that the thickness of an oleic acid film spread on water corresponded to the dimensions of one molecule. Pockels[124] found little change in the surface tension of a spread film of fatty acid until it was confined to an area which corresponded to approximately 20 $\AA^2$/molecule, the Pockels point. After this point had been reached further compression of the film produced a reduction in the surface tension with little change in area.

This difference between the surface tension of the spread film, γ, and that of the pure liquid, γ_o, is defined as the surface pressure, namely,

$$\pi = \gamma_o - \gamma$$

This is a two-dimensional force acting in the plane of the surface. The units of surface pressure are the same as those for surface tension, that is mN m^{-1}.

The character of the spread film can usually be determined from the plot of surface pressure against the area occupied per molecule. There are three broad categories that spread monolayers can be divided into, gas-like,

Figure 6/1 : Langmuir Trough Curves

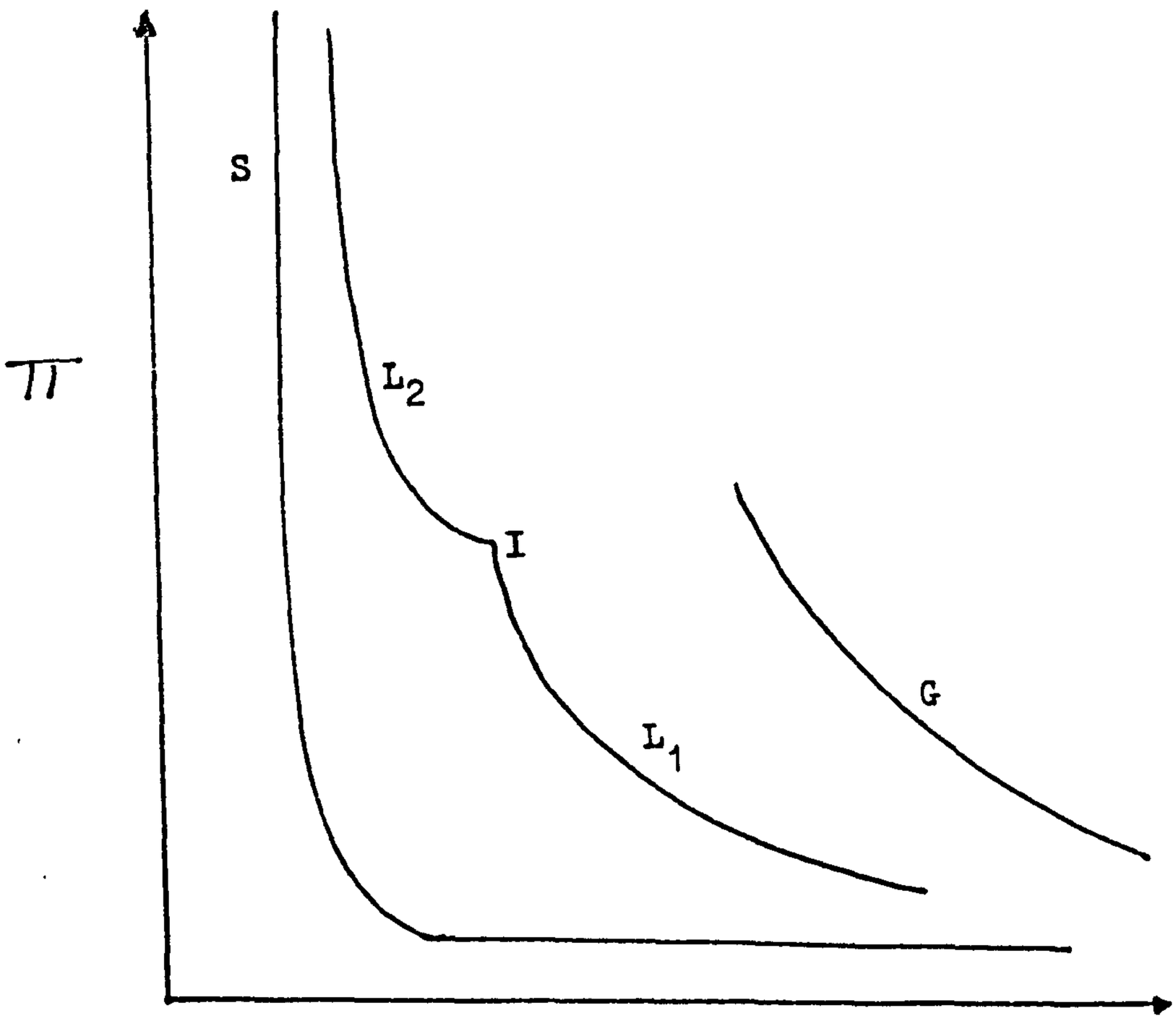

G - gaseous film

L_2 - condensed liquid film

I - intermediate

L_1 - expanded liquid film

S - solid-like film

liquid-like and solid-like.

Gaseous films can behave as a two-dimensional gas, and for this situation an equation of state can be given for the film in the form

$$\pi A = kT$$

where A is the area per molecule, k the Boltzmann constant and T the absolute temperature. However this assumes the intermolecular attraction and co-area both to be negligible; a correction can be introduced to allow for these by writing an equation in the form

$$\pi (A - A_o) = x\,kT$$

where x is a parameter involving cohesive forces and A_o is the co-area correction. The gaseous film is highly expanded. Figure 6/1 shows the behaviour of such a film at a liquid-vapour interface.

Films which are mobile, that is with molecules still free to move in the plane of the interface, but have some degree of molecular attraction, are termed liquid-like. There are two types of liquid films: the liquid-expanded film (L_1) and the liquid-condensed film (L_2). The expanded film shows a high compressibility as defined by

$$-\frac{1}{A}\left(\frac{\partial A}{\partial \pi}\right)_T$$

where A is area and π the surface pressure of the film. On compression the film normally passes through a phase transition (I) into the more compact condensed phase (L_2) as shown in figure 6/1. The latter, at small areas per molecule, has a low compressibility. The transition I represents a phase change from a mobile state to a more condensed one, that is a disorder-order transition.

In solid-like films the molecules form a compact rigid film which has a low compressibility as a result of strong molecular interactions. The solid film behaviour is shown in figure 6/1 as curve S.

Surface pressure can be measured directly by means of a film balance. One of the first balances was devised by Langmuir[125] and consisted of a

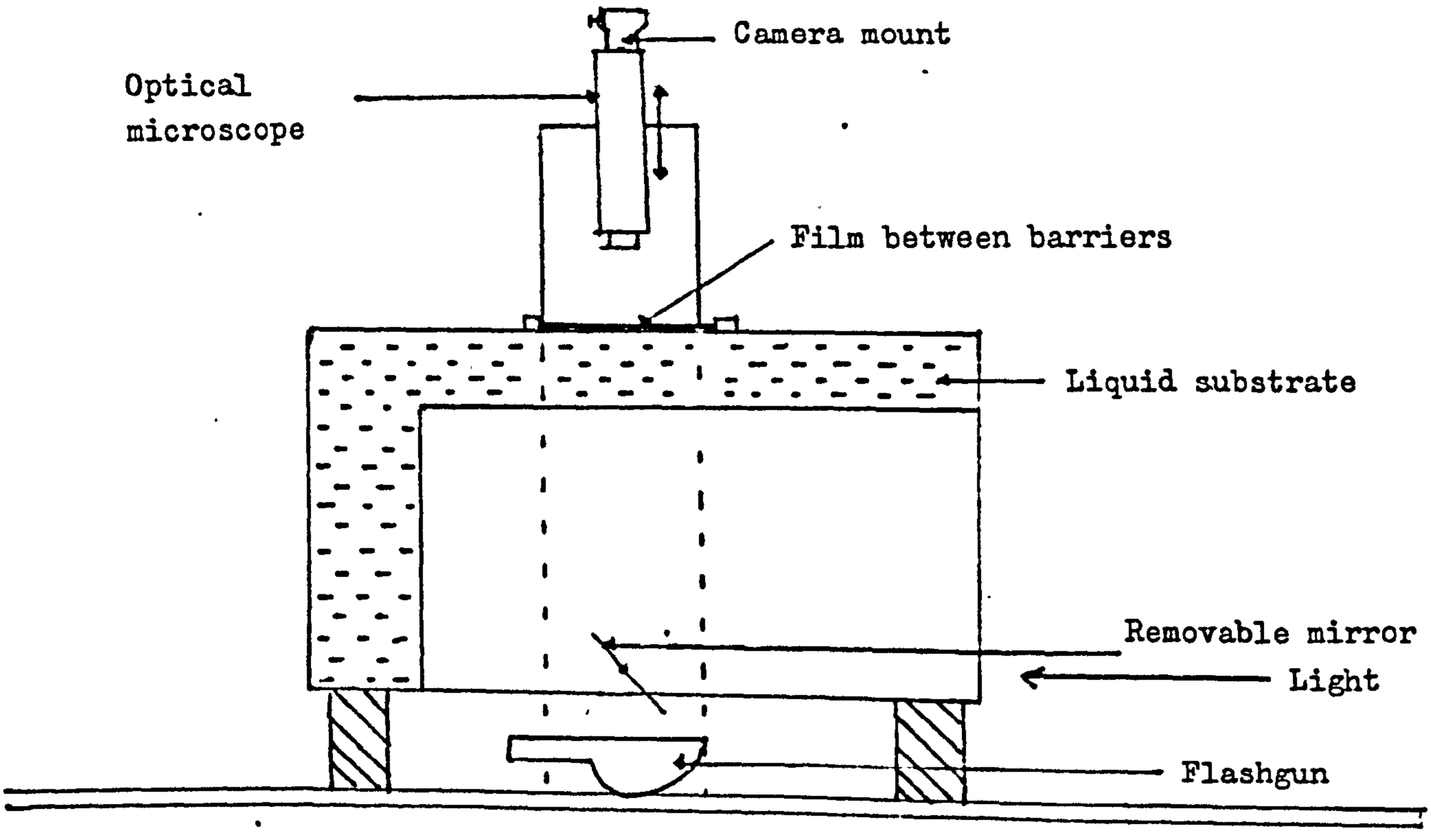

Figure 6/2 : Langmuir Trough

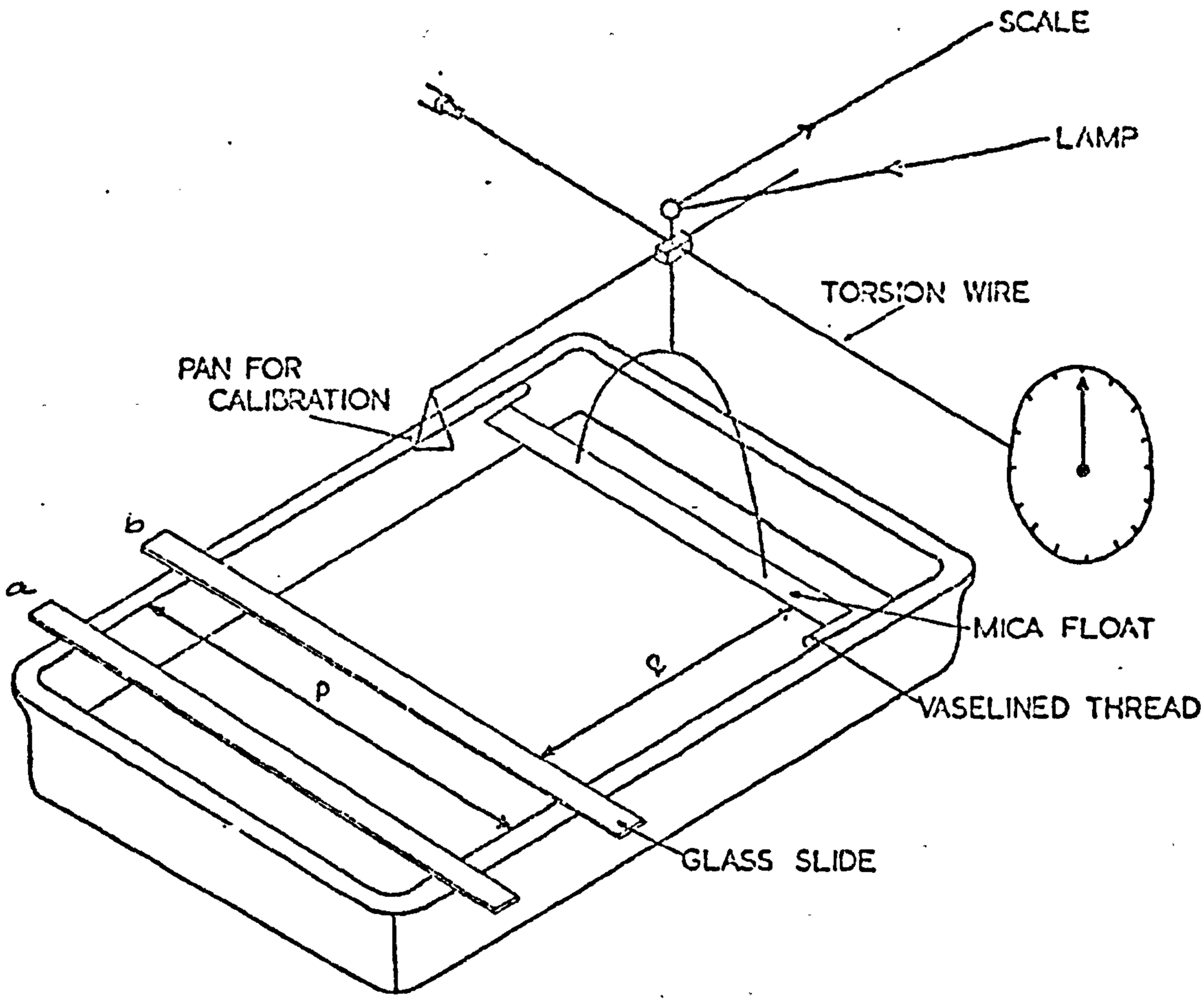

FILM BALANCE.

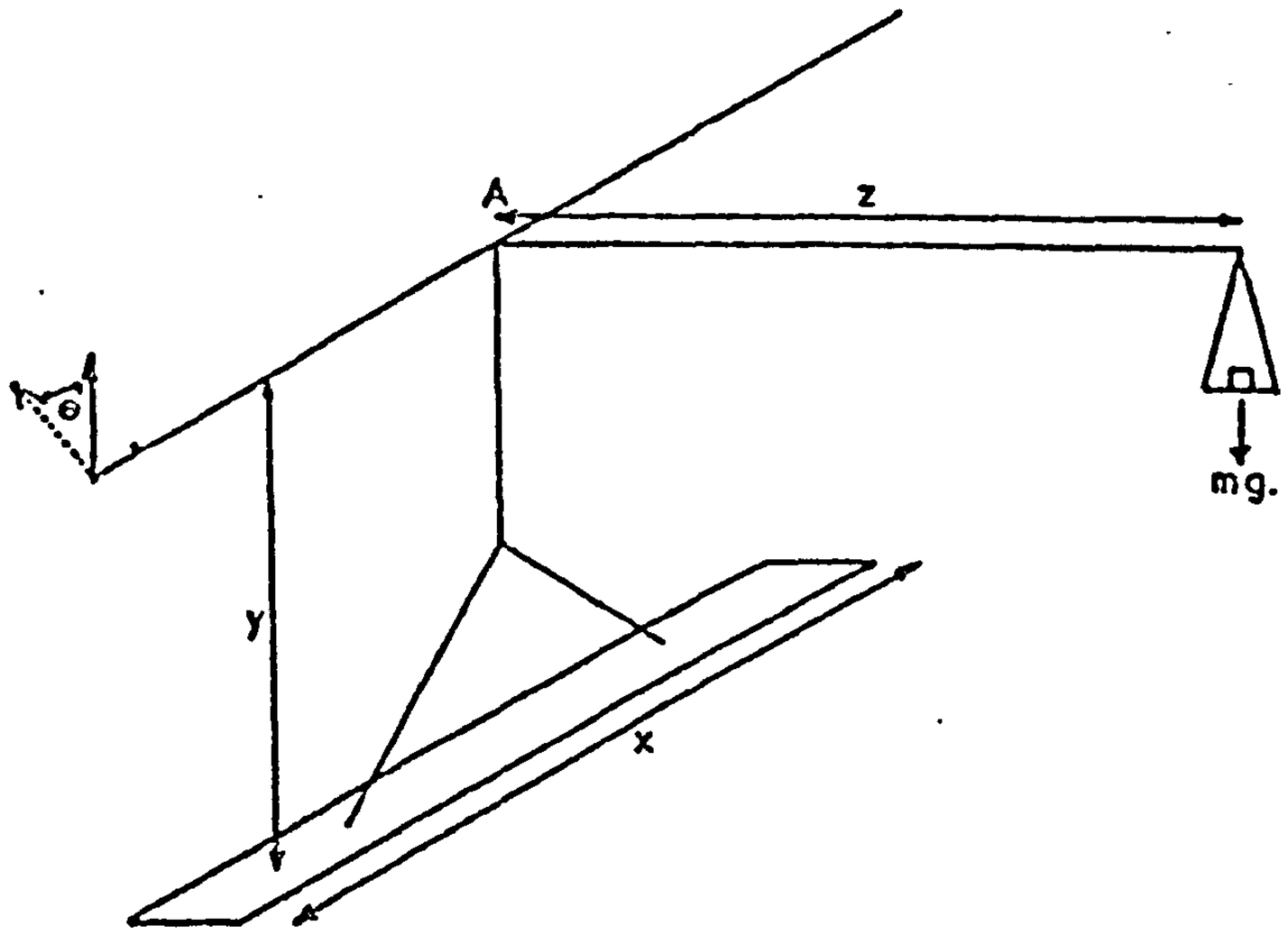

SUSPENSION FOR FILM BALANCE.

Figure 6/3 : The Langmuir Trough

horizontal float suspended from an arm attached to a torsion wire, the latter forming part of a torsion balance. The balance measured the difference between the film coated surface on one side and the clean surface on the other side of the float.

In the present work the formation of surface films from solid particles was investigated. The particles used were polystyrene spheres which had been formed as polymer latices. Techniques were devised for spreading the particles as a monolayer and the compression behaviour of the particles in the surface was observed under various conditions.

6.1.2 Experimental

A perspex trough as described in diagram 6/2 was used as this was transparent to light. The trough was placed on a platform above an optical bench and the light passed up through the trough from underneath. The height of each leg of the support platform was adjusted until the trough was horizontal. The pan of the torsion balance was then counterbalanced with the weights until the boom was horizontal. The stirrup was attached to the mica float with melted paraffin wax. Vaselined threads were then attached lightly with wax to the float and the sides of the trough so that they formed equal and opposite areas, Guastella[126]. A solution of paraffin wax in petroleum ether was applied to the sides of the trough and the mica float, to increase their hydrophobicity. The movable barriers were also made from perspex.

Before commencing an experiment the barriers were tested for leaks. This was achieved by filling the trough with once distilled water until the liquid level was just above the sides of the trough. Talc was then sprinkled on the liquid surface close to the float. A barrier was placed on the surface and moved slowly towards the float, see figure 6/3.

When leaks occurred the talc could be seen streaming past the vaselined threads. If leakage occurred the threads were replaced and retested.

The trough was filled with the salt solution required. Then the surface of the liquid was cleaned by sweeping the areas on both sides of the float with perspex barriers. Two barriers shown as a and b in figure 6/3 were placed in front of the float, roughly 10 cm apart. The area within the barriers was used to spread polystyrene latex particles on the liquid surface.

(i) Procedures for spreading latex particles

Two different methods of spreading the latex particles were used. In one case freeze-dried polystyrene particles and in the other a dispersion of latex in ethanol and water were applied to the trough.

(a) Freeze-dried latex

The polystyrene latex JC, mean diameter 3.89 μm, was freeze dried using a container with a glass cold finger, containing liquid nitrogen, inserted in it. The latex suspension in water was sprayed onto the inner walls of the container which was placed in an ethanol/solid carbon dioxide bath. The apparatus was evacuated, using a rotary pump, for twenty-four hours.

The freeze-dried latex was applied to the trough by means of a glass rod. A clean rod was coated with dried latex and then one rod was dipped in and out of the surface of the substrate until the majority of the particles floated off. This was repeated several times until a compact film of several cm^2 was visible on the surface of the trough.

The salt solution used as the substrate lay in the range 10^{-1} to 10^{-5} mol dm^{-3} sodium chloride.

The layer formed was not very good; clumps of latex particles could be seen on the surface. It required a lot of patience, on behalf of the operator, to suck up any badly spread layers and apply more latex until eventually a relatively good layer was formed. A more serious problem was that there was no method of determining the amount of latex on the surface except by taking photographs of the layer and finding the packing fraction from them.

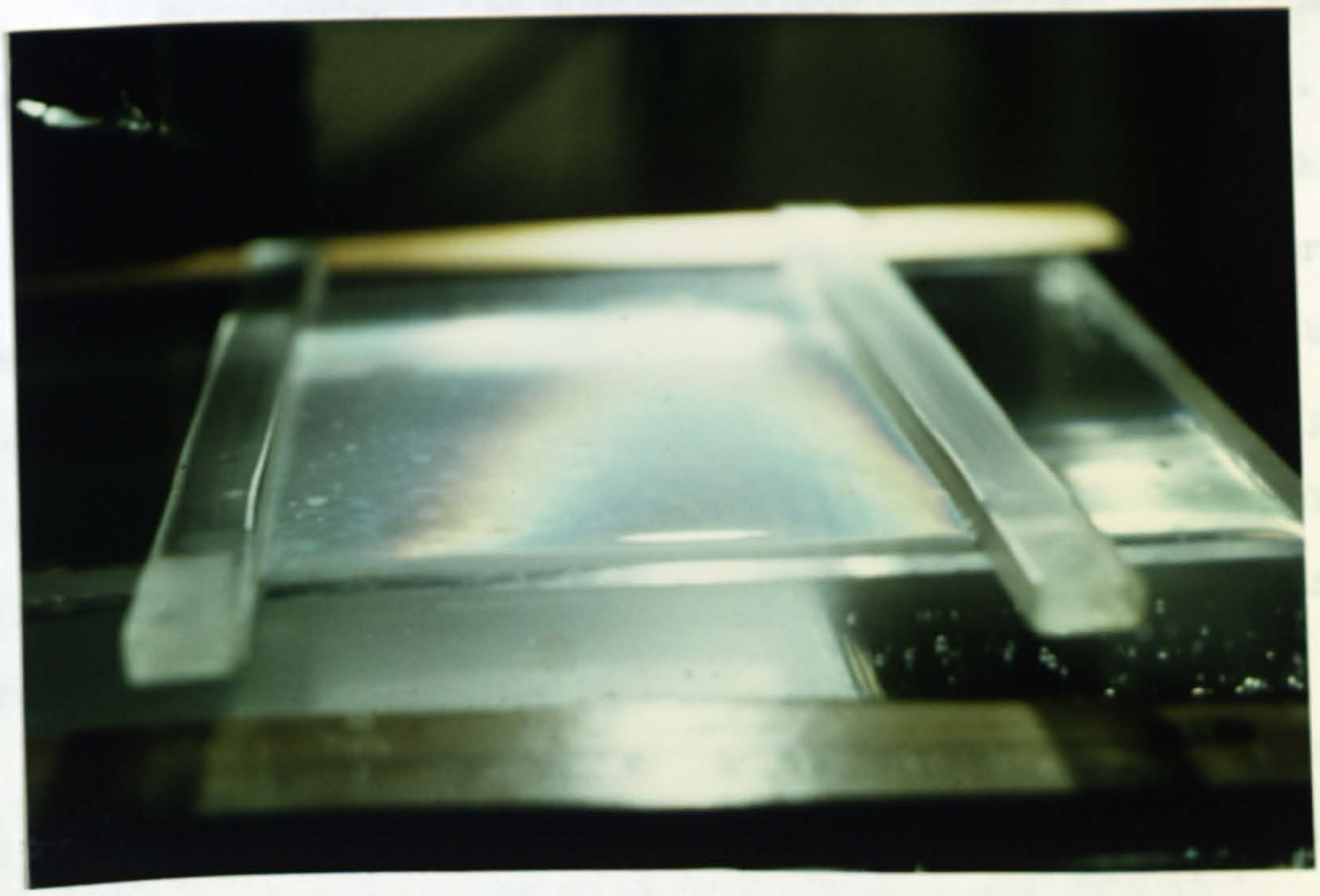

Figure 6/4: A Layer of Polystyrene Particles splitting White Light into its Component Colours

(b) Latex dispersion in an ethanol and water mixture

A concentrated suspension of latex in water, about 13% w/v, was mixed in a 1:1 ratio, by volume, with ethanol. The monodisperse latices used for these runs were JC, S67 and RB55. Latex systems with mixed particle sizes were also studied; these were 1:1 mixtures of latex JC with S67, JC with S17, and JC with RB55.

The latex in the ethanol-water mixture was then applied in 50 μl amounts to the surface of the trough by a Pipetman P200. The pipette was held close to the surface at the moment of detachment of the drop.

The substrate for all these runs was 0.5 mol dm^{-3} sodium chloride.

A very good layer of polystyrene particles was formed effortlessly. Light from above the trough was split into its component colours by the layer, figure 6/4. The regular packing of the polystyrene latex particles on the surface acted as a diffraction grating. No 'dry' solid clumps of polystyrene were seen. However some of the particles from the dispersion when it was dropped onto the surface did appear to sink.

Two methods were used to calculate the amount of latex on the trough: one using the volume added and the other using the packing fraction of the particles as calculated from photographs of the layer. This enabled the amount of polystyrene latex which sank to be estimated.

(ii) Compression of the film

After the layer had been spread by one of these methods it was compressed by moving the two barriers a, b, figure 6/3, towards each other. A photograph of the surface layer using a microscope magnification of 400 x was taken. Illumination was provided by a flash gun placed under the trough. The film used was Ilford Pan F, A.S.A.50, which was developed using Promicrol to increase the film speed. The area of the compact layer was also measured.

The nearest barrier, b, to the float was carefully removed (see figure 6/3); the area of clean surface behind the float reswept. The

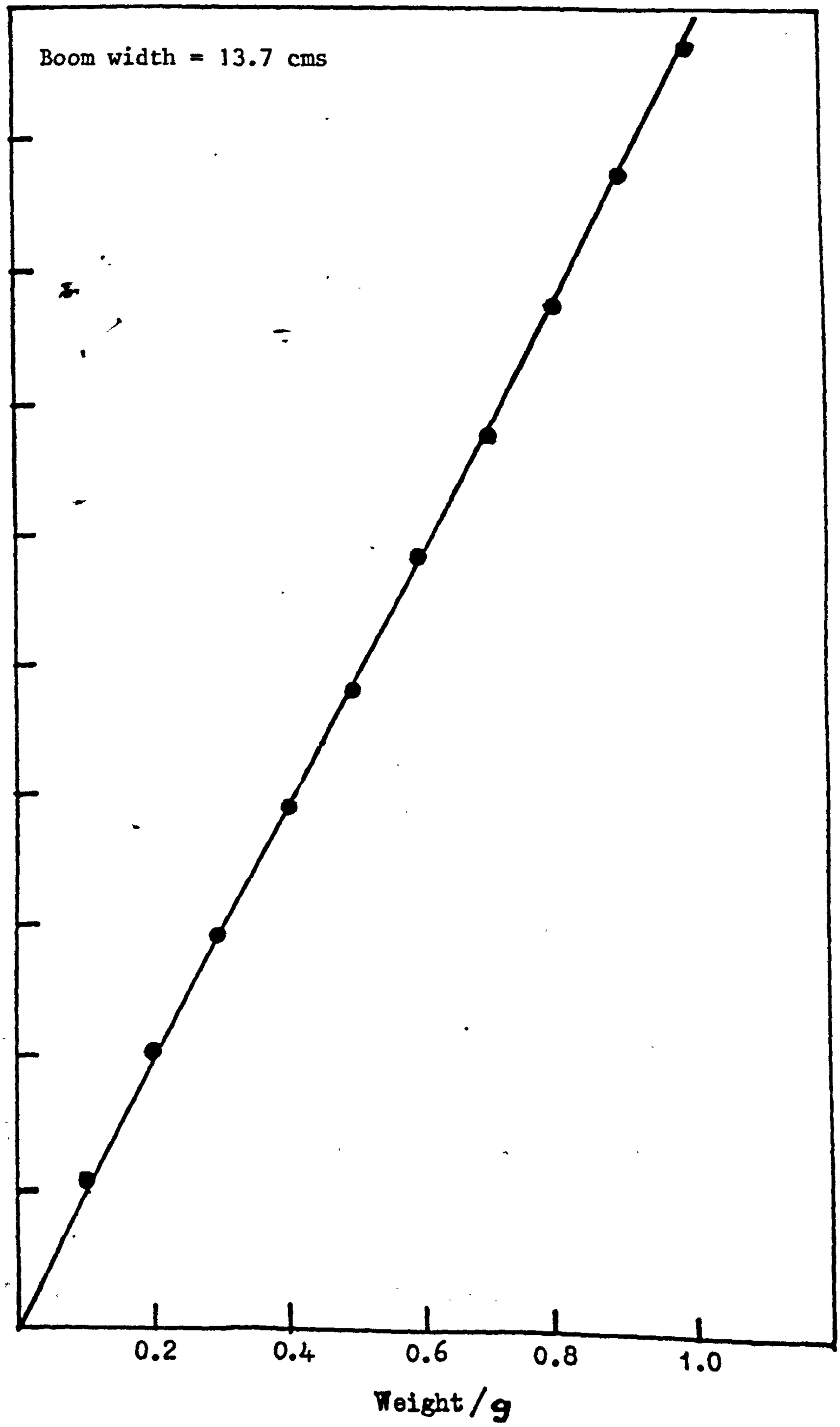

Figure 6/5 : Calibration Curve

remaining barrier, a, in front of the mica was slowly moved towards the float until a compact film was formed against it. Any contamination on the surface was removed by gentle suction.

The barrier a was then moved away from the float to a reference distance. The film was allowed to spread out to cover the larger area. Movement of the torsion head was observed by means of a lamp and scale, see figure 6/3. At this point the barrier was carefully brought towards the float. As soon as any deflection of the float was seen, preferably as small as possible, the barrier was stopped and the force required to bring the float back to the horizontal was determined. The distance of the barrier from the float was recorded before moving it a further small distance. This procedure was repeated until folding of the surface film was observed visually.

6.1.3 Calibration of the wire

The torsional coefficient of the wire, K, was determined by placing weights, in the range 0.1 - 1 g, on the pan provided, see figure 6/3. After each addition the force required on the torsion wire to return the float to the horizontal was recorded as a deflection on a circular scale. A graph of the deflection of the float from the horizontal against the weight added was drawn. The slope of the line is equivalent to the torsional constant for the wire, figure 6/5.

Certain dimensions of the trough were also measured. These were the width of the trough, q, the distance from the torsion wire to the point of suspension of the scale pan, z, the distance from the torsion wire to the mica float, y, and the length of mica float, x. The surface pressure, Π, was determined from the torque acting on the float, using the expression

$$\Pi = \frac{zg}{K\,xy}\,\theta$$

where θ is the deflection of the float.

6.1.4 Calculations

(i) Calculations on the Langmuir trough results

(a) Determination of packing fraction

Several photographs of each layer were taken, via the microscope, and from these the average packing fraction from each run was determined.

For each photograph a random area, approximately 2×10^{-8} m^2, was drawn so as to include a number of whole polystyrene particles. Using a Carl Zeiss particle size analyser Type TGZ3, the number and size of the particles were determined. The particle size distribution was determined via a histogram. The area was traced onto tracing paper which was then weighed; hence the area of the layer, A_L, could be determined. Knowing the average particle diameter and the total number of particles, the total particle area was determined, A_{PSL}. Now the packing fraction ϕ can be defined as

$$\phi = \frac{A_{PSL}}{A_L}$$

(b) The area term

The area of the trough occupied by the film, A, was given by the product of the width of the trough, q, and the length of the trough between the barrier and the float, p, figure 6/3. To normalise each run with regard to another this area, A, was then divided by the cross-sectional area of the polystyrene particles, A^o, as given by

$$A^o = N \pi R^2$$

where N is the number of particles and R the number average particle radius. Thus the normalised area $\bar{A}$ was obtained as a dimensionless quantity defined by the expression

$$\bar{A} = \frac{A}{A^o}$$

The total cross-sectional area of polystyrene can be defined as

$$A^o = A' \bar{\phi}$$

where A' is the area of the compact film and $\bar{\phi}$ is the packing fraction of the compact film.

Therefore when $\bar{A}$ is equal to $1/\phi$ the film is compact

(c) Calculation of the number of latex particles on the surface from the packing fraction and the volume of suspension added

The total surface area of the polystyrene latex particles, A^o, can be calculated as described above. The number of particles on the surface, N, is then given by

$$N = \frac{A^o}{\pi R^2}$$

where R is the average particle radius as determined from the electron micrographs, section 3.1.1.

From the volume of the suspension added to the surface V^1, the volume of the polystyrene particles V^o can be calculated, knowing the volume fraction, V, and hence the number of particles added to the trough, N^1, can be determined :

$$V = \frac{V^o}{V^1} \times 100$$

$$N^1 = \frac{3V^o}{4\pi R^3}$$

By comparing these two numbers the percentage of latex particles which sank was found as

$$\% \text{ sinkage} = \frac{N^1 - N}{N^1} \times 100$$

For the single latex systems the percentage sinkage was found to be 7% for the large latex JC and 86% for the harder to resolve smaller latex S67.

(ii) <u>Refraction of a parallel beam of light through a polystyrene latex particle</u>

The particles on the surface of the trough were photographed by using a flash placed under the air/liquid interface. However for observing the layer down the microscope a narrow parallel light beam was used. Figure 6/11 shows the difference between the appearance of the particular

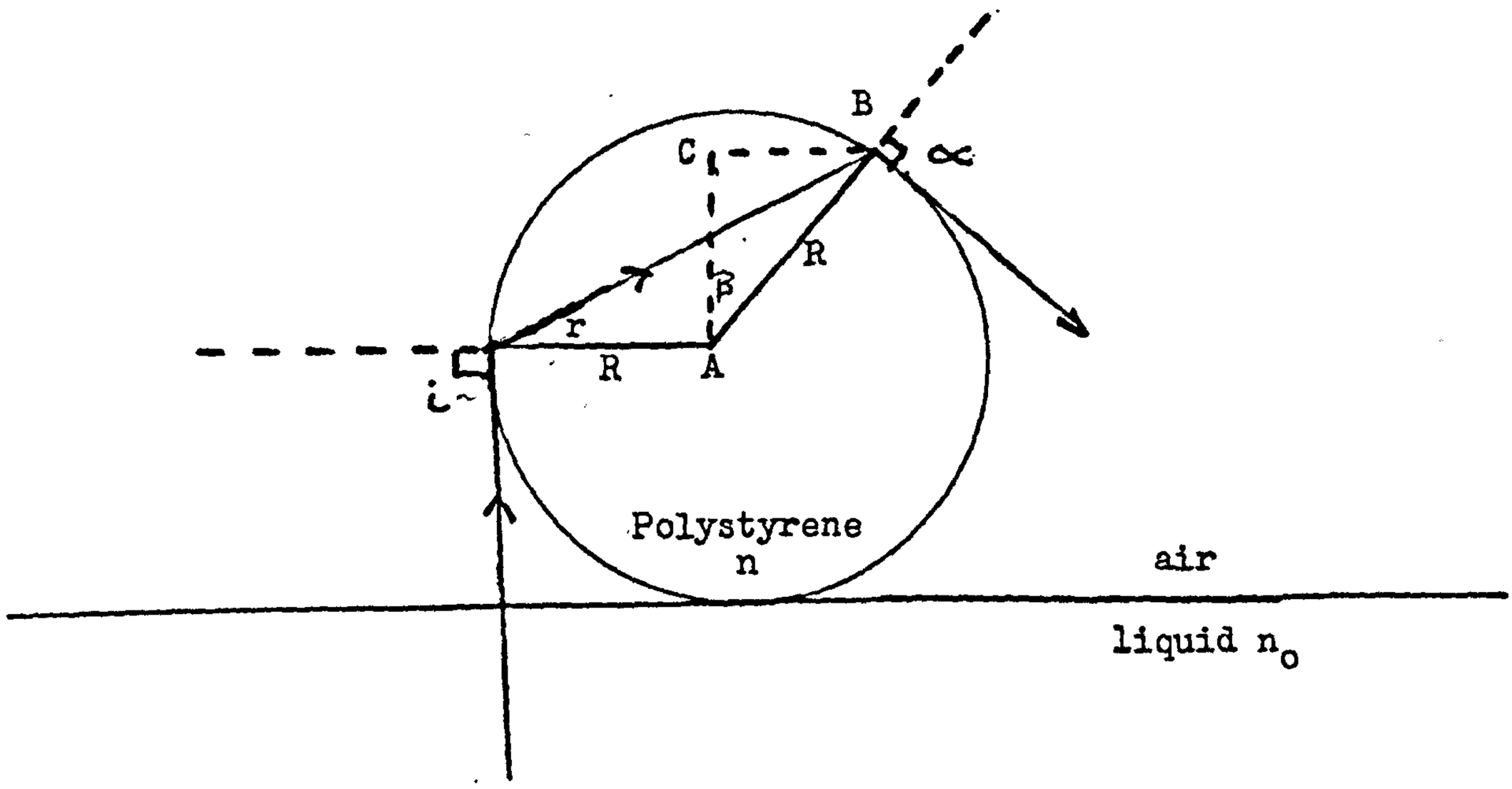

Figure 6/6 : Refraction of Light through a Polystyrene Latex Particle in Air

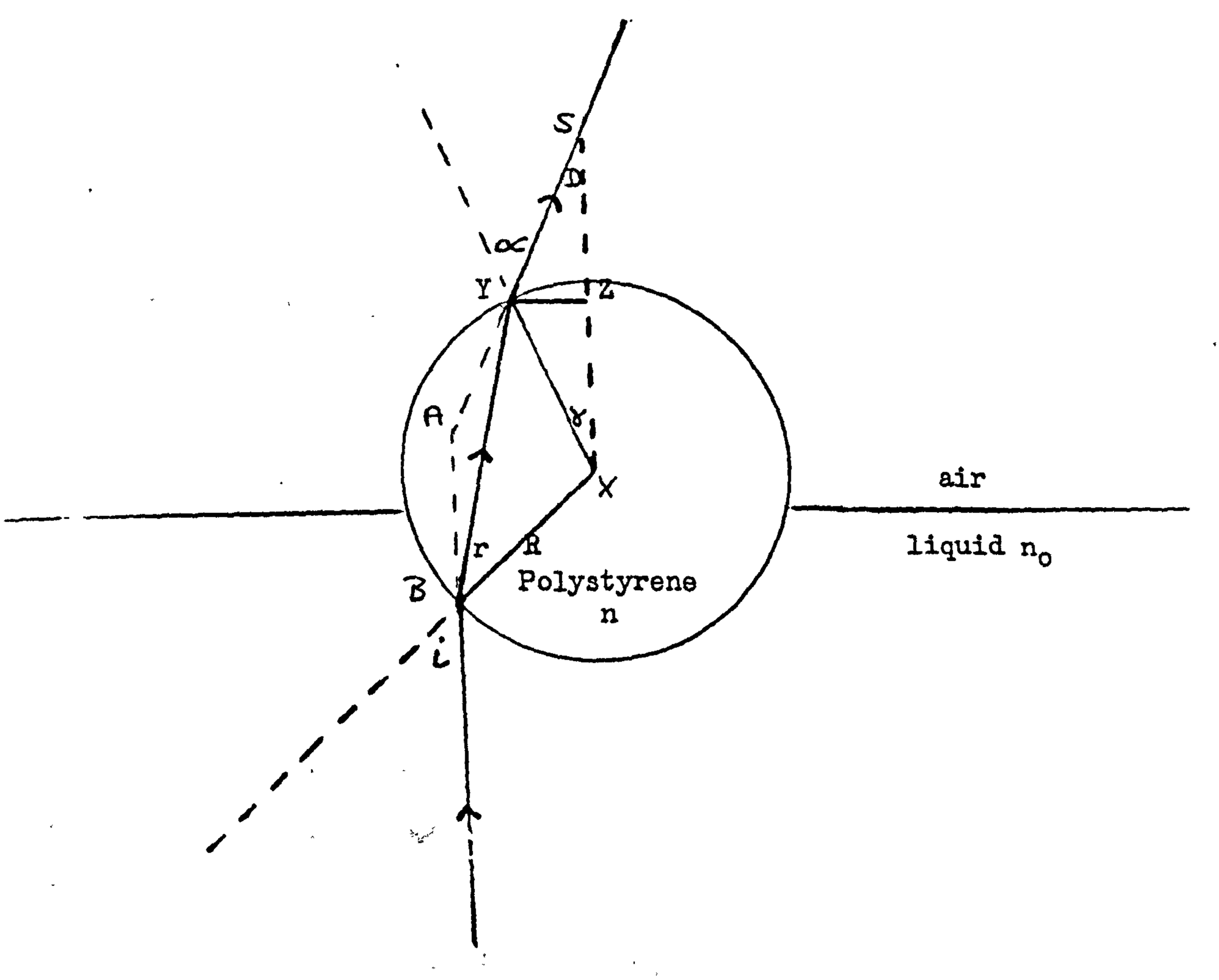

Figure 6/7 : Refraction of Light through a Polystyrene Latex Particle in Liquid

layer using the two different types of illumination. As can be seen the parallel light beam causes a bright area in the centre of the particle to appear, whereas the wider source of illumination, the flash gun, does not. The next two sections deal with refraction of a light beam through a polystyrene particle with regard to where the liquid/air interface is with respect to the particle.

(a) Polystyrene particle in air

For total internal reflection of the light beam, in the particle, the angle of emergence, α, of the beam must be equal to or greater than 90°. It follows that for a particle in air, refractive index of 1, the angle of incidence, i, must also be equal to 90°, figure 6/6.

By Snell's law : $\sin i = n \sin r$

and $n \sin r = \sin \alpha$

where n is the refractive index for polystyrene and i, r are the angles of incidence and refraction respectively.

The radius of the bright area is equivalent to CB and can be defined in terms of the angle β in triangle ABC :

$$\beta = 90 - 2r$$

$$CB = R \sin \beta$$

Since for polystyrene n = 1.6005

$$CB = 0.22 R$$

(b) Polystyrene latex particle partly submerged in liquid

It will be shown, section 9.2.1, that for particles of 4 μm diameter, and smaller, the deformation of the meniscus at the point of contact with the particle surface is minute. Therefore the profile of the liquid surface can be assumed to be planar.

A similar treatment to the above can be used. Here the angle, γ, defines the radius, YZ, of the bright area, figure 6/7. At the latex-water interface

$$n_o \sin i = n \sin r$$

where n_o is the refractive index of the liquid.

At the latex-air interface

$$n \sin r = \sin \alpha$$

$\triangle$ XYS $\qquad \gamma = \alpha - D$

$\triangle$ ABY $\qquad D = \alpha + i - 2r$

Therefore for polystyrene n = 1.6005 and for water n_o = 1.3337, hence

$$YZ = 0.481\,R$$

This is the maximum radius of the bright area. Therefore if the liquid/air interface is halfway, or greater, up the particle the bright area will still have the same radius.

From the photographs of the layer it can be seen that the diameter of the bright area is roughly a half that of the particle. Therefore it can be concluded that the latex particle is wetted by the liquid but the precise position of the meniscus cannot be calculated.

6.1.5 Results

(i) Freeze-dried latex

Typical photographs of the particulate surface films are shown in figures 6/8 and 6/9. Table 1 shows the average packing fraction calculated for each run. The theoretical packing fraction for hexagonally close packed particles in a monolayer is 0.907. The packing fraction appears to increase with salt concentration, the highest value attained being 0.625.

TABLE 1

Variation of Packing Fraction with Salt Concentration

Salt concentration /mol dm^{-3}	Packing fraction of compact film
10^{-5}	0.35
10^{-4}	0.39
10^{-3}	0.53
10^{-1}	0.625

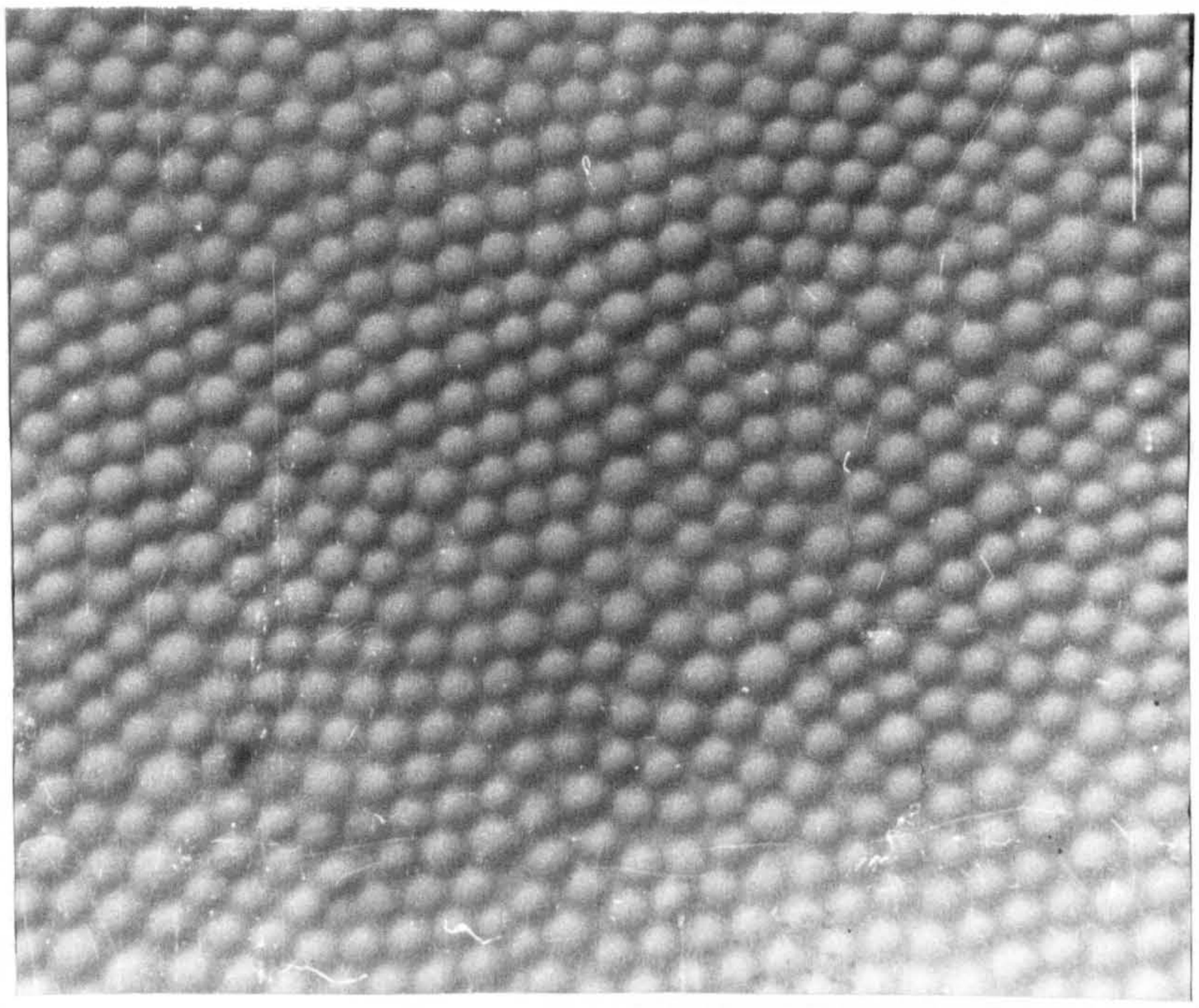

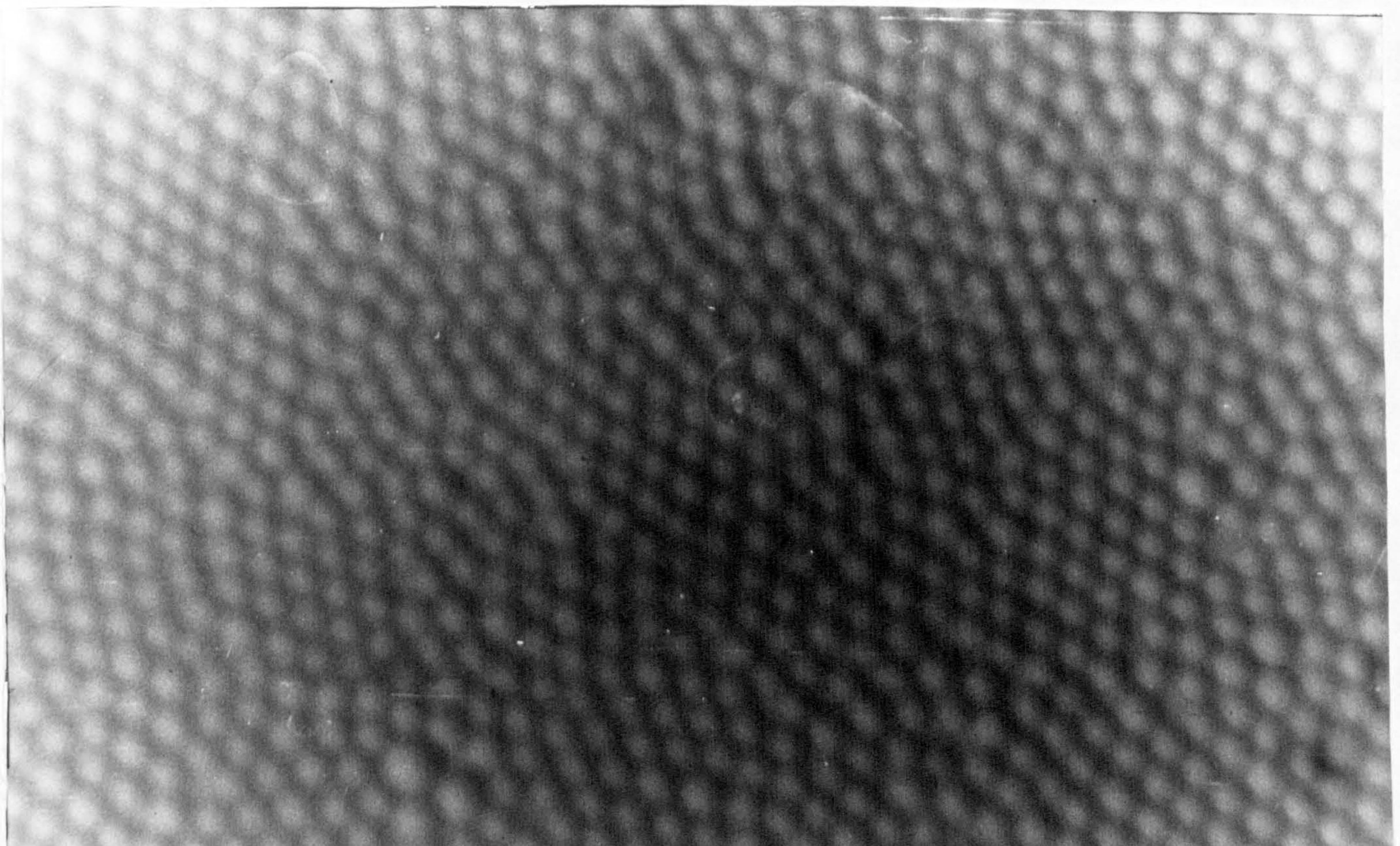

Figures 6/8 & 6/9: Latex Particles on 10^{-3} mol dm^{-3} Sodium Chloride

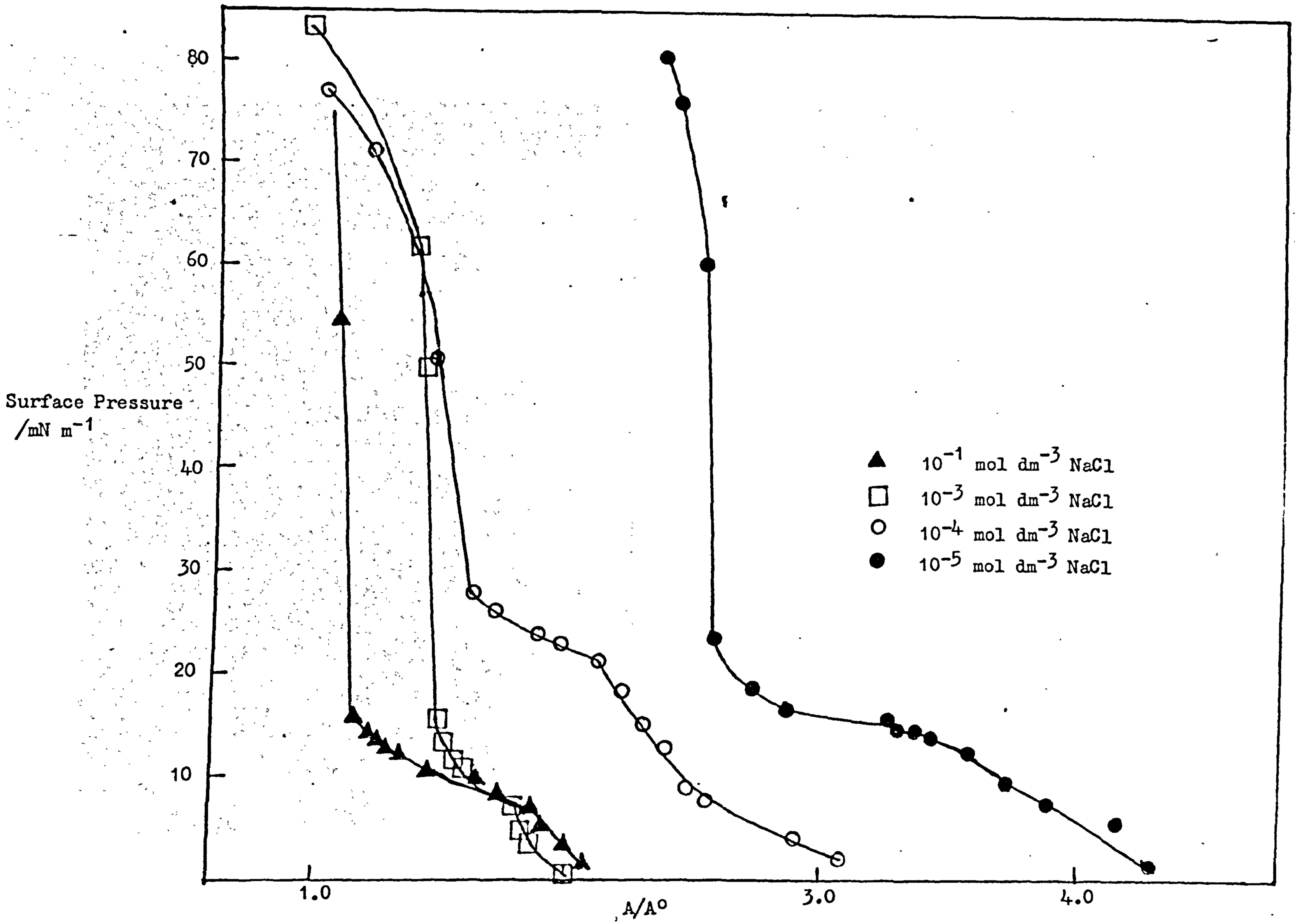

Figure 6/10 : Variation of Surface Pressure with Area at different sodium chloride concentrations for the freeze-dried samples

Figure 6/11 : A Layer of Latex JC on 0.5 mol dm^{-3} Sodium Chloride

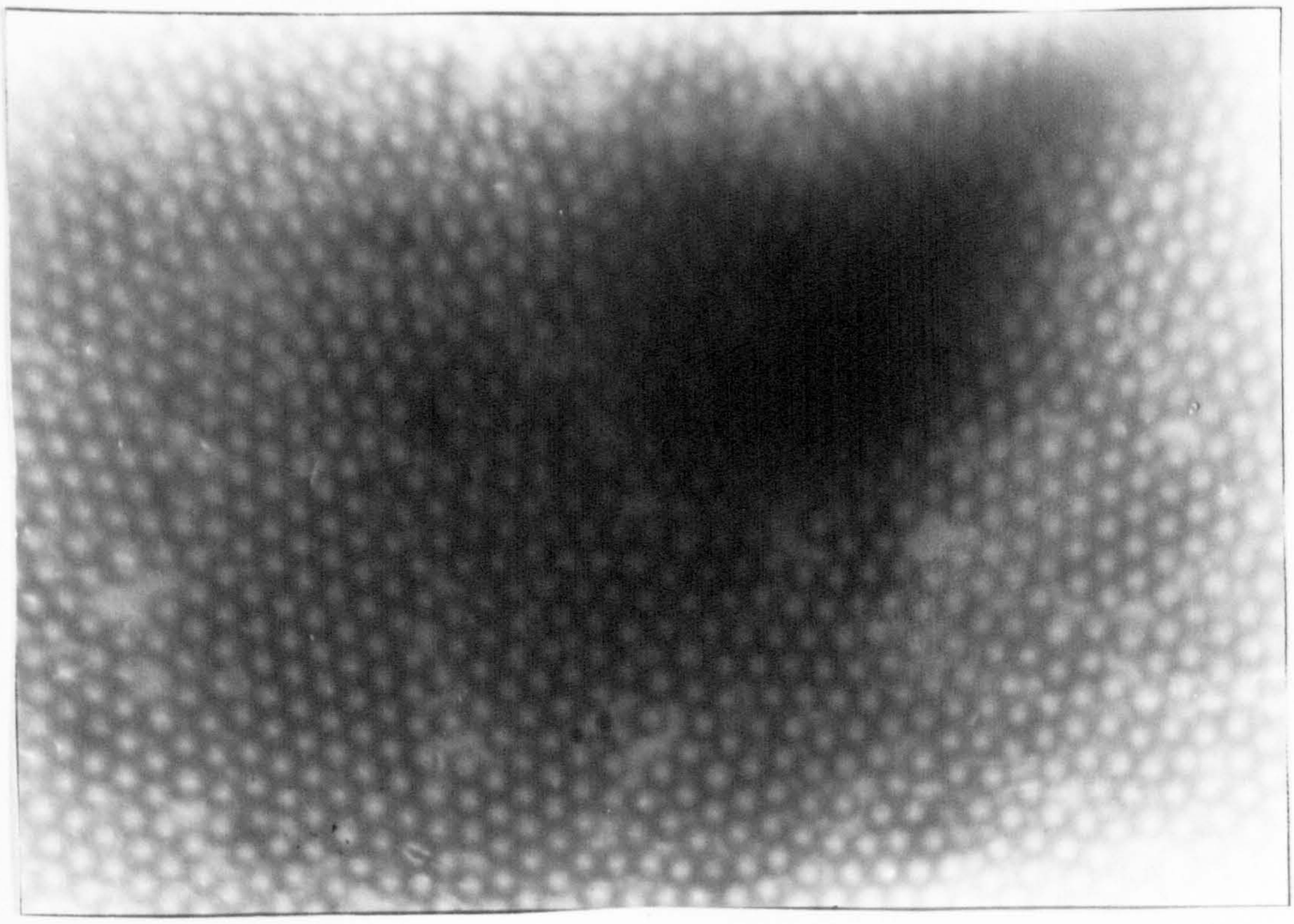

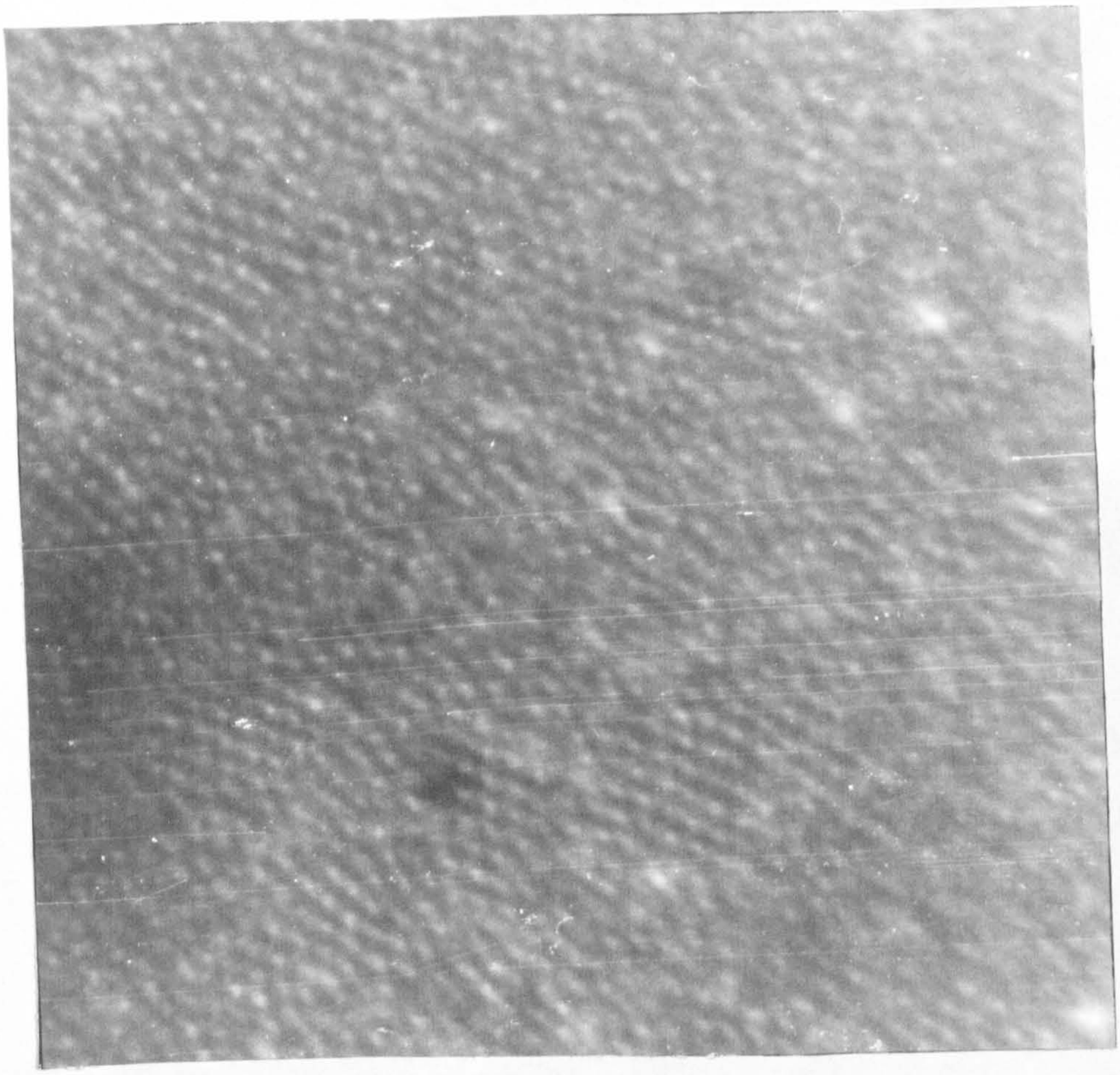

Figure 6/12: A Layer of Latex S67 on 0.5 mol dm^{-3} Sodium Chloride

Figure 6/13 : A Layer of Latex RB55 on 0.5 mol dm^{-3} Sodium Chloride

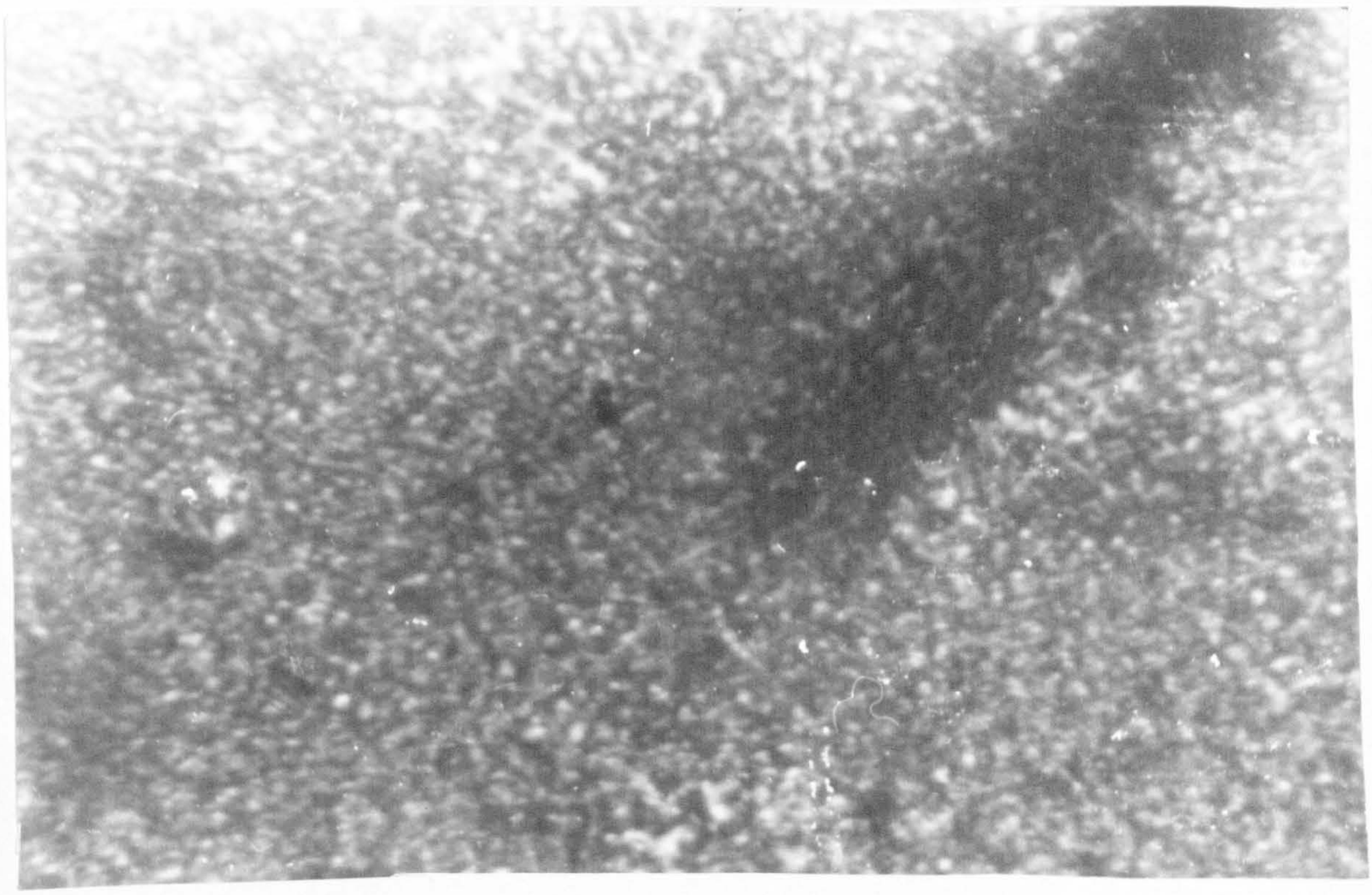

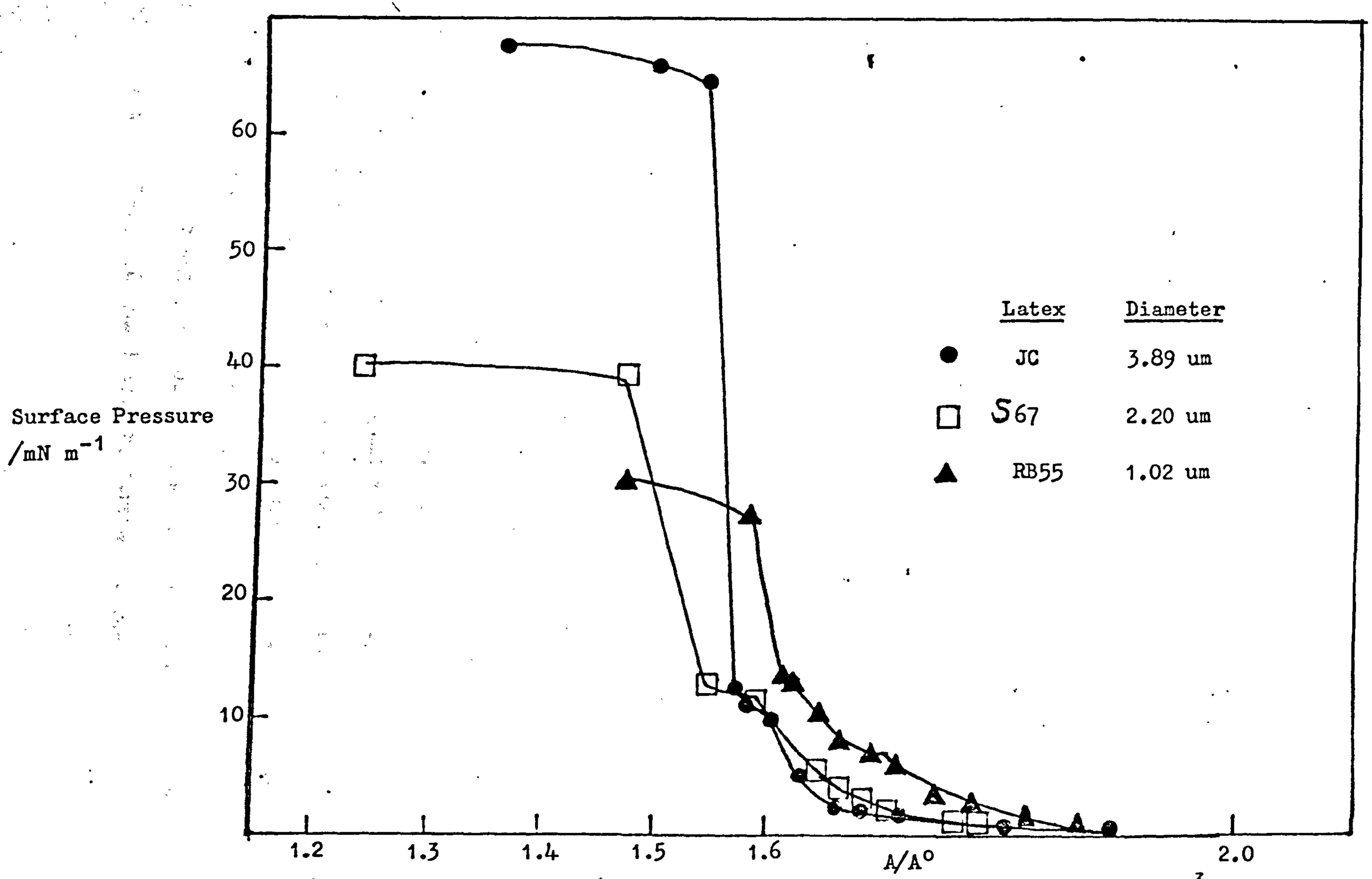

Figure 6/14 : Surface Pressure / area curves for different Latices on 0.5 mol dm^{-3} sodium chloride

Figure 6/10 summarises the π-A curves found for different sodium chloride solutions and a layer of polystyrene particles of diameter 3.89 μm. All the runs show a transition through an intermediate phase. The transition of a mobile latex film to a compact, non-compressible, solid-like film takes place over a larger range of area the more dilute the salt solution. Before the film broke, for all the curves, surface pressures as high as 80 mN m^{-1} were found. These high surface pressures indicated the high two-dimensional compressional strength of the films, as measured by the surface compressibility, $-\frac{1}{A}\left(\frac{\partial A}{\partial \pi}\right)_T$.

(ii) Latex suspended in water/ethanol

(a) Single latex systems

The effect of varying the size of the latex particle was established using this spreading technique. The photographs in figure 6/11 show the packing of latex JC, diameter 3.89 μm, on 0.5 mol dm^{-3} sodium chloride as the substrate. The packing fraction was 0.68.

Photographs of the layers of S67, diameter 2.2 μm, and RB55, diameter 1.05 μm, are shown in figures 6/12 and 6/13. The microscope was at the limit of its resolution in focusing on these small particles. Accurate packing fractions could not be determined for them. Since these latices were monodisperse it seems reasonable to assume they would be hexagonally close-packed and the packing fractions were the same as for latex JC.

Figure 6/14 summarises the runs for the three different latex sizes on 0.5 mol dm^{-3} sodium chloride. For all three a change in packing of the particles from a mobile film to a compact film was observed. The intermediate state for all three was formed at the same surface pressure within experimental error. The only appreciable difference between these three was the pressure at which the film ruptured. This increased with particle size in the order RB55, S67 and latex JC. This indicates that the larger polystyrene particles, 3.89 μm diameter, form a stronger condensed film

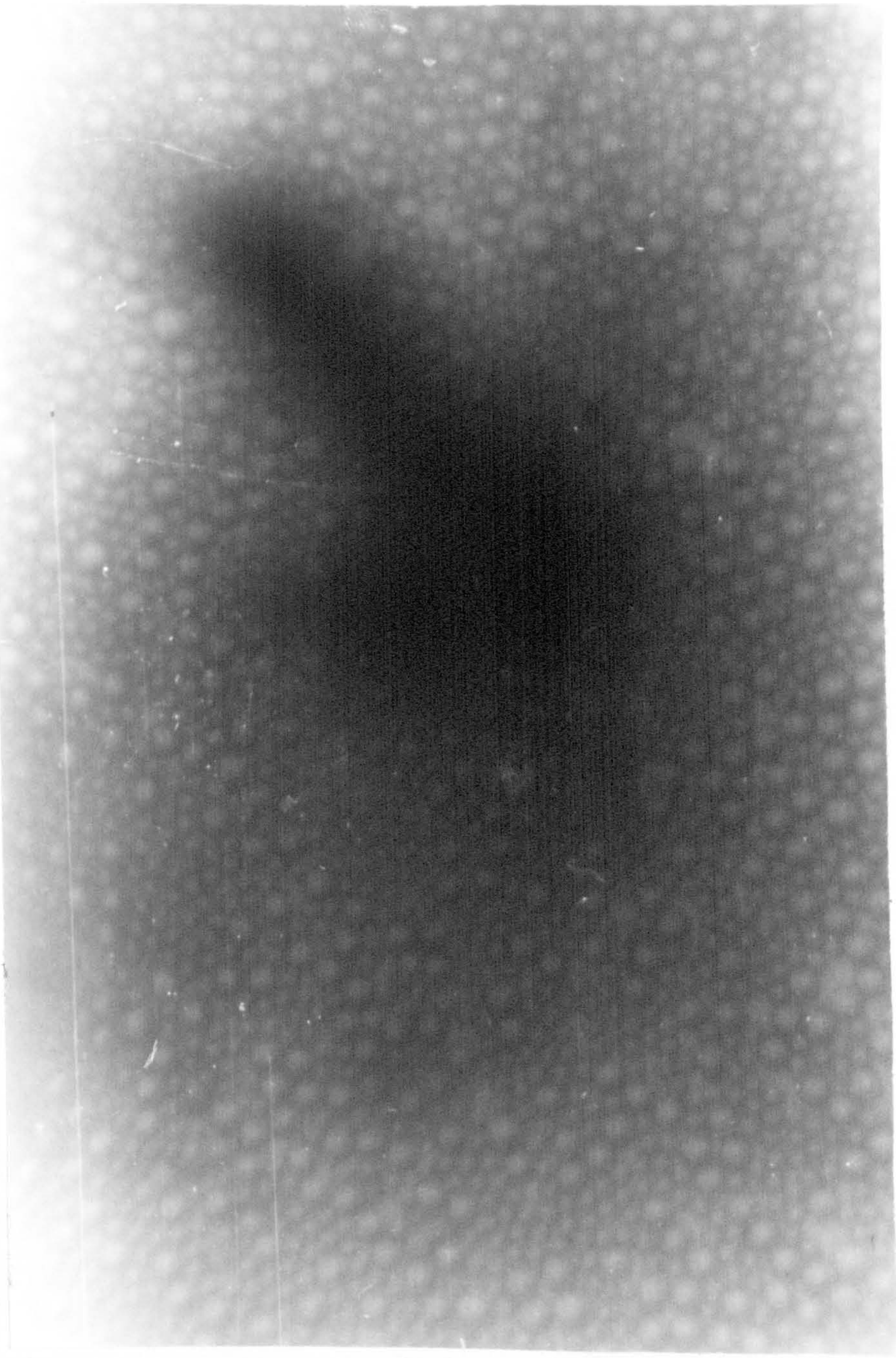

Figure 6/15 : A Layer of Latex JC/S67 on 0.5 mol dm^{-3} Sodium Chloride

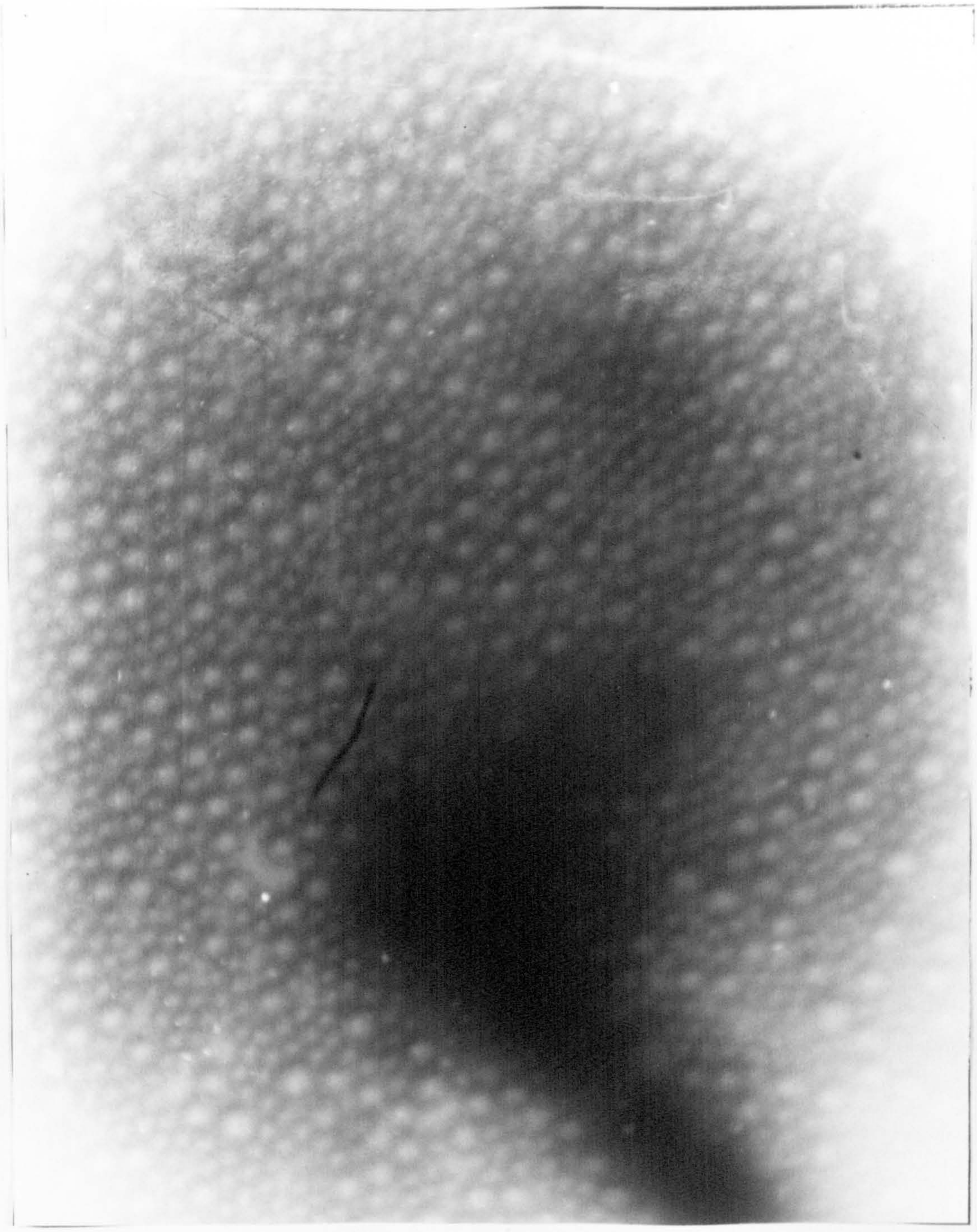

Figure 6/16 : A Layer of Latex JC/S67 on 0.5 mol dm^{-3} Sodium Chloride

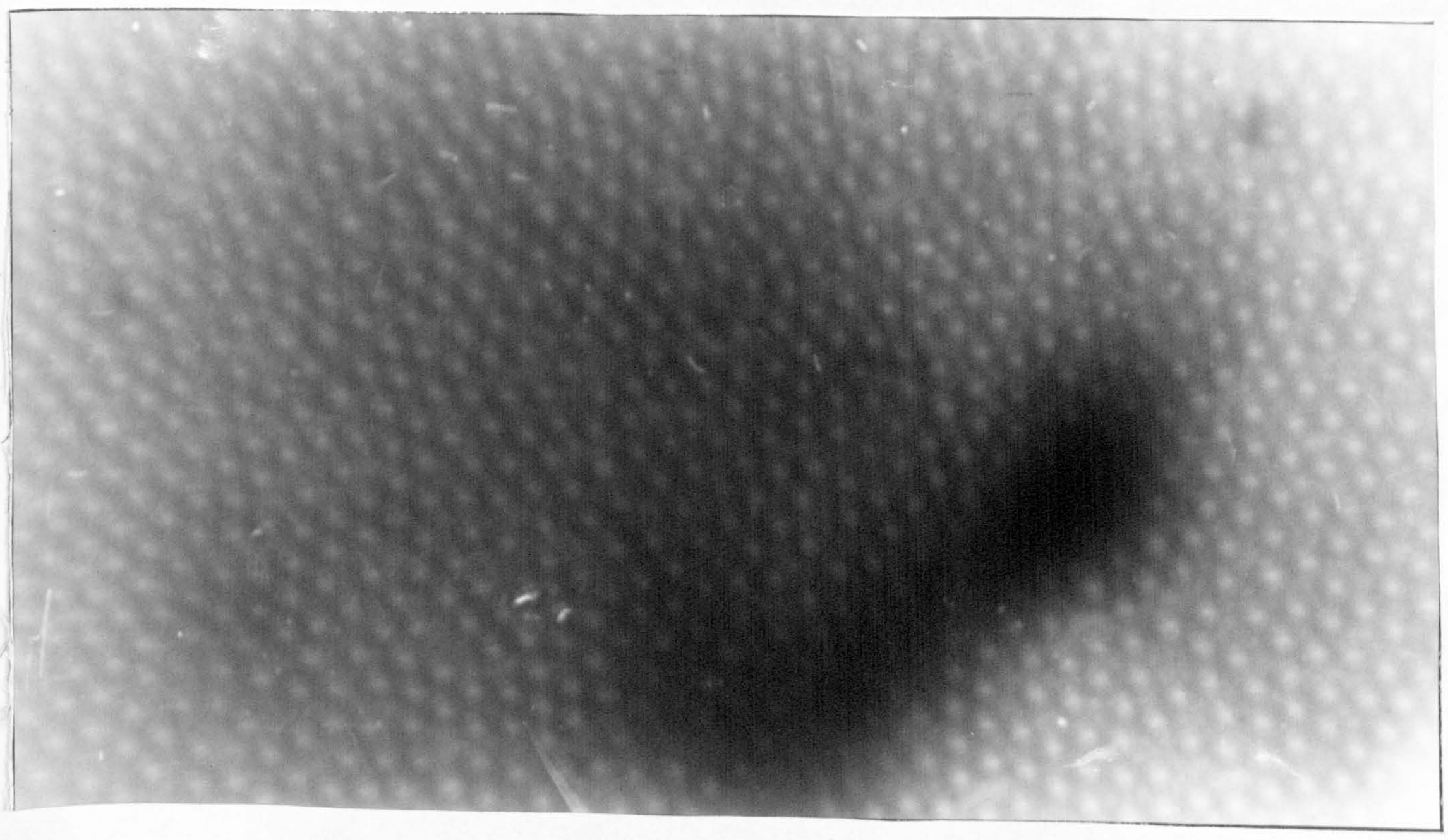

Figure 6/17 : A Layer of Latex JC/S17 on 0.5 mol dm^{-3} Sodium Chloride

Figures 6/18 & 6/19 : A Layer of Latex JC/RB55 on 0.5 mol dm^{-3} Sodium Chloride

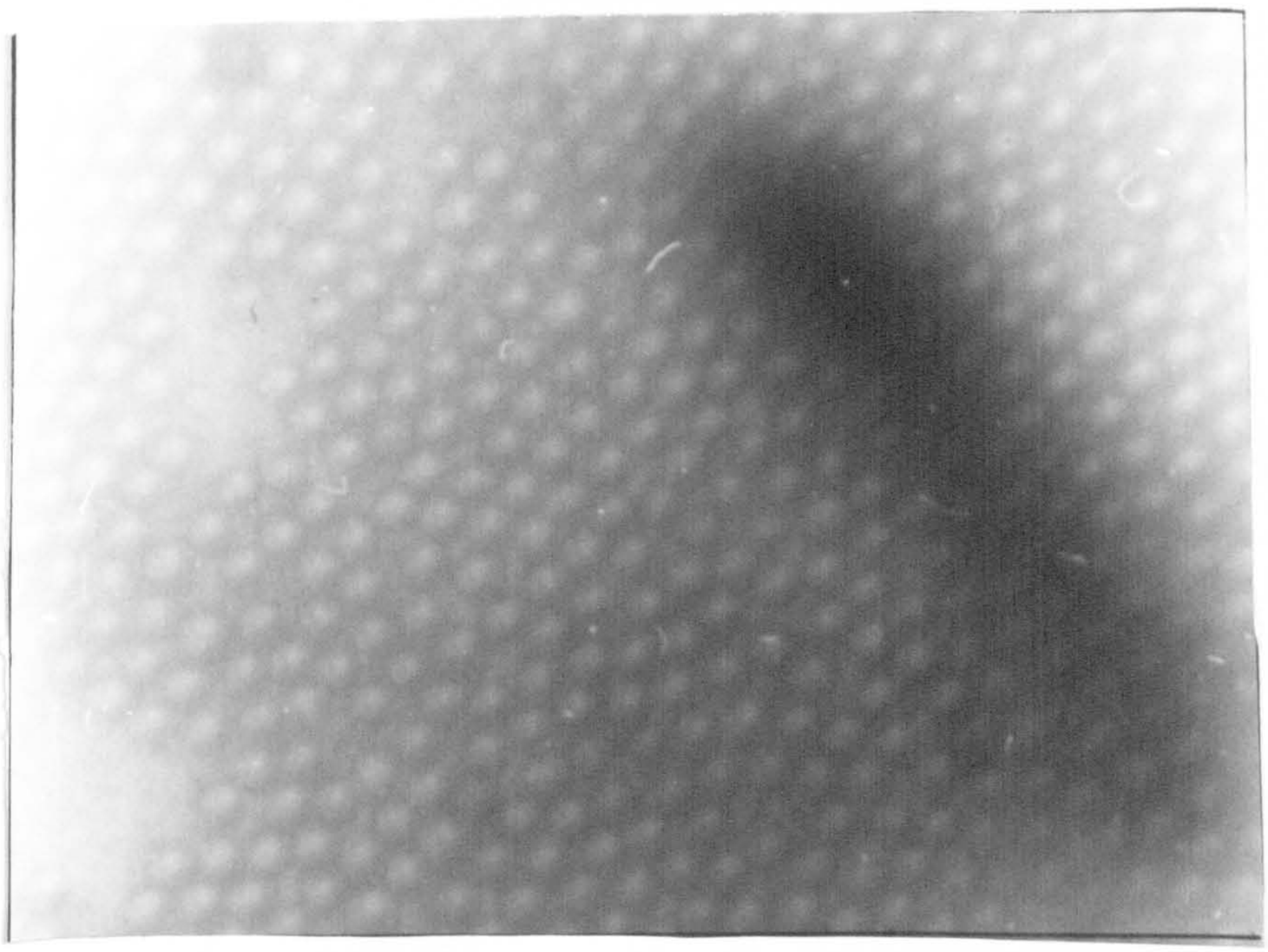

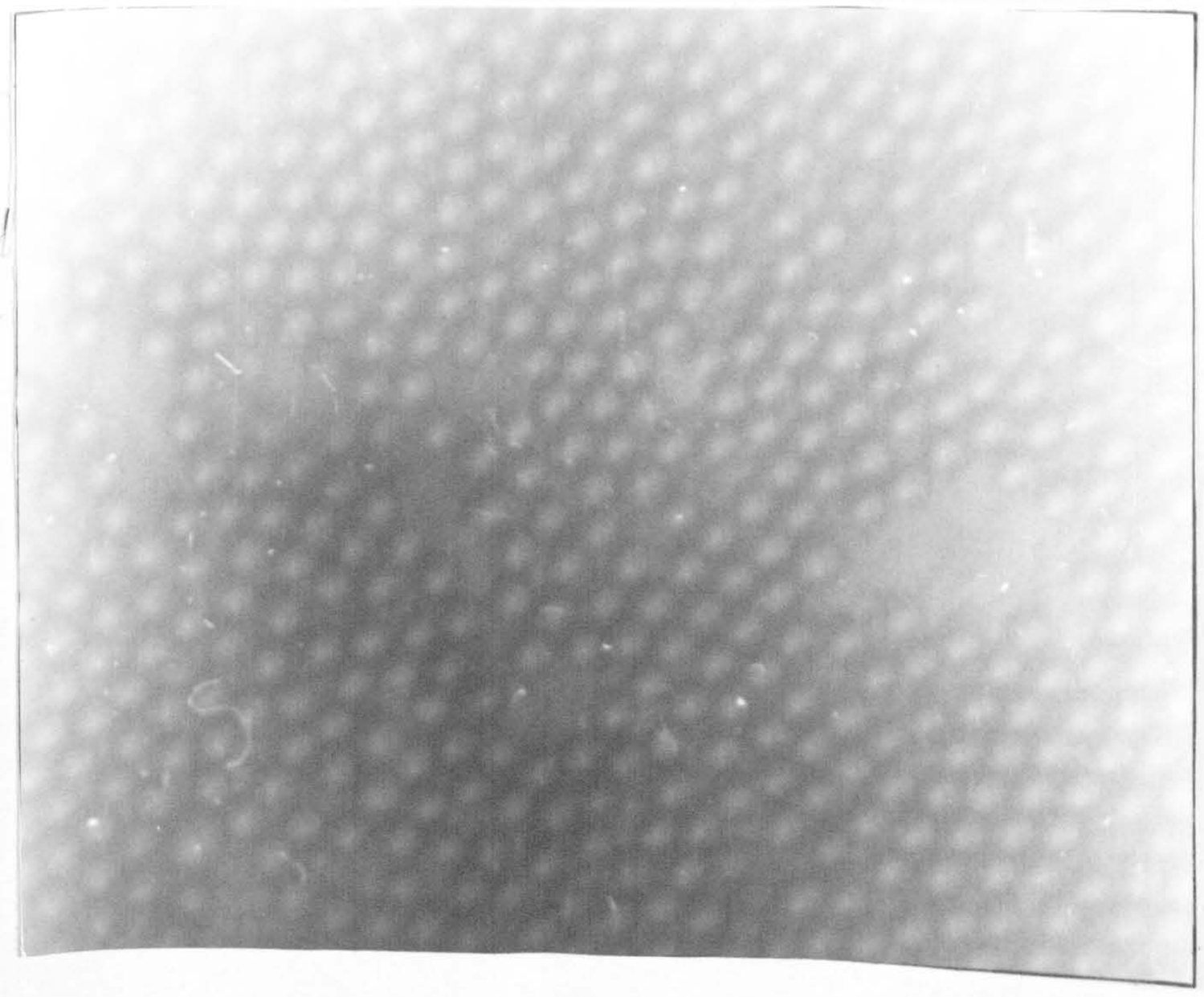

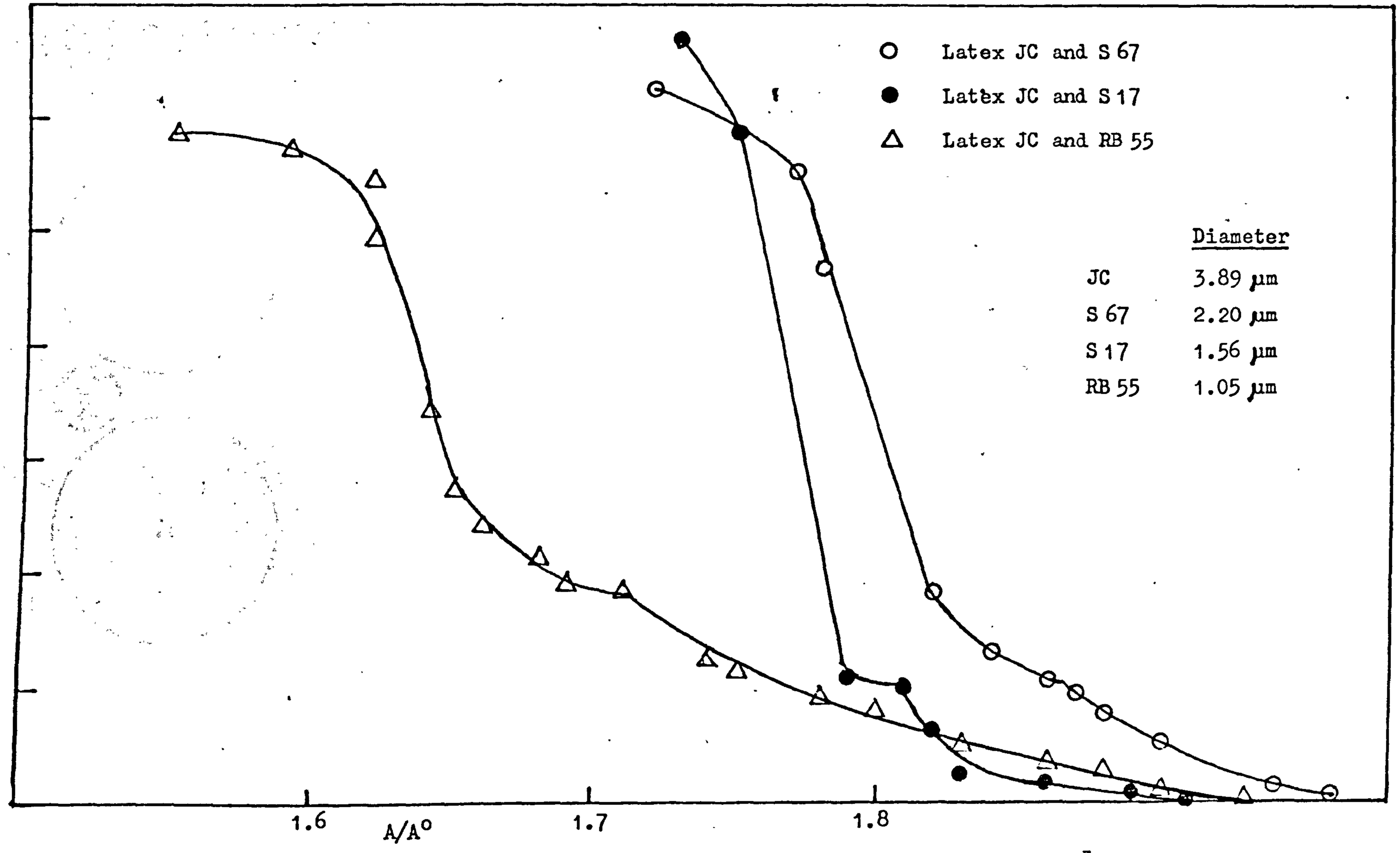

Figure 6/20 : Surface Pressure/Area curves for mixed Latex Systems on 0.5 mol dm^{-3} sodium chloride

Figure 6/21 : The Relative Size of the Polystyrene Particles

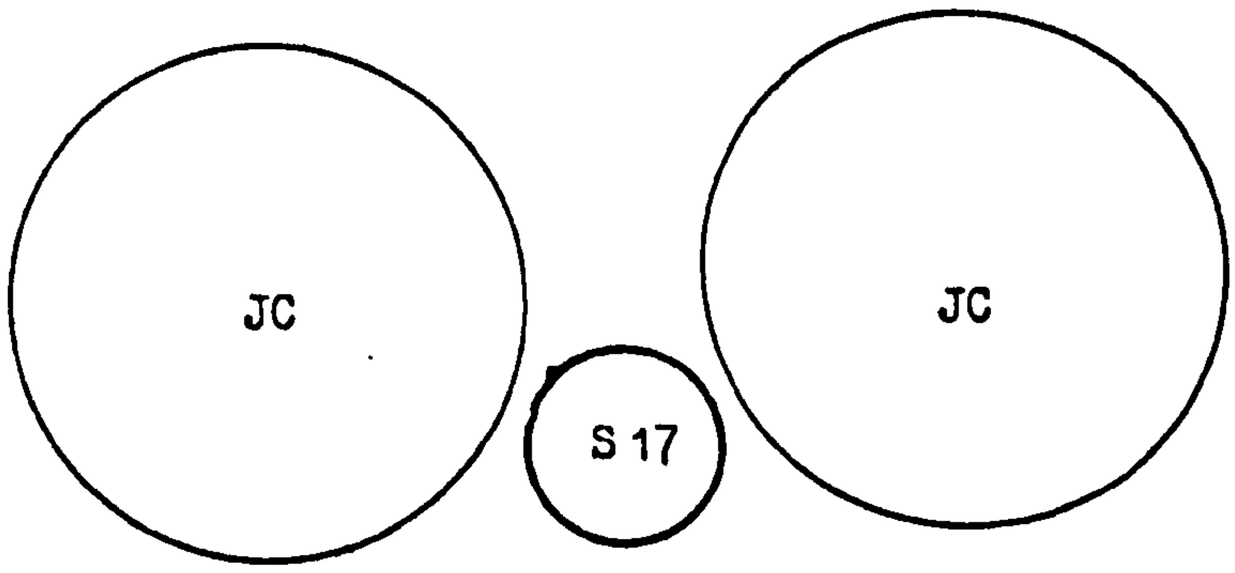

than the smaller particles of diameter 1.05 μm. Therefore the cohesive forces appear to increase as the particle diameter increases.

(b) Systems of mixed particle sizes

Photographs in figures 6/15 - 6/19 show the layers obtained from latex JC mixed with S67, S17 amd RB55.

For latex JC/S67 mixture, diameters respectively 3.89 and 2.2 μm, a dispersion of the large JC particles in hexagonally close-packed S67 was found. Figure 6/20 shows the surface film results for these mixed systems. It can be seen that latex JC/S67 is an expanded film without any apparent transition.

When the mixed latex JC/S17 was applied to the surface of an 0.5 mol dm^{-3} sodium chloride, S17, diameter 1.5 μm, appeared to sink leaving a layer of latex JC on the surface. No small particles were seen in the photographs and the percentage of particles sunk appears to be high.

The variation in amount which sinks is due to a number of factors, some of which vary with each run. These include the number of syringe loads used; this depends on the area of the surface of the trough to be covered with a latex film. Also the concentration of the latex suspension and the height of the syringe above the interface affect the sinkage percentage.

The same is true for the mixed latex JC/RB55 with particle diameters of 3.89 and 1.05 μm. Here the layer appears to be a hexagonally close-packed layer of latex JC particles, figure 6/19.

However the relative sizes of the latex particles mean that a small particle can fit in between two larger particles without being necessarily visible from above, figure 6/21.

The Langmuir trough result for the latex JC/S17 system is similar to that for the single latex system. However for the latex JC/RB55 mixture a more expanded film was observed and the transition occurs at a higher surface pressure than before. This would be consistent with the proposal that there are smaller particles in the surface which are repelling the larger particles, and hence a more expanded film is formed on the liquid substrate.

For all three systems the film appears to break at the same surface pressure within experimental error, that is 55 - 60 mN m^{-1}; this is lower than the same parameter for single latex systems. For all the mixed systems the same packing fraction, 0.57, was found.

6.1.6 Conclusion

Polystyrene latex particles of a certain size, that is from 1 μm to 4 μm, float on the surface of salt solutions forming a layer which on compression has solid-like properties such as low compressibility.

The strength of this layer decreases with decrease in particle size.

If mixed latex films are studied, then for latex particles below 2 μm diameter the smaller latex appears to sink leaving a film containing particles ca. 4 μm diameter which resembles that of the monodisperse 3.89 μm diameter particles. However for latex particles larger than 2 μm diameter a mixed film is observed in which the large particles are dispersed in the film of close-packed smaller particles. Due to interactions between the different particles a more liquid film was to be found. The surface pressure, on the rupture of the film, is lower than the single latex systems. This indicates that the films for the mixed systems are weaker.

6.2 Surface Tension

6.2.1 Introduction

The method used for determining interfacial tension of the surface of a latex/salt suspension was the Du Noüy Ring. This involves the measurement

of the force required to detach a platinum ring from the surface of a liquid. The force can then be equated to the product of the surface tension and the periphery of the surface in contact with the ring. There are two assumptions involved with this method, the first being the equating of the total contact length with twice the circumference of the ring. The second neglects the mass of liquid raised above the surface of the liquid.

The first assumption is corrected for by measuring the distance from the centre of the ring to the inner edge of the wire, R', and the radius of the wire, r. Then the correction factor, f, becomes

$$f = \frac{L}{2\pi R' + 2\pi(R' + 2r)}$$

where L is the total contact length obtained from calibration using a known weight.

To allow for both the nature of the ring and the air/liquid interface, Harkins and Jordan[127] derived a correction factor, F. If the apparent surface tension is γ' then

$$\gamma' = \frac{mg}{4\pi R}$$

where m is the mass of liquid raised above the surface of the liquid and R is the distance from the centre of the ring to the centre of the wire.

Therefore $R = R' + r$

Now $\gamma = \gamma' F$

where γ is the absolute surface tension and F is the Harkins and Jordan correction factor.

$$F = f\left(\frac{R^3}{V}, \frac{R}{r}\right)$$

where V is the volume of liquid raised above the surface.

So $$\gamma = \frac{mg}{4\pi R} F$$

Tables of correction factors can be found in Harkins and Jordan's original paper[127].

6.2.2 Experimental

The surface tension measurements were made on a Kruss tensiometer using a platinum ring. The tensiometer was calibrated using known weights in the range 0.05 to 0.45 g.

Latex JC, diameter 3.89 μm, was suspended in salt solutions in the range 0.005 to 0.5 mol dm^{-3} and poured into the steel dish on the tensiometer platform. The latex percentage used was 0.06%. One run was done with the surface coated with freez-dried latex particles for latex suspended in 0.35 mol dm^{-3} sodium chloride.

The platinum ring was flamed and then placed on the boom. The table was raised until the ring was submerged in the suspension. This was then lowered until the ring lay in the surface. Slowly the motorised platform was lowered, making sure that the boom was kept horizontal, until with a sudden jerk the ring came free of the surface. The final reading on the deflection scale was noted. This procedure was repeated until five readings were found to be within 0.5 mN m^{-1} of each other. The average surface tension was calculated for each run. The temperature for these runs was 20 ± 2°C.

6.2.3 Calculations

(a) Calibration

Let the weight added be x grams, then this is equivalent to

$$\frac{xg}{2c}$$

where c is the mean circumference; for the ring supplied this was 6.011 cm.

If the reading on the scale was d, for the weight x, then the correction is

$$\frac{xg}{2c} \Big/ d$$

(b) Harkins and Jordan correction

To find the correction factor, F, from the tables, R/V and R^3/V must be known.

R/r is given for the ring used as 51.7, while R can be calculated

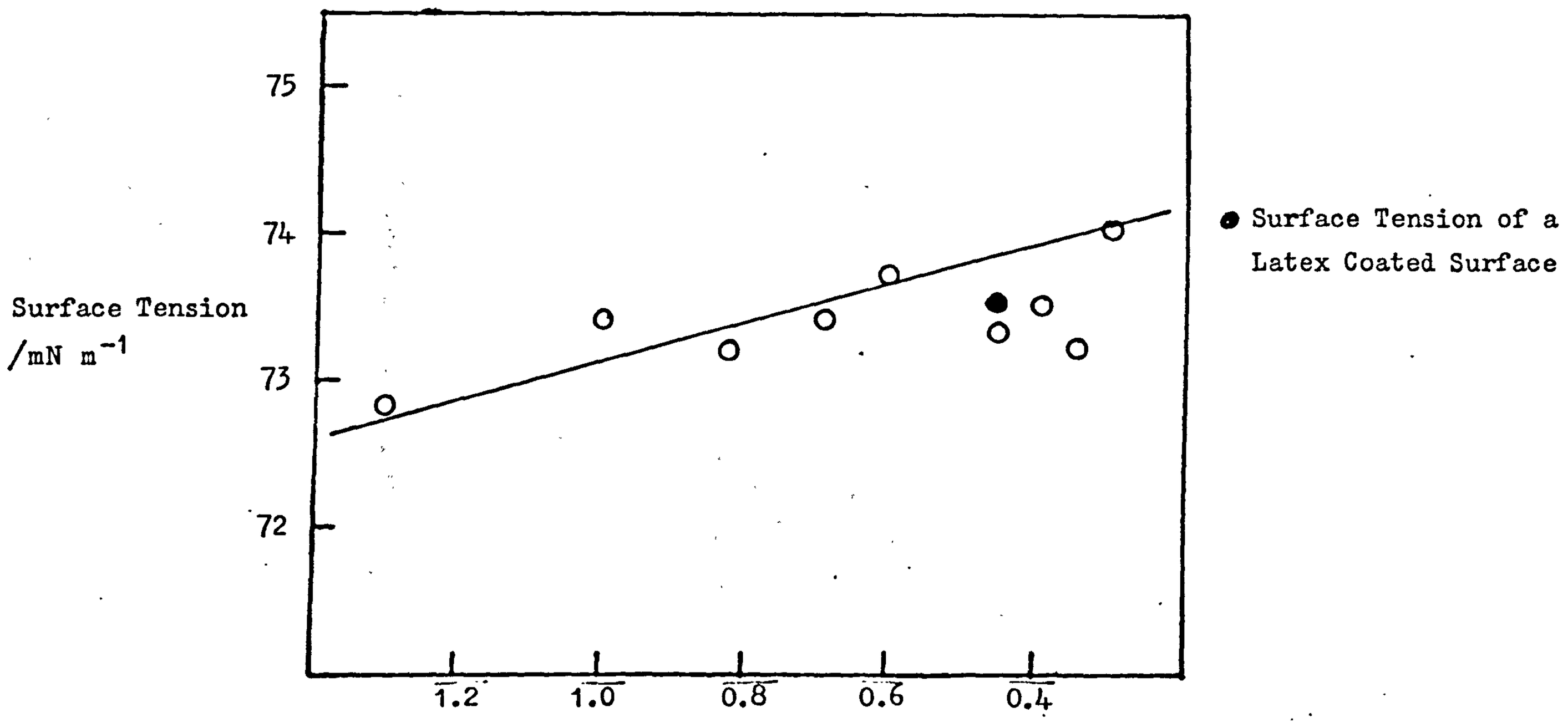

Figure 6/22 : Surface Tension measurements of Latex in sodium chloride solutions at 20°C

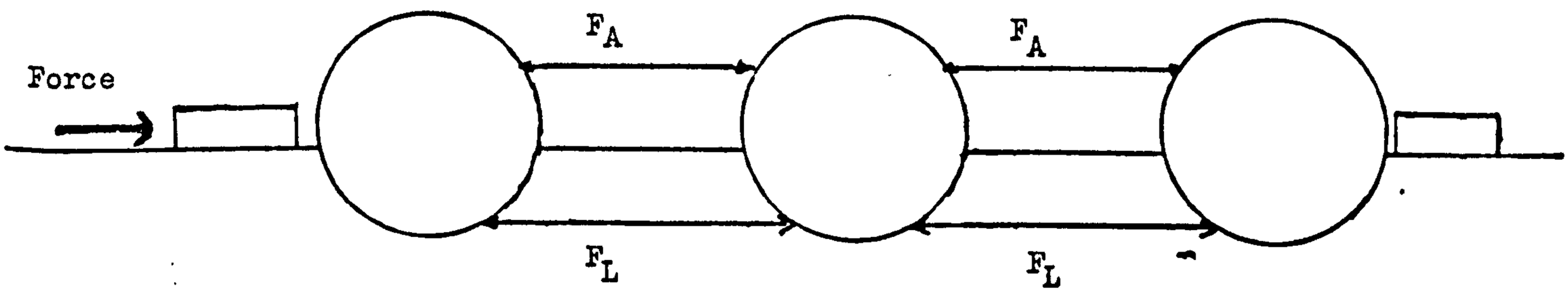

$$F_L = F_R^{el} + F_A^{vdW} \quad ; \qquad F_\sigma = F_A^{vdW}$$

Figure 6/23 : Forces acting in a Monolayer

from the mean circumference

$$2\pi R = c$$

For small masses of water V ∝ m and m can be found from the apparent surface tension γ'.

$$\gamma' = \frac{mg}{2c}$$

6.2.4 Results and Conclusion

The results are summarised in figure 6/22. There is a small increase in the surface tension of the latex suspension in the range 0.005 to 0.5 mol dm^{-3} sodium chloride as would be expected.

In this experiment the force required to pull a ring through a latex/salt surface was observed. No difference is seen in this force for a range of salt solutions and its value is close to that for a clean water surface, namely 72.8 mN m^{-1} at 20°C. Also the surface tension of a latex coated surface is, within experimental error, the same as for a clean latex/salt suspension. This shows that the adhesive force of the layer to the surface is very small.

6.3 Summary of Results from Film and Surface Tension Studies

Figure 6/23 shows a schematic representation of a monolayer of close-packed latex particles on the surface of a Langmuir trough. From considerations of the attractive and repulsive forces it can be clearly seen that all the forces act within the plane of the monolayer. The only forces acting perpendicular to the plane of the monolayer are to those concerned in maintaining the equilibrium of a single sphere at an interface, that is buoyancy, surface tension and gravity. Therefore the stronger forces act in the plane of the interface, producing a strong cohesive force within the layer, as indicated by the Langmuir trough results, whereas weaker forces are acting perpendicular to the interface producing a weak adhesive force of the layer to the liquid surface, as indicated by the surface tension results.

The lateral forces acting in the plane can be divided into two sets,

those acting in the liquid phase F_L and those in the gaseous phase, F_G. F_L consists of the electrostatic repulsion and the van der Waals attraction, whereas F_G consists of just the van der Waals attraction.

$$F_L = F_R^{el} + F_A^{vdW}$$

$$F_G = F_A^{vdW}$$

This results in the attractive force in the gaseous phase pulling the particles closer together than they would be if the particles were completely submerged in the liquid media.

CHAPTER 7

ELECTROPHORETIC MEASUREMENTS

7.1 Microelectrophoresis Studies

7.1.1 Introduction

Electrophoresis is an electrokinetic technique which can be used to determine the zeta-potential of a charged colloidal particle.

Experimentally the velocity of the particles is accurately measured in a well-defined electric field in order to determine the mobility; the latter quantity can then be converted to a zeta-potential. Measurements of mobility must be carried out at a position in the cell where the fluid velocity is zero, that is at the stationary layer. In fact this is the position, in a closed cell, where the electro-osmotic flow exactly balances the return viscous flow of the liquid.

In the present work the velocity profile across the cell was measured. Some data are shown in figure 7/1. The profile is parabolic. At a distance $a\sqrt{2}$ from the axis of the cylindrical capillary, where a is the radius of the capillary, the liquid velocity is zero and this corresponds to the stationary layer.

The observed mobility, u, of a colloidal particle at a point distance, d, from the centre of the capillary is equal to the sum of the electrophoretic mobility at that point, u_t, and the electro-osmotic mobility, u_o. In the absence of particles, the liquid velocity at any distance, d, is given by

$$u = u_o\left[\frac{2d^2}{a^2} - 1\right]$$

This is equal to zero when $d^2 = \frac{a^2}{2}$ and this locates at this level the position of the stationary layer.

In this research the electrophoretic mobility was measured for some of the latices used in the foaming studies.

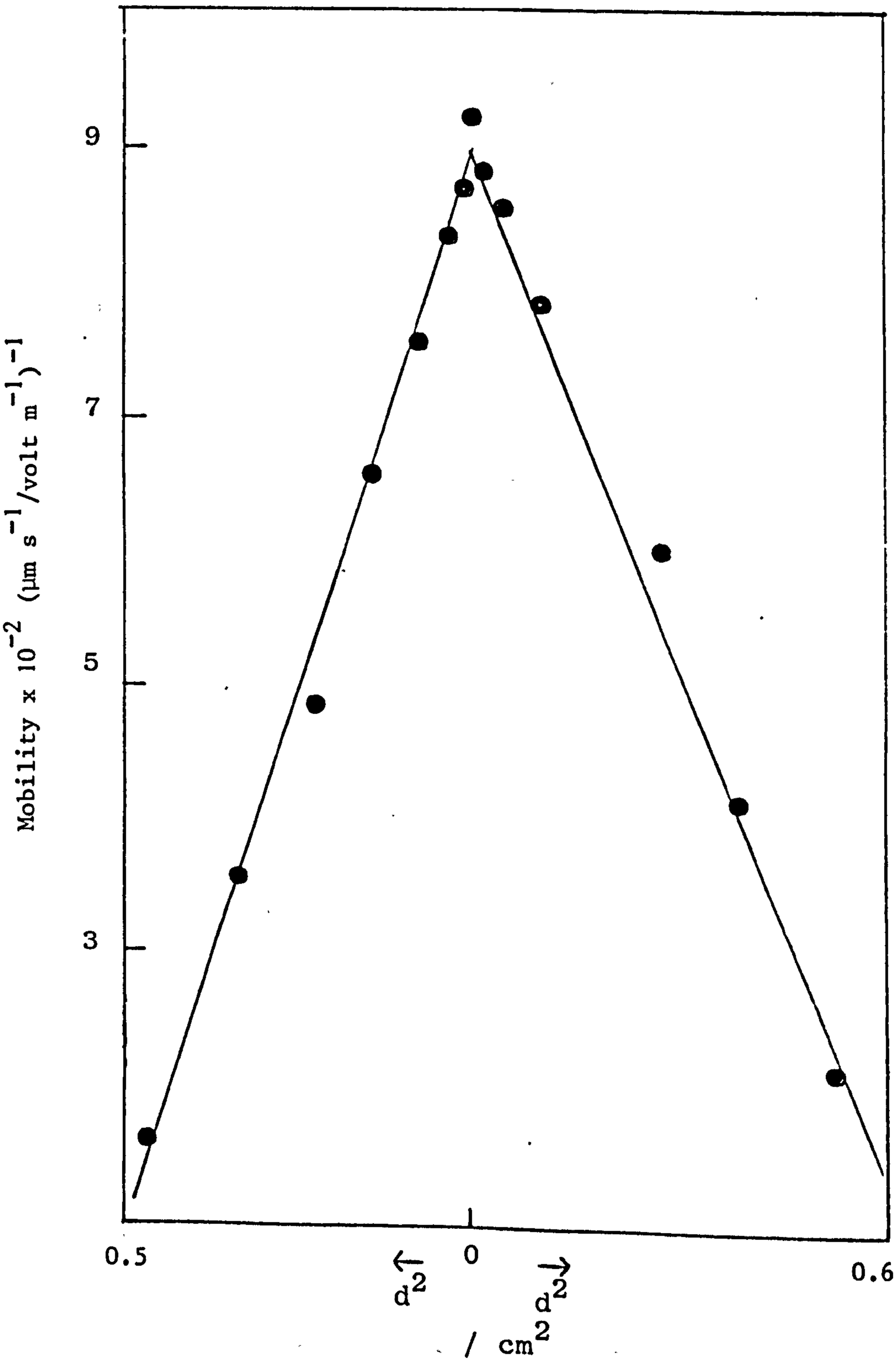

Fig.7/1: Mobility Profile across the Cell

7.1.2 Experimental

(a) Apparatus

The measurements were carried out on a Rank Brothers microelectrophoresis apparatus using a cylindrical cell of the Kruyt / van Gils type. This was a constant bore capillary with thin glass walls, internal diameter 1.73 cm and length 7.96 cm between the electrodes. The platinum electrodes were blackened to reduce polarisation effects.

The cell was illuminated perpendicular to the viewing direction; the width of the beam used was narrow. The latex particles, seen as bright specks of light in the ultramicroscope, at a magnification of 350 x were timed across a graticule fitted in the eyepiece of the microscope. The graticule division corresponded to a distance of 28.6 μm in the cell.

(b) Determination of the stationary layer

Initially, the microscope was focused on the front outer wall of the cell. This appeared very speckled and all the spots were in focus in the same plane. The microscope was then moved down until the inner face came into focus. This appeared less speckled and the spots did not come to focus together owing to the curvature of the cell. The scale reading was taken when the spots in the centre were focused. This procedure was repeated for the lower wall; the light beam was brought down to illuminate the lower part of the cell. The radius of the cell could therefore be found.

From the radius of the cell the position of the stationary layer was calculated as explained above. The microscope was then set so that the mobility determinations were made at the upper stationary layer.

(c) Experimental procedure

The cell was filled with each dispersion in turn; care being taken to ensure that there were no air bubbles trapped in it. After each run the dispersion was sucked out by the action of a water pump and the cell cleaned by repeatedly filling it with twice-distilled water.

A potential was applied to the outer platinum electrodes and the actual potential experienced by the solution measured using the inner electrodes, on an Advanced Instruments digital multimeter DMM 3.

The time taken for a focused particle to cross two graticule divisions was recorded. After each measurement the polarity was reversed and the particles were timed moving in the opposite direction. Approximately ten measurements were made in each direction for each latex system.

(d) Latex suspended in sodium chloride solutions

The latex JC particles, diameter 3.89 μm, were suspended in sodium chloride solutions in the concentration range 0.05 to 0.5 mol dm^{-3}. The latex concentration was found to give a number concentration in the microscope suitable for accurate measurements. All measurements were carried out at room temperature which was $21^{o} \pm 1^{o}C$.

(e) Latex suspended in DTAB solutions

Latex JC was suspended in DTAB solutions covering the concentration range 5×10^{-6} to 5×10^{-2} mol dm^{-3}, the latex concentration being 0.05%. The procedure used was the same as that described above. However for the more mobile latex suspensions the particles were measured over a greater number of graticule divisions at a lower applied potential.

7.1.3 Calculations

The applied potential causes the counterions to move in the opposite direction to that of the particle. This produces a retardation effect on the particle. Henry formulated this effect for the case of spherical symmetrical electrical electrical double layers using the Debye-Hückel approximation[128] and found the result that

$$u = \frac{\epsilon \zeta}{6 \pi \eta} f(\chi a)$$

where u is mobility, ϵ is relative permittivity, η is viscosity, ζ is zeta-potential, a is the radius of the particle and $1/\chi$ is the Debye-Hückel

reciprocal length. There are two uniting cases ;

for $\kappa a >> 1$ $f(\kappa a) = 3/2$

giving $u = \frac{\epsilon \zeta}{4 \pi \eta}$, the Smoluchowski relationship

for $\kappa a << 1$ $f(\kappa a) = 1$

giving $u = \frac{\epsilon \zeta}{6 \pi \eta}$, the Hückel relationship

In the present work the particles have diameters of 3.89 μm and (κa) values > 100. Hence the Smoluchowski relationship could be used to calculate the zeta-potential from the mobility where the mobility itself has been obtained from

$$u = \frac{\bar{V}_E}{x}$$

where $\bar{V}_E$ is the average velocity of the particles and x the applied field strength.

7.1.4 Results

(a) Dispersions in sodium chloride solutions

Figure 7/2 shows the variation in mobility and zeta-potential with salt concentration within the foaming region 0.05 to 0.5 mol dm^{-3} sodium chloride. Both the mobility and the zeta-potential decrease with sodium chloride concentration as would be expected owing to compression of the electric double layer. However the zeta-potential is still appreciable, the lowest zeta-potential being -34 mV at 0.5 mol dm^{-3} sodium chloride.

(b) Dispersions in DTAB solutions

Figure 7/3 shows the variation in zeta-potential in the range 5×10^{-6} to 5×10^{-2} mol dm^{-3} DTAB. The zeta-potential starts with a negative value, goes through zero and then becomes positive; this indicates a reversal of zeta-potential at a DTAB concentration of 1.8×10^{-5} mol dm^{-3}.

7.1.5 Discussion of Results

Latex JC particles in sodium chloride solutions show a decrease in zeta-potential with sodium chloride concentration. This is due to the

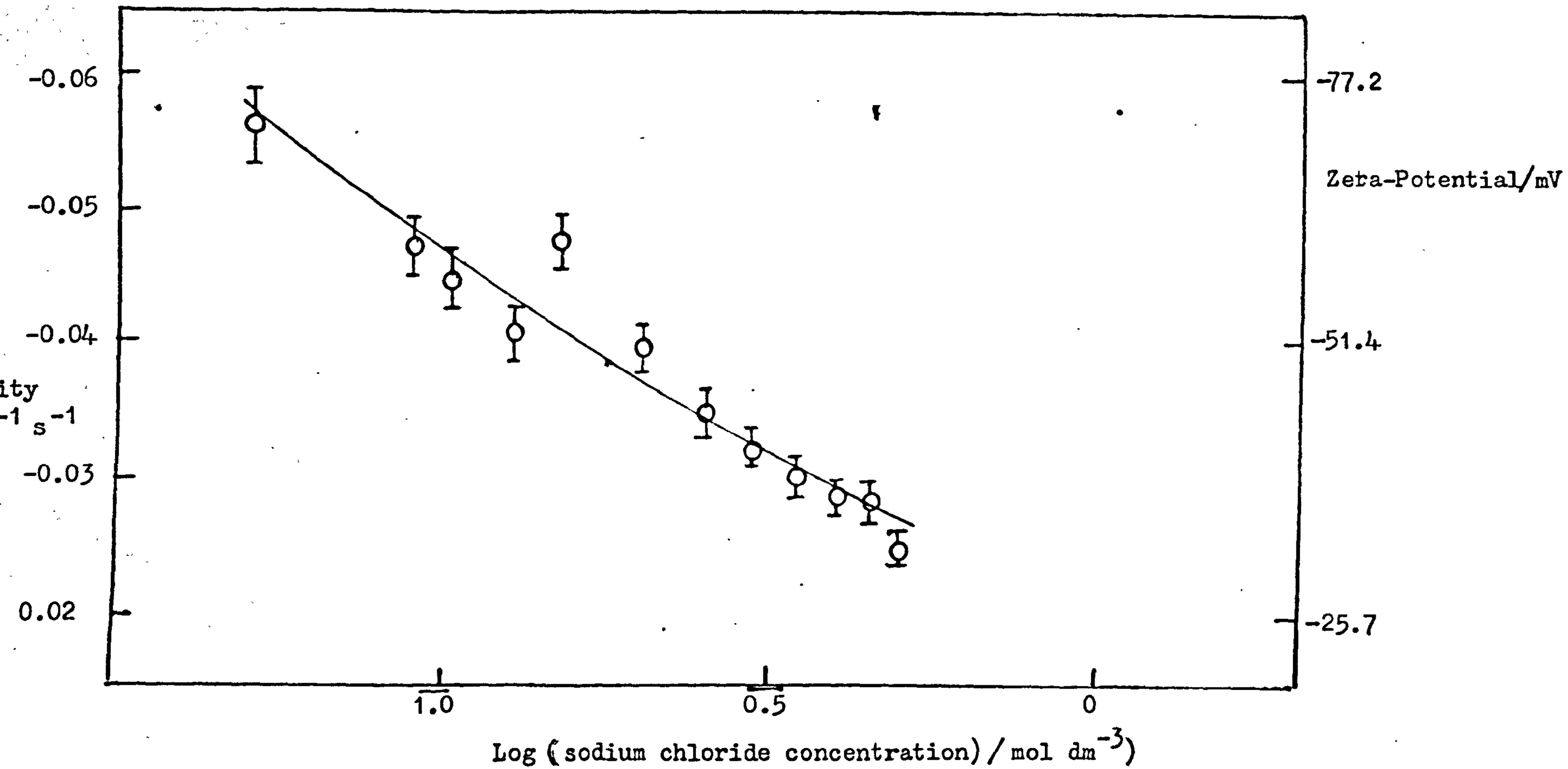

Figure 7/2 : Electrophoretic Measurements for Latex JC in Sodium Chloride Solutions

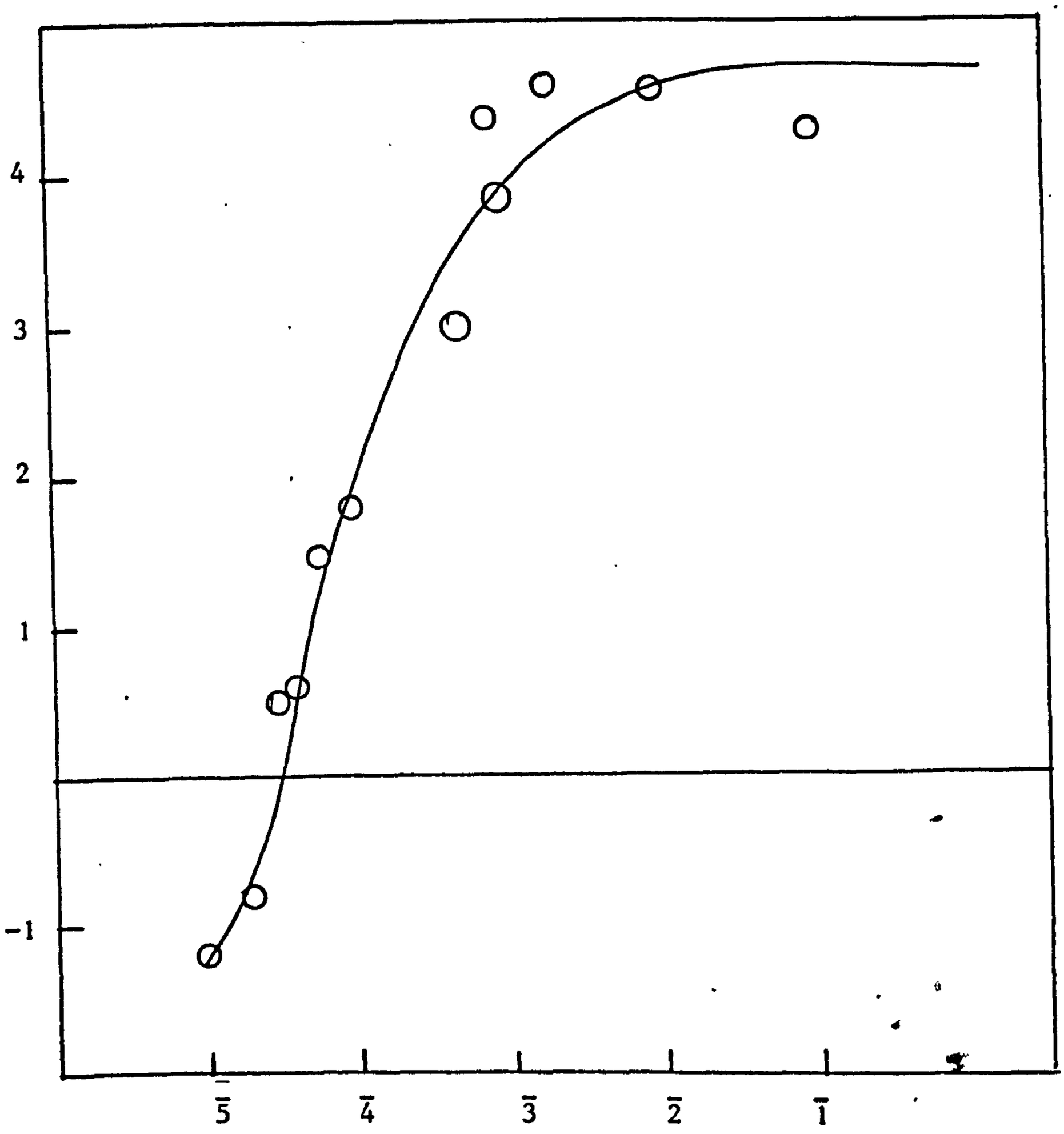

Figure 7/3: Variation of mobility with DTAB concentration for Latex JC

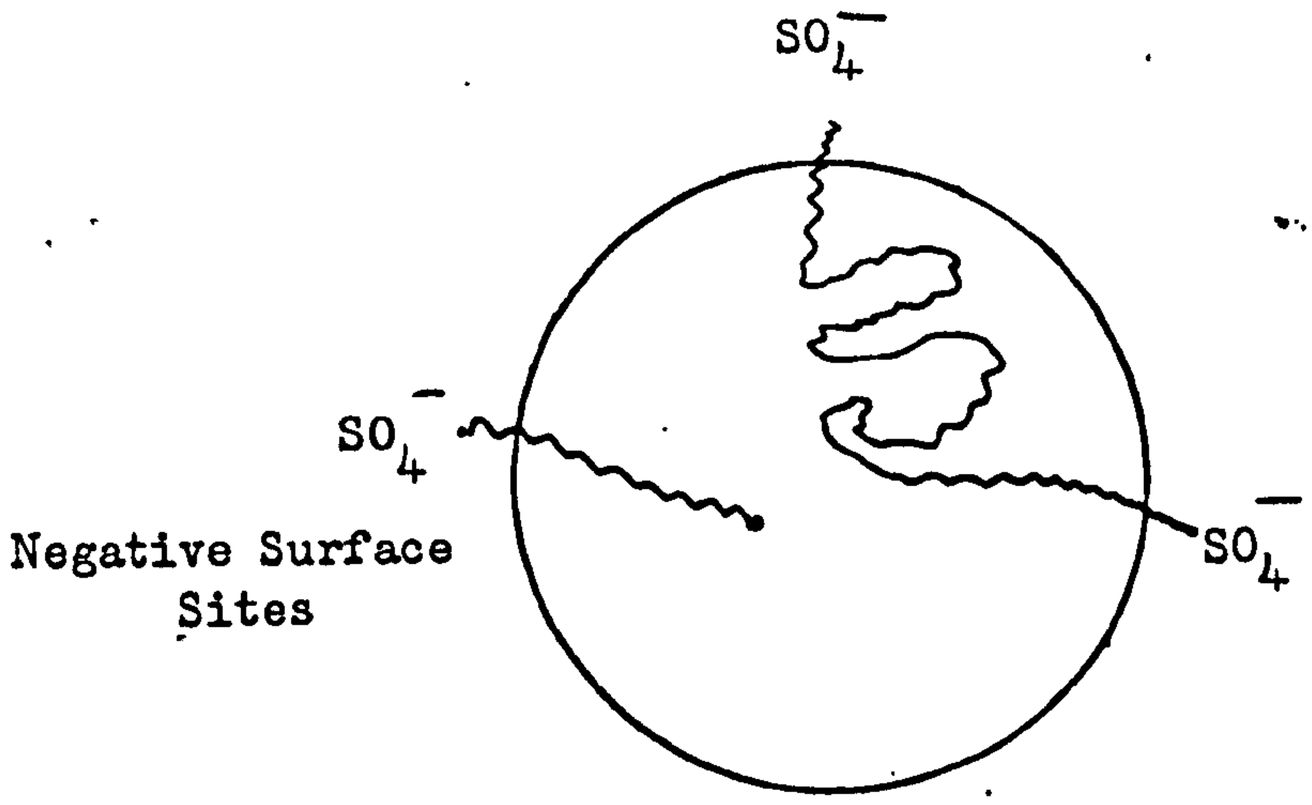

Figure 7/4: Polystyrene Latex Particle

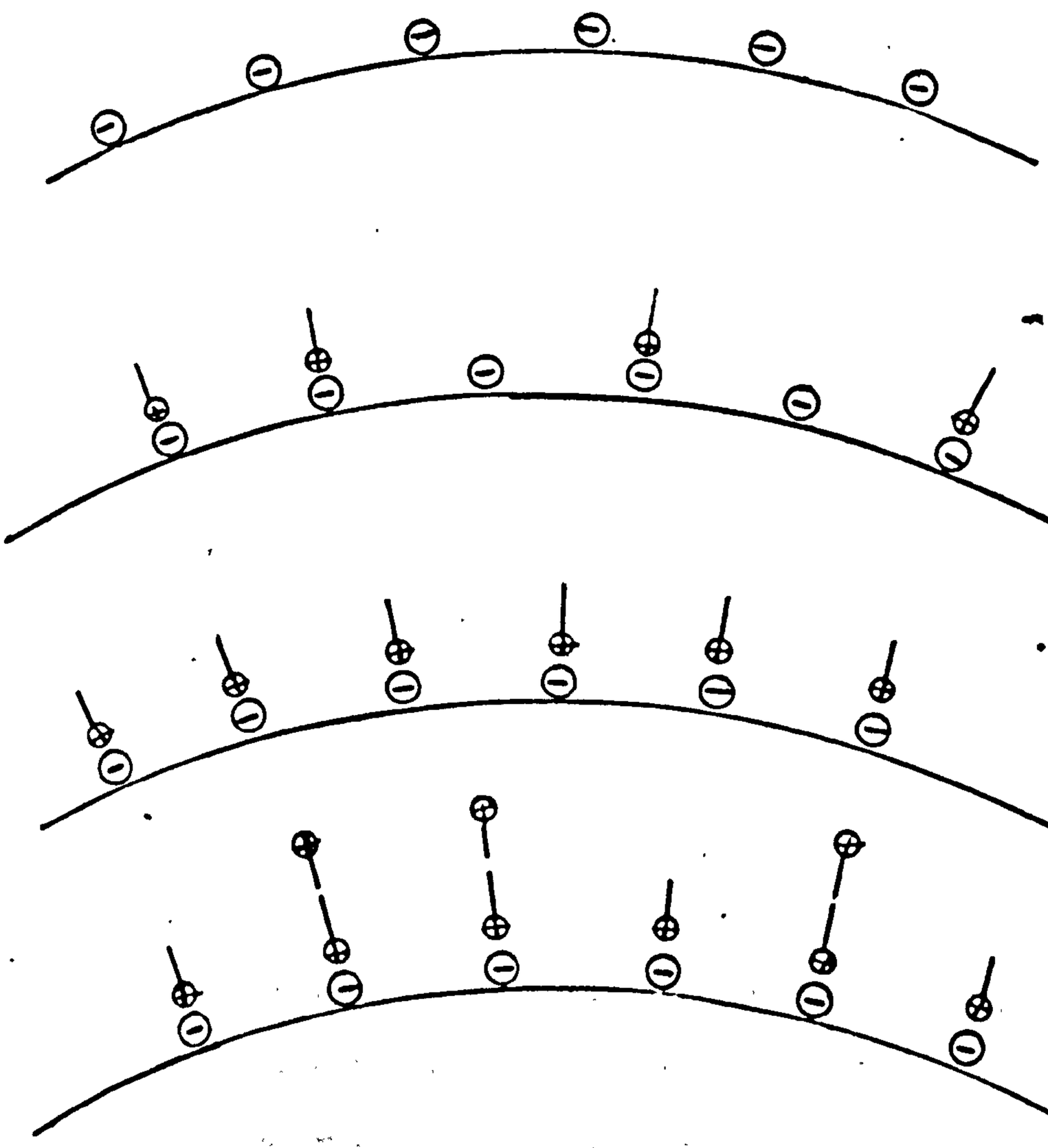

Figure 7/5: Adsorption of DTAB

compression of the electrical double layer with increase in salt concentration. However, a fairly large potential -34 mV is still observed in 0.5 mol dm^{-3} sodium chloride. In the foam tests the latex appeared to be coagulated at this salt concentration. The coagulation could have been the result of shaking the suspension, thus causing surface coagulation to take place[95-99] as the bulk system approaches the critical coagulation concentration.

For latex particles in DTAB solutions the zeta-potential does go through zero, indicating a reversal of charge at 1.8×10^{-5} mol dm^{-3} DTAB. The surfactant molecules are adsorbed at the negative sites on the particle's surface. These negative surface charges arise from the ionised end-groups on the polymer chains which for these latices are the sulphate groups, figure 7/4. The positively charged head groups adsorb onto the negative sites, figure 7/5. This causes the zeta-potential to decrease. As the DTAB concentration is increased the surfactant adsorbs onto the polymer latex particle until a completely hydrophobic shell is formed. Now the zeta-potential goes through zero. Then as the DTAB concentration is increased the surface charge will be reversed as additional surfactant molecules are adsorbed on top of this hydrophobic shell.

The surfactant concentration region close to the concentration of DTAB which produces reversal of charge on the surface should correspond to the polystyrene latex foaming region, since at these concentrations the zeta-potential is low and this factor in turn causes the repulsive forces to be lowered, This enables closer approach of the particles to each other. Also the nature of the surface has been changed; the surface hydrophobility has been increased due to the adsorbed surfactant molecules being oriented with the hydrophobic tails towards the liquid phase. Both low surface charge and high hydrophobicity favour the polystyrene particles resting at the air/liquid interface in a close-packed array.

The reversal of zeta-potential corresponded to a DTAB concentration

1.8×10^{-5} mol dm^{-3} while the best polystyrene foam was formed at 5×10^{-4} mol dm^{-3} DTAB. The latex concentration was diluted by a hundred times for the zeta-potential determination. As the DTAB is causing this reversal of charge by adsorption onto the particle, the larger the number of particles the higher the concentration of surfactant must be to give adsorption at all the surface charges and bring the net surface charge to zero. Since the results are expressed in terms of the initial DTAB concentrations taken it is not surprising that the DTAB concentration giving maximum foam and that giving zero mobility are different. However, if these could be corrected to allow for the amount of DTAB adsorbed by the particles, it would be anticipated that maximum latex foaming would occur at the concentration of DTAB corresponding to zero mobility of the particles, see section 4:3:3.

CHAPTER 8

CONTACT ANGLE MEASUREMENTS

8.1 Introduction

When a liquid is brought into contact with a solid it can either spread out and wet the solid, that is a wetting situation, or form a drop with a finite angle of contact against the solid, non-wetting. In the wetting case, figure 8/1, the contact angle is zero or close to it. For the optimum non-wetting the contact angle should be close to 180^{o}.

When liquid and solid phases are in contact there are usually two limiting contact angles. The maximum contact angle, θ_A, occurs when the liquid meniscus advances over a part of the solid not previously wetted by the liquid. The other is the minimum angle, θ_R, where the liquid meniscus is receding over a part of the solid which has already been wetted by the liquid.

The difference between these two indicates the roughness and heterogeneity of the solid surface. Contact angle measurements are macroscopic, whereas the roughness of the surface is a microscopic phenomenon. Therefore within the same system large differences in contact angle can be found due to slight differences in the surface roughness. Care is needed in the interpretation of such contact angle data.

8.2 Theory

Young's equation can be written in the form

$$\gamma_{LV} \cos\theta = \gamma_{SV} - \gamma_{SL}$$

where γ_{LV}, γ_{SV} and γ_{SL} are the interfacial tensions of the liquid-vapour, solid-vapour and solid-liquid interfaces respectively, and θ is the contact angle. This equation basically deals with the force balance at a three-phase point of contact, as shown in figure 8/1.

The validity of Young's equation has been questioned by several authors on various grounds[1,2,129]. However their arguments have not been

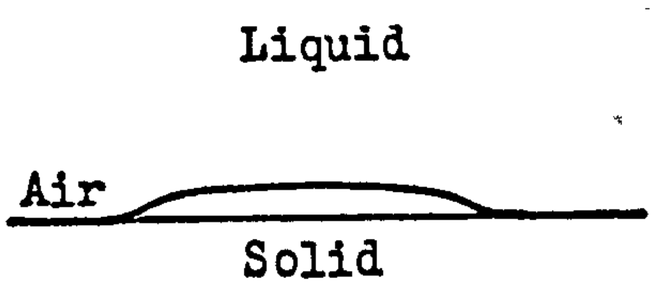

Wetting situation

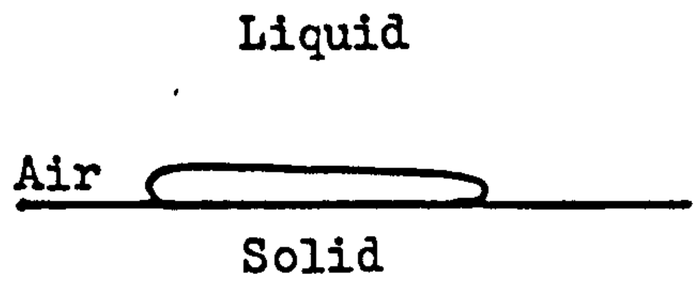

Non-wetting situation

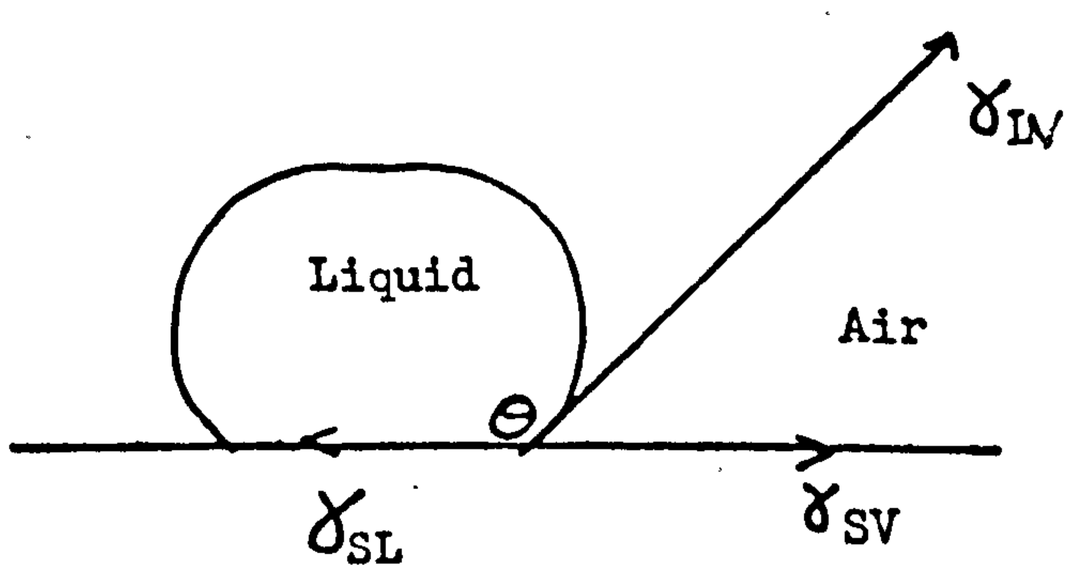

Balanced when

$$\gamma_{SV} = \gamma_{SL} + \gamma_{LV} \cos\theta$$

Young's Equation

Figure 8/1

generally accepted and at the present time it still appears safe to use this equation for the majority of situations.

It soon becomes apparent that for a single system several different values of contact angle could be obtained. Sulman postulated that these differences in contact angle were due to the hysteresis caused by the movement of the three-phase line[130]. The magnitude of this hysteresis can be defined as the difference in the advancing and receding angles.

8.2.1 Roughness

Several authors have discussed the effect that the physical conditions of the surface have on wetting; the contact angle is a measure of the resistance of the solid to wetting[131-134]. Wenzel was the first to attempt to correct Young's equation for a rough surface[131] with the equation

$$\cos\theta = r\cos\hat{\theta}$$

thus giving

$$r\gamma_{LV}\cos\hat{\theta} = \gamma_{SV} - \gamma_{SL} \qquad \text{Wenzel's equation}$$

where r is the roughness factor and $\hat{\theta}$ is the Wenzel angle.

The roughness parameter, r, is the ratio of an area of the microscopically rough surface to an area of the microscopically smooth surface. Since the area of a rough surface is greater than that of a theoretically smooth one, then this factor is always greater than one and is equal to unity for a smooth surface.

A rough surface means that there is more surface to wet per unit area than on a smooth surface. Roughness magnifies the wetting character of the solid surface; for $\theta < 90^{\circ}$, the surface becomes more easily wetted, that is its resistance to wetting is lowered. The adhesion tension, which is a measure of this resistance, has been defined by Wenzel[131] as

$$\bar{A} = \gamma_{SV} - \gamma_{SL}$$

where $\bar{A}$ is the adhesion tension.

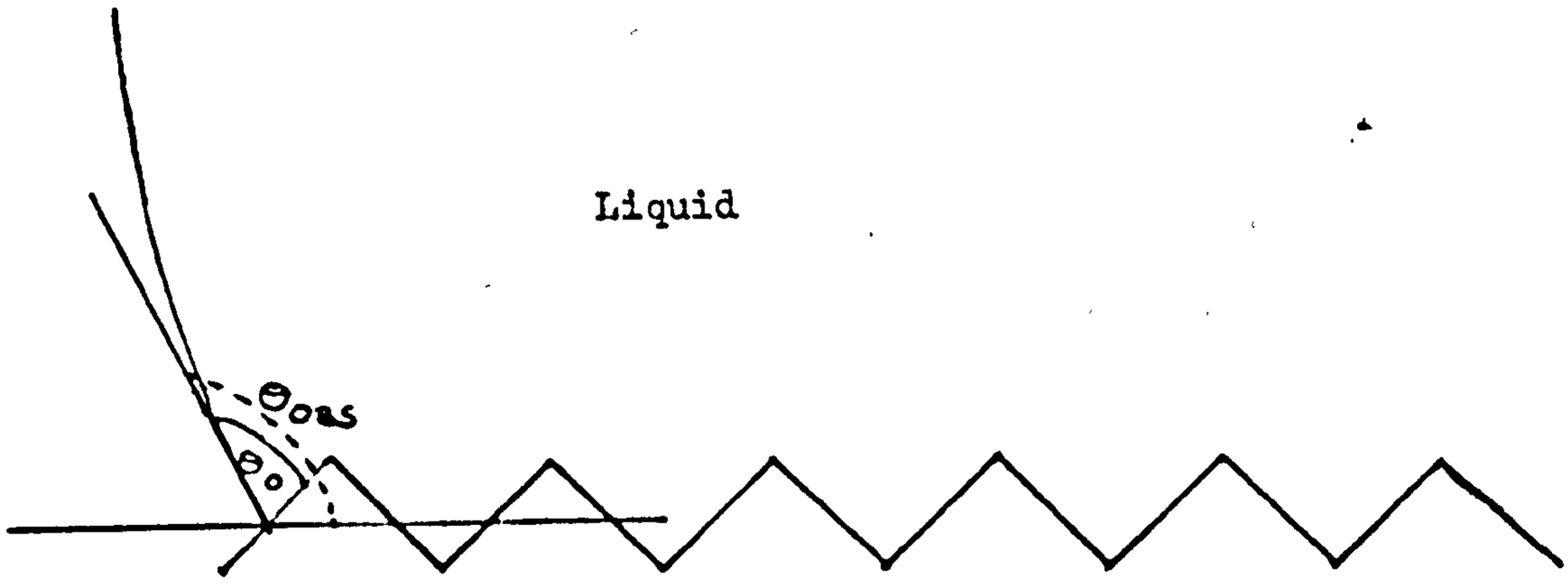

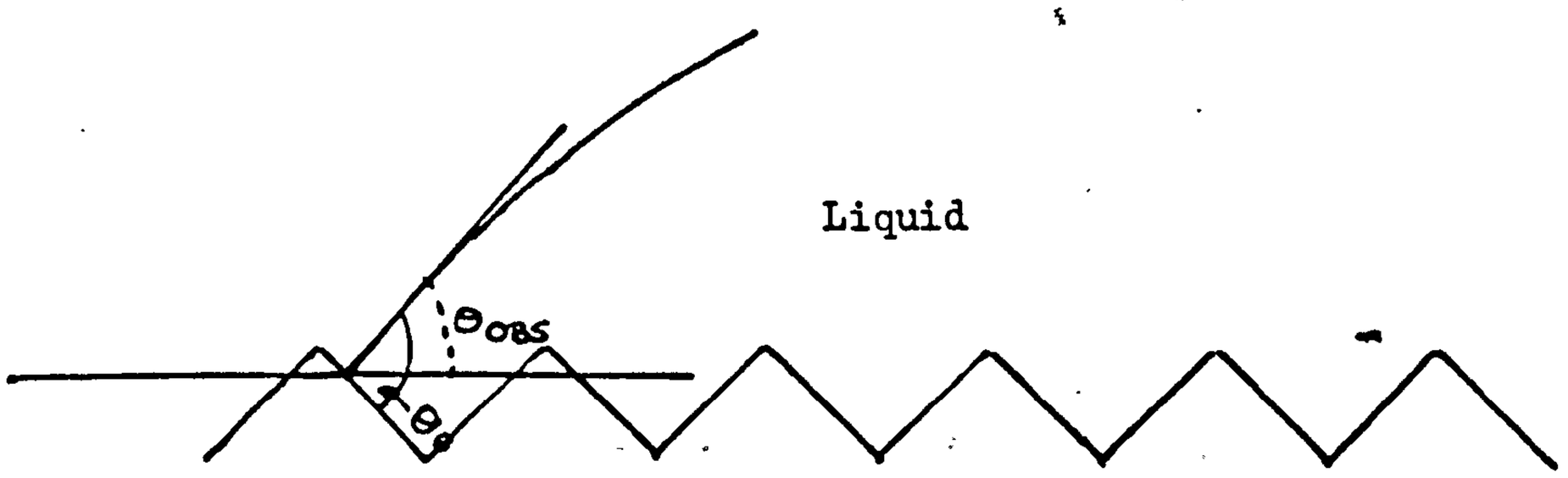

Figure 8/2 : Effect of roughness on the macroscopic contact angle

Good[135] has given a thermodynamic derivation of Wenzel's equation.

There are several reviews which discuss the possibility of surface roughness being a cause of contact angle hysteresis[136-138].

Johnson and Dettre[139] have set up a simple model based on concentric grooves to simulate a rough surface, the dimensions of which were large compared with molecular dimensions. They assumed that the microscopic angle, θ_o, was constant and that the observed contact angle θ_{obs} could be defined by

$$\theta_{obs} = \theta_o + \alpha$$

where α was the inclination of the surface at the three-phase point of contact, see figures 8/2. The second assumption was that only certain values of contact angle are allowed. The stability of each configuration was measured by the surface energy. The free energy curve is shown in figure 8/3.

There existed energy barriers which separate adjacent metastable configurations. The barriers were highest near $\hat{\theta}$ which was called the Wenzel angle since it obeyed his equations. The energy barriers were reduced to zero at the advancing and receding contact angles. To remain in the metastable configuration the vibrational energy of the system needed to be less than the height of the energy barrier.

There are several reports in the literature of contact angle studies on model rough surfaces[140-142]. For example, Bartell and Shepard[142] found the advancing and receding contact angles to be independent of the height of the pyramids they produced on their surfaces. However, they found the results to be in disagreement with the Wenzel equation.

8.2 2 Composite surfaces

A different type of surface is a composite one. A composite surface can be defined as one composed of different materials; a common composite surface is a porous one where one of the phases is air[139]. Cassie and Baxter[143] have studied the wettability of a porous solid, the

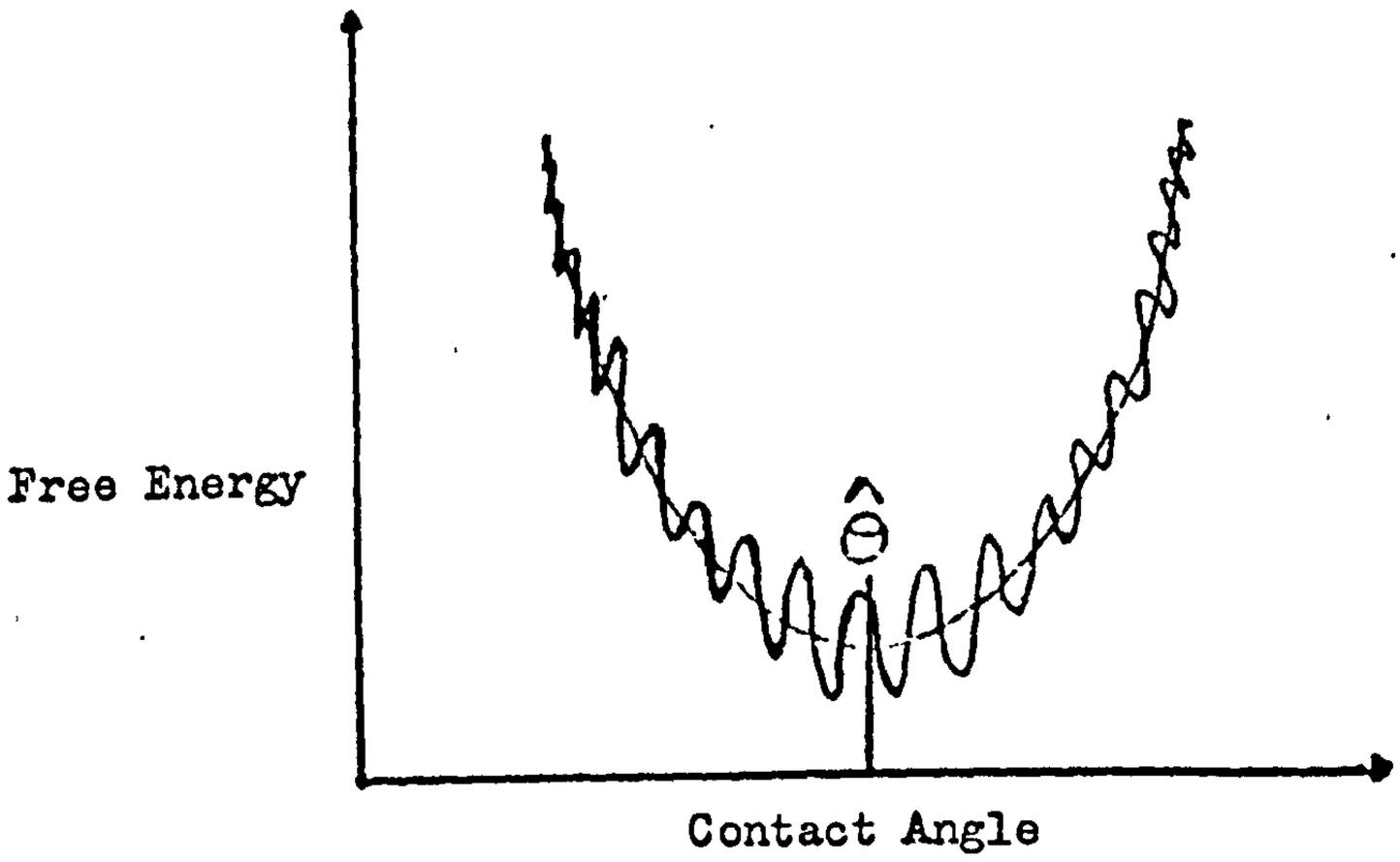

$\hat{\theta}$: minimum angle ≡ angle which obeys Wenzel's Equation.

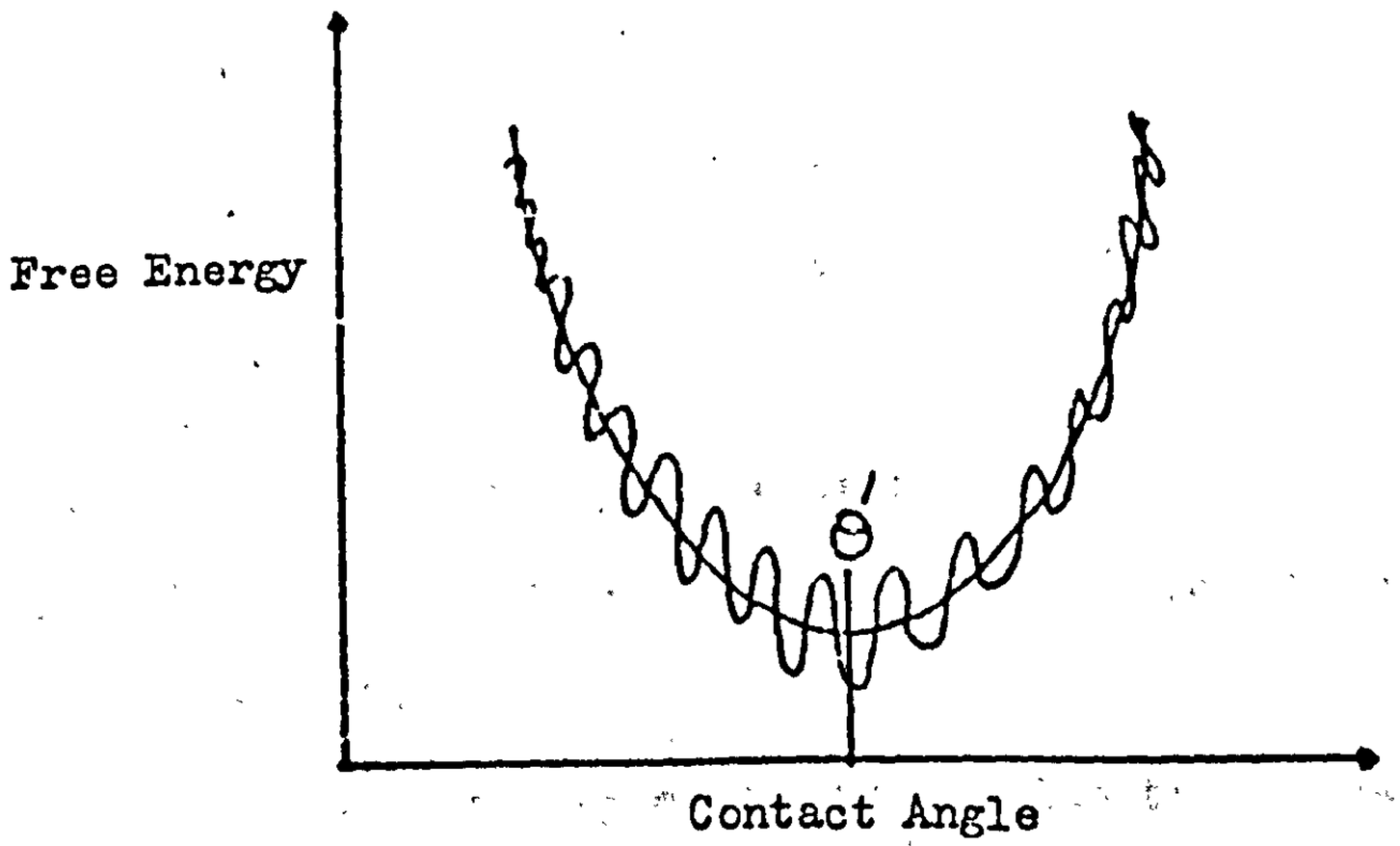

θ' : minimum angle ≡ angle which obeys Cassie's Equation.

Figure 8/3 : Free energy calculation created by Johnaon and Dettre[139,144,145]

surface being a composite of fibre and air. Cassie[143] has postulated an equation defining the contact angle for this system :

$$\cos\theta_c = f_1 \cos\theta_1 - f_2$$

where θ_c is the composite contact angle, f_1 the fraction of the surface which is solid, f_2 the fraction of the surface which is air, and θ_1 the contact angle of the solid surface.

8.2.3 Surface heterogeneity

Johnson and Dettre have studied surface heterogeneity, a factor which provides another cause of contact angle hysteresis[139,144,145]. Here again the surface heterogeneity must be small compared to the size of the drop. Cassie[146] has corrected the Young equation for use with heterogeneous surface to give

$$\cos\theta_H = f_1 \cos\theta_1 + f_2 \cos\theta_2$$

where θ_H is the contact angle due to surface heterogeneity, f_1 the fraction of the surface having contact angle θ_1 and f_2 the fraction of surface having contact angle θ_2.

Johnson and Dettre have postulated a theory based on an idealised heterogeneous surface[144]. This involved alternate circular bands of different surface energy. They made the following assumptions.

(1) The liquid was incompressible.

(2) The boundary between the regions had no effect on the energy of the system.

The free energy curve was similar to the one for the surface roughness, figure 8/3. Here the minimum angle corresponded to the angle which obeyed Cassie's equation. As in the case of the surface roughness model the curve obtained was not continuous. There was a finite number of closely spaced points, each representing a metastable equilibrium. The height of the energy barrier was directly proportional to the band width. Here again the barrier was reduced to zero at the advancing and receding contact angles.

Figure 8/4 : Electron Micrographs of gold-coated Layers of Latex JC

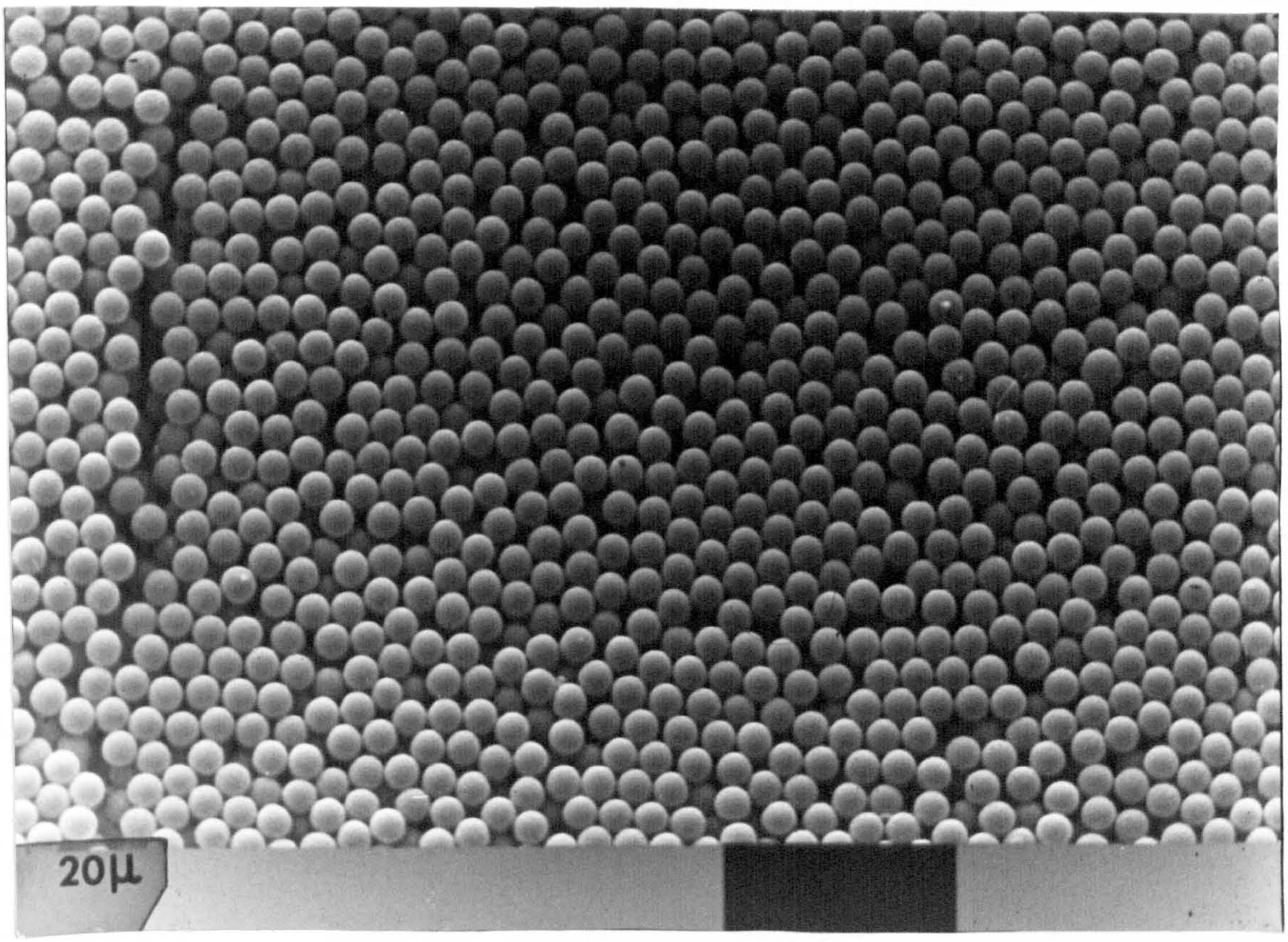

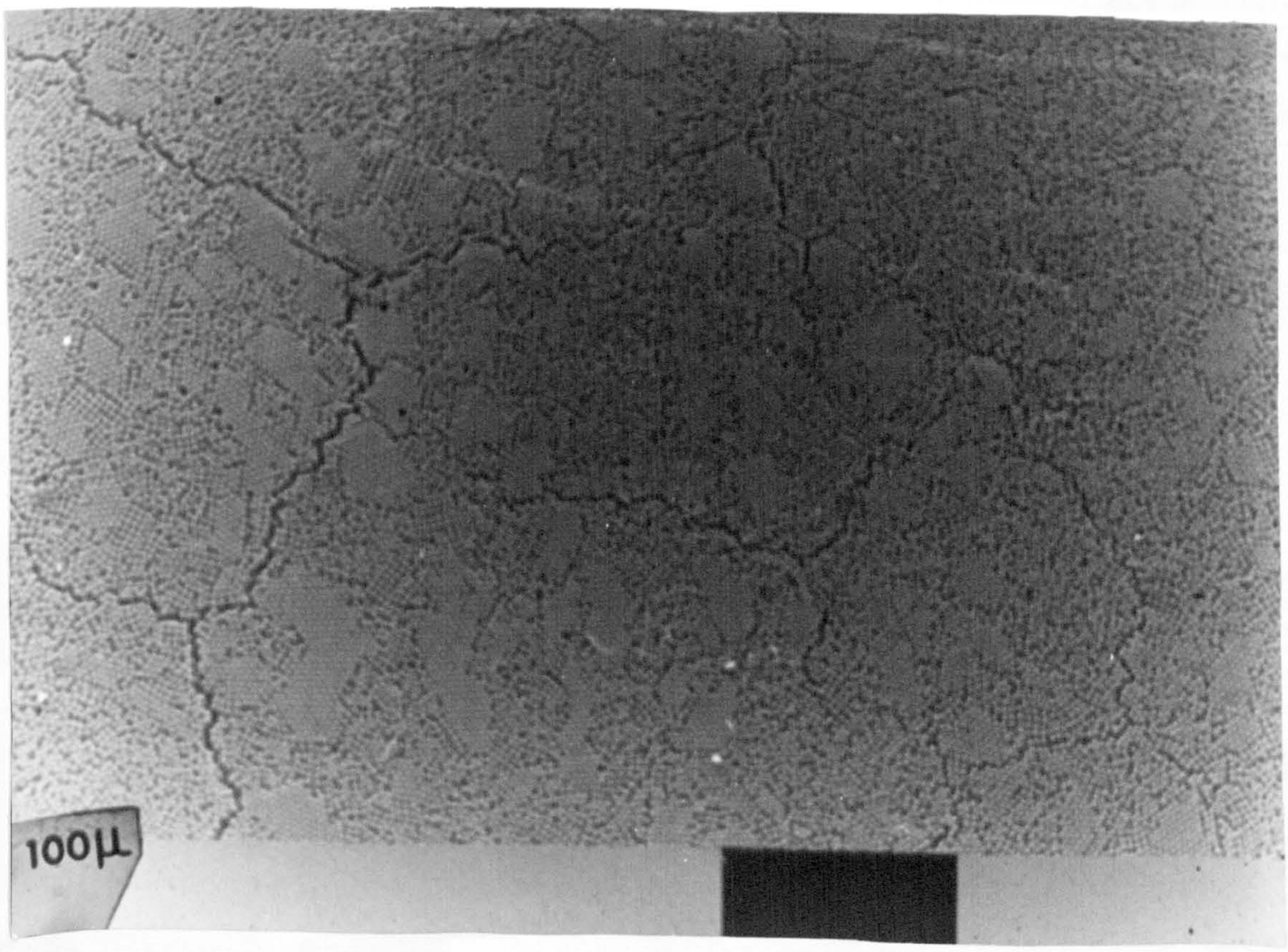

Another type of model they considered was one where the two different types of surface were combined in such a way that they gave a non-circular distribution. Now the drop periphery moved between the barriers as well as across them. This increased the number of metastable regions and reduced the barriers between them.

In their second paper[145] Johnston and Dettre discussed the experimental measurements that they had made. They chose a paraffin wax model system where the surface roughness at the most was only a second order effect on hysteresis. They found reasonable agreement with the theory considering the assumptions made. The advancing contact angle was found to be insensitive to the coverage of high contact angle regions after fifty percent coverage.

8.3 Measurement of Contact Angle in the Present Work

This proved to be a difficult problem. Firstly, the captive bubble method was tried. Here a layer of polystyrene latex particles, dried down on a glass slide, was immersed in the liquid and an air bubble touched onto the layer. Unfortunately the moment the layer was immersed in the sodium chloride solution it became detached from the solid substrate and floated off.

Two other methods were eventually tried and these will be discussed in the following sections.

8.4 Captive Drop Method

8.4.1 Experimental

Latex JC and S67, 3.89 μm and 2.2 μm diameters, were dried down, from concentrated suspensions in water, onto glass cover slides. The layers were dried and kept in a desiccator over silica gel.

An estimate of the roughness of the surface was obtained from scanning electromicrographs of the layers themselves. Figure 8/4 shows some examples of the micrographs obtained from the gold-coated layers at various magnifications.

Figure 8/5 : Optical Bench for the Captive Bubble Method

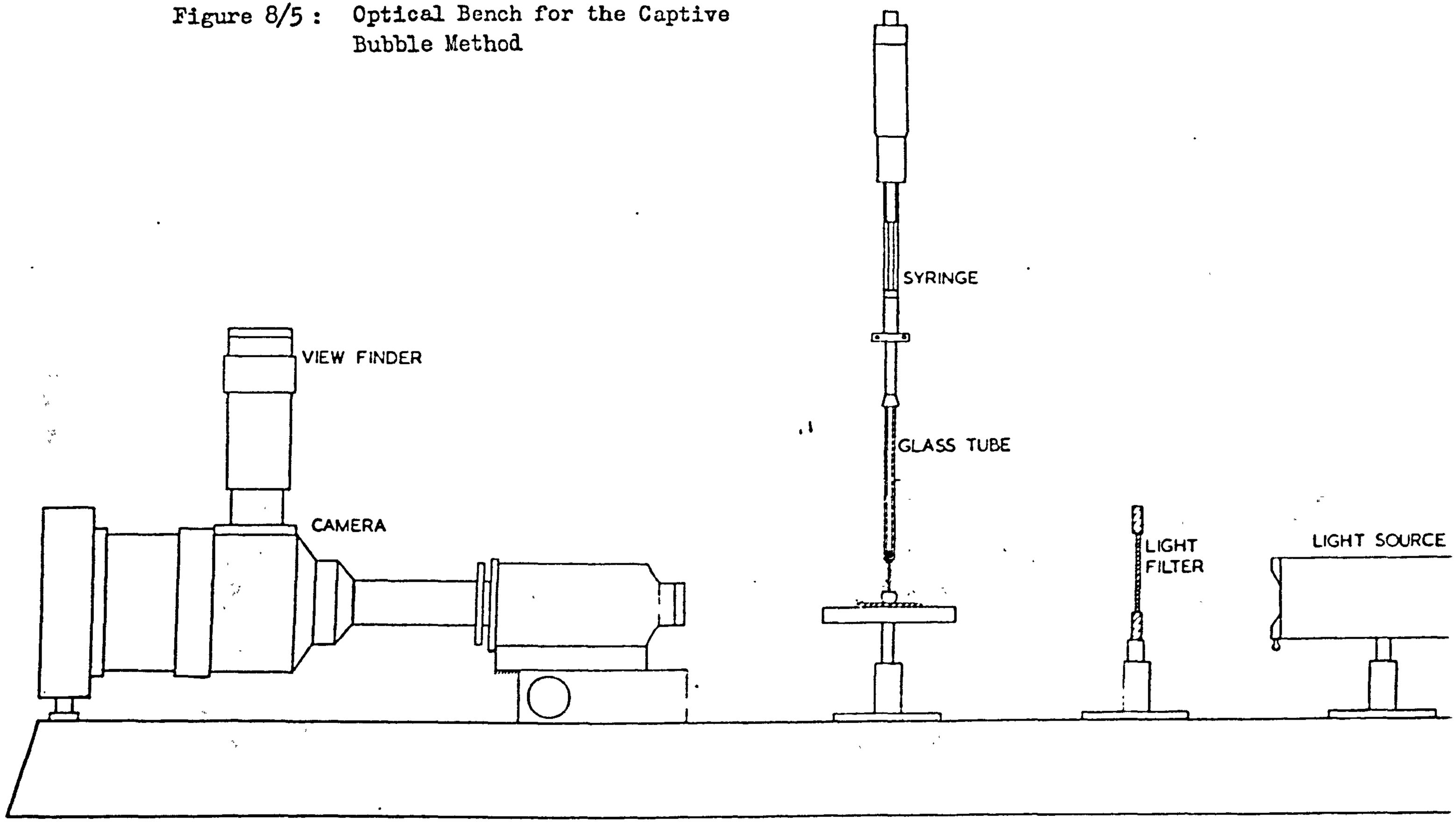

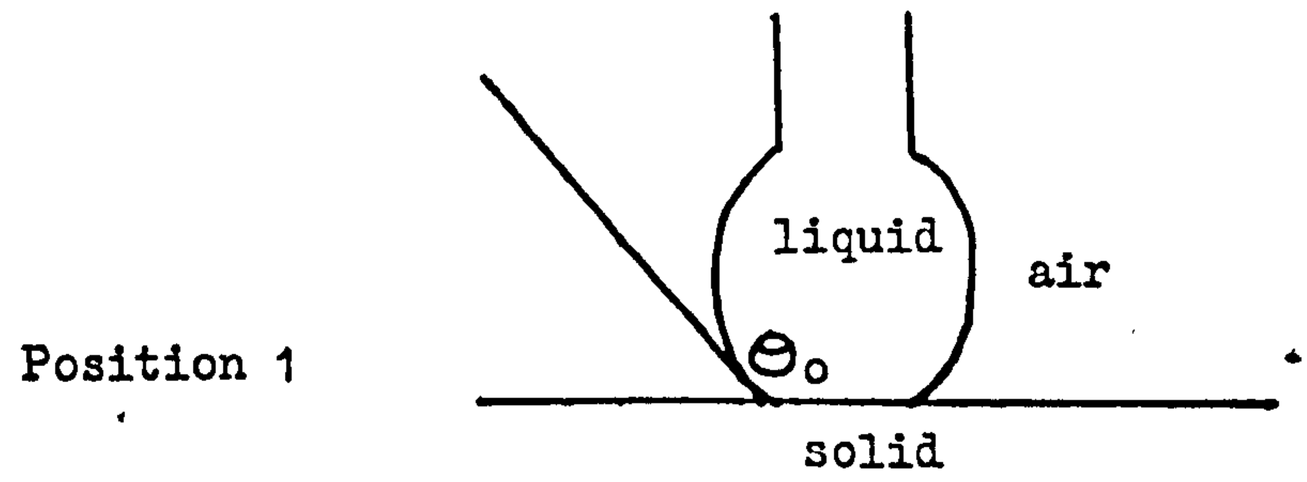
Position 1
liquid
air
θ_o
solid
Position 2
θ'_a
Position 3
θ_r
Position 4
θ''_a

Figure 8/6

For each run a slide was placed on the adjustable table of the apparatus sketched in figure 8/5. The micrometer, mounted on the syringe containing the liquid, was turned. A drop was allowed to touch the layer. After two minutes two photographs of the drop were taken; using a camera with an exposure time of $\frac{1}{2}$ second and Ilford FP4 film. A green filter was used in conjunction with a tungsten lamp to provide monochromatic illumination. The micrometer was then turned further until the point of contact of the liquid with the solid moved. Two further photographs were taken after two minutes. The micrometer was turned in the opposite direction and the liquid was sucked up from the layer until it was below the tip of the needle. After waiting two minutes two photographs were taken. The drop was advanced again by adding more liquid until the point of contact with the solid surface moved; photographs were taken after two minutes. For each run a total of five drops were photographed in each of the four positions, figure 8/6.

The contact angles were measured by taking the developed film and projecting it onto white paper. The angles were drawn and measured with a protractor. The mean angle in each position was found by averaging all the angles drawn.

Sodium chloride solutions in the range 0.05 to 0.5 mol dm^{-3} were investigated when in contact with layers of latices JC and S67. Also DTAB solutions in the range 1×10^{-5} to 2×10^{-3} mol dm^{-3} for layers of latex JC were studied.

8.4.2 Results

(a) Defining the angles

The contact angles measured in position 1, figure 8/6, were denoted by θ_o. These are the equilibrium contact angles measured macroscopically on the drop at rest in contact with the solid.

The mean advancing angle for each run, $\overline{\theta}_A$, was found by averaging the angles in position 2, θ'_a, and those in position 4, θ''_a. In both cases

Figure 8/7: A drop of 0.2 mol dm^{-3} Sodium Chloride on a Layer of Latex JC

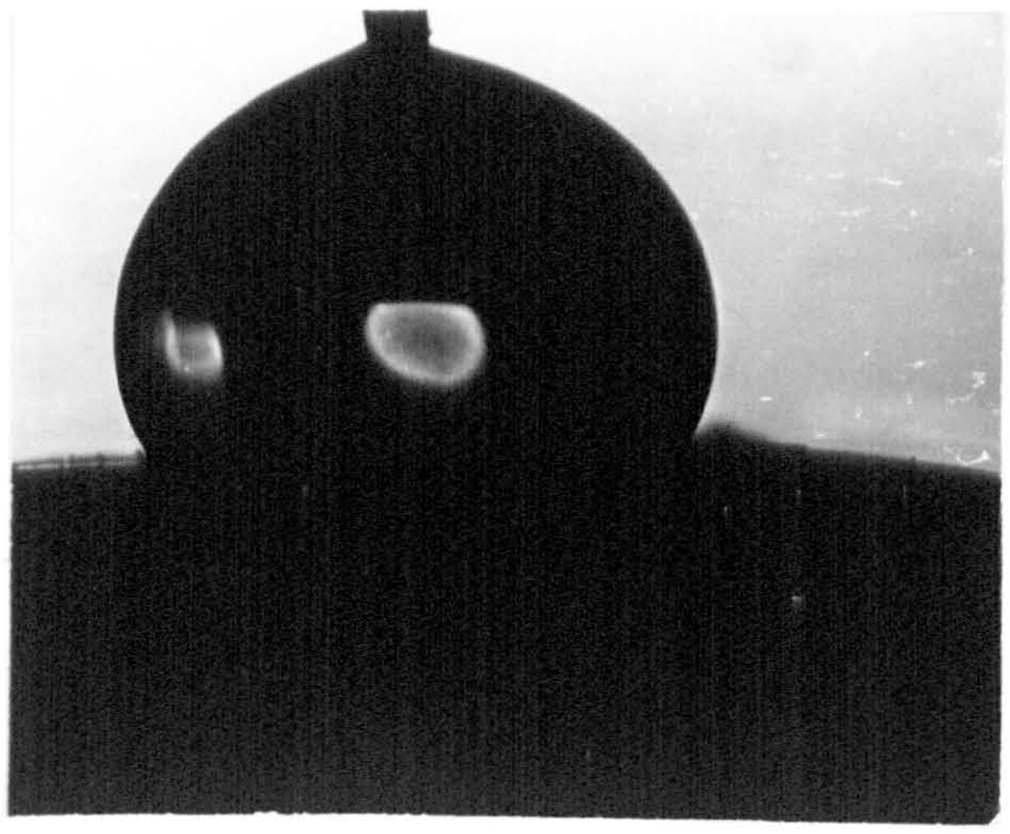

Position 1

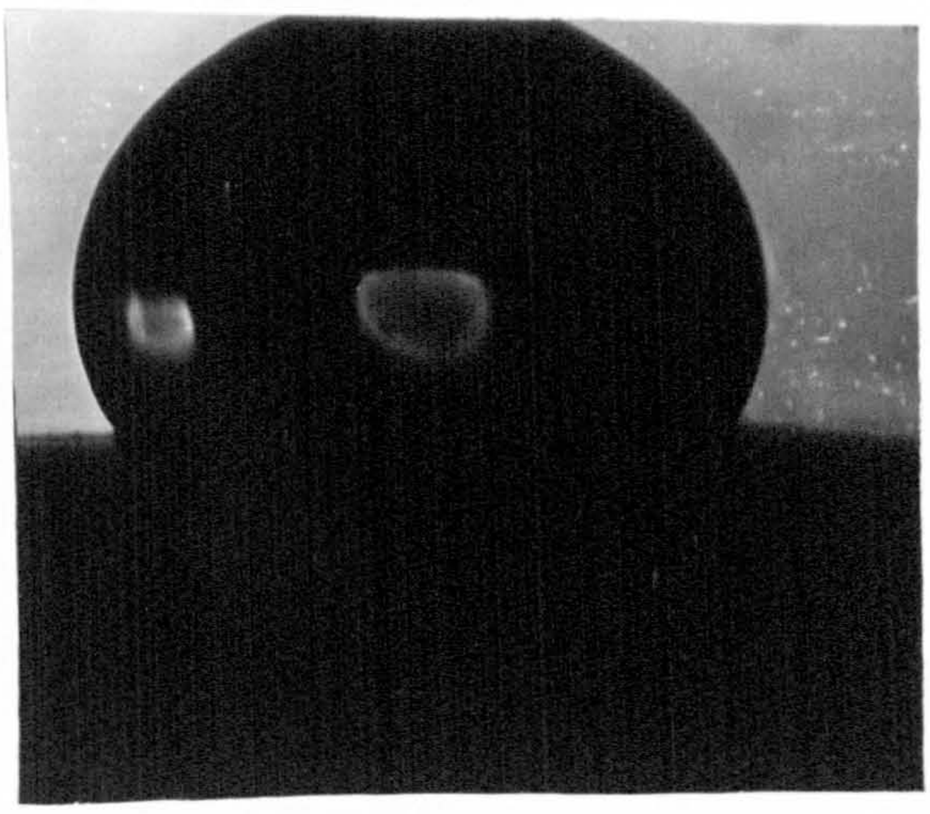

Position 2

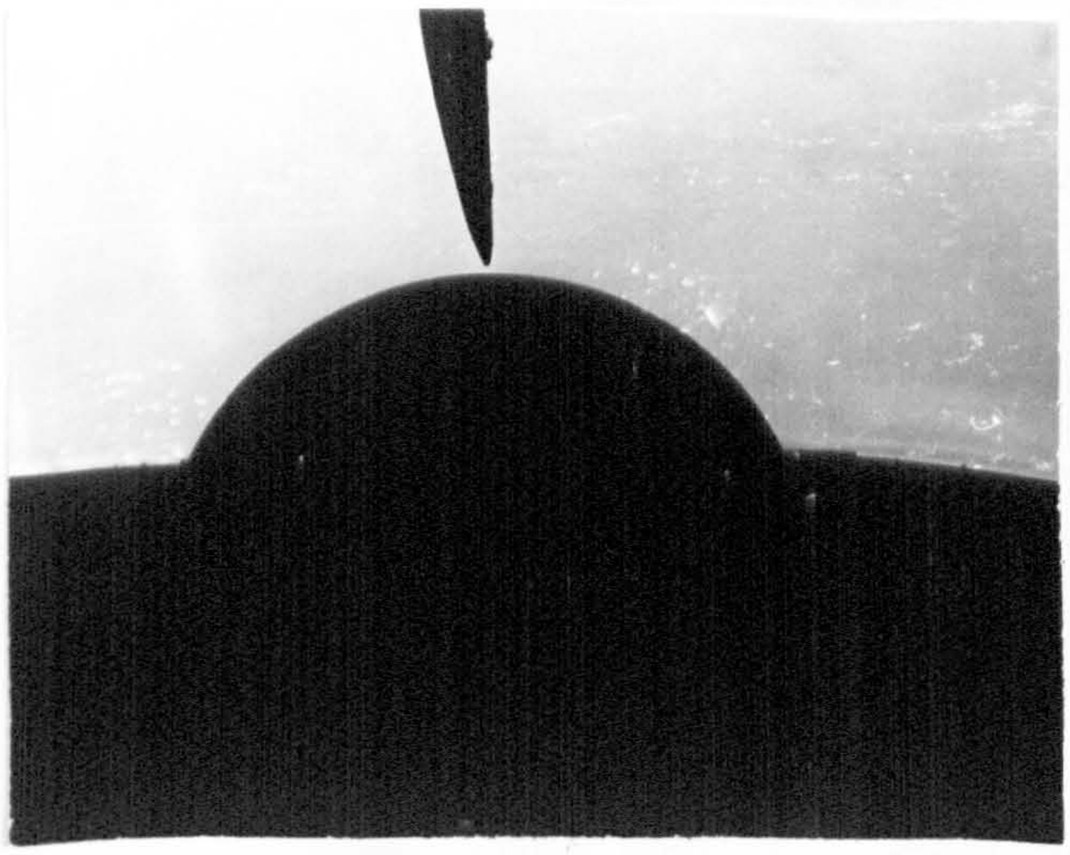

Position 3

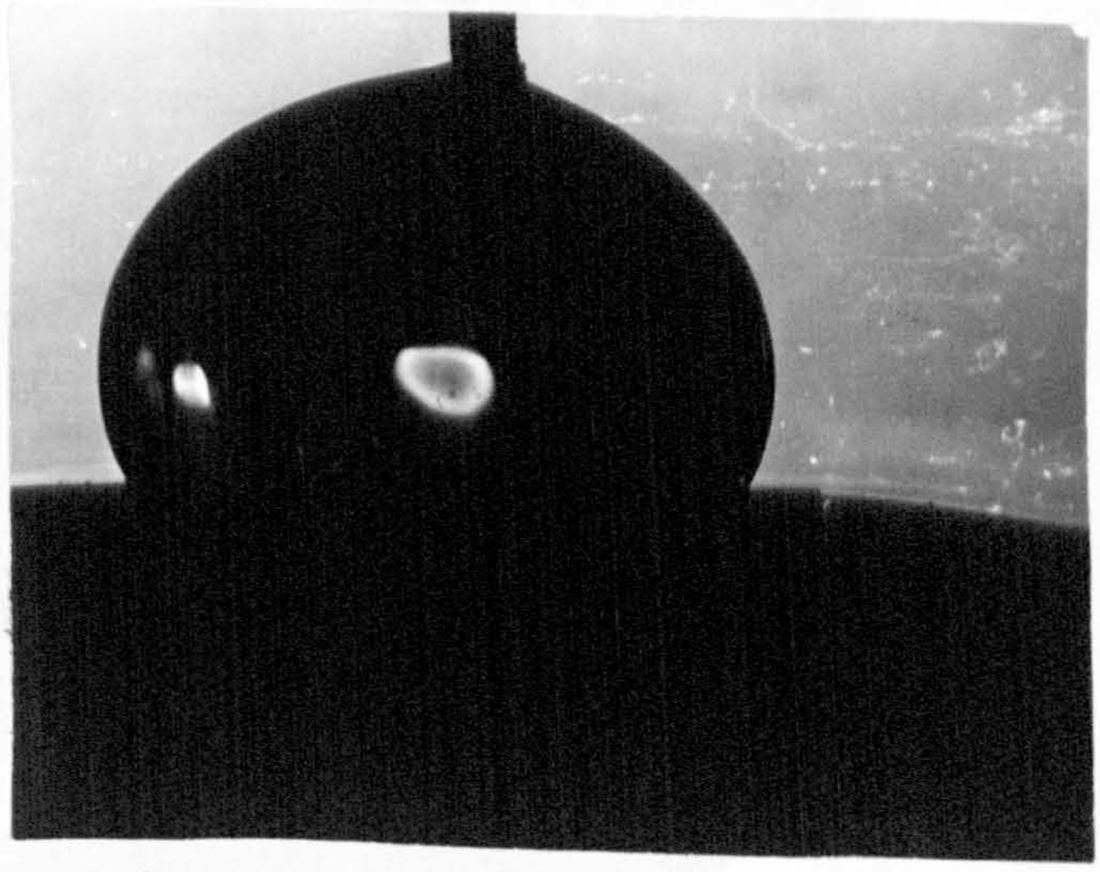

Position 4

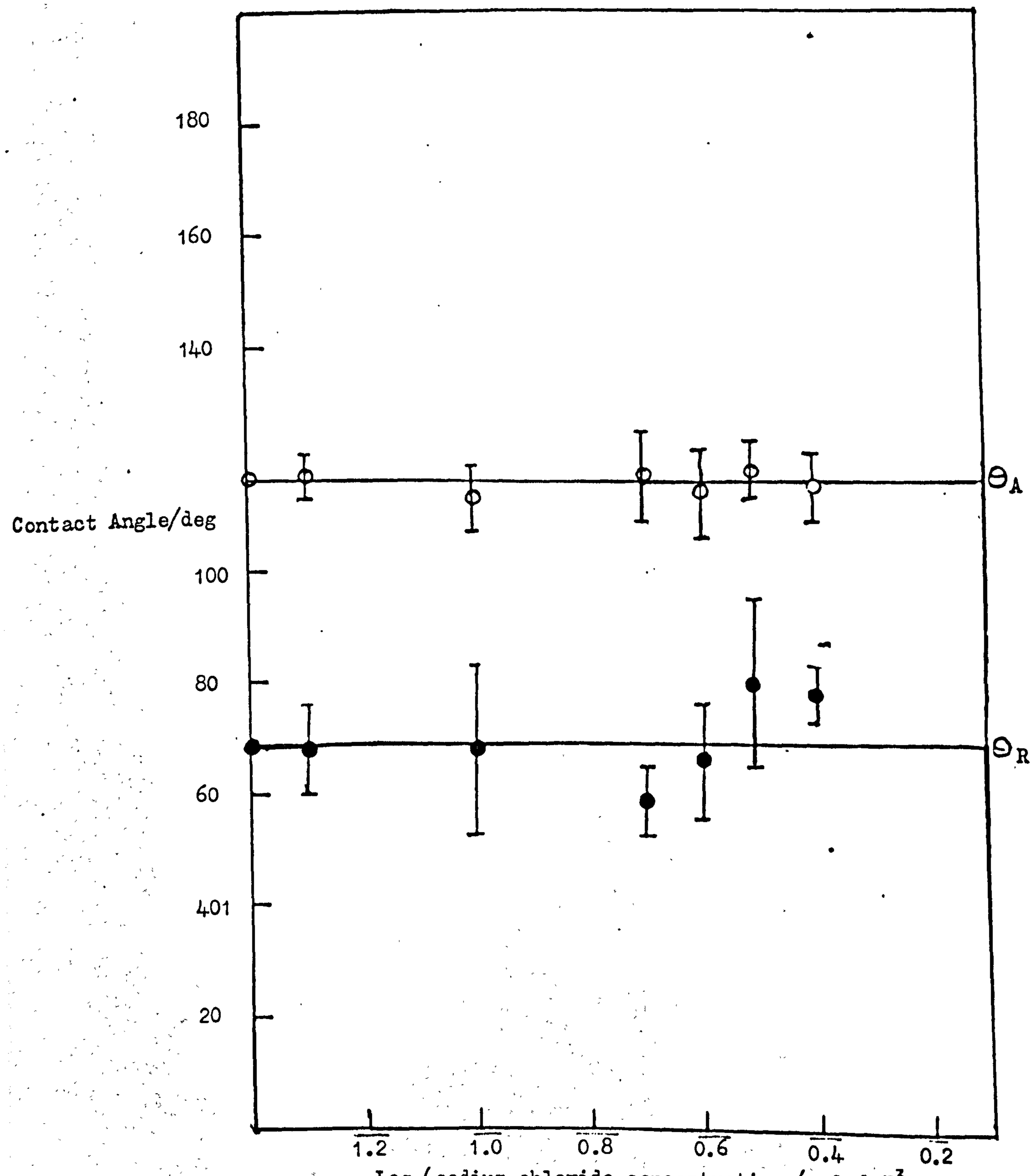

Figure 8/8 : Contact Angles of Salt Solutions on Latex JC

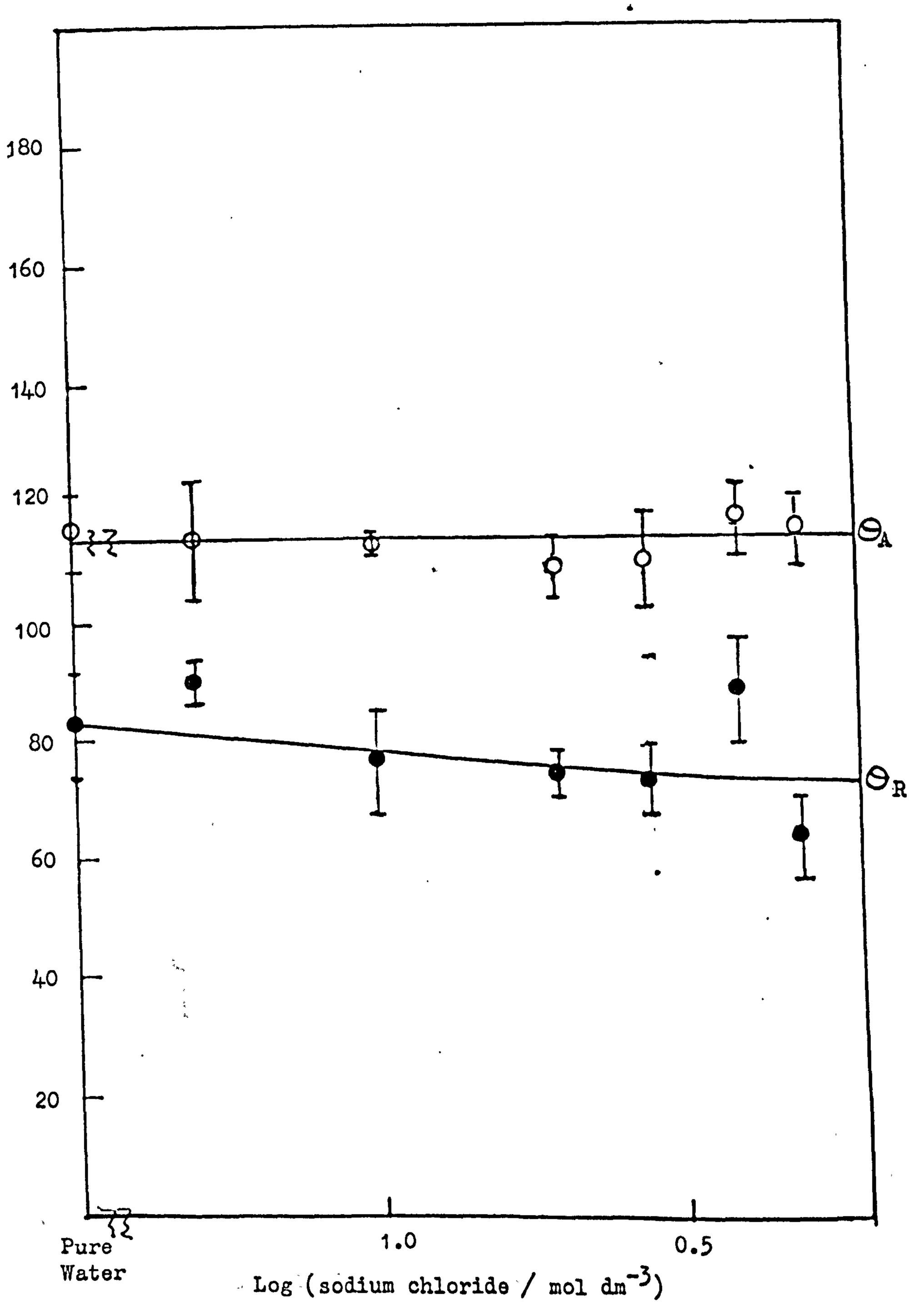

Figure 8/9 : Contact Angles of Salt Solutions on S 67

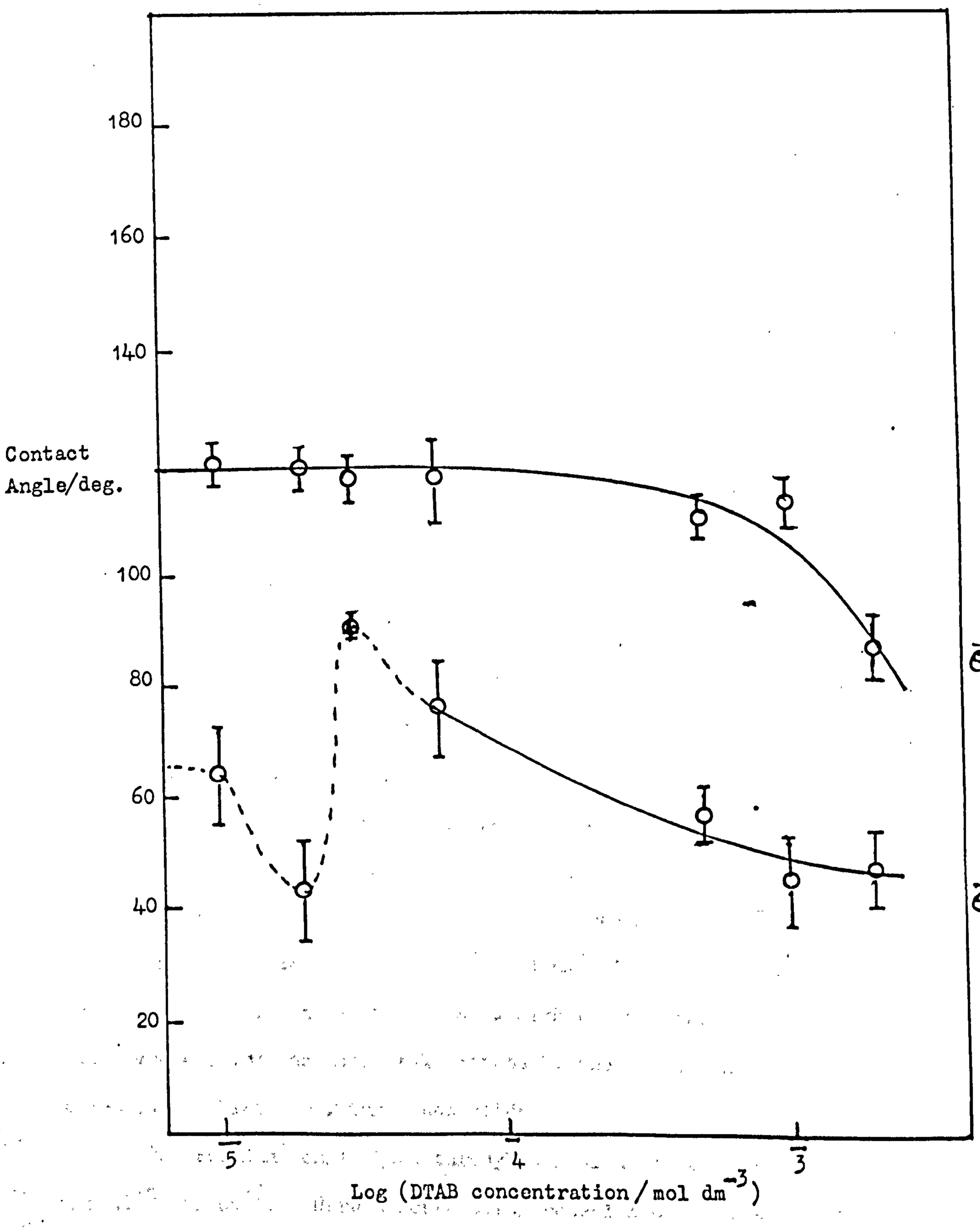

Figure 8/10 : Contact Angles of DTAB Solutions on Latex JC

the point of contact of the liquid and solid phases has been moved.

The receding angle for each run $\overline{\theta}_R$ was calculated by averaging all the angles determined in position 3.

(b) Salt solutions on latex JC

Figure 8/7 shows a typical series of photographs of the four different positions for 0.2 mol dm^{-3} sodium chloride on latex JC.

Figure 8/8 shows the averaged contact angles for the salt solutions studied. The standard deviation of each set of results has been determined.

There is no appreciable difference in contact angle in this range. The advancing angles are, within experimental error, 116°. The receding angles show a larger overall error but can be averaged out to 68°. These are the same as the corresponding angles for twice-distilled water.

(c) Salt solutions on latex S67

Figure 8/9 shows the contact angle data for salt solutions touching a compact layer of latex particles. The advancing angles show no appreciable difference with salt concentration and are, within experimental error, 114°. The receding angles show a general decrease with salt from 90° to 72°. The advancing and receding contact angles for twice-distilled water were found to be 115° and 83° respectively.

(d) DTAB solutions on latex JC

The variation in contact angle for the range 1×10^{-5} to 2×10^{-3} mol dm^{-3} DTAB is shown in figure 8/10. The advancing angle is constant, at about 117°, until the DTAB concentration reaches 5×10^{-4} mol dm^{-3} where it begins to decrease. At 2×10^{-3} mol dm^{-3} it drops below 90°, showing an improved wetting situation. At a higher concentration of DTAB the polystyrene layer was completely wetted by the surfactant solution and as a result was lifted off the glass slide.

The receding angle goes through a maximum at a DTAB concentration of 3×10^{-5} mol dm^{-3}. Here a non-wetting receding contact angle of 91° was found.

Wetting situation $\theta < 90^{\circ}$

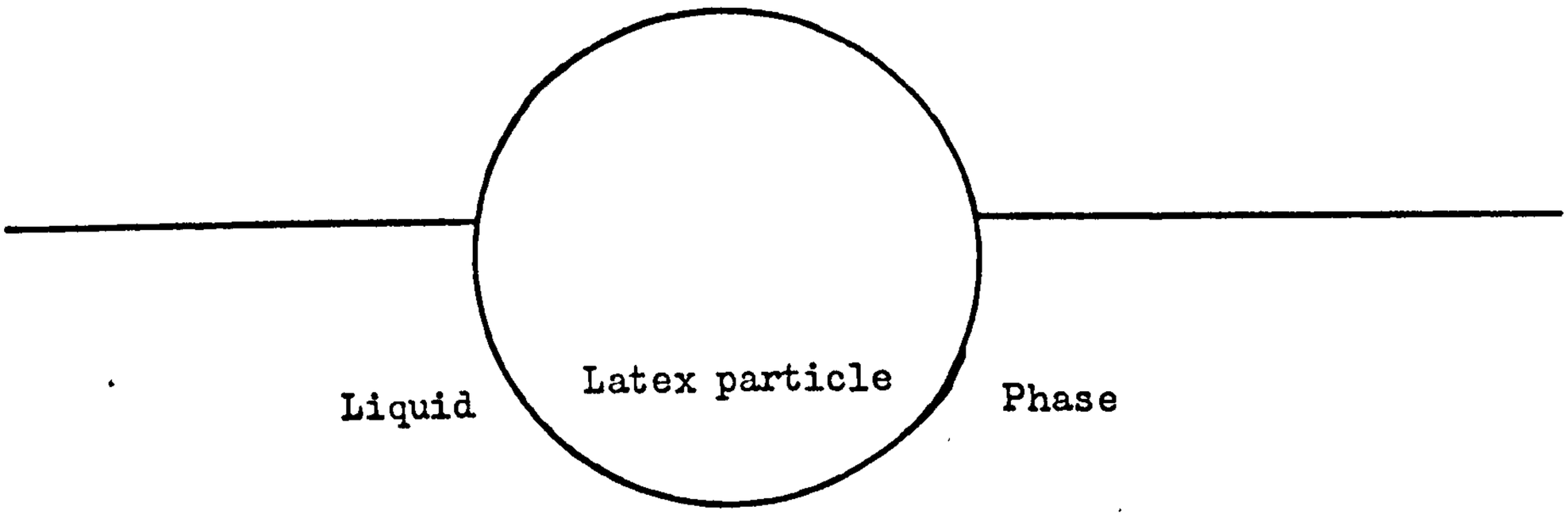

Non-wetting situation $\theta > 90^{\circ}$

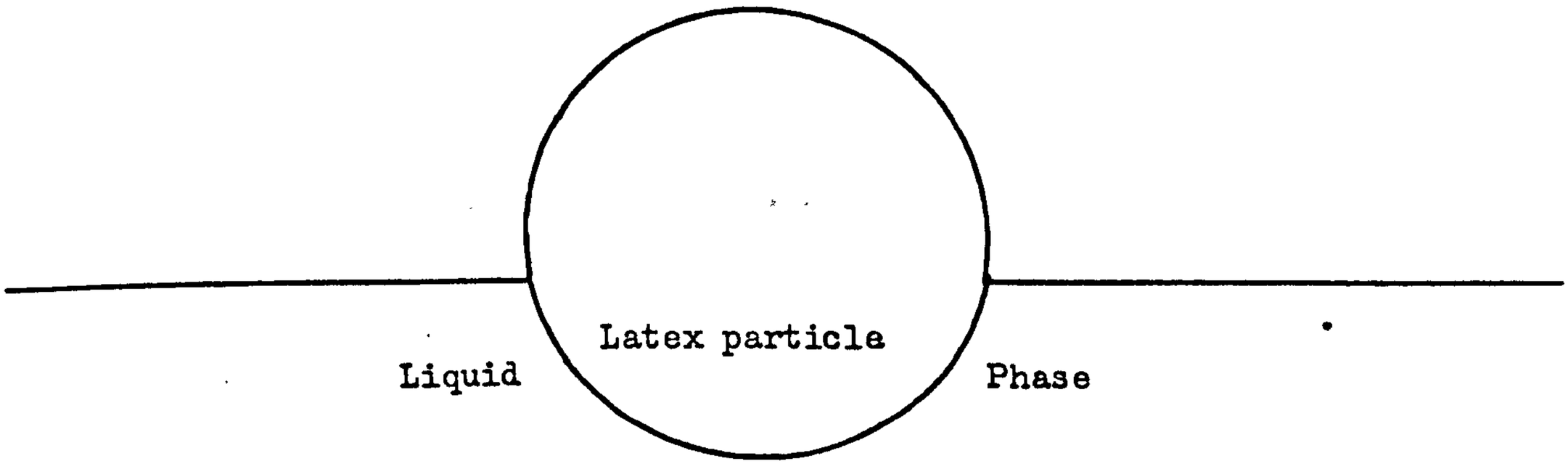

Figure 8/11

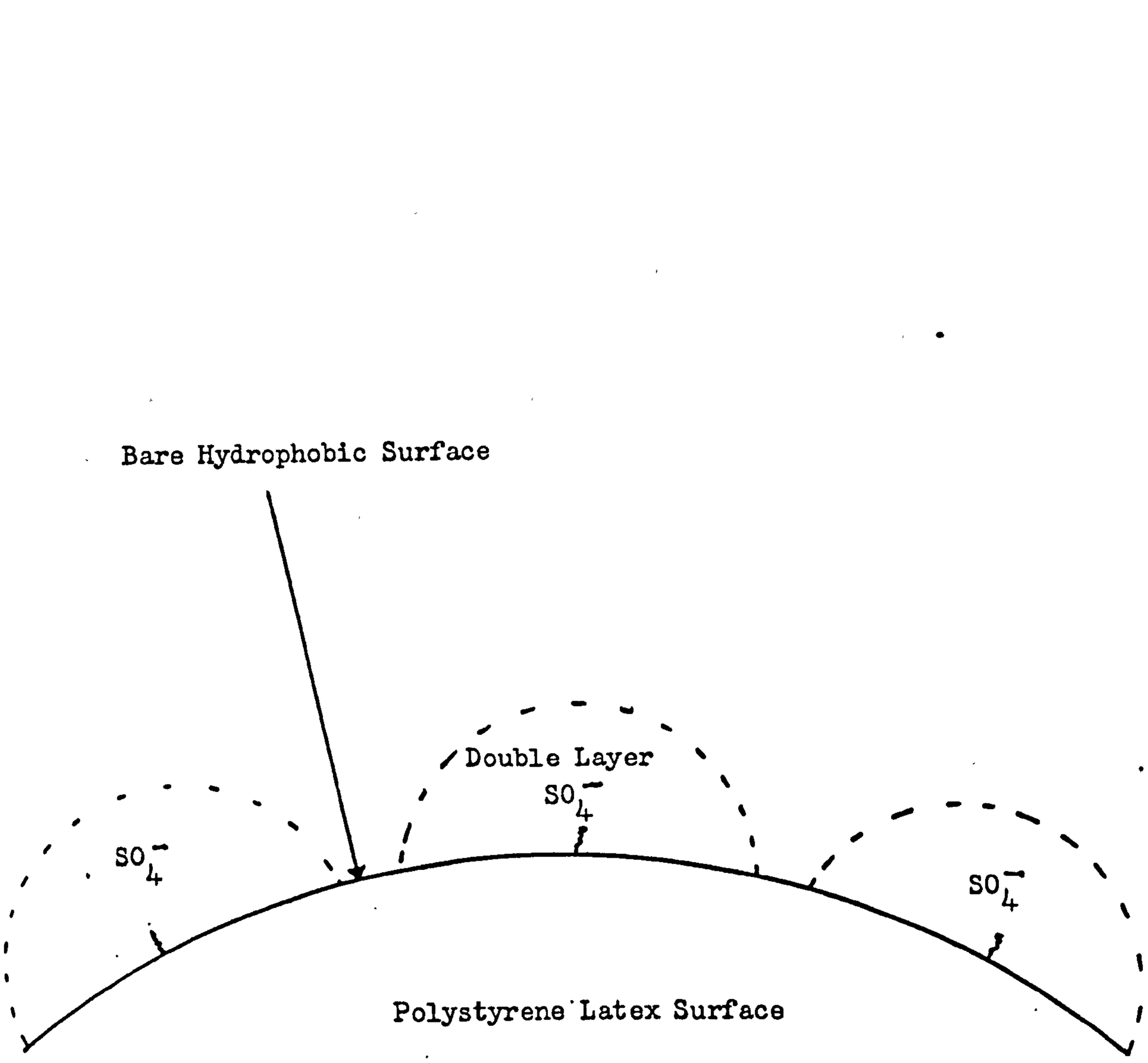

Figure 8/12 : Compression of the Double Layer

8.4.3 Conclusions

If a polystyrene particle is situated at an air-liquid interface part of its surface will not be wetted by the liquid phase, that is the contact angle must be greater than zero. Depending on whether the polystyrene latex particle favours a wetting situation ($\theta < 90^{\circ}$) or a non-wetting situation ($\theta > 90^{\circ}$), the height of the liquid meniscus and consequently the area of the particle in the gaseous phase will vary as shown in figure 8/11.

Therefore although the DTAB results show an increase in contact angle in the latex foaming region to an angle greater than 90° as would be expected, the sodium chloride results do not appear to vary in the foaming region.

With the DTAB experiments the surface charge is being neutralised as the surfactant is adsorbed on the polystyrene surface. This is a different mechanism of changing the surface character than with the salt solutions.

With the highly concentrated sodium chloride suspensions, the electrolyte is causing the double layer of counterions around the surface charges to shrink. Eventually there will be a point where this shrinkage will cause bare hydrophobic polystyrene surface to be exposed, figure 8/12.

This method of measuring contact angle appears to be sensitive to changes in surface nature due to adsorption of a surfactant, but does not indicate the effect that decreasing the double layer thickness has on the wetting character of the solid. As a method for contact angle measurements it gives no information on the effect of the roughness of the solid surface.

With this in mind the next section concerns the development of a method of Wolfram[147] which attempts to eliminate any surface roughness and by so doing enable the microscopic equilibrium contact angle to be estimated from macroscopic measurements.

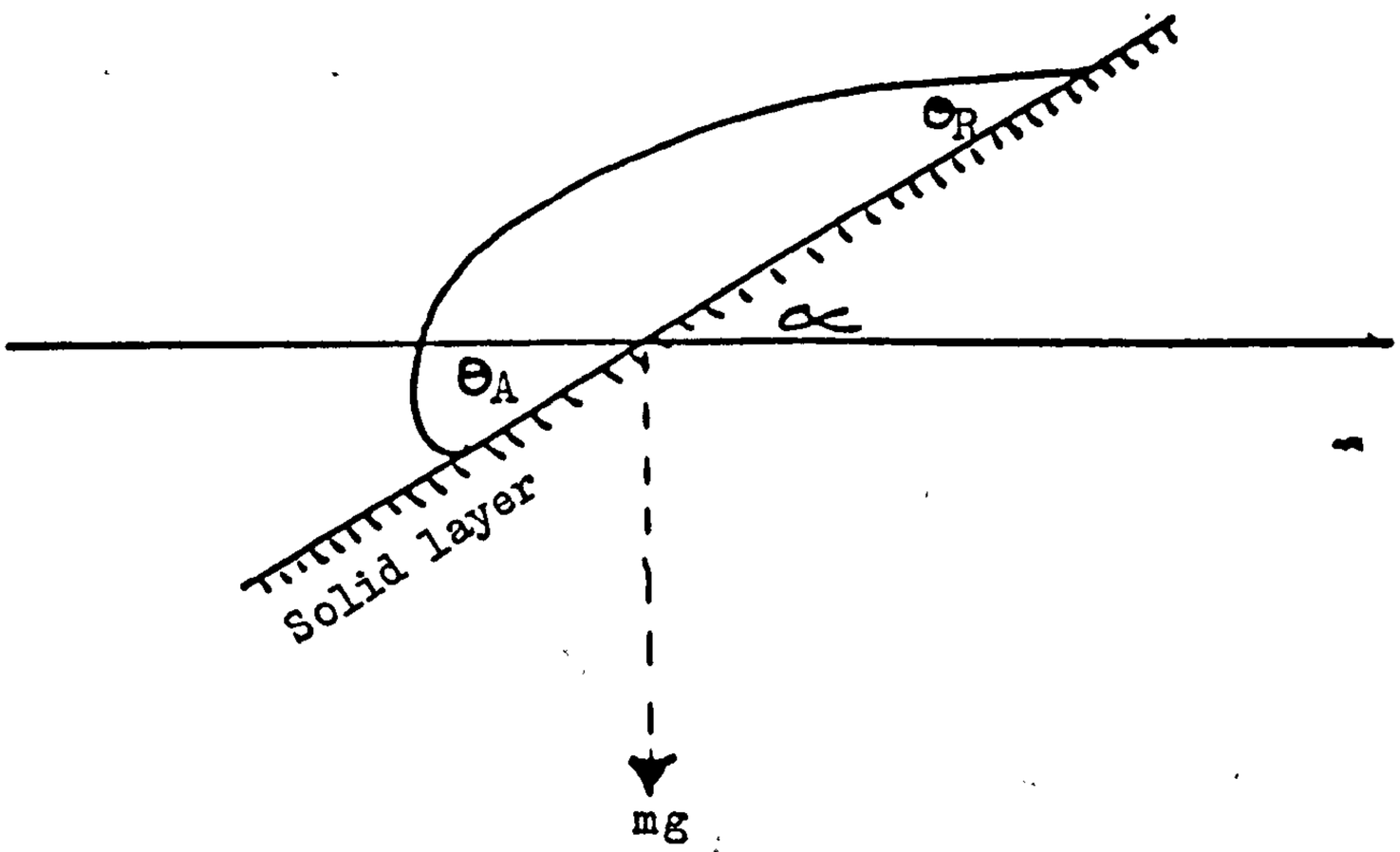

Figure 8/13: Drop on a tilting plate

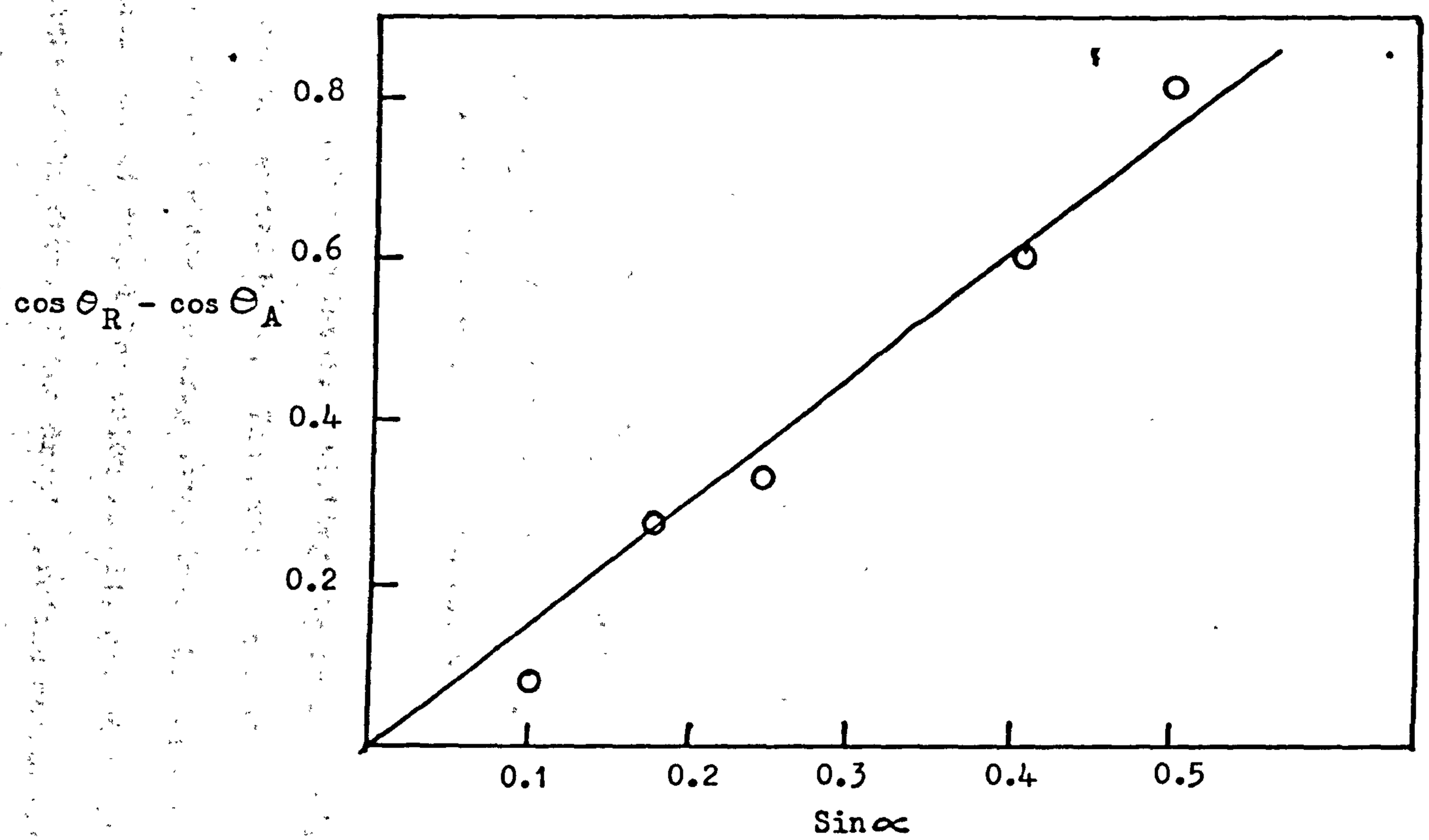

Figure 8/14: Graph of the Difference of the Cosines of the Receding and Advancing Contact Angles against the Sine of the Angle of Tilt for Latex S67 and 0.05 mol dm^{-3} Sodium Chloride.

8.5 Contact Angle by Tilt

8.5.1 Introduction

MacDougall and Ockrent originated the method of using a drop of liquid on a tilted solid plate, in 1942.[148] In the present work a drop was placed on a layer of the solid deposited on a glass plate and then the whole system was slowly tilted.

MacDougall and Ockrent postulated a theory dealing with the equilibrium forces acting on the drop as it is tilted, figure 8/13. They proposed the following equation:

$$\cos\theta_R - \cos\theta_A = K_1 A \sin\alpha$$

with $$K_1 = \frac{\rho g}{\gamma}$$

where A is the area of contact of the drop with the solid and ρ is the density. Therefore the graph of the difference in the cosines of the two contact angles, θ_R and θ_A, against the sine of the tilt angle should be linear. Figure 8/14 shows this graph plotted for a set of data of a drop of 0.05 mol dm^{-3} sodium chloride on a layer of latex S67.

8.5.2 Theory of the Tilting Plate Method

For a liquid drop on a horizontal geometrically smooth surface the equilibrium contact angle should be such that Young's equation is obeyed. That is

$$\gamma_{SV} = \gamma_{SL} + \gamma_{LV}\cos\theta$$

where γ_{SV}, γ_{SL} and γ_{LV} are the interfacial tensions for the solid-vapour, solid-liquid and liquid-vapour interfaces, and θ is the equilibrium contact angle.

This technique involves tilting the solid surface to an angle of tilt which can be denoted by α. The layer is tilted until a critical value of tilt is reached where the drop moves down the solid surface. There is a critical mass of drop below which it will not roll off. As the drop moves the angle at the front of the drop's profile corresponds to the advancing angle, while the back angle is the receding angle. The angle of tilt when

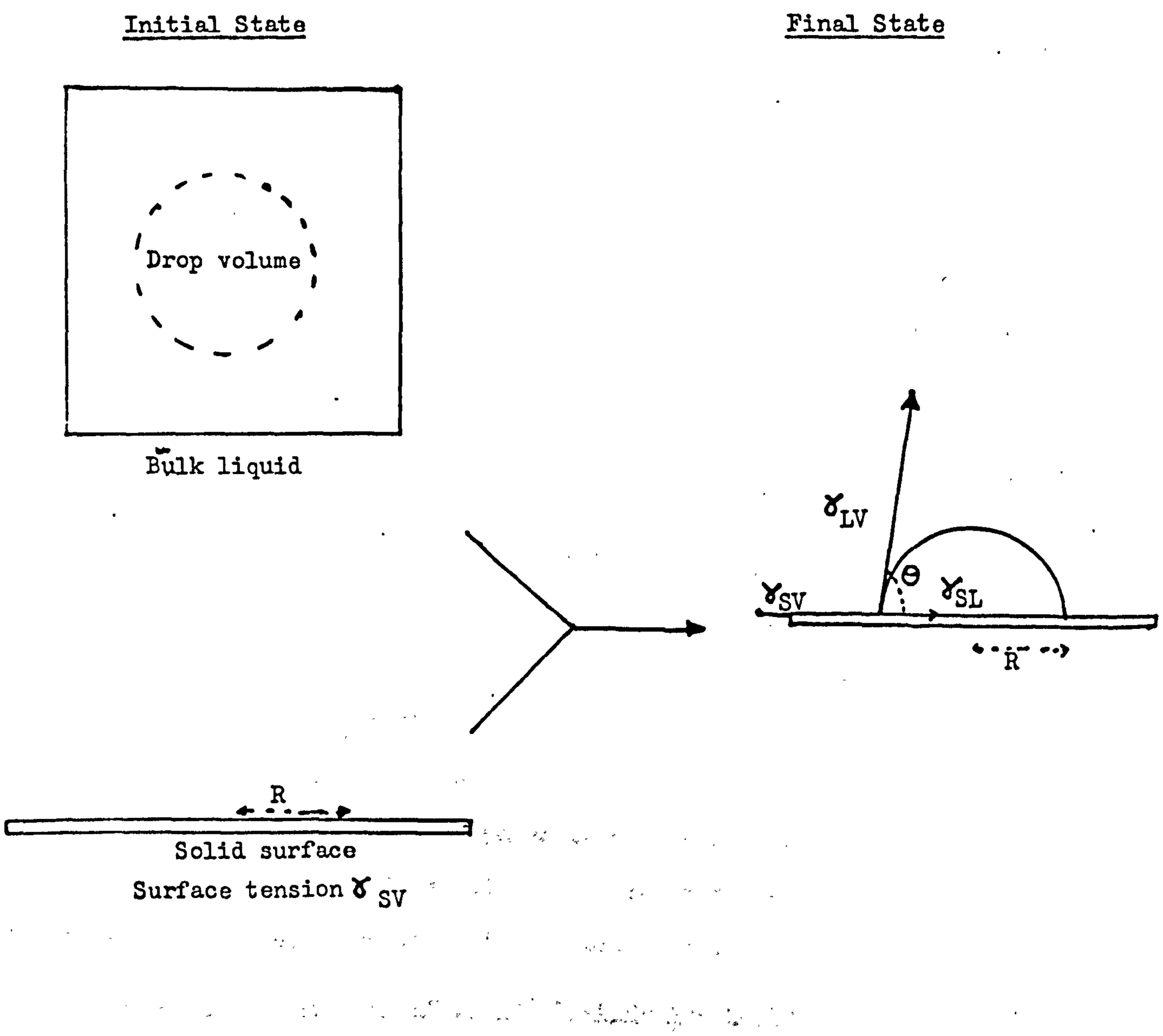
Initial State
Drop volume
Bulk liquid
Final State
γ_{LV}
γ_{SV}
Θ
γ_{SL}
R
R
Solid surface
Surface tension γ_{SV}

Figure 8/15

this situation occurs can be denoted as the critical angle tilt, α_{crit}.

If the surface is rough then the values of the advancing and receding angles depend on the degree of roughness. The critical tilt angle depends on the roughness of the solid surface. As α_{crit} increased Wolfram found the advancing angle to increase while the receding contact angle decreased[147]. The data for the advancing and receding angles at different degrees of roughness, that is at different α_{crit}, will therefore extrapolate back to zero critical angle of tilt. This is equivalent to a smooth planar surface. Both sets of data were found to extrapolate back to a single value of contact angle which corresponds to the angle obeying Young's equation, θ_Y, see section (a).

Therefore using this technique to measure the critical tilt angle the effect of roughness on contact angle is eliminated and Young's angle can be determined. Experimentally the values of the advancing and receding angles are measured for surfaces having different roughness factors.

(a) The spreading of a liquid drop on a solid surface

The process can be considered to involve taking a drop of liquid, volume V, from the interior of the bulk liquid and spreading it on the clean solid surface, figure 8/15. The drop is assumed to form a spherical liquid cap having a base radius of R. The contact angle, which is a measured macroscopic quantity for an apparently smooth surface, is denoted by θ. This does not necessarily equal the thermodynamic equilibrium angle, that is Young's angle, which is a microscopic quantity.

(b) Thermodynamics of drop formation on the plate

Since the interior of the bulk liquid can be taken as the standard state, see figure 8/15, and therefore has no interfacial term, the initial free energy F_i can be defined as

$$F_i = A_{SV} \cdot \gamma_{SV}$$

where A_{SV} is the area of solid surface which will be covered by the liquid.

Correspondingly the final free energy, F_f, is equal to

$$F_f = \gamma_{SL} A_{SL} + \gamma_{LV} A_{LV}$$

where γ_{SL} and γ_{LV} correspond to the interfacial tensions, and A_{SL} and A_{LV} the areas of the solid-liquid and liquid-vapour interfaces. This enables the free energy change, $\triangle F$, to be defined as

$$\triangle F = \gamma_{SL} A_{SL} + \gamma_{LV} A_{LV} - A_{SV} \gamma_{SV}$$

However, since $A_{SV} = A_{SL}$, it follows that

$$\triangle F = (\gamma_{SL} - \gamma_{SV}) A_{SL} + \gamma_{LV} A_{LV} \qquad (1)$$

The thermodynamic equilibrium is defined by the Young equation as

$$\gamma_{SV} = \gamma_{SL} + \gamma_{LV} \cos\theta_Y \qquad (2)$$

where θ_Y is the true, microscopic, thermodynamic contact angle.

Rewriting equations (1) and (2) the following is obtained:

$$(\gamma_{SL} - \gamma_{SV}) = -\gamma_{LV} \cos\theta_Y$$

and

$$\triangle F = \gamma_{LV} A_{LV} - \gamma_{LV} \cos\theta_Y A_{SL}$$

The area terms can for the first approximation be taken as the area of a spherical cap and a circle, respectively; hence

$$A_{LV} = \frac{2\pi R^2}{1 + \cos\theta} \qquad \text{(see Appendix I)}$$

$$A_{SV} = \pi R^2$$

$$\triangle F = \frac{2\pi R^2 \gamma_{LV}}{(1 + \cos\theta)} - \pi R^2 \gamma_{LV} \cos\theta_Y \qquad (3)$$

It should be noted that θ is a macroscopic quantity since it has been defined assuming that the solid surface is smooth, whereas θ_Y is the true microscopic contact angle.

For a rough solid surface a similar treatment to the above can be performed and the corresponding free energy change becomes

$$\triangle F' = \frac{2\pi R^2 \gamma_{LV}}{(1 + \cos\theta)} - r\pi R^2 \gamma_{LV} \cos\theta_Y \qquad (4)$$

(c) Force acting along the perimeter of the drop

The force can be obtained by differentiating the free energy change, equation (4) with respect to the radius of the liquid spherical cap:

$$\left(\frac{\partial \Delta F'}{\partial R}\right)_{\gamma_{LV}} = \frac{4\pi R \gamma_{LV}}{(1+\cos\theta)} + \frac{2\pi R^2 \gamma_{LV} \sin\theta}{(1+\cos\theta)^2}\frac{\partial\theta}{\partial R} - \overset{\frown}{2\pi R \gamma_{LV} \cos\theta_Y} \qquad (5)$$

The macroscopic angle θ is a variable dependent on the radius of the spherical cap, R, whereas the Young angle, θ_Y, is not.

Wolfram has defined the parameter f, which is the force per unit length of perimeter, as

$$f = \frac{1}{2\pi R}\left(\frac{\partial \Delta F''}{\partial R}\right)_{\gamma_{LV}} = \left[\frac{2\gamma_{LV}}{(1+\cos\theta)} + \frac{\gamma_{LV} R \sin\theta}{(1+\cos\theta)^2}\frac{\partial\theta}{\partial R}\right] - r\gamma_{LV}\cos\theta_Y \qquad (6)$$

This equation can be simplified by evaluating $\partial\theta/\partial R$.

This achieved by differentiating the volume of a spherical cap, radius R, with respect to both the radius R and contact angle θ. However as the drop is tilted, although the contact angle θ changes, which will mean that the dependent variable, the radius of the drop will also, the volume of the drop is assumed to remain constant. Equation (6) now becomes

$$f = \gamma_{LV}\cos\theta - r\gamma_{LV}\cos\theta_Y$$

As the drop moves down the inclined solid surface the macroscopic angle will be the advancing angle at the front and receding at the back. Forces corresponding to these two contact angles can be defined:

advancing case $f_A = \gamma_{LV}(\cos\theta_A - r\cos\theta_Y)$

receding case $-f_R = \gamma_{LV}(\cos\theta_R - r\cos\theta_Y)$

Equating these two forces, the roughness factor is given by

$$r = \frac{\cos\theta_A + \cos\theta_R}{2\cos\theta_Y}$$

and can be estimated from the two macroscopic measured angles and the extrapolated Young angle.

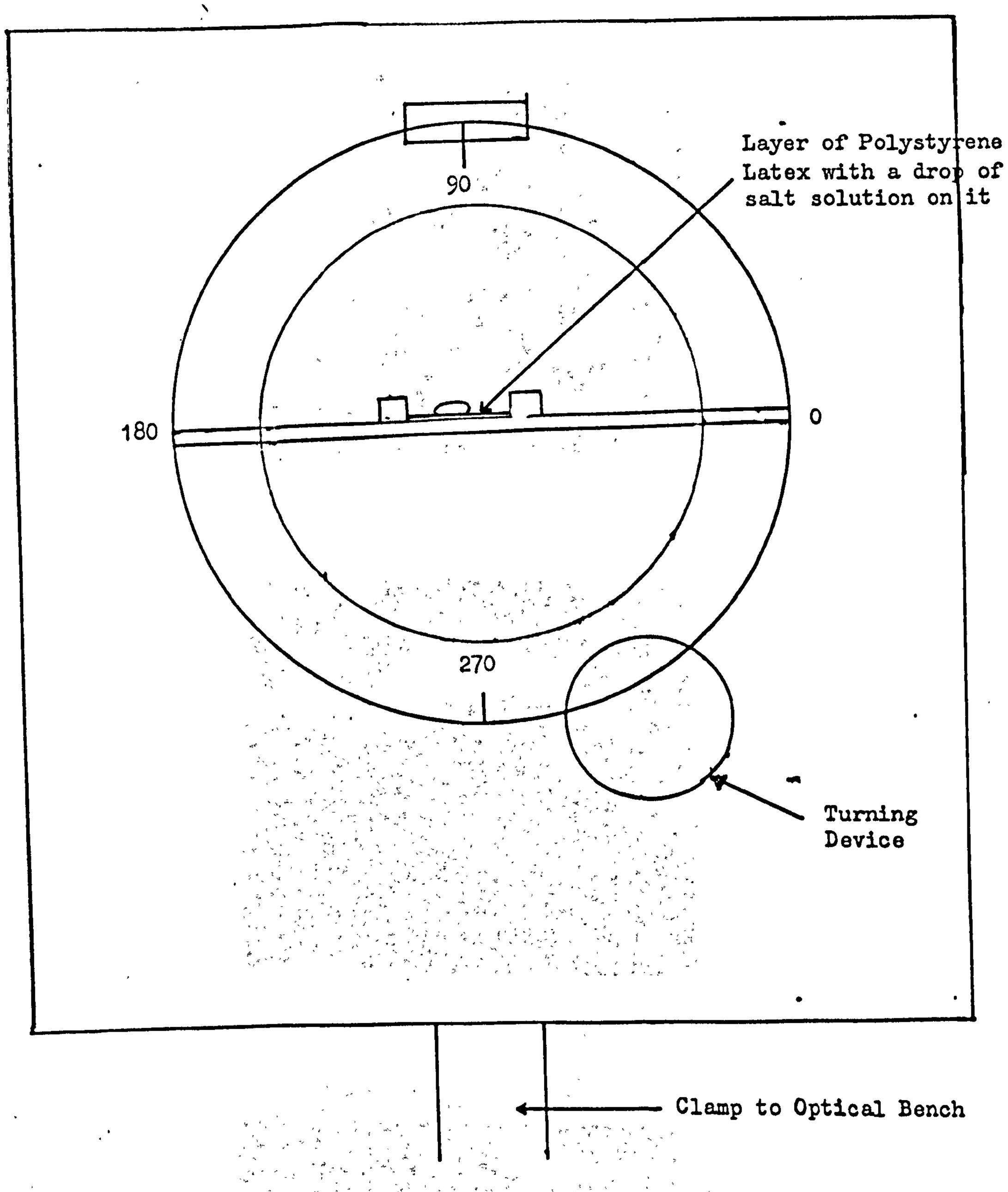

Figure 8/16 : Apparatus for the Tilting Drop Technique

Figure 8/17 : Deformation of a Drop on Tilting

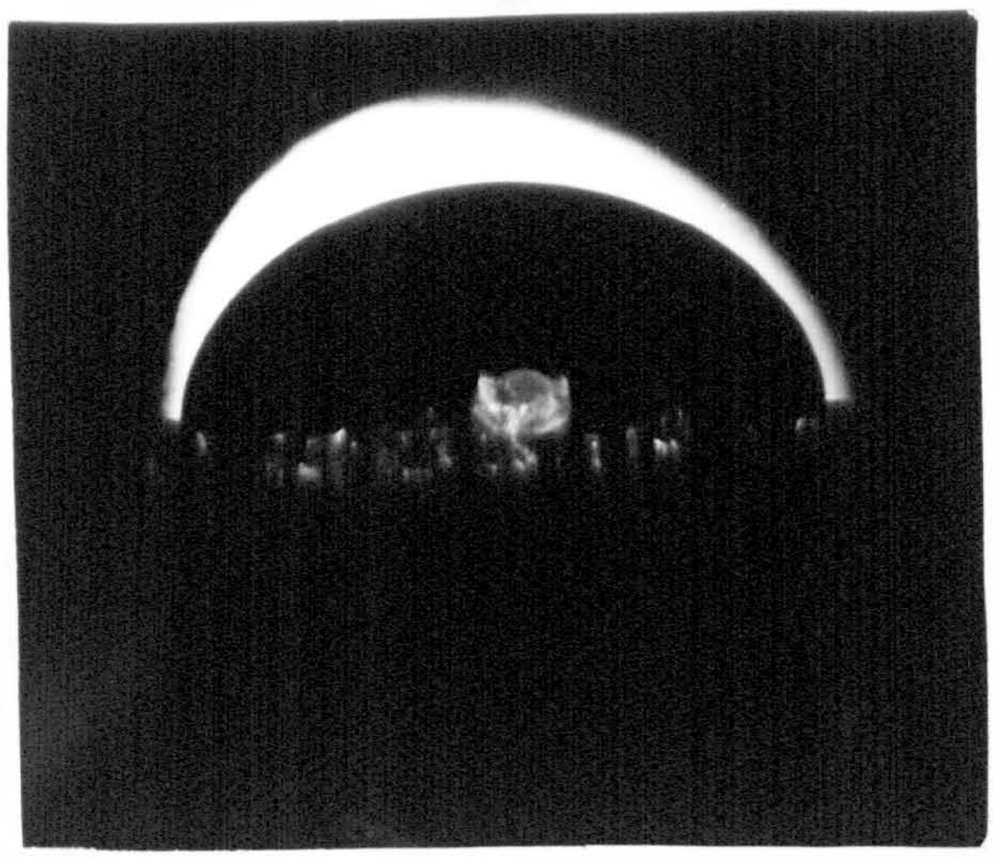

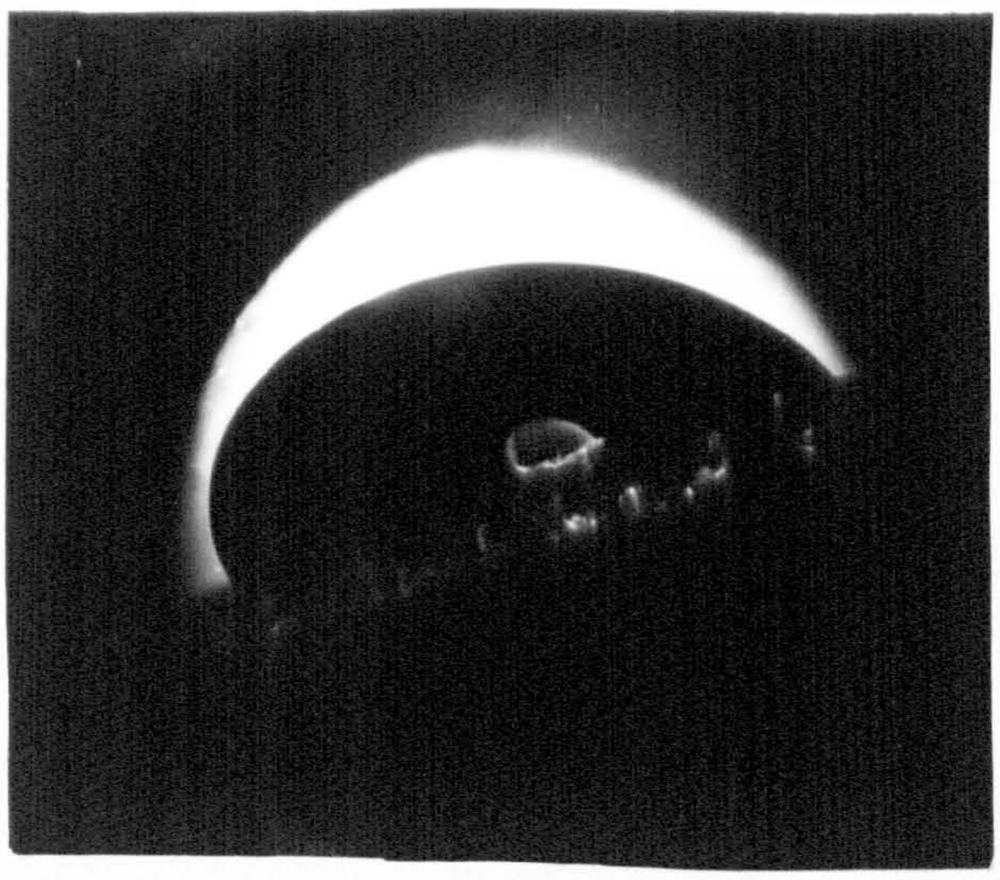

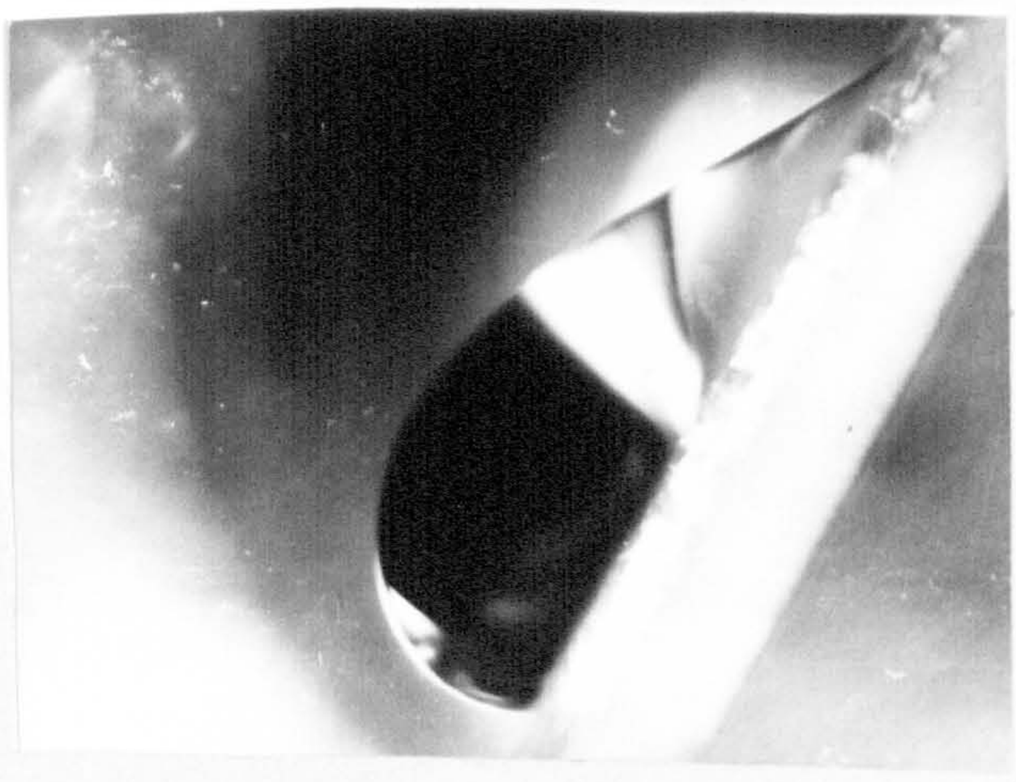

Figure 8/18 : Variation of Advancing and Receding Contact Angle with Tilt

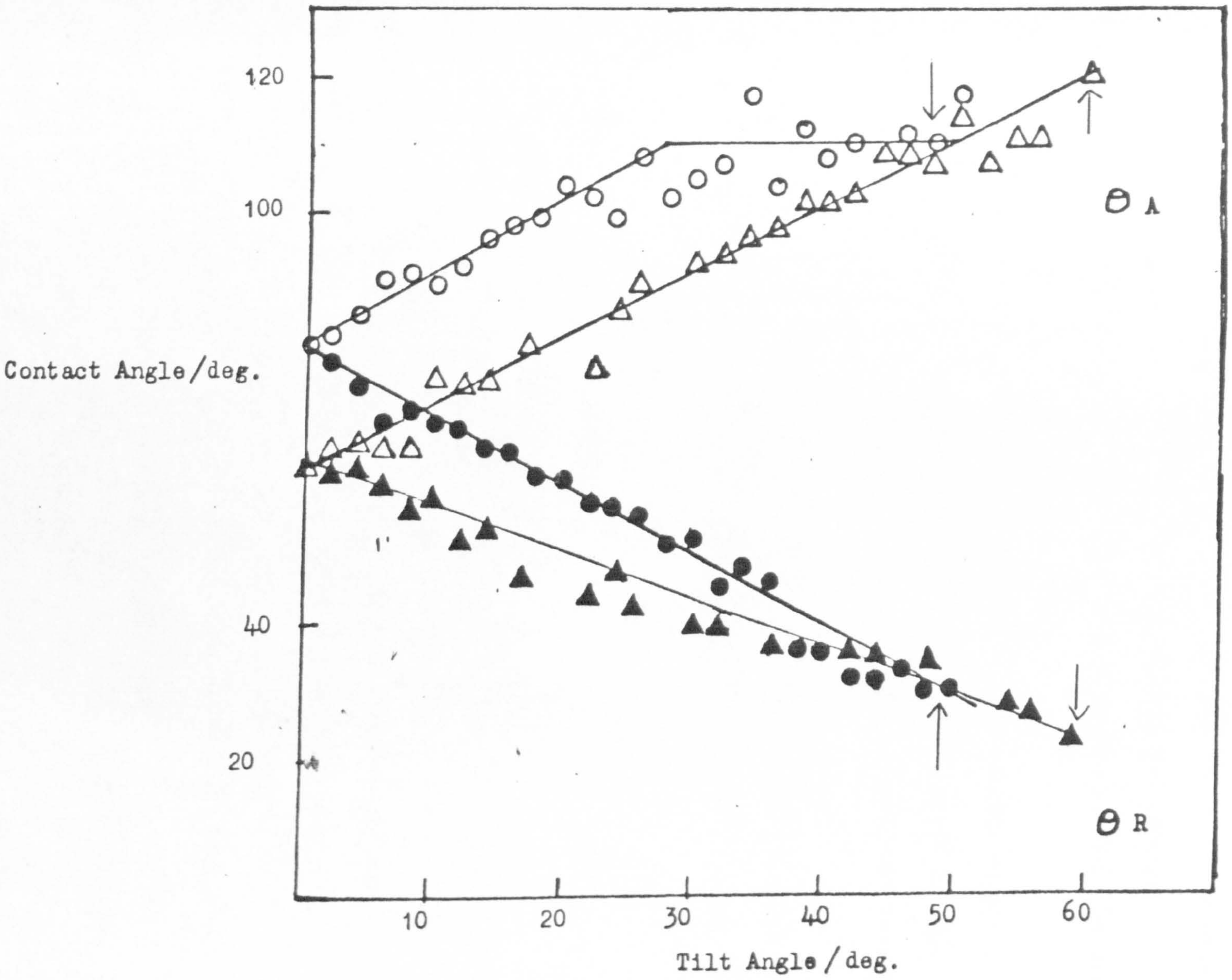

8.5.3 Experimental

The apparatus described in figure 8/16 was designed to hold the polystyrene coated cover slide as it was slowly tilted through a known angle. It was placed on the optical bench in figure 8/5 instead of the table.

The layers were prepared as described in section 8.4.1. The drop volume used was 0.1 cm^3, formed by using an interchangeable syringe. A large drop was required as there was a critical mass below which the drop would not roll off.

The layers were tilted through two degrees, left for two minutes, after which a photograph was taken. Three drops were tilted on layers deposited on three different slides for each run. The angles were measured as before, section 8.4.1.

Salt drops in the range 1×10^{-8} to 0.5 mol dm^{-3} sodium chloride were tilted on layers of latex JC, and for S67 in the range 0.05 to 0.5 mol dm^{-3} sodium chloride.

8.5.4 Results

(a) Latex JC

Figure 8/17 shows photographs of the deformation of a drop on tilti... A typical set of experimental data plotted as contact angle, θ, against th tilt angle, α, is shown in figure 8/18. Wolfram's method depends on obtaining the advancing and receding angles at the critical angle of tilt, that is α_{crit}. The experimental problem is to determine this point. Figure 8/18 shows typical sets of data and the arrows indicate the points at which the drops started to slide. The ordinate at this point is therefore equal to α_{crit} and the advancing and receding angles are those required by the Wolfram analysis.

In general the receding angles were more precisely determinable than the advancing ones. This is illustrated in figure 8/18, where the advancing angles show more scatter at the positions just prior to the drop tilting. It should be noted that it is also harder to measure the larger angles from the photographs due to the high curvature of the liquid profile for the advancing case.

Latex JC

Figure 8/19

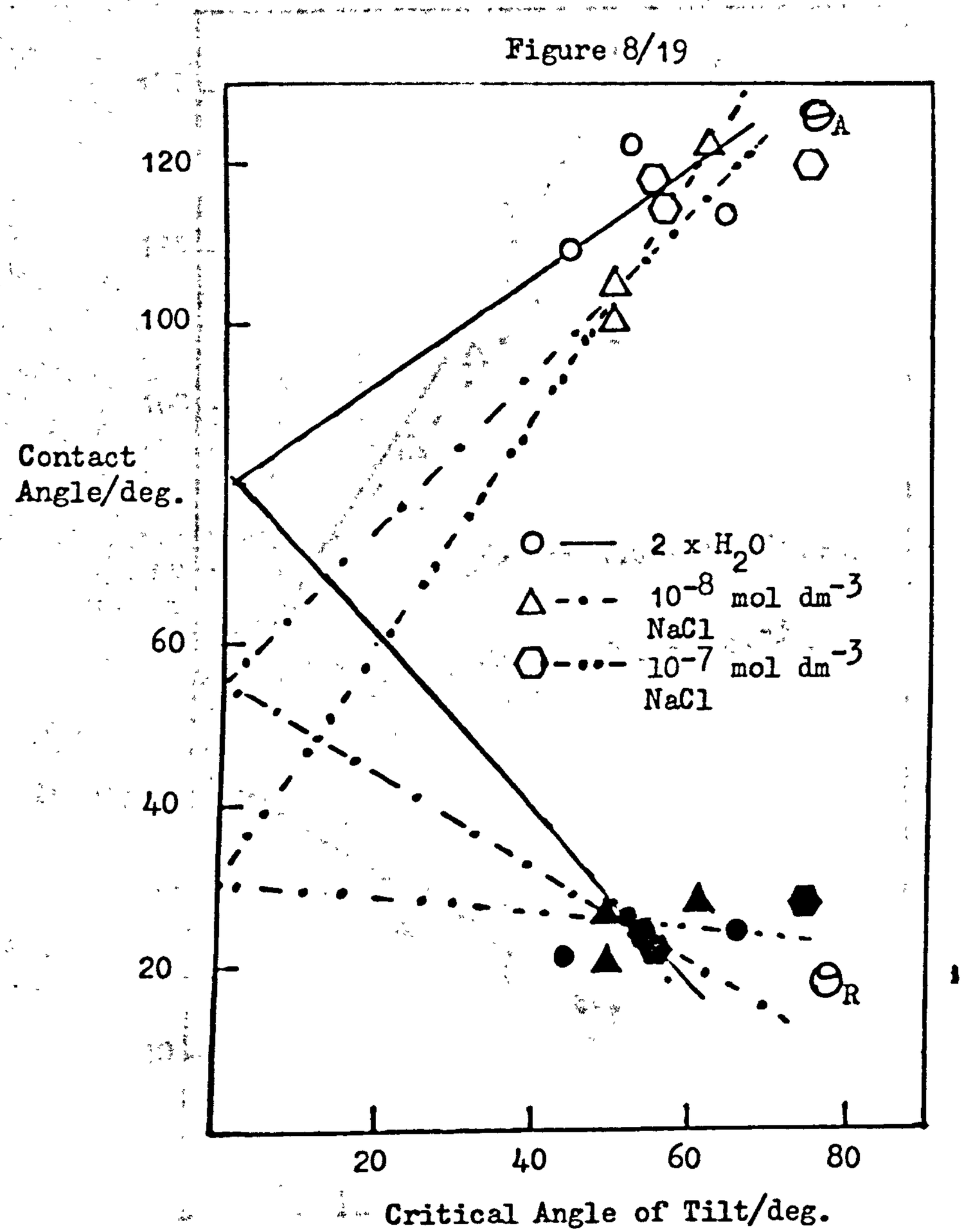

Figure 8/20

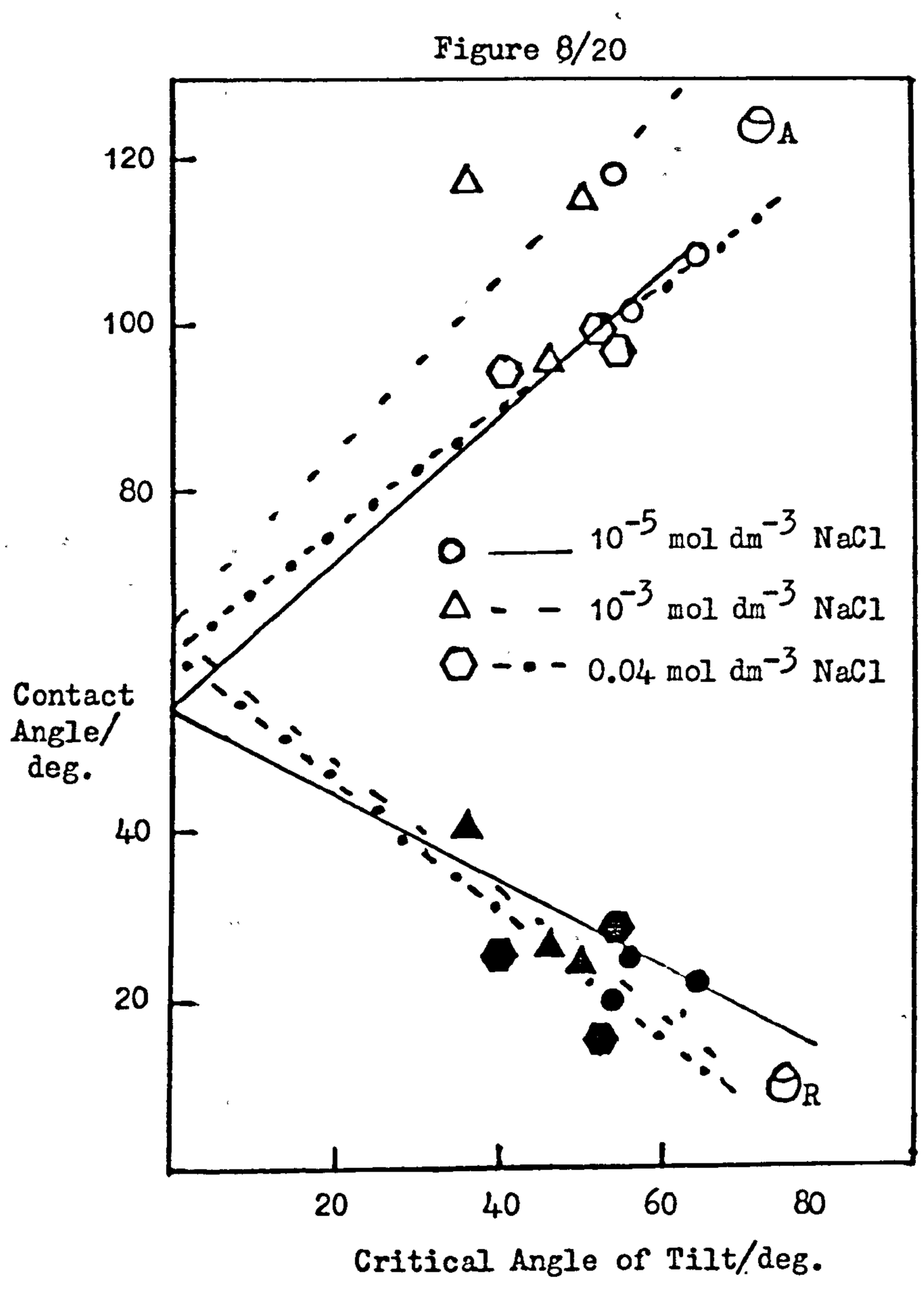

Figure 8/21

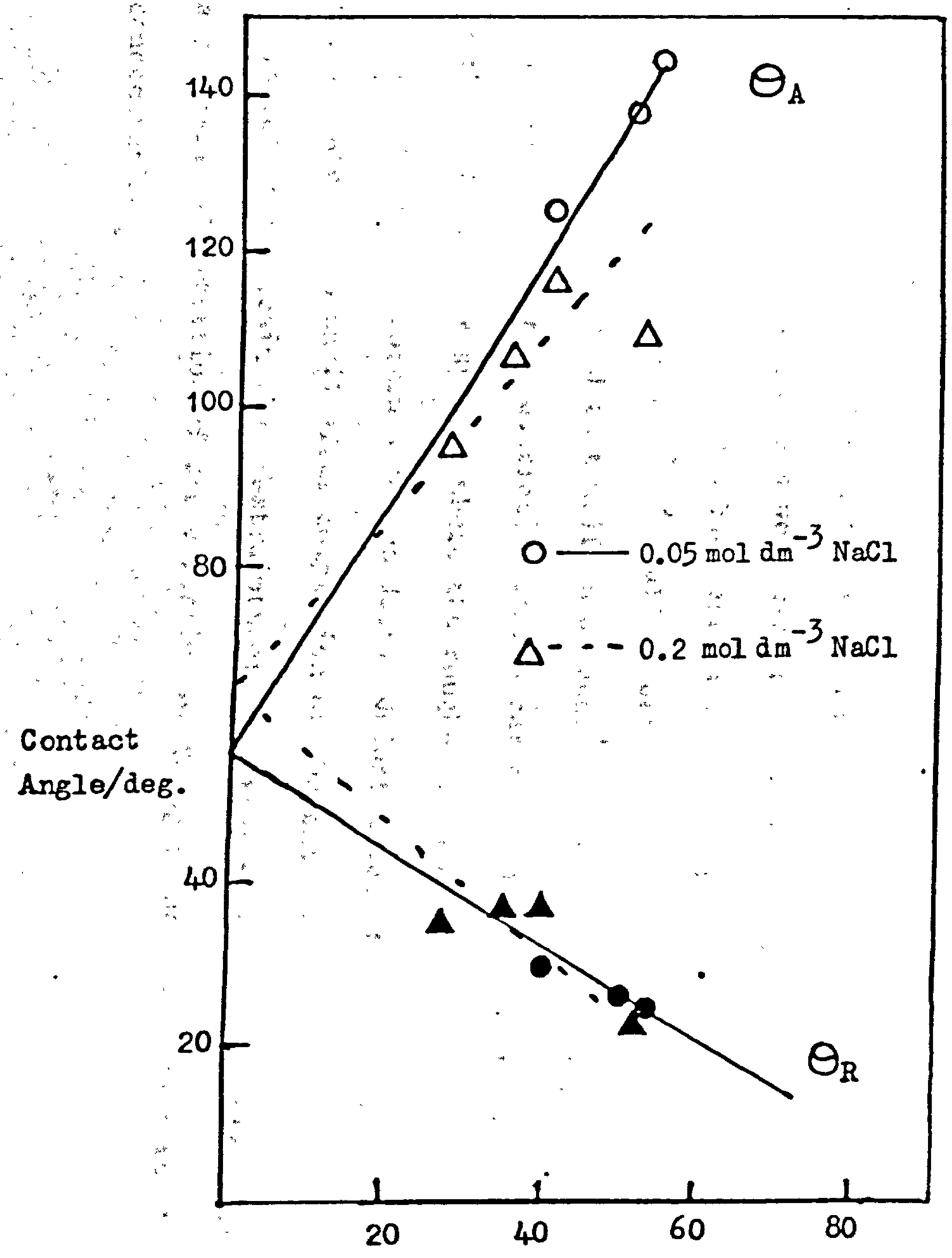

Figure 8/22

Latex JC

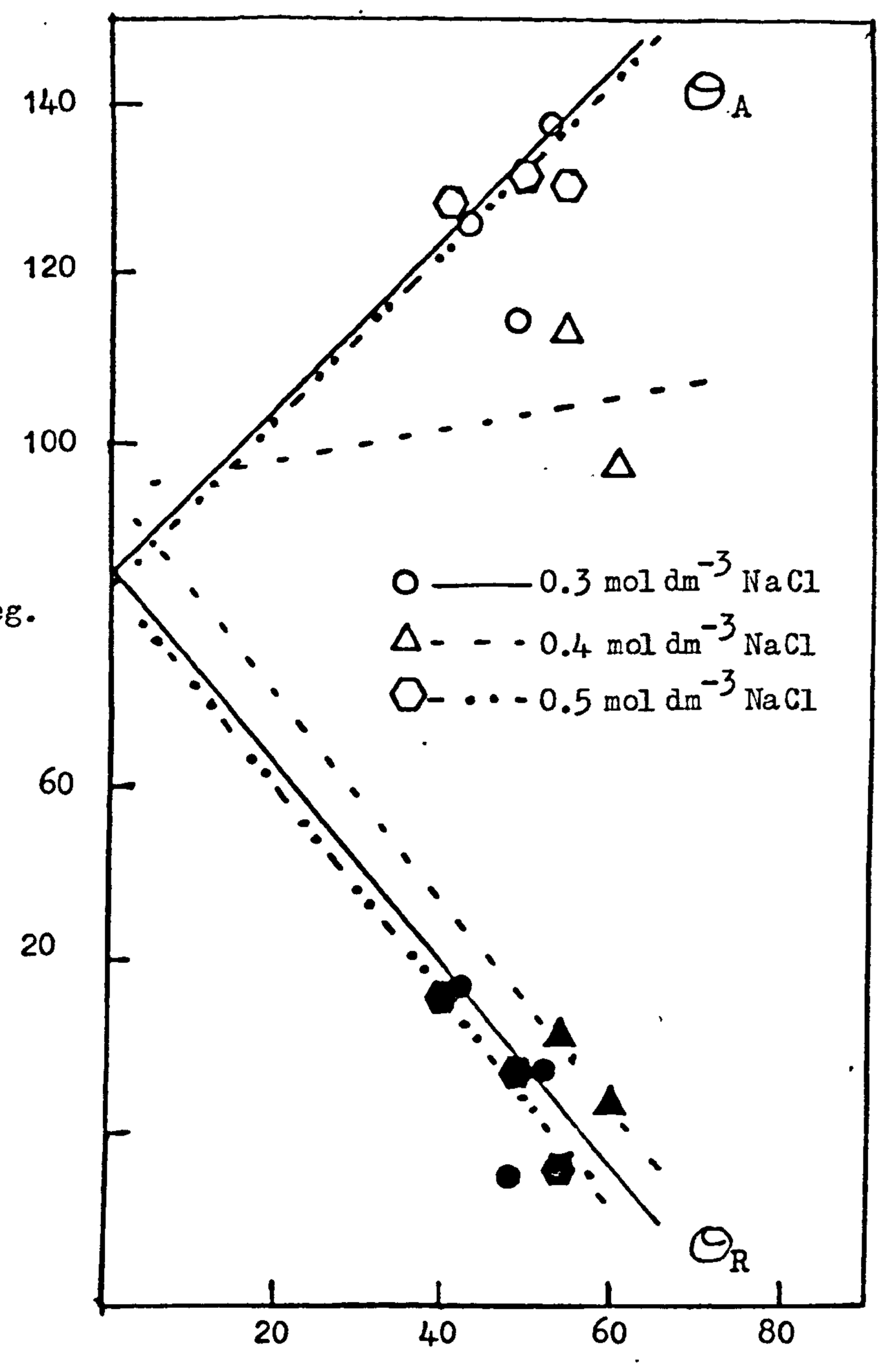

Figures 8/19 - 8/22 summarise the results. The results for 10^{-8} mol dm^{-3} and 10^{-7} mol dm^{-3} sodium chloride solutions, formed from dilution of a concentrated salt solution, were combined to give a single extrapolated value of Young's angle, since there should be little difference between these very dilute salt solutions and water.

One of the problems of this technique is illustrated by these graphs. The fact that the surfaces were fairly reproducible in terms of the packing of the latex spheres meant that there was only a small variation of roughness possible; unlike the situation experienced by Wolfram[147] where a wide variation in roughness was produced thus giving a wide spread of critical angles of tilt.

In order to obtain the Young angle from the data it is necessary to extrapolate to zero critical angle of tilt. This was achieved by the following procedure.

(1) Since the receding angle data proved to be more reliable than the advancing ones, the best straight line was drawn for the receding case.

(2) This enabled the range of possible Young Angles to be defined.

(3) Now the advancing angles were used to estimate the best intersection of the ordinate. It has been estimated that for these results, Young's angles within $\pm 5^{o}$ could be determined.

It should be noted that Wolfram's paper[147] can be misleading. It is not apparent the restriction that a narrow band of roughness has on this method. For systems where the roughness cannot be readily varied, it is advisable to obtain numerous data. Unfortunately this problem was not isolated by us until after completion of the experiments. However, it is felt that within the constraints of the experiment, figure 8/23 gives a realistic illustration of the variation of Young's angle with electrolyte concentration.

Figure 8/23 : Variation in Young's Angle with Sodium Chloride Concentration for Latex JC

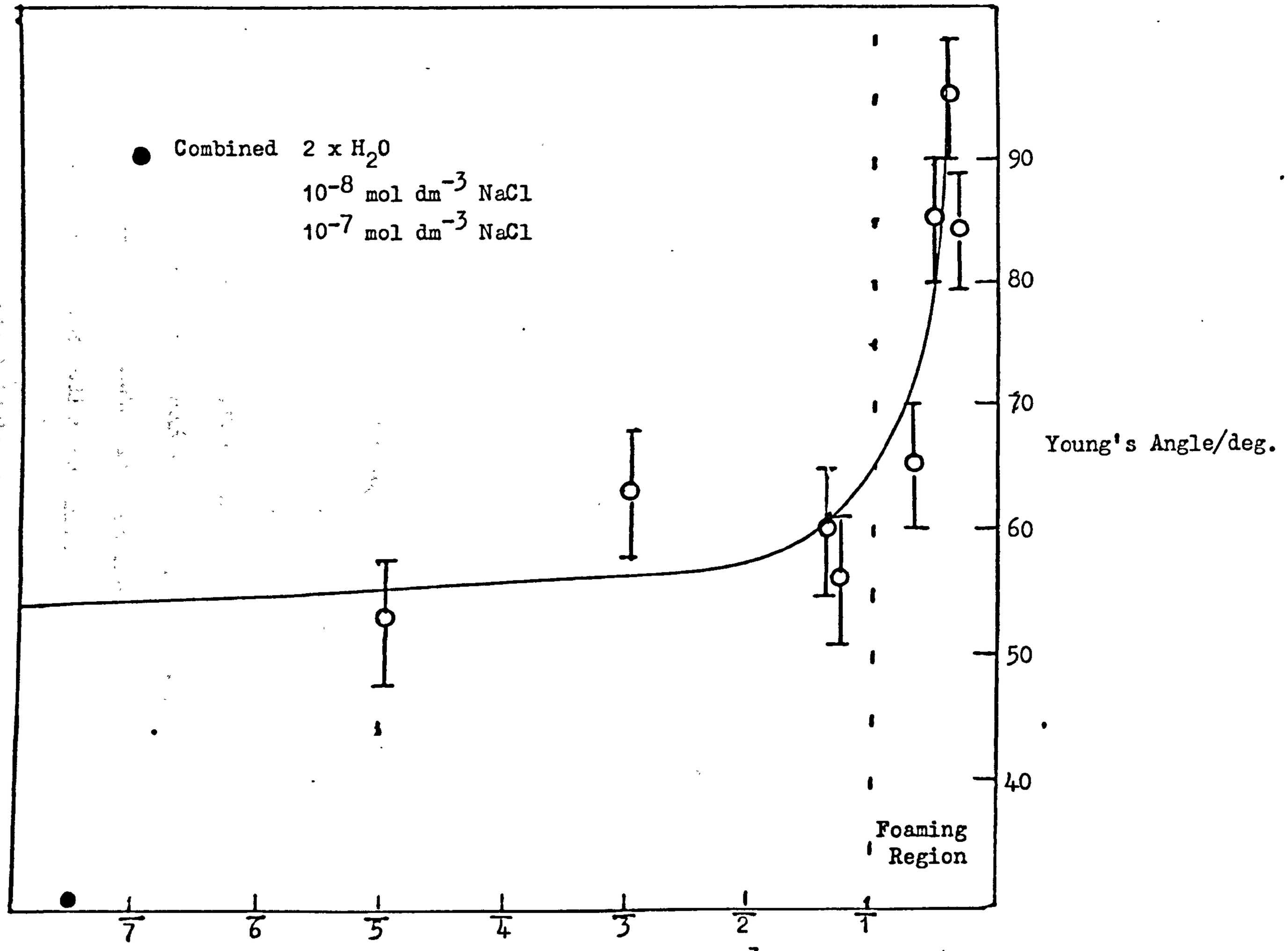

The results show a slight increase in contact angle with salt concentration until the foaming region is reached where now there is a sharp increase in contact angle, a θ_Y value, of greater than 80° being found.

(b) Latex S67

Only three solutions were used for latex S67, diameter 1.1 μm. These are shown in figure 8/24. For the 0.05 mol dm^{-3} salt solution data the advancing angles are all 117°; however the receding angles clearly extrapolate back to 39°.

If this is taken for Young's angle for 0.05 mol dm^{-3} salt, which lies just outside the foaming region, then it would appear that the Young angle for S67 also shows an increase in the foaming region. The Young angles for 0.2 and 0.5 mol dm^{-3} salt were found to be 73° and 70° respectively.

8.5.5 Conclusion

This method enables the Young angle which is a macroscopic angle obeying the Young equation to be determined. It also eliminates any effect roughness has on the equilibrium macroscopic contact angle. In previous experiments, section 8.4.2, the effect of surface roughness obscured the increase of contact angle with increasing sodium chloride concentration.

For both 4 and 2 μm diameter latices there is a sharp increase in Young's angle in the foaming sodium chloride range 0.1 to 0.5 mol dm^{-3}.

8.6 Discussion of the Contact Angle Data

8.6.1 Comparison of the two methods used

The captive drop method only produces values for the advancing and receding contact angles. Both these will vary with the roughness of the polystyrene layer as well as any surface heterogeneity produced from different surface groups on the surface of each latex particle. However

Figure 8/24

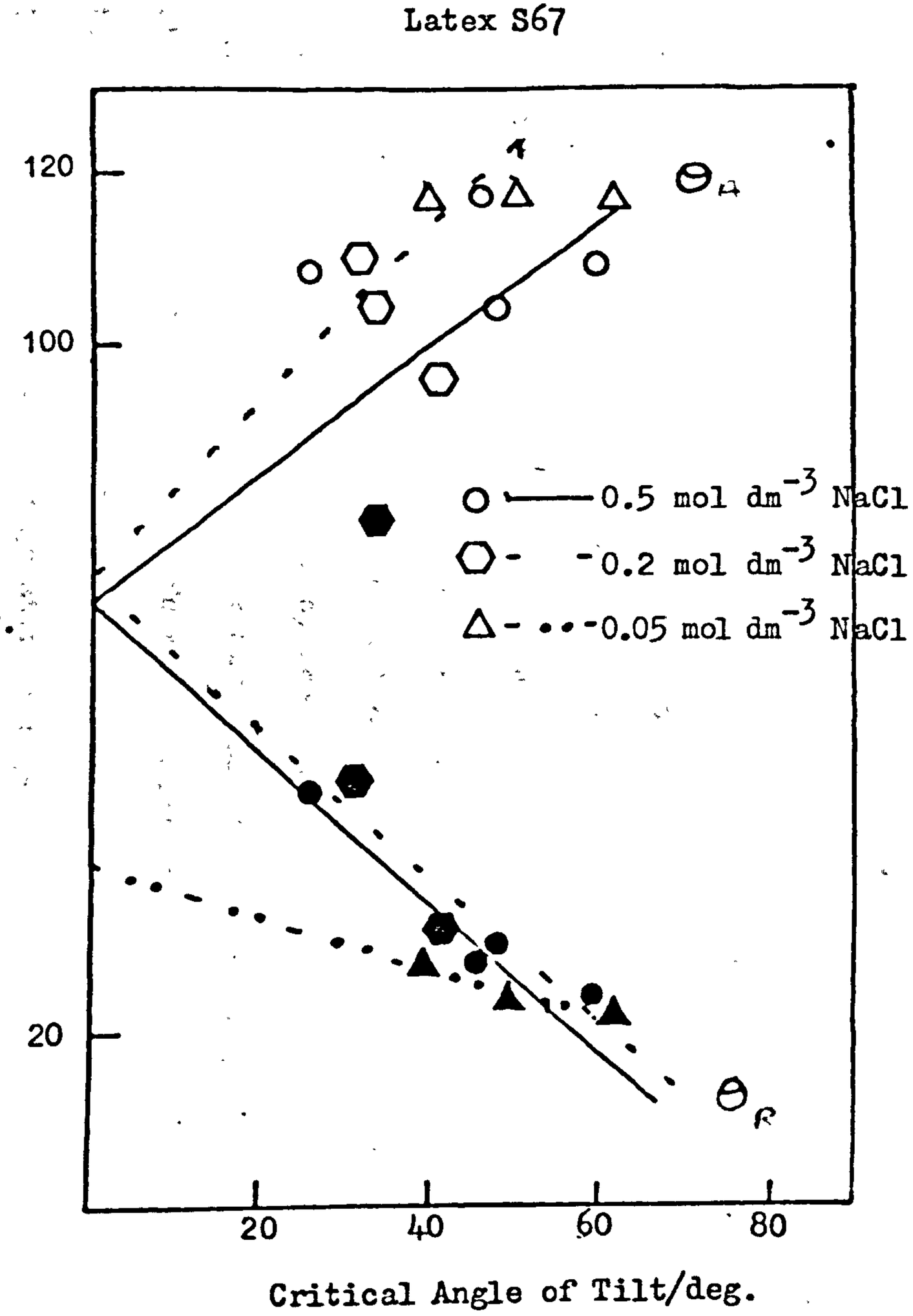
Latex S67
120
100
20
Contact Angle/deg.
θ_A
θ_R
0.5 mol dm^{-3} NaCl
0.2 mol dm^{-3} NaCl
0.05 mol dm^{-3} NaCl
20
40
60
80
Critical Angle of Tilt/deg.

the tilt method gives a more fundamental quantity, Young's angle, which is a microscopic quantity and as such cannot be measured directly unless very smooth surfaces are available.

By the captive drop method changes in the contact angle were observed with variation of surfactant concentration. However the sensitivity of this technique was such that changes in contact angle with variation in salt concentration could not be detected.

8.6.2 Conclusions

There is a sharp increase in Young's angle at sodium chloride concentrations in the foaming region. Young's angles of 50° to 60° were observed for solutions in the range 10^{-5} to 10^{-1} mol dm^{-3}, whereas in the foaming region these increased to 95° for 0.4 mol dm^{-3} sodium chloride.

For the DTAB - latex system both the advancing and receding angles were greater than 90° in the latex foam region, whereas for the surfactant foam region both had decreased to approximately 0°.

Therefore it can be concluded that polystyrene latices of a certain size can be made to foam, either by compression of the electrical double layer, that is adjustment due to a high salt concentration, or by adsorption of a cationic surfactant. The foaming conditions in both cases correspond to situations where the contact angle of the liquid phase on the solid particle must be close to or greater than 90°.

CHAPTER 9

DISCUSSION OF RESULTS

9.1 General Conclusions

Polystyrene latices containing particles of 1 to 4 μm diameter will form very stable foams. In the latter the individual air cells are stabilised by layers of hexagonally close-packed latex particles. The regularity of this packing has been shown both by optical micrographs and by laser diffraction patterns.

The two foaming systems examined in this thesis were latices containing electrolytes and latices in the presence of surfactant. Each system illustrates a different foaming mechanism. The basic mechanism of foam formation is discussed in the following sections.

9.1.1 Electrolyte/Polystyrene Latex Foams

Although the results reported in this section were obtained in the presence of sodium chloride, it will be assumed that the mechanism postulated will be similar for the foam studies in the presence of other electrolytes, such as barium chloride, magnesium sulphate and lanthanum nitrate, as well as the foams produced due to decreasing the pH of the latex suspension.

The tilting drop method of determining contact angle indicated that an increase in Young's angle, θ_Y, the true equilibrium contact angle, occurred with an increase in sodium chloride concentration, figure 9/1. There was a gradual increase in θ_Y with salt concentration until the foaming region was reached at about 0.05 mol dm^{-3} sodium chloride. At this point the results showed a sudden increase in θ_Y to give angles of greater than 90°. This indicated the increased hydrophobic nature of the surface of the polystyrene particles.

The effect of the high ionic strength of the dispersion is to cause the electrical double layer surrounding the surface charges on the latex particle to contract. This in turn causes the wetting films to be non-

Figure 9/1 Summary of Foam Data for Latex JC/ Sodium Chloride Suspensions

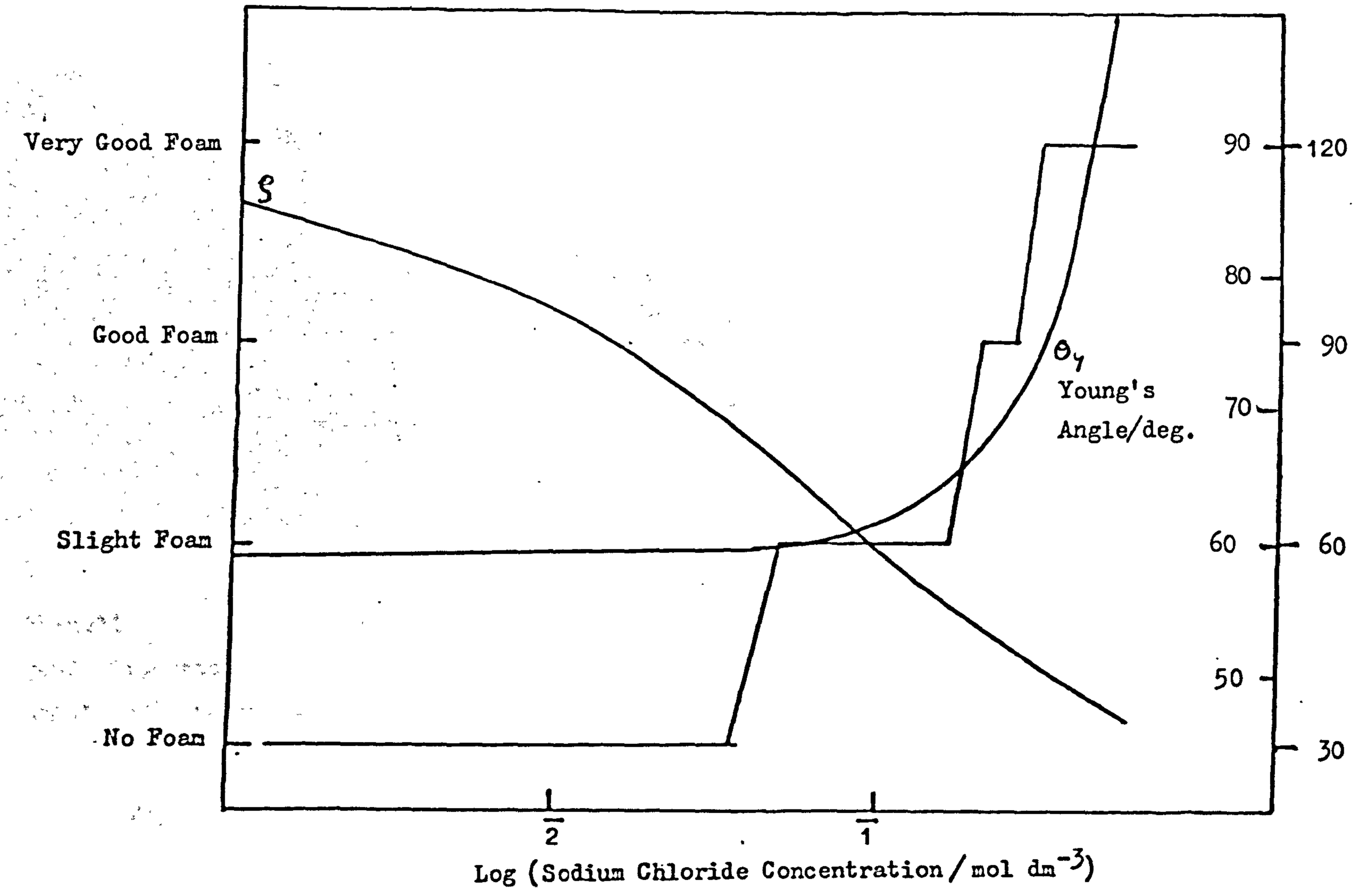

Low DTAB Concentration

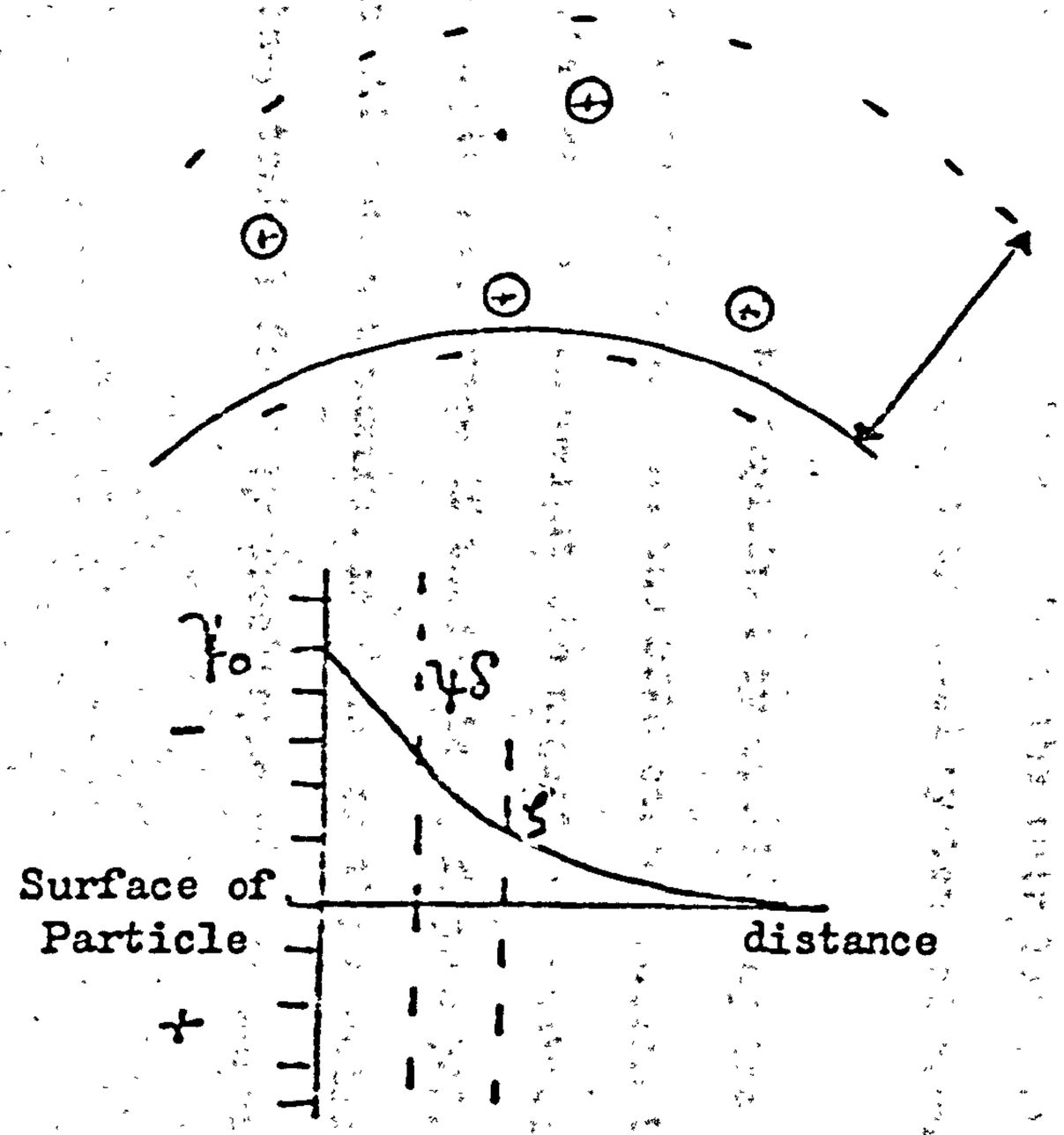

θ small

good dispersion

negative ζ -potential

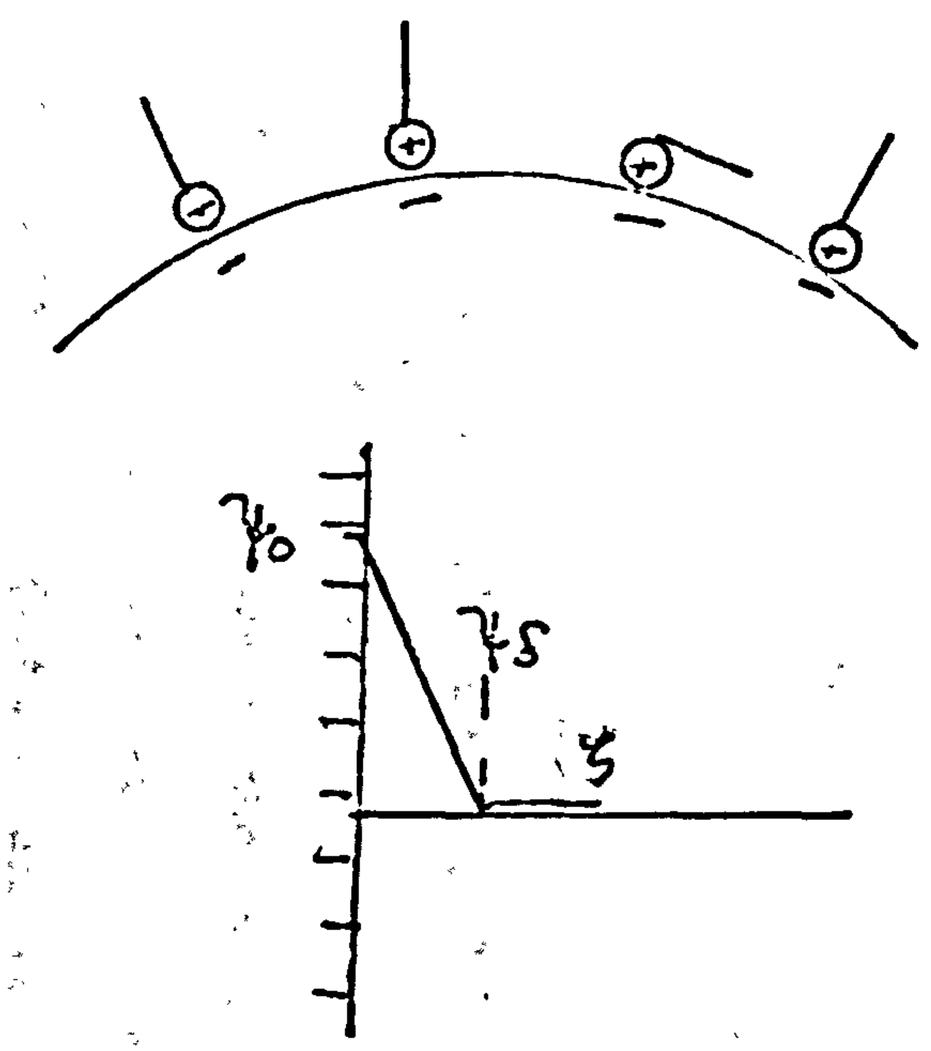

θ large

tendency for coagulation and/or flocculation

zero ζ -potential

High DTAB Concentration

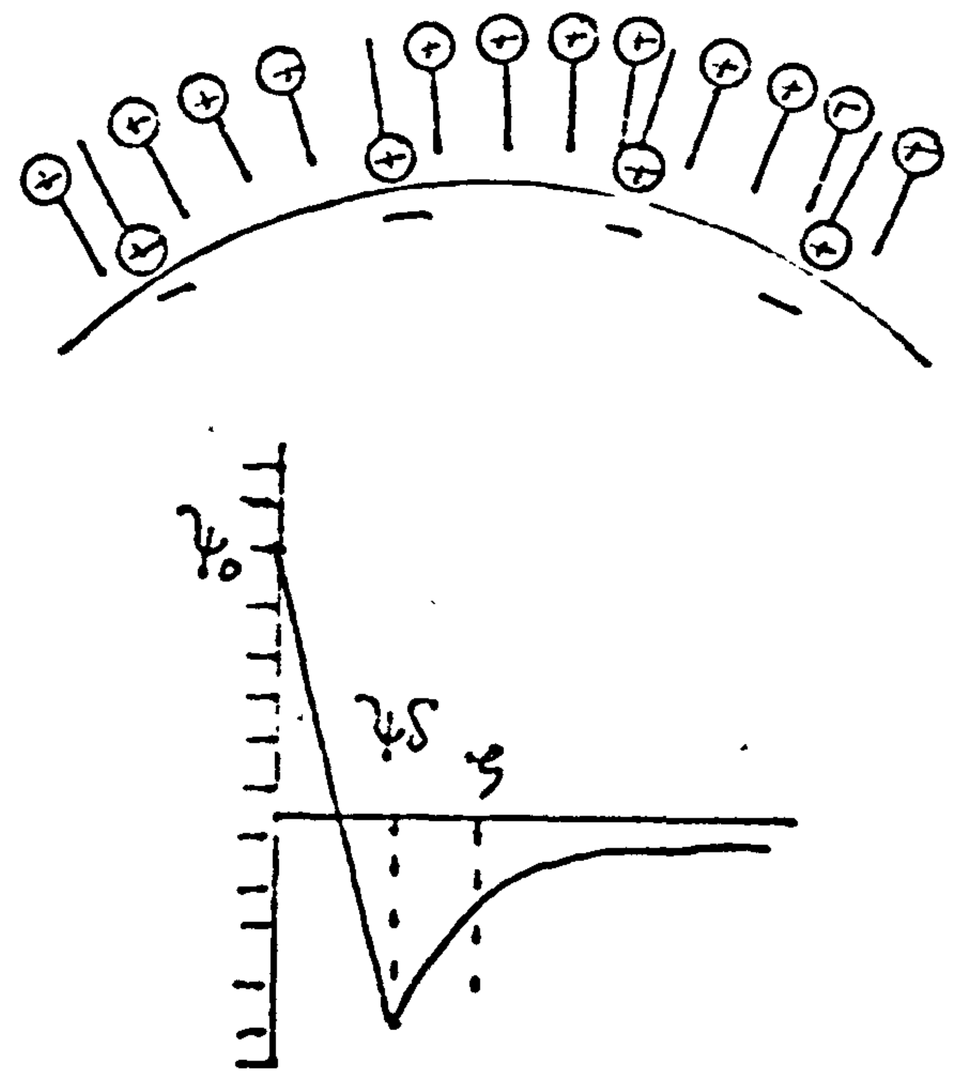

θ small

good dispersion

positive ζ -potential

Key : ψ_o Surface Potential ψ_δ Stern Potential ζ zeta Potential

Figure 9/2

continuous and to form liquid 'beads' around the surface charges. If this is the case bare hydrophobic patches will be exposed and hence it is more energetically favourable for the sphere to be situated at the air/liquid interface.

As can be seen from the data in figure 9/1, a slight foam is first observed at the salt concentration of 0.05 mol dm^{-3} corresponding to the beginning of the increase in contact angle and the decrease in zeta-potential. At sodium chloride concentrations, 0.3 to 0.4 mol dm^{-3}, where now good to very good foams were observed, the contact angle can be seen to increase steeply to angles of 80° - 90° while the zeta-potential continues to fall. This indicates that increased hydrophobicity of the polystyrene particle surface occurs at the same sodium chloride concentration range where the zeta-potential has been lowered, by the high salt concentration, and so enables a closer approach of the latex particles which in turn helps to stabilise the foam produced.

9.1.2 Surfactant / Polystyrene Latex Foams

No foaming of the latex was observed with anionic surfactants, but foams were formed in the presence of the cationic surfactant DTAB.

The latex systems were observed to go from a 'no foam' situation to a latex foam and then to a surfactant foam as the DTAB concentration was increased. Coupled with this the bulk latex changed from being a good dispersion to being a coagulated system and then changed to a dispersion again.

This can be explained by considering the adsorption of the DTAB on the latex surface. As the DTAB concentration increases the cationic surfactant is adsorbed at the negatively charged sites, eventually leading to complete coverage of these sites, figure 9/2. This corresponds to the situation when a maximum is found in the contact angle data and to the zero zeta-potential found by electrophoresis measurements. Under these conditions

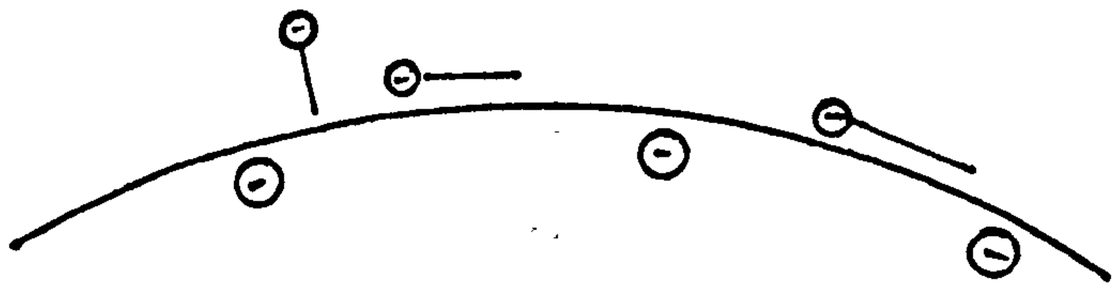

Polystyrene Latex Particle

Figure 9/3 : Adsorption of Sodium Dodecyl Sulphate

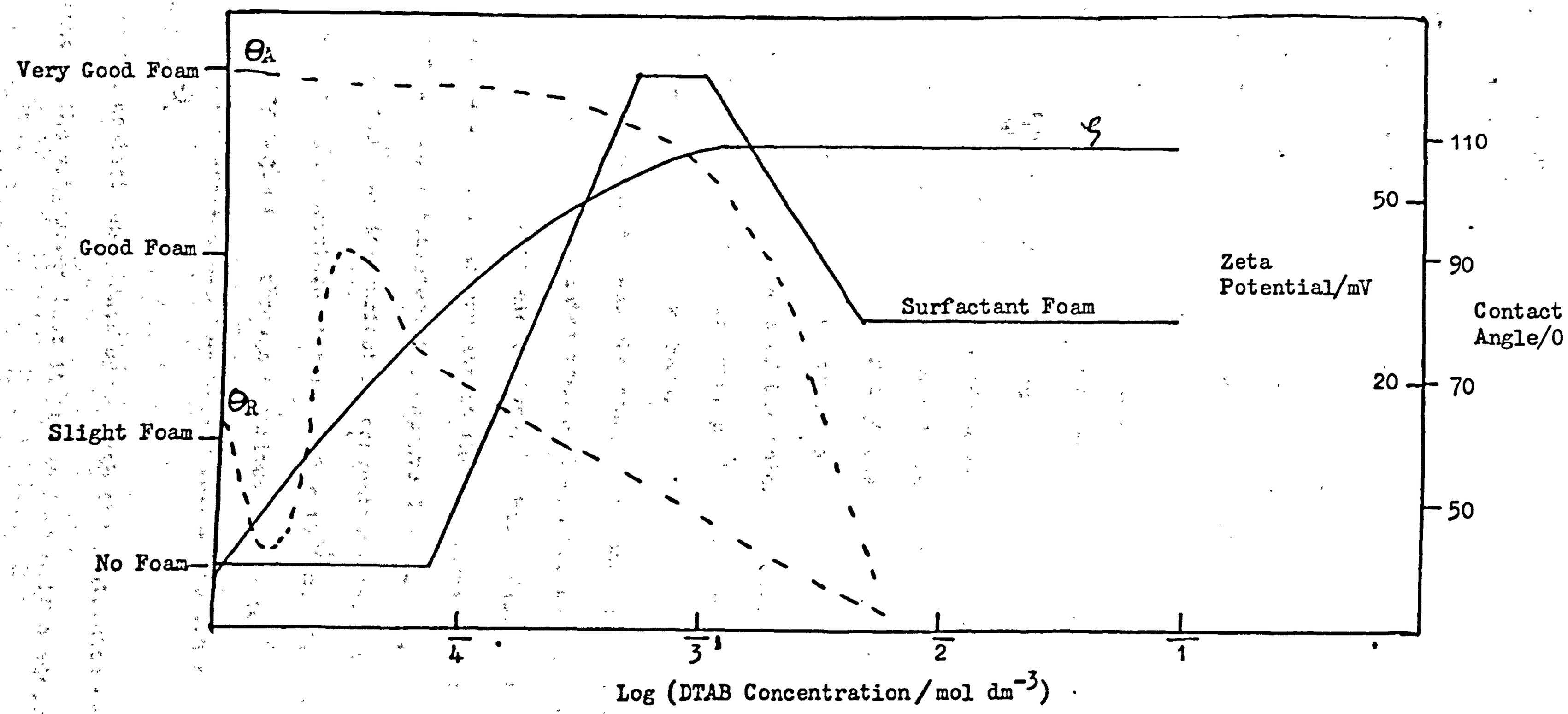

Figure 9/4 : Summary of Foam Data for Latex JC / Surfactant Suspensions

more particles are preferentially adsorbed at the interface, forming a closely packed layer. This enables a foam to be formed, and since the zeta-potential is low bulk coagulation also occurs.

As more surfactant is added, more dodecyltrimethylammonium ions are adsorbed on the particle surface, which subsequently means that the zeta-potential becomes positively charged and the particle easier to wet. Now the particles cannot approach each other as closely as before due to the increased repulsion between them. As they are now more hydrophilic in nature they tend to move preferentially into the bulk phase where they form a stable dispersion. If the DTAB concentration is increased to beyond its critical micelle concentration a surfactant foam is formed.

For the anionic surfactant/latex systems the surfactant is physically adsorbed on the particle's surface and not specifically adsorbed via the head groups as was the case for the DTAB/latex system. Figure 9/3 shows schematically how the surfactant molecules adsorb on the surface. This clearly shows that the head groups of the anionic surfactant cause the polystyrene particle to become more hydrophilic and hence remain preferentially wetted in the bulk phase.

A particle size effect was observed. The smallest latex, RB55, 1 μm diameter, did not form a latex foam although the bulk phase did undergo coagulation on the addition of electrolyte. This indicated the reluctance of these small particles to accumulate at the air/liquid interface.

The contact angle measurements, captive drop method, showed a large advancing angle, 118°, at low surfactant concentrations, 5×10^{-4} mol dm^{-3}, which decreased to give complete wetting at 2×10^{-3} mol dm^{-3} DTAB, figure 9/4. The receding angle went through a maximum at 3×10^{-5} mol dm^{-3} DTAB, corresponding to a dewetting angle at higher surfactant concentrations, 2×10^{-3} mol dm^{-3}.

Hence the contact angle data agree with the postulated mechanism of foaming, that is the suggestion that it is due to specific adsorption of the

cationic surfactant at the negative charged sites on the latex particle surface.

From figure 9/4, it would appear that the appropriate changes in foaming behaviour, contact angle and zeta-potential data did not correspond with each other, However it must be noted that the measurements were determined for different latex particle number concentrations and hence for different equilibrium bulk DTAB concentrations.

9.2 Theory

9.2.1 Theory for a Spherical Polystyrene Latex Particle situated at an Air/Liquid Interface

There are three main forces to be considered: the surface tension, F_1, the gravitational force, F_2, and the hydrostatic pressure, F_3. Figure 9/5 defines the parameters for the equilibrium position of a sphere at an interface for the general case.

Now the vertical force, F_1, acting upwards, due to the surface tension becomes

$$F_1 = 2\pi r \gamma \cos (90 - \phi)$$

where r is the radius of the circular cap of the sphere at the point of contact with the liquid, γ is the interfacial tension and ϕ the angle between the tangent to the liquid surface at the point of contact, relative to the horizontal. However r can be defined in terms of the radius of the sphere :

$$r = R \sin \alpha$$

and since ϕ is the difference between the contact angle θ and α, the angle between the radius at the point of contact and the vertical, it can be written as

$$\phi = \theta - \alpha$$

Now F_1 becomes

$$F_1 = 2\pi R \gamma \sin \alpha \sin (\theta - \alpha)$$

if α is less than 90°.

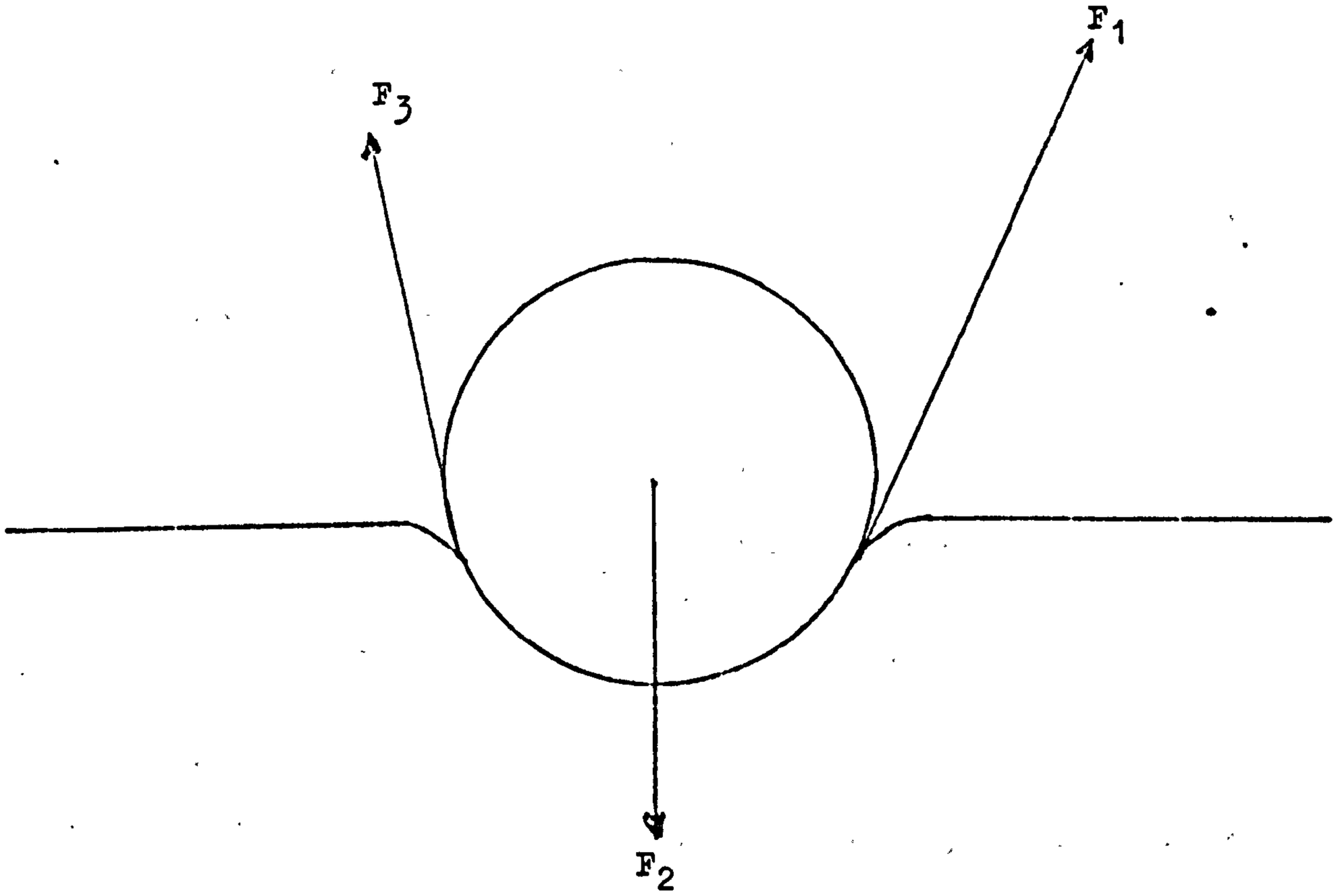

Figure 9/5

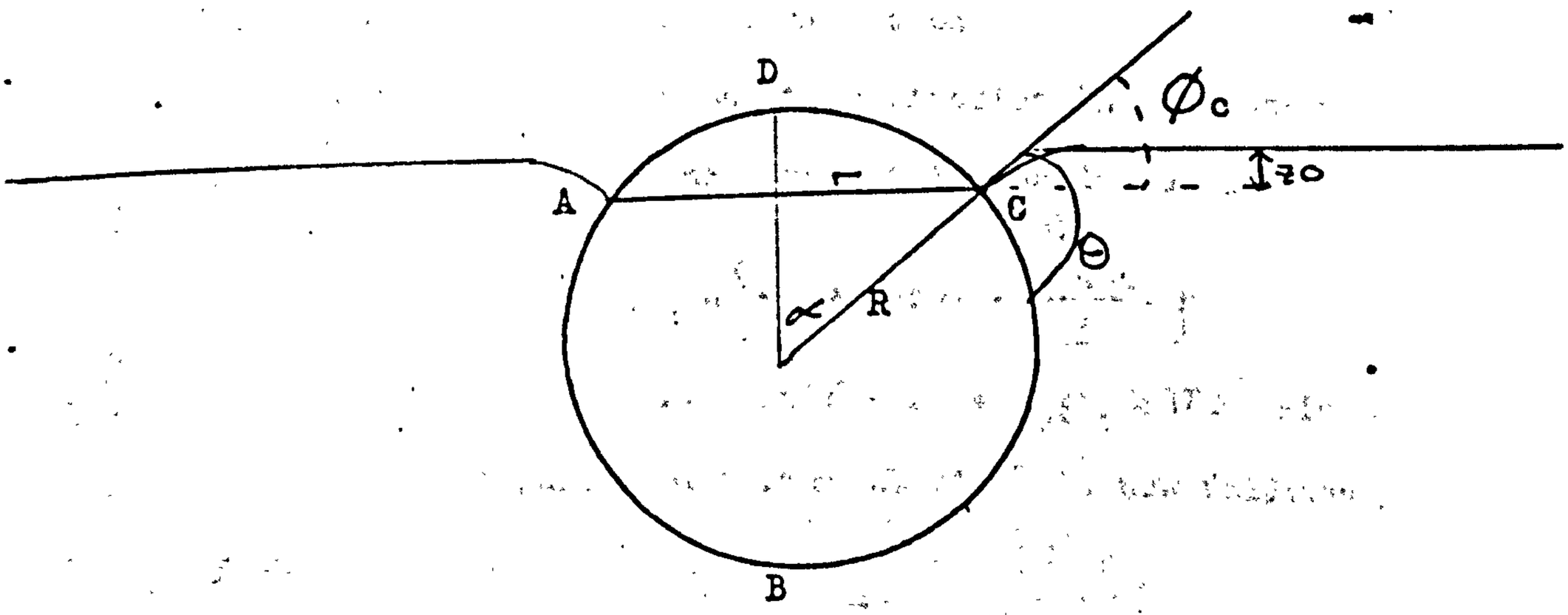

Figure 9/6

For the gravitational force, F_2, the apparent mass of the sphere must first be defined. From figure 9/6 the apparent mass is equivalent to

$$V_{ABCD}\,\varrho - V_{ABC}\,\varrho_o$$

where V_{ABCD} and V_{ABC} are the volumes of the segments ABCD and ABC respecitvely, and ϱ and ϱ_o are the densities of the sphere and the liquid media respectively. Taking the volume of ADC as being that of a spherical cap the apparent mass of the sphere becomes

$$\frac{4}{3}\pi R^3 (\varrho - \varrho_o) + \frac{\pi R^3 \varrho_o}{3} (1 - \cos\alpha)^2 (2 + \cos\alpha)$$

and hence

$$F_2 = \frac{4}{3}\pi R^3 \varrho g - \pi R^3 \varrho_o g \left\{\frac{2}{3} + \cos\alpha - \frac{\cos^3\alpha}{3}\right\}$$

Finally, the hydrostatic pressure F_3 which is the force acting over the effective area of the disc AC is

$$\pi r^2 z_o \varrho_o g$$

Therefore $F_3 = z_o \varrho_o g \pi R^2 \sin^2\alpha$

This is acting in the upward direction.

For the sphere to be at equilibrium in the interface the total downward force must balance the total upward one, so

$$\frac{4}{3}\pi R^3 \varrho g - \pi R^3 \varrho_o g \left\{\frac{2}{3} + \cos\alpha - \frac{\cos^2\alpha}{3}\right\}$$

$$= 2\pi R \gamma \sin\alpha \sin(\theta - \alpha) + z_o \varrho_o g \pi R^2 \sin^2\alpha$$

If the argument of Torbin et al.[74] is now followed, z_o can be defined by the equation

$$z_o = -R \sin\alpha \tan(\theta - \alpha) \left[\ln\left(\frac{R \sin\alpha}{2\sqrt{\frac{\gamma}{\varrho_o g}}}\right) + 0.58\right]$$

Now the balance of the forces can be written to give

$$\frac{4}{3}\pi R^3 \varrho g = 2\pi R \gamma \sin\alpha \sin(\theta - \alpha) + \pi R^3 \varrho_o g \left\{\frac{2}{3} + \cos\alpha - \frac{\cos^3\alpha}{3} + \frac{z_o \sin^2\alpha}{R}\right\}$$

Figure 9/7 : Graph of $(\theta - \alpha)$ against Radius of the Sphere

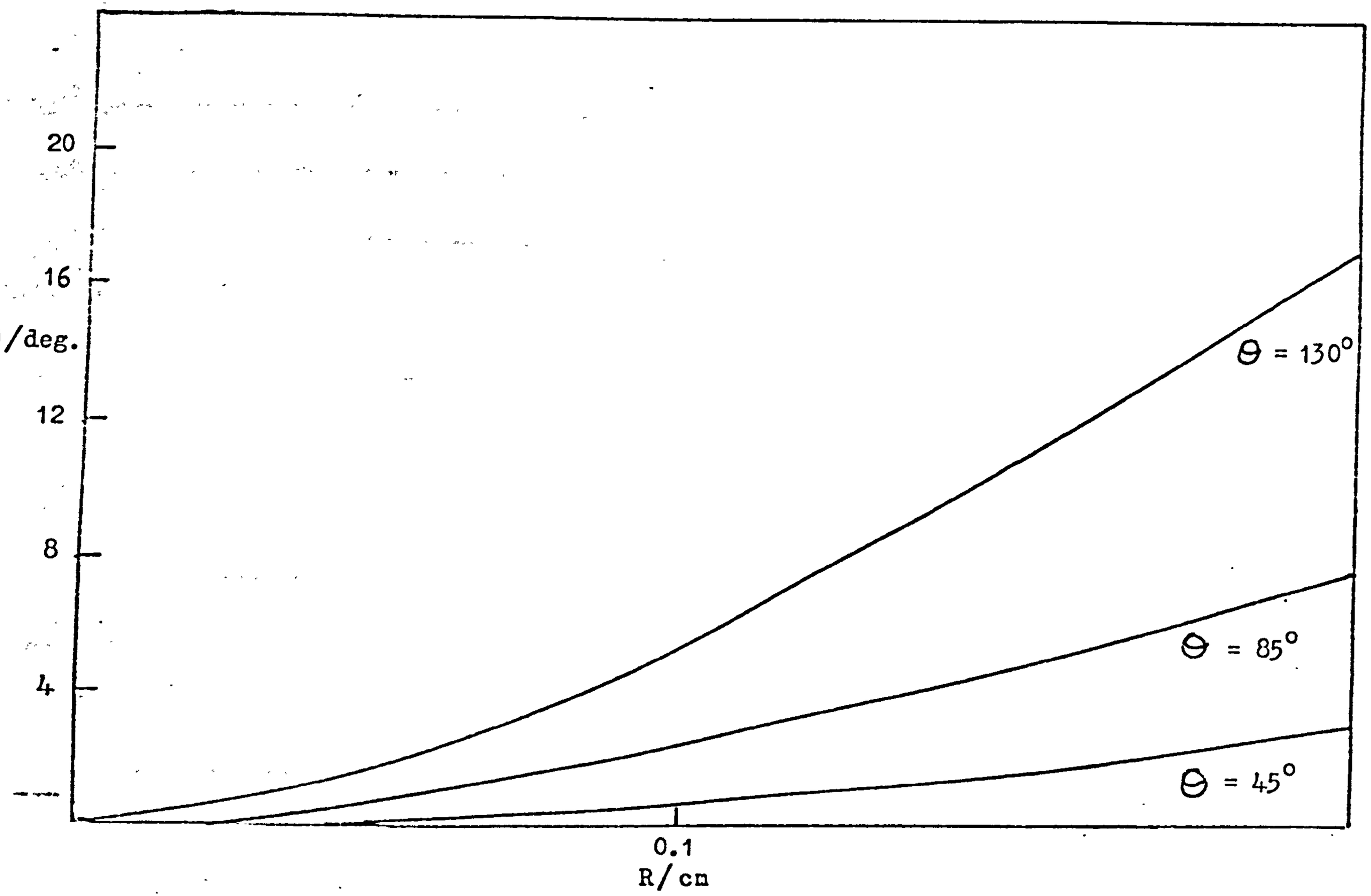

Figure 9/8 : α versus Particle Radius at Constant Contact Angle

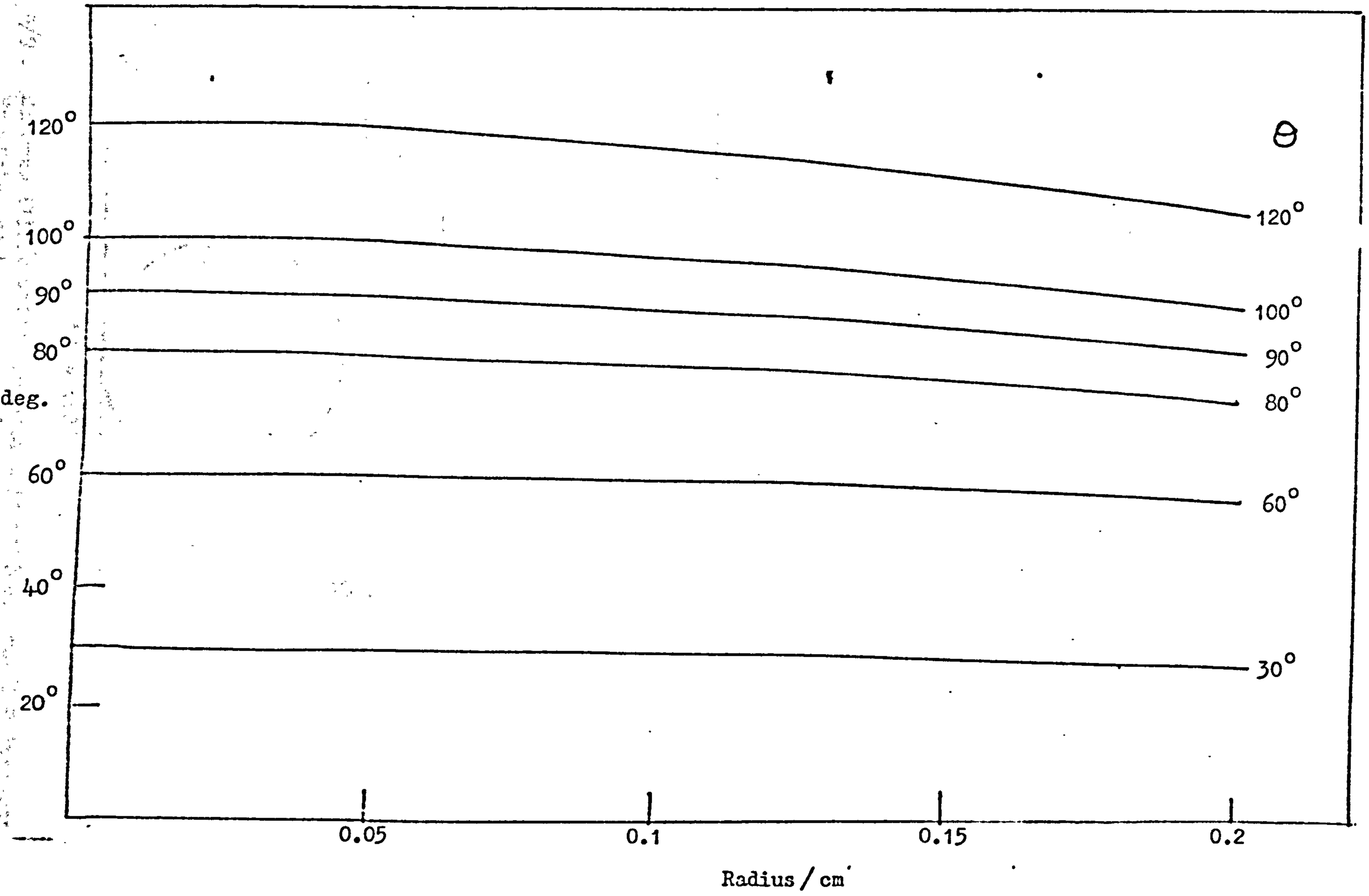

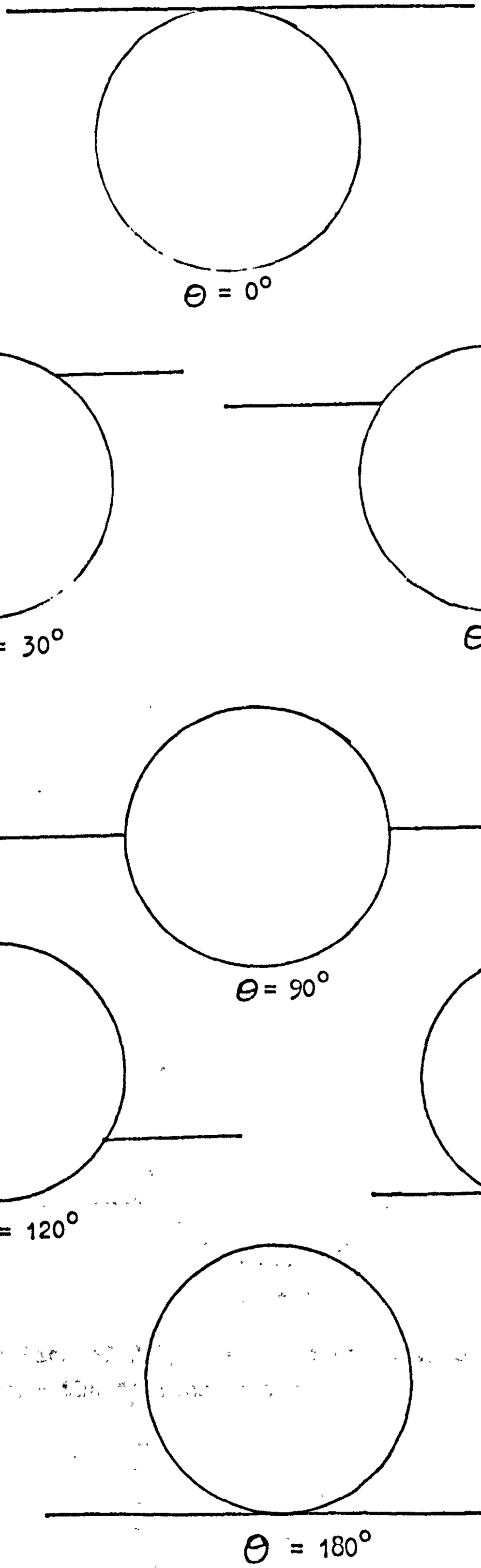

Figure 9/9 : Diagram illustrating the height of meniscus for a Polystyrene Particle, radius 1.94 μm, density 1.057, at an air/water interface for increasing contact angle.

Figure 9/10

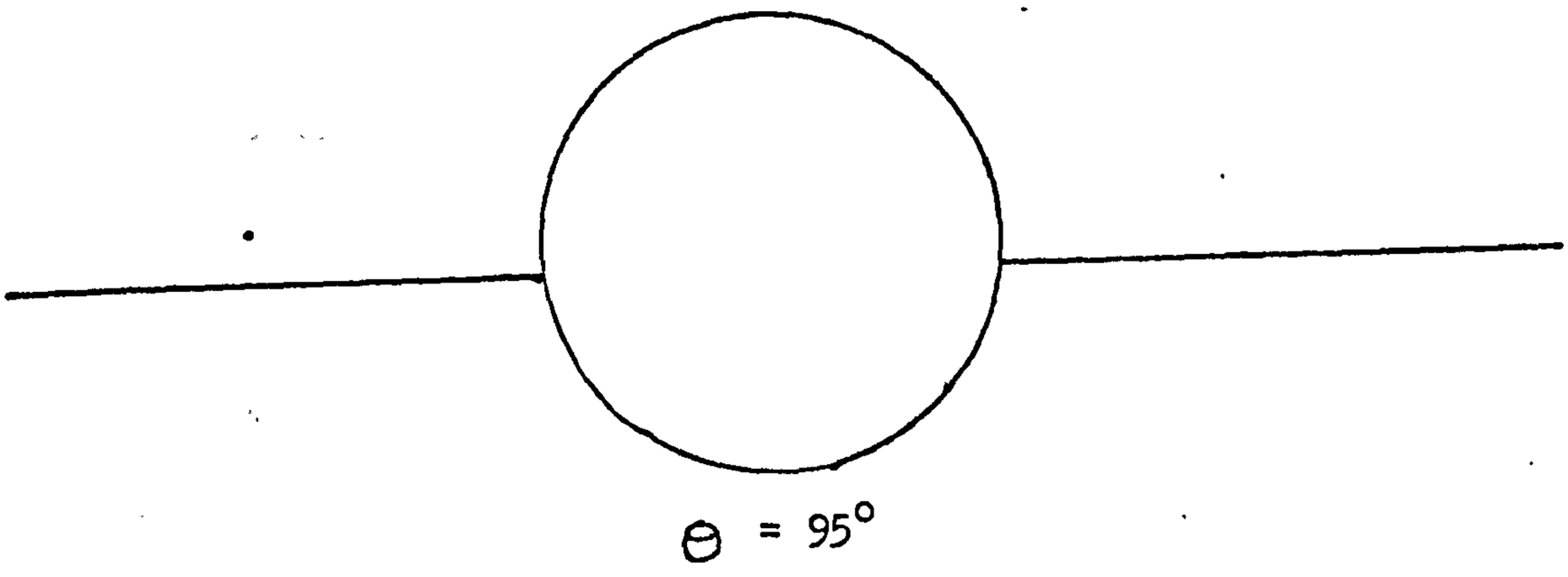

Position of Polystyrene Latex Particle in
Sodium Chloride Solutions 0.05 to 0.5 mol dm^{-3}

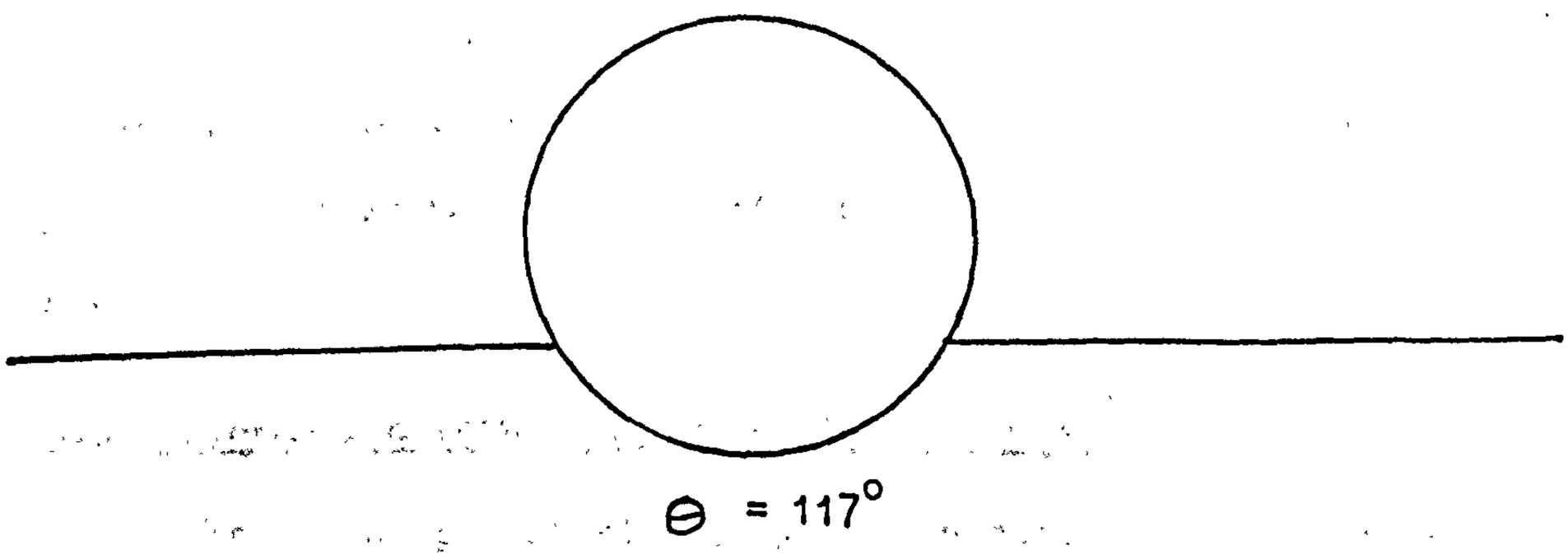

Position of Polystyrene Particle in DTAB Solution
within the foaming region

A computer program was written based on this equilibrium which enabled the variables such as ϕ, $(\theta - \alpha)$ to be plotted against the particle radius for a known constant value of the equilibrium contact angle, θ. Figure 9/7 shows such plots. It can be seen that for a particle diameter of 4 μm the angle between the meniscus at the point of contact and the horizontal, ϕ, is zero. Hence it can be concluded that the liquid interface shows no perturbations and is in fact planar at the point of contact with the solid sphere for these small particles.

Also if the parameter α is plotted against R, as in figure 9/8, it can be seen that there is no difference between α and θ for particles having radii smaller than 100 μm.

The position of the sphere in the interface, that is the height of the meniscus relative to the particle, will depend directly on contact angle, and hence since $\theta = \alpha$, $h = R \cos\alpha$. For a wetting contact angle, 30°, the sphere is virtually submerged, while for a dewetting angle, 120°, the majority of the sphere is now in the gaseous phase, figure 9/9.

If the Young angle for latex particles in contact with salt solutions within the foaming region, 0.05 and 0.5 mol dm^{-3}, is taken as 95° then the height of a sphere of diameter 3.89 μm above the interface is 2.15 μm. Taking the advancing angle for DTAB / polystyrene as 117°, see captive drop results, then this height becomes 2.88 μm. Both indicate that in the polystyrene foam the majority of the sphere's surface is situated in the air, figure 9/10.

9.3 Interaction between Latex Particles in a Liquid

The total potential energy of a particle in a liquid medium can be taken as the sum of the attractive and repulsive energies as defined in chapter 1:

$$V_T = \frac{\epsilon_r R \psi_o^2}{2} \ln \left[1 + \exp(-\kappa H_o)\right] - \frac{A_{net} R}{12 H_o} \qquad (1)$$

Figure 9/11 : A Potential Energy Curve for Latex JC

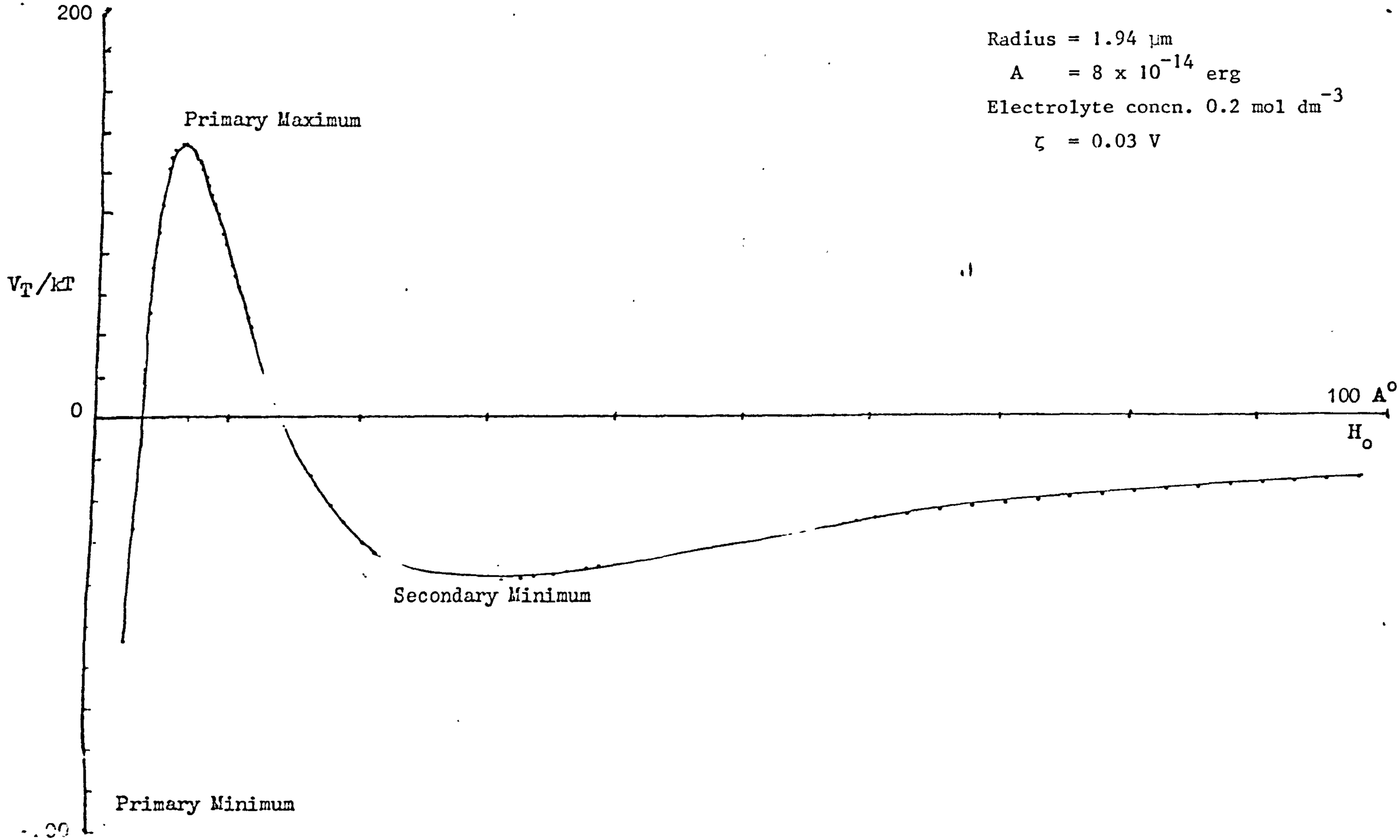

Table 1

Variation of $1/\kappa$ with Sodium Chloride Concentration

Electrolyte Concentration/mol dm^{-3}	$1/\kappa$/Å
0.05	13.6
0.10	9.6
0.20	6.8
0.30	5.6
0.50	4.3
0.70	3.6
1.00	3.0

Figure 9/12 : Potential Energy Curves for Latex JC Particles in Various Sodium Chloride Solutions

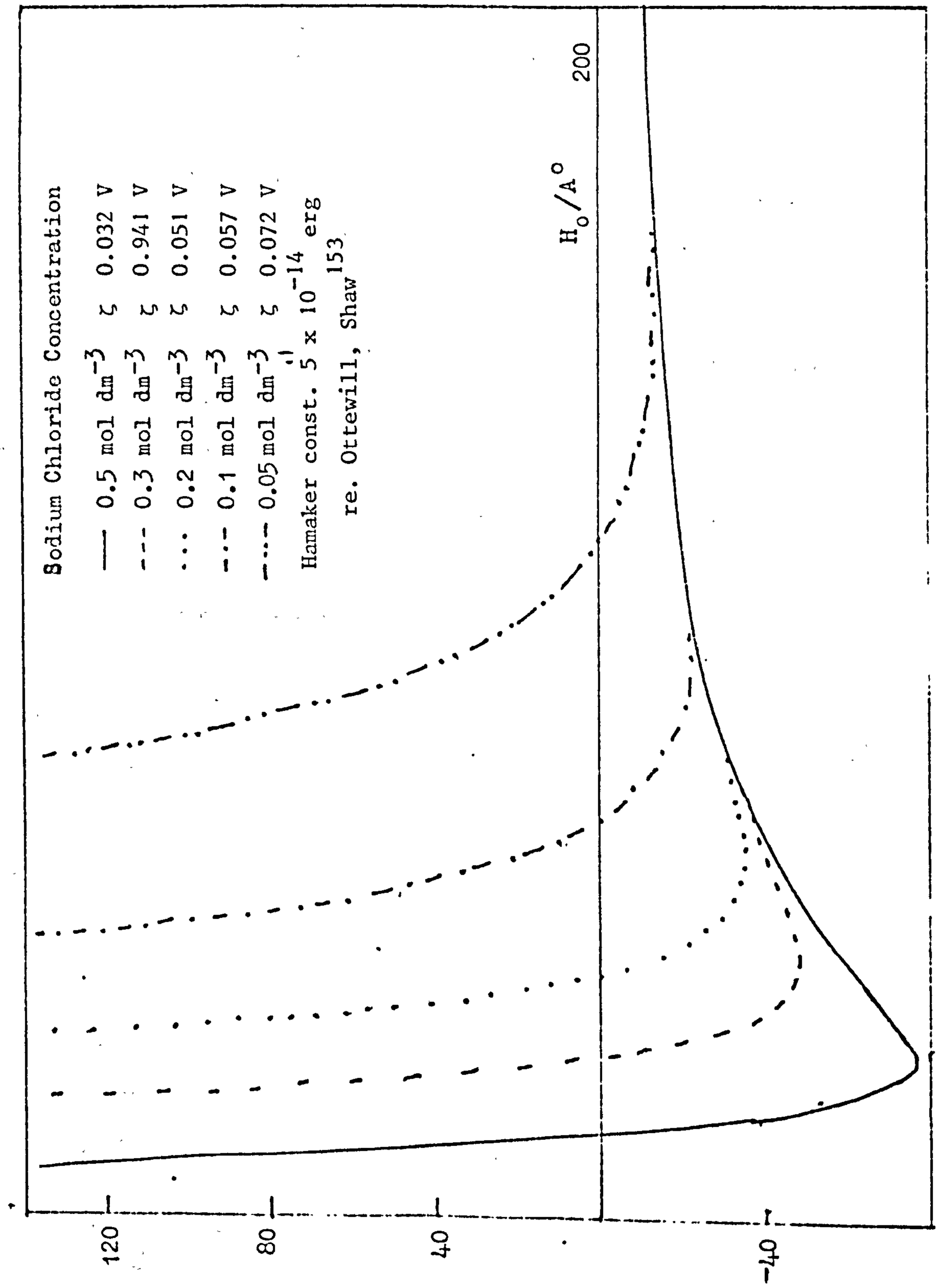

The thickness of the electrical double layer, $1/\kappa$, can be determined using the following equation as a function of salt concentration, table 1,

$$\kappa = \sqrt{\frac{8\pi\, n_o\, z_1 z_2\, e^2}{\varepsilon_r\, kT}} \quad \text{(section 1.5.2)}$$

where z_1, z_2 are the charge on the anion and cation. The zeta-potential, determined from the electrophoretic measurements, is required to calculate the repulsive potential energy of interaction.

A typical plot of the variation of potential energy of a charged particle with distance of separation between the surfaces of two spheres is shown in figure 9/11.

The diffraction of a laser beam by the bubble surface seemed to be indicative of a bilayer of particles. If this is the case then the particles in the two adjacent layers would interact in pairs and the potential energy of interaction is described by equation 1. The particles would be in positions of secondary minimum with respect to each other.

Particles will only form such a closely packed network if the particles in the bulk phase are approaching the conditions for coagulation. One method of achieving this potential energy state is to reduce the zeta-potential associated with the particles. This is the mechanism by which the DTAB/latex suspensions foam in the region of reversal of charge. Another way of making this close approach of two particles energetically favourable is to reduce the double layer repulsion, by increasing the ionic strength of the solution.

9.3.1 The Foaming Mechanism due to Increased Ionic Strength of the System

The potential energy curves have been calculated for latex JC, diameter 3.89 μm, within the foaming region, 0.05 to 0.5 mol dm^{-3} sodium chloride, figure 9/12.

The depth of the secondary minimum increases with sodium chloride concentration. This indicates that although the attraction between the particles in the bilayer increases as the secondary minimum increases in depth there is still a very strong repulsive force, indicated by the gradient of the energy curve; this helps to prevent the very close approach of the two particles. Moreover this will probably allow some mobility of the particles with the liquid layer between them. The bubble coalescence results, appendix II, show an increase in foam stability within the foaming region, that is in the range of 0.05 to 0.5 mol dm^{-3} sodium chloride. However, a ceiling in this stability appeared to be reached at the higher salt concentrations. This corresponded to the bulk coagulation region.

The other electrolytes studied showed behaviour similar to that observed in sodium chloride solutions. However a less stable foam was formed with higher valency electrolytes, as measured by both foam volume and its lifetime, than with the 1:1 electrolyte, sodium chloride. The ease of foaming of polystyrene latex particles when suspended in the following electrolytes increased in the order $La(NO_3)_3$, $BaCl_2$, $MgSO_4$, NaCl, that is 3:1, 2:1, 2:2 and 1:1 electrolytes.

The effect of varying the pH of the system was also studied. A good foam was formed in a strongly acidic environment, as the bulk phase approached the critical coagulation concentration.

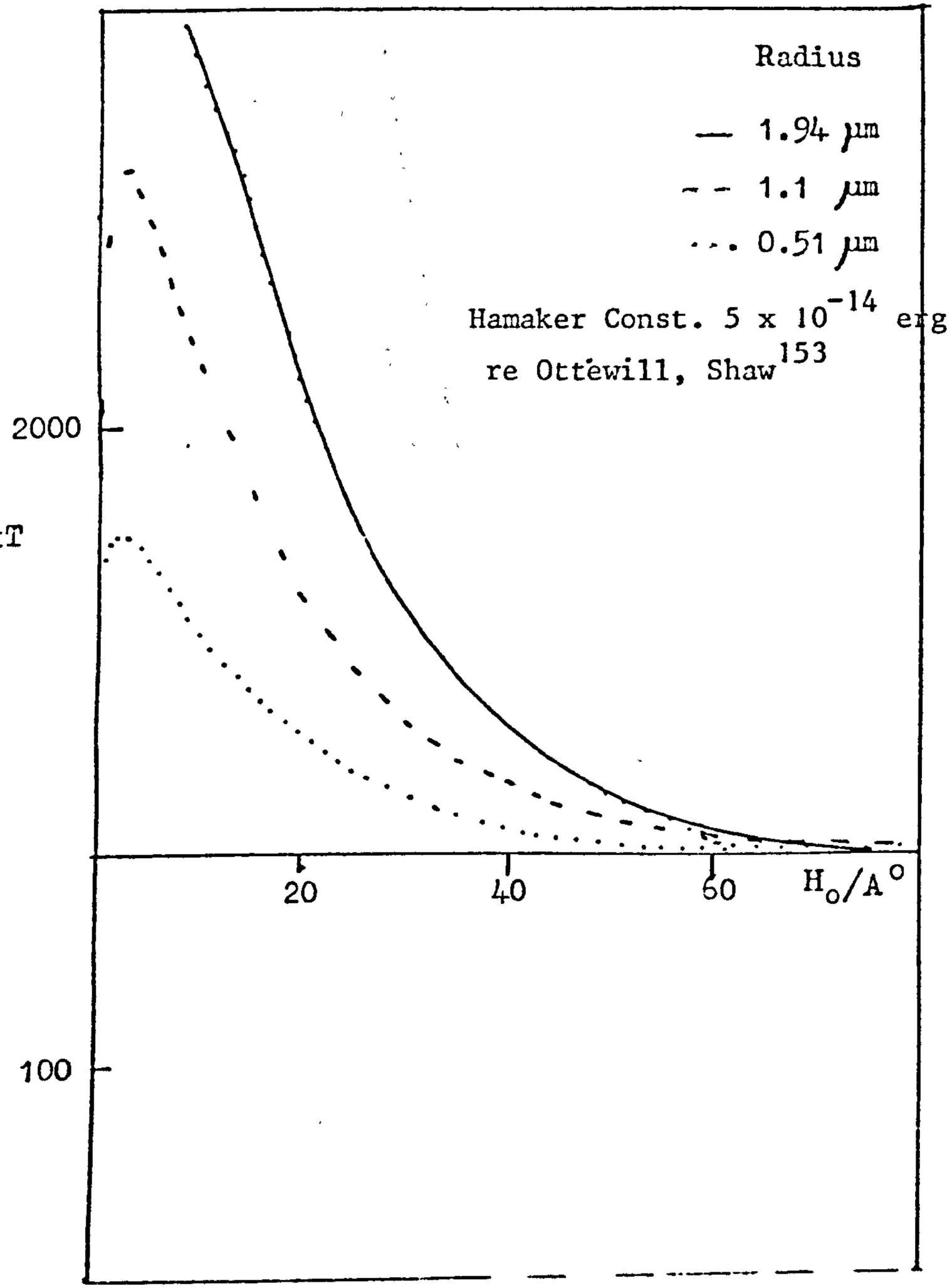

Figure 9/13 : Potential Energy Curves of Various Sized Polystyrene Particles in 0.05 mol dm^{-3} Sodium Chloride Solutions

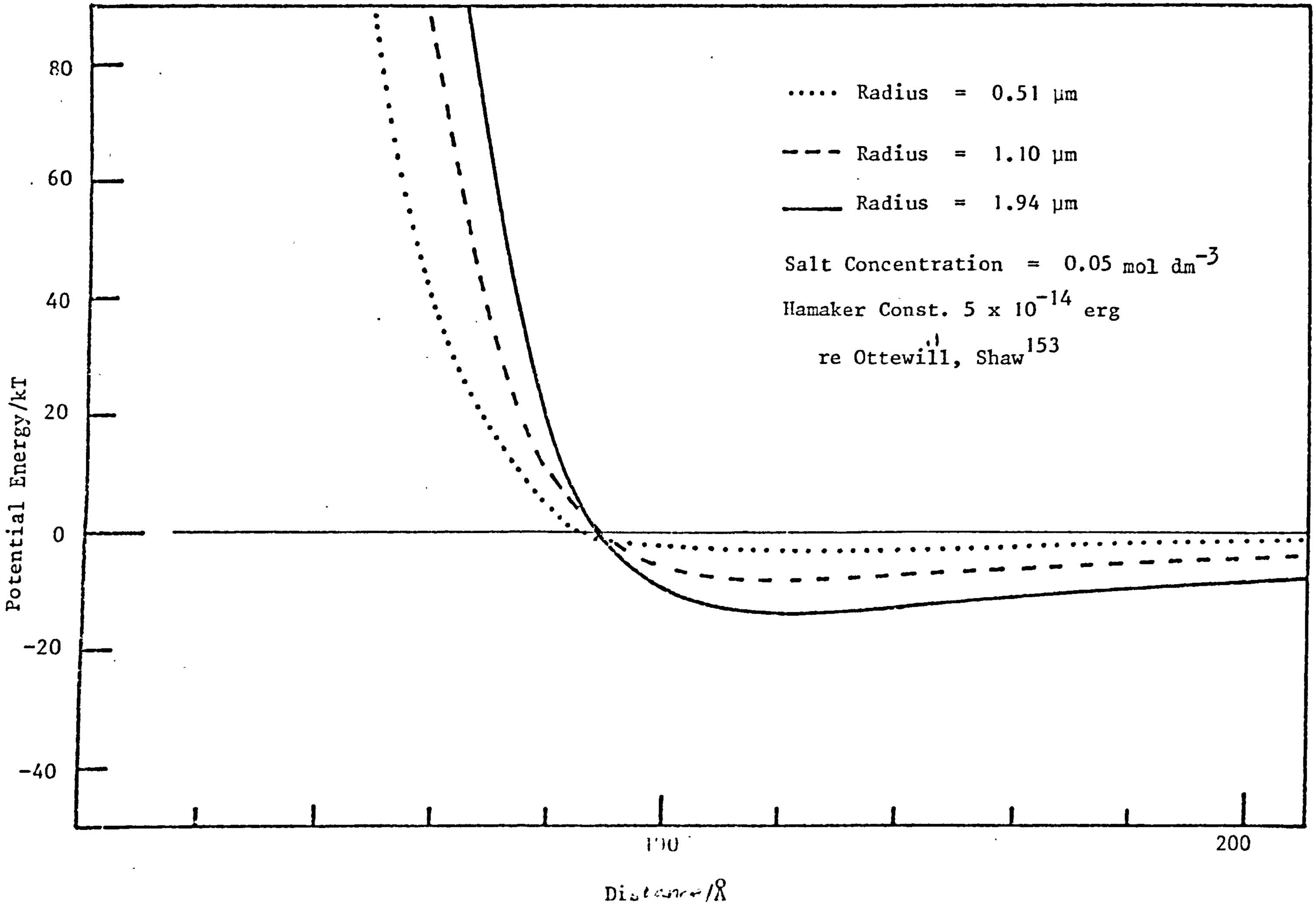

Figure 9/14: Potential Energy Curve for Polystyrene Particles of Various Sizes in 0.05 mol Sodium Chloride Solutions

9.3.2 Particle Size Effect

Different foaming behaviour was observed with varied sized latex particles. For latex JC, 3.89 μm diameter, a 'good' foam was observed before bulk coagulation occurred. Latices S61 and S67, diameters 2.1 and 2.2 μm, also formed a good foam near the point of bulk phase coagulation. A good foam was formed after coagulation had occurred in the bulk phase for latex particles with diameters of 1 μm. Therefore there appears to be a particle size dependency in the foaming behaviour.

The positions of secondary minimum for different sized latex particles in 0.05 mol dm^{-3} sodium chloride have been plotted in figures 9/13 and 9/14. For the smaller latices the zeta-potential has been assumed to be the same as that of latex JC, diameter 3.89 μm in 0.05 mol dm^{-3} sodium chloride, namely 72 mV.

It can be seen that the larger the particles the more pronounced is the secondary minimum and the higher the primary maximum. Therefore this could suggest that the bilayer of latex particles will be residing in a deeper secondary minimum the larger the particle. For the 1 μm diameter particle hardly any minimum is observed, and this corresponds to 'no foam' behaviour observed from foam studies with this salt concentration. Here there is no tendency for the particles to reside in a secondary minimum and in so doing form a foam.

A particle size effect was also observed for the latex/surfactant foams where no latex foam was formed for the 1 μm diameter latex.

9.4 Interactions within the Latex Layer

The latex particles are hexagonally close-packed on the bubble's surface, with part of the sphere in the liquid and the rest in air, figure 9/10. In section 9.2.1 the depth of immersion of the sphere has been calculated from such parameters as contact angle, density and surface tension.

The part of the sphere in the gaseous phase will probably only experience van der Waals attraction and the electrostatic repulsion will be primarily present in the liquid phase. This means that the particles within each layer can be drawn into close contact with each other, since there is only a small electrostic repulsive contribution to the total potential energy. The following sections describe the potential energy curves for two spheres situated within the same layer having the majority of their surface in the gaseous phase.

9.4.1. Theory

For simplicity the total interaction energy has been calculated for two particles situated in a monolayer with half of the particle in air and the other half submerged in the aqueous phase. The interaction energy in the air is then given by

$$V_T \text{ (air)} = \frac{A_{pp} R}{24 H_o}$$

where A_{pp} is the Hamaker constant for the interaction between polystyrene particles in a vacuum.

For the submerged hemisphere the total interaction is half that for the interaction of two spheres in a liquid, that is,

$$V_T \text{ (aqueous)} = \frac{\varepsilon_r R \psi_o^2}{4} \ln\left[1 + \exp(-\kappa H_o)\right] - \frac{A_{net} R}{24 H_o}$$

Hence the total interaction of two spheres situated in a monolayer can be defined as

$$V_T = \frac{\varepsilon_r R \psi_o^2}{4} \ln\left|1 + \exp(-\kappa H_o)\right| - \frac{R}{24 H_o}\left|A_{pp} + A_{net}\right|$$

A computer program has been devised to calculate this energy, Appendix IV. It should be noted that for both the computer programs, Appendices III and IV the full expression for the attractive energy term has been used, that is, in this case,

$$V_A = - \frac{A_{net}}{24}\left(\frac{1}{x^2 + 2x} + \frac{1}{x^2 + 2x + 1} + 2 \ln \frac{x^2 + 2x}{x^2 + 2x + 1}\right)$$

where $x = \frac{H_o}{2R}$

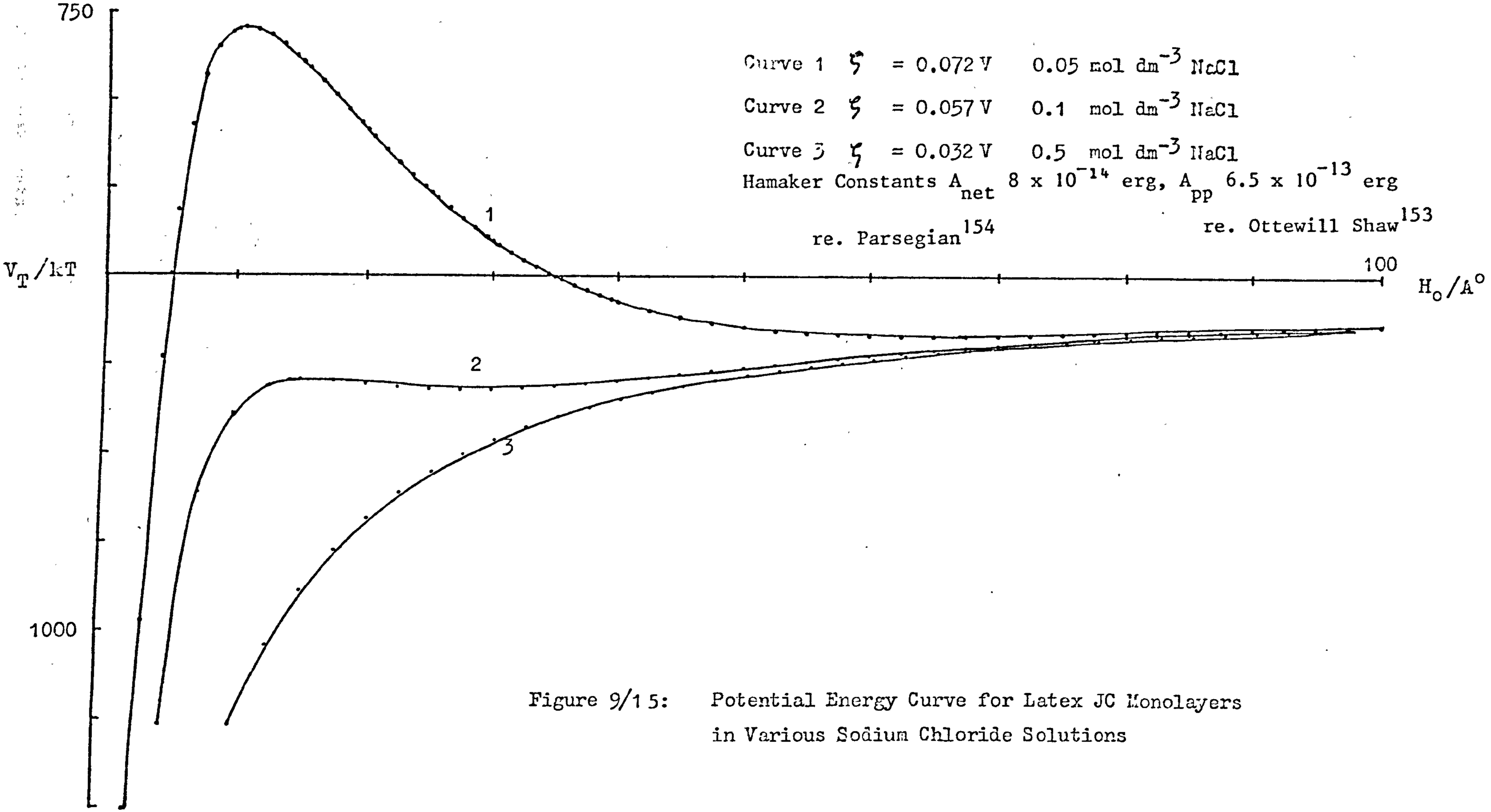

Figure 9/15: Potential Energy Curve for Latex JC Monolayers in Various Sodium Chloride Solutions

However for these systems x is much less than unity and the attractive energy approximates to

$$V_A = - \frac{A_{net} R}{24 H_o}$$ for half-submerged spheres.

The contact angle data indicate that in fact the portion of the particle dewetted, that is in the gaseous phase, is greater than half, section 9.2.1. The calculated energy therefore contains less attractive energy than that actually experienced by two adjacent particles in the monolayer.

9.4. The Total Interaction Energy experienced by Monolayers submerged in Sodium Chloride Solutions

Figure 9/15 illustrates the interaction energies of two adjacent particles in monolayers half-submerged in different sodium chloride solutions.

Curve 1 represents a monolayer of latex JC particles, radius .94 μm, where half of each particle is wetted by 0.05 mol dm^{-3} sodium chloride. There is a large primary maximum in the potential energy for the monolayer at this salt concentration. This energy barrier will prevent the particles from packing closely together in the layer. No foam was found at this salt concentration in the foam tests conducted on latex JC.

Curve 2 illustrates the calculated interaction energy for a monolayer of latex JC half submerged in 0.1 mol dm^{-3} sodium chloride. Here there is a minute potential energy barrier. Hence the particles in the monolayer can approach each other closer than before, and this sodium chloride concentration corresponds to a slight foam as determined by the foam tests on this latex.

Finally, curve 3 is the calculated potential energy for two adjacent particles, latex JC, in a monolayer submerged in 0.5 mol dm^{-3} sodium chloride. No primary maximum exists and in fact this curve is indicative of a very strong attractive force resulting in the particles being very closely packed in the monolayer. At this salt concentration a very good foam was found in the foam tests.

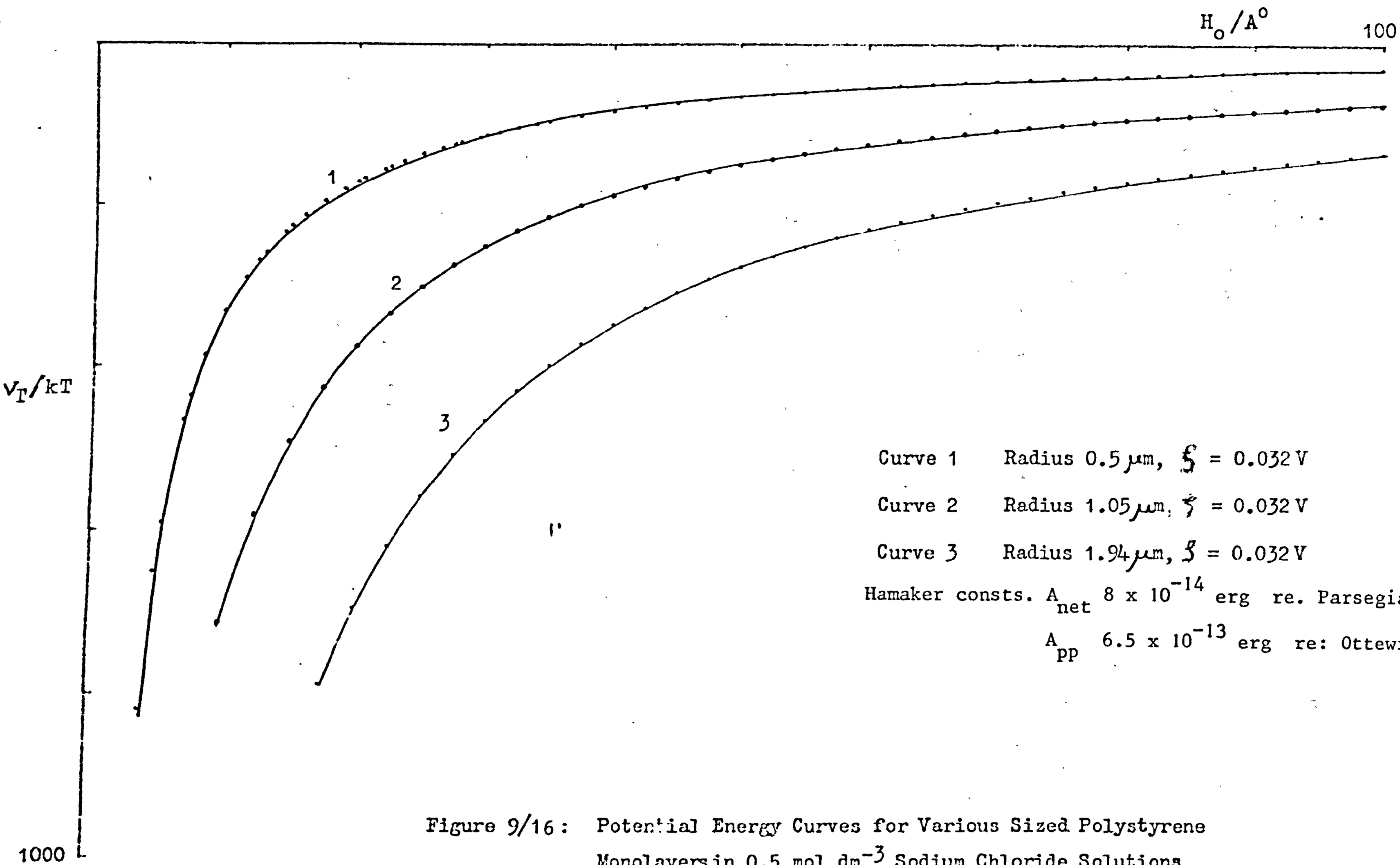

Curve 1 Radius 0.5 μm, ζ = 0.032 V

Curve 2 Radius 1.05 μm, ζ = 0.032 V

Curve 3 Radius 1.94 μm, ζ = 0.032 V

Hamaker consts. A_{net} 8×10^{-14} erg re. Parsegian[154]

A_{pp} 6.5×10^{-13} erg re: Ottewill, Shaw[15]

Figure 9/16: Potential Energy Curves for Various Sized Polystyrene Monolayers in 0.5 mol dm^{-3} Sodium Chloride Solutions

Clearly for a good latex foam, where the particles in the monolayer must be able to pack closely together, the interaction energy must be dominantly attractive. This is found to be the case for the calculated interaction energy of a monolayer of half submerged particles. Also it has been shown that if there exists a potential barrier, causing the monolayer to be more expanded, then the foam produced is not stable.

9.4.3 Particle Size Effect

From the Langmuir trough measurements the strength of the monolayer decreased with particle diameter, that is a monolayer of latex JC, radius 1.94 μm, had a higher collapse pressure than RB 55, radius 0.5 μm, while floating on 0.5 mol dm^{-3} sodium chloride. The collapse pressures were 67.5 and 30 mN m^{-1} respectively.

Figure 9/16 shows the calculated interaction energies for particles with radii 0.5 μm, 1.0 μm and 1.94 μm, half submerged in 0.5 mol dm^{-3} sodium chloride solution. For the large latex particles, JC, the attractive force in the monolayer is greater than that for the smaller latices. It can be concluded that the larger the latex particles, the greater the attractive force between them, the closer they can be packed in a monolayer and the greater the cohesion in the layer.

The mixed latex monolayer on the Langmuir trough indicated that the latex particles less than 1.6 μm diameter were squeezed out of the interface by the larger 3.89 μm diameter particles. This indicated that a smaller particle, diameter less than 1.6 μm, was not held at the interface as strongly as the 2.2 or 3.89 μm particle. The stronger attractive forces between the bigger particles might squeeze the smaller ones out of the interface.

9.4.4 The Rigidity of a Monolayer of Polystyrene Latex Particles

A monolayer of the polystyrene latex particles floating on a salt solution has a high degree of rigidity associated with it on compression. A solid-like film is formed which has a very high collapse pressure; for latex JC this parameter is 68 mN m^{-1}. This indicates that these particles can approach close to each other and can reside in positions of primary minimum in the potential energy curve.

For foam stability the film covering the bubble must be able to withstand vibrations set up in the system. Obviously the higher the rigidity of the film the more stable the foam will be. However there still must be a degree of mobility within the film. The presence of a second layer of particles, the two layers being in positions of secondary minimum with each other, will enable there to be a degree of mobility both within the plane of the film and also across it. The repulsion of the two layers will balance the capillary suction taking place via the Plateau borders.

It follows from this that for foams to be formed there must be sufficient particles to cover the air-liquid interface generated as has been found from the foam studies. If the number of latex particles is too small, insufficient of the bubble's surface will be coated with particles causing 'patches' in the latex layer which act as rupture centres.

For the mixed monolayer, for particles smaller than 2 μm with the large 3.89 μm latex the smaller particles appeared to sink. However, the relative sizes of the particles are such that the large particles could easily hide the smaller ones. This would appear to be the case for the 3.89 μm / 1.02 μm layer. This layer was characteristic of an expanded liquid, indicating repulsion within the layer preventing the close-packed, solid-like layer previously observed with only the 3.89 μm particles.

Surface tension measurements using a Du Noüy tensiometer indicated that the adhesion of a layer of polystyrene latex particles to the air/liquid interface was very small. Since the surface tension of a polystyrene layer

on a salt/latex suspension's surface was, within experimental error, the same as without the layer.

Therefore the cohesion force within the layer, indicated by the Langmuir trough experiments, is larger than the adhesion of the particle to the air/liquid interface.

9.5 Summary of Conclusions

Polystyrene particles will only form a foam when the system is approaching the conditions required for bulk coagulation. This can be brought about either by an increase in the ionic strength or by specific adsorption of ions. They will not foam when suspended in water alone.

It seems very probable on the basis of experimental evidence that the air cell is coated by a bilayer of latex particles, which are hexagonally close-packed. It also seems possible that the particles within the phase of each monolayer are in positions of the primary minimum energy due to the strong attraction of particles in air; whilst in adjacent layers with aqueous electrolyte solution in between the two particles are in positions of the secondary minimum. The depth of this secondary minimum and hence the foam stability increase within the salt foaming region and with particle size.

A particle size effect has been observed. Latices having diameters of 1 μm are reluctant to foam. They will not foam even in the DTAB system.

The single monolayers are rigid and solid-like in character. The interaction energy and the strength of the monolayer increase with particle size. Mixed particle size monolayers illustrated the formation of a more liquid-expanded film.

The zeta-potential of the polystyrene particles decreased within the electrolyte foaming region and a reversal of charge occurred with the DTAB system, at a concentration corresponding to the latex foam region.

The contact angle data for both types of foaming systems indicated an increase in contact angle to give angles greater than 90° as the foaming

region was approached. Therefore the particles acquire a hydrophobic nature making it more energetically favourable to be situated at the air-liquid interface than in the bulk phase and so form a latex stabilised foam.

REFERENCES

1. Adamson, A.W. "Physical Chemistry of Surfaces", 2nd Ed., Interscience, N. York (1967).
2. Shaw, D.J. "Introduction to Colloid and Surface Chemistry", Butterworth (1966).
3. Goodwin, J.W., Ottewill, R.H., Pelton, G. and Yates, D.E. Brit. Polym. J. 10, 173 (1978).
4. Derjaguin, B.V. and Landau, L. Actaphysics-chim. U.R.S.S., 14, 633 (1941).
5. Verwey, E.J.W. and Overbeek, J.Th.G. "Theory of Stability of Lyophobic Colloids", Elsevier (1948).
6. Ottewill, R.H. Chem. Soc. Spec. Per. Report Coll. Sci., vol. 1, 173 (1973).
7. Plateau, J.A.F. "Statique Experimentale et Théorique des Liquides", Paris, vol.1, chap.5 (1873).
8. Ross, S. Ind. Eng. Chem. 61, 48 (1969).
9. Hardy, Sir William J. Chem. Soc. 127, 1224 (1925).
10. Corkill, J.M., Goodman, J.F., Haisman, D.R. and Harrold, S.P. Trans. Farad. Soc. 57, 821 (1961).
11. Laing, M.E. Proc. Roy. Soc. A.109, 28 (1925).
12. Bikermann, J.J. Ind. Eng. Chem. 57, 56 (1965).
13. Manegold, E. "Schaum", Chemie und Techik. Verlagsgesellschaft, Heidelberg (1953).
14. Kitchener, J.A. and Cooper, C.F. Quart. Revs. 13, 71 (1959).
15. Kitchener, J.A. Rec. Prog. Surf. Sci. 1, 51 (1964).
16. de Vries, A.J. Rec. trav. chim. 77, 81 (1958).
17. Dewar, J. Engineering, 101, 87 (1916).
18. Rennie, J. and Smith, W. Nature, 192, 419 (1961).
19. Hartland, S. and Barber, A.D. Trans. Inst. Chem. Engrs. 52, 43 (1974).
20. Sebba, F. J. Coll. Int. Sci. 40, 468 (1972).

21. Kruglyakov, P.M. and Taube, P.R. Coll. J. U.S.S.R. (trans), 34, 194 (1972).

22. Ross, S. and McBain, J.W. Ind. Eng. Chem. 36, 570 (1944).

23. Ross, S. J. Phys. Chem. 54, 429 (1950).

24. Ross, S., Hughes, A.F., Kennedy, M.L. and Marid, A.R. J. Phys. Chem. 57, 684 (1953).

25. Burcik, E.J. J. Coll. Int. Sci. 5, 421 (1950).

26. Chang, R.C., Schoen, H.M. and Grove, C.S. Ind. Eng. Chem. 48, 2035 (1956).

27. Clark, N.O. and Blackman, M. Trans. Farad. Soc. 44, 7 (1948).

28. Gibbs, J.W. "The Collected Works of J. Willard Gibbs", chap.III, vol.1, Longmans Green & Co. 1928.

29. Schütz , F. Trans. Farad. Soc. 38, 85 (1942).

30. Schütz, F. Trans. Farad. Soc. 38, 94 (1942).

31. von Bartsch, O. Koll. Beih. 20, 1 (1925).

32. Brady, A.P. and Ross, S. J.A.C.S. 66, 1348 (1944).

33. Foulk, C.W. and Miller, J.N. Ind. Eng. Chem. 23, 1283 (1931).

34. Nash, T. J. Appl. Chem. 8, 440 (1958).

35. Brown, A.G., Thuman, W.C. and McBain, J.W. J. Coll. Sci. 8, 491 (1953).

36. Clark, N.O. Trans. Farad. Soc. 44, 13 (1948).

37. Bikerman, J.J. Trans. Farad. Soc. 34, 634 (1938).

38. Barmore, M. Tech. Bull. Colorado Agric. Coll. 9 (1934).

39. Clark, N.O. and Blackman, M. Trans. Farad. Soc. 44, 1 (1948).

40. de Vries, A.J. Rec. trav. chim. 77, 283 (1958).

41. Brown, A.G., Thuman, W.C. and McBain, J.W. J. Coll. Sci. 8, 508 (1953).

42. de Vries, A.J. Rec. trav. chim. 77, 209 (1958).

43. Bikerman, J.J. Sepn. Sci. 7, 647 (1972).

44. Lyklema, J. Rec. trav. chim. 81, 890 (1962).

45. Scheludko, A. Adv. Coll. Inter. Sci. 1, 391 (1967).

46. Jones, T.G., Durham, K., Evans, W.P. and Camp, M. Proc. 2nd Int. Congr. Surf. Act., London, 1, 225 (1957).

47. Miles, C.D., Ross, J. and Shedlovsky, L. J. Amer. Oil Chem. Soc., 27, 268 (1950).

48. Sporek, C.R. J. Amer. Oil Chem. Soc. 30, 190 (1953).

49. Dasher, G.F. and Mabis, A.J. J. Phys. Chem. 64, 77 (1960).

50. Mysels, K., Sherioda, K. and Frankel, S. "Soap Films", chap.II, Pergamon Press (1959).

51. Derjaguin, B.V. and Titijevskaya, A.S. Proc. 2nd Int. Congr. Surf. Act., London, 1, 211 (1957).

52. Haas, P.A. and Johnson, H.F. Ind. Eng. Chem. Fund. 6, 225 (1967).

53. Derjaguin, B.V. Trans. Farad. Soc. 33, 203 (1940).

54. Derjaguin, B.V. and Churaev, N.V. Coll. J. U.S.S.R. (trans) 38, 402 (1976).

55. Van den Tempel, M. Proc. Scand. Symp. Surf. Activ. 2, 306 (1964).

56. Ivanov, I.B. and Dimitrov, D.S. Coll. Polym. Sci. 252, 982 (1974).

57. Radeov, B.P., Dimitrov, D.S. and Ivanov, I.B. Coll. Polym. Sci. 252, 50 (1974)

58. Miles, G.D., Schedlovsky, L. and Ross, J. J. Phys. Chem. 49, 93 (1945).

59. Thompson, W. J. Appl. Chem. 12, 12 (1962).

60. Scriven, L.E. and Sternling, C.V. Nature, 187, 186 (1960).

61. Davies, J.T. Proc. 2nd Int. Congr. Surf. Act. 1, 220 (1957).

62. Jashnani, I.L. and Lemlich, R. J. Coll. Int. Sci. 46, 13 (1974).

63. Mannheimer, R.J. A.I. Ch. E.J. 13, 751 (1967).

64. Joly, M. Rec. Prog. in Surf. Sci. 1, 1 (1964).

65. Shih, F.S. and Lemlich, R. A.I. Ch. E.J. 13, 751 (1967)

66. de Vries, A.J. Rec. trav. Chim. 77, 383 (1958).

67. de Vries, A.J. Rec. trav. Chim. 77, 441 (1958).

68. Shearer, L.T. and Akers, W.W. J. Phys. Chem. 62, 1264 (1958).

69. Malysa, K., Pawlikowska-Czubak, J. Bull. Acad. Pol. Sci. Ser. 23, 423 (1975).

70. Corkill, J.M., Goodman, J.F., Ogden, C.P. and Tate, J.R. Proc. Roy. Soc. A273, 84 (1963).

71. Ivanov, I.B., Radeov, B.P., Manev, E. and Scheludko, A. Trans. Farad. Soc. 66, 1262 (1970).

72. Barber, A.D. and Hartland, S. Trans. Inst. Chem. Eng. 53, 106 (1975).

73. Maru, H.C., Wasan, D.T. and Kintner, R.C. Chem. Eng. Sci. 26, 1615 (1971).

74. Torbin, M.V., Chesha, I.I. and Dukhin, S.S. Coll. J. U.S.S.R. (trans) 32, 643 (1970).

75. Boucher, E.A. and Kent, H.J. J. Chem. Soc. Fara. 74, 846 (1978).

76. Rapacchietta, A.V. and Neumann, A.W. J. Coll. Int. Sci. 59, 555 (1977).

77. Hartland, S. J. Coll. Inst. Sci. 26, 383 (1968).

78. Hartland, S. and Robinson, J.D. J. Coll. Int. Sci. 35, 372 (1971).

79. Princen, H.M. Surf. Coll. Sci. 2, 36 (1969).

80. Dukhin, S.S. and Rulev, N.N. Coll. J. U.S.S.R. (trans) 39, 231 (1977).

81. Derjaguin, B.V., Dukhin, S.S. and Rulev, N.N. Coll. J. U.S.S.R. (trans) 38, 277 (1976).

82. Princen, H.M. J. Coll. Sci. 18, 178 (1963).

83. Princen, H.M. and Mason, S.G. J. Coll. Sci. 20, 246 (1965).

84. Hartland, S. Chem. Eng. Sci. 24, 987 (1969).

85. Hartland, S. and Robinson, D. Chem. Eng. Sci. 25, 227 (1970).

86. Nutt, C.W. Chem. Eng. Sci. 12, 133 (1960).

87. Derjaguin, B.V., Rulev, N.N. and Dukhin, S.S. Coll. J. U.S.S.R. (trans) 40, 598 (1978).

88. Huh, C. and Scriven, L.E. J. Coll. Int. Sci. 30, 323 (1969).

89. Huh, C. and Mason, S.G. J. Coll. Int. Sci. 47, 271 (1974).

90. Padday, J.F. and Pitt, A. J. Coll. Sci. 38, 323 (1972).

91. Scheludko, A. and Nikavov, A.D. Coll. Polym. Sci. 253, 396 (1975).

92. Huh, C. and Mason, S.G. Can. J. Chem. 54, 969 (1976).

93. Heller, W. J. Phys. Chem. 41, 1041 (1937).

94. Heller, W. and Roeder, H.L. Trans. Farad. Soc. 38, 191 (1942).

95. Heller, W. and Peters, J. J. Coll. Int. Sci. 32, 592 (1970).

96. Peters, J. and Heller, W. J. Coll. Int. Sci. 33, 60 (1971).

97. Heller, W. and De Lauder, W.B. J. Coll. Int. Sci. 35, 60 (1971).

98. Heller, W. and Peters, J. J. Coll. Int. Sci. 35, 300 (1971).

99. De Lauder, W.B. and Heller, W. J. Coll. Int. Sci. 35, 308 (1971).

100. Ottewill, R.H. Chem. Soc. Spec. Per. Rep. Coll. Sci. 1, 205 (1973).

101. Stark, H.M. J.A.C.S. 52, 2730 (1930).

102. Roe, C.P. and Brass, P.D. J. Coll. Sci. 10, 194 (1958).

103. Freundlich, von H. and Woronersensky, S. Koll. Z. 33, 222 (1925).

104. Fair, G.M. and Geminell, R.S. J. Coll. Sci. 19, 360 (1964).

105. Webb, B.H. and Johnson "Fundamentals of Dairy Chemistry", Avi Publishing Company (1965).

106. Mulder and Walstra, P. "Milk Fat Globule", Commonwealth, Agri. Bureaux.

107. Wang, J.C. and Kinsella, J.E. J. Food Sci. 41, 498 (1976).

108. Monaghan-Watts, B. Ind. Eng. Chem. 29, 1009 (1937).

109. Richert, S.D., Morr, C.V. and Cooney, C.M. J. Food Sci. 39, 42 (1974).

110. Slosberg, H.M., Hanson, H.L., Stewart, G. and Lowe, B. Poultry Sci. 27, 294 (1948).

111. Henry, W.C. and Barbour, A.D. Ind. Eng. Chem. 25, 1054 (1953).

112. Peter, P.N. and Bell, R.W. Ind. Eng. Chem. 22, 1124 (1930).

113. Cumper, C.W.N. Trans. Farad, Soc. 49, 1360 (1953).

114. Sechler, C., Manargh, G. and Mangel, M. Food Res. 24, 198 (1959).

115. Leviton, A. and Leighton, A. J. Dairy Sci. 18, 105 (1935).

116. Bailey, M.I. Ind. Eng. Chem. 27, 973 (1935).

117. Goodwin, J.W., Hearn, J., Ho, C.C. and Ottewill, R.H. Br. Polym. J. 5, 347 (1973).

118. Jayasuriya, D.S. Ph.D. thesis, Univ. Bristol (1978).

119. Goodwin, J.W., Ottewill, R.H. and Yates, D.E. J. Coll. Int. Sci. 62, 356 (1977).

120. Wark, I. and Sutherland, I. "Principles of Flotation", Australasian Institute of Mining and Metallurgy.

121. Krieger, I.M. and O'Neill, F. J.A.C.S. 90, 3114 (1965).

122. Alonso, M. and Finn, E.J. "Fundamental University Physics", vol.2, p.914.

123. Lord Rayleigh. Proc. Roy. Soc. (London), 47, 364 (1890).

124. Pockels, A. Nature, 43, 437 (1891).

125. Langmuir, I. J.A.C.S. 39, 1848 (1917).

126. Guastella, J. "Surface Chemistry", Butterworth (1947).

127. Harkins, W.D. and Jordan, H.F. J.A.C.S. 52, 1751 (1930).

128. Henry, D.C. Proc. Roy. Soc. A133, 106 (1931).

129. Elliott, G.E.R. and Riddiford, A.C. Rec. Prog. Surf. Sci. 2, 111 (1964).

130. Sulman, H.L. Trans. Inst. Min. & Met. 20, 88 (1920).

131. Wenzel, R.N. Ind. Eng. Chem. 28, 988 (1956).

132. Bartell, F.E. and Wooley, A.D. J.A.C.S. 55, 3578 (1933).

133. Bartell, F.E. and Hatch, G.E. J. Phys. Chem. 39, 11 (1935).

134. Bartell, F.E. and Ray, B.K. J.A.C.S. 74, 778 (1952).

135. Good, R.J. J.A.C.S. 74, 5041 (1952).

136. Schwartz, A.M. and Minor, F.W. J. Coll. Sci. 14, 584 (1959).

137. Cassie, A.B.D. Diss. Fara. Soc. 3, 11 (1948).

138. Shepard, J.W. and Bartell, F.E. J. Phys. Chem. 57, 458 (1953).

139. Johnson Jr., R.E. and Dettre, R.H. Surf. Coll. Sci. 2, 85 (1969).

140. Bikerman, J.J. J. Phys. Coll. Chem. 54, 653 (1950).

141. Bartell, F.E. and Shepard, J.W. J. Phys. Chem. 57, 211 (1953).

142. Bartell, F.E. and Shepard, J.W. J. Phys. Chem. 57, 455 (1953).

143. Cassie, A.B.D. and Baxter, S. Trans. Fara. Soc. 40, 546 (1944).

144. Johnson Jr., R.E. and Dettre, R.H. J. Phys. Chem. 68, 1744 (1964).

145. Dettre, R.H. and Johnson Jr., R.E. J. Phys. Chem. 69, 1507 (1965).

146. Cassie, A.B.D. Diss. Fara. Soc. 3, 11 (1948).

147. Wolfram, E. and Faust, R. "Wetting, Spreading and Adhesion", p.213. Ed. J.F. Padday, Acad. Press (1978).

148. MacDougall, G. and Ockrent, C. Proc. Roy. Soc. A180, 151 (1942).

149. Wilson, J.C. M.Sc. thesis, Univ. Bristol (1976).

150. Connors, P. and Ottewill, R.H. J. Coll. Int. Sci. 37, 642 (1971).

151. Heller, W. and Quimfe, G. C.R.Acadm.Sci. Paris, 178, 445 (1936)

152. van den Hul, H.J., Vanderhoff, J.W., Br.Polym.J. 2, 121 (1970).

153. Ottewill, R.H., Shaw, J.N., Disc.Farad.Soc. 42, 154 (1966).

154. Gingell, D., Parsegian, V.A., J.Coll.Int.Sci. 44, 456 (1973).

APPENDIX I

Geometry of the Spherical Liquid Cap (Section 8.5.2)

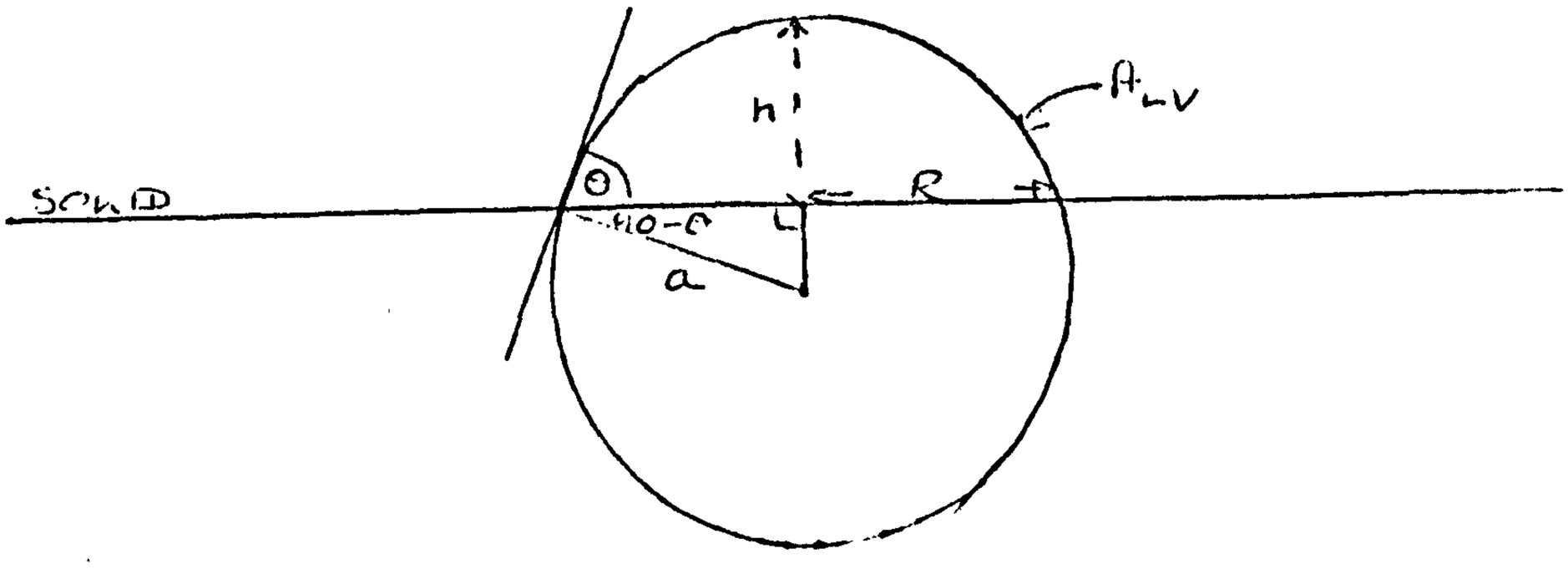

The liquid forms a spherical cap, height h, radius R; where the radius of the sphere is a.

Surface Area $A_{LV} = 2\pi a h$

$$R = a \cos(90 - \theta)$$

$$h = a \sin\theta$$

Similarly

$$(a - h) = a \sin(90 - \theta)$$

$$h = a(1 - \cos\theta)$$

$$A_{LV} = 2 \frac{\pi R^2}{\sin^2\theta}(1 - \cos\theta)$$

$$A_{LV} = \frac{2\pi R^2}{1 + \cos\theta}$$

Simplification of Expression (6) p.92

If V is the volume of a spherical cap then

$$V^2 = \frac{\pi^2 R^6}{9}\left[\frac{2}{(1 + \cos\theta)^3} + \frac{3}{(1 + \cos\theta)^2} - 1\right]$$

As the layer tilts the volume of the drop, that is a spherical cap, remains constant while R and θ vary.

Let $x = 1 + \cos\theta$

then $V^2 = \frac{\pi^2 R^6}{9} \left[\frac{2}{x^3} + \frac{3}{x^2} - 1\right]$

Differentiating,

$$0 = \frac{6\pi^2 R^5}{9} \left[\frac{2}{x^3} + \frac{3}{x^2} - 1\right] dR - \frac{6\pi^2 R^6}{9} \left[\frac{1}{x^4} + \frac{1}{x^3}\right] dx$$

$$\therefore \quad \frac{dx}{dR} = \frac{x^4}{R(1 + x)} \left[\frac{2}{x^3} + \frac{3}{x^2} - 1\right]$$

However $x = 1 + \cos\theta$

$$\therefore \quad dx = -\sin\theta \, d\theta$$

and $$\frac{d\theta}{dR} = -\frac{x^4}{R \sin\theta(1 + x)} \left[\frac{2}{x^3} + \frac{3}{x^2} - 1\right]$$

In expn. 6

$$\left[\frac{2\gamma_{LV}}{(1 + \cos\theta)} + \frac{\gamma_{LV} R \sin}{(1 + \cos\theta)^2} \frac{d\theta}{dR}\right] = \gamma_{LV} \left[\frac{2}{x} - \frac{R \sin\theta}{x^2} \frac{x^4}{R \sin\theta(1 + x)} \left(\frac{2}{x^3} + \frac{3}{x^2} - 1\right)\right]$$

$$= \gamma_{LV} \left[\frac{2}{x} - \frac{1}{(1 + x)} \left(\frac{2}{x} + 3 - x^2\right)\right]$$

$$= \gamma_{LV} (x - 1)$$

$$= \gamma_{LV} \cos\theta \, .$$

APPENDIX II

Bubble Coalescence

These experiments were conducted to see if a measure of foam stability within the latex foam region could be obtained. However as such this method proved inadequate due to insufficient temperature control.

1. Experimental

The simple apparatus illustrated in figure 1 was used to study the coalescence of a bubble, with a liquid-air interface. The bubble was formed at the end of a capillary and then released to float upwards towards the air-water interface.

In order to carry out the experiment a dilute latex JC suspension in sodium chloride solution in the range 0.05 to 0.45 mol dm^{-3} sodium chloride was stirred with a magnetic follower. A layer of polystyrene latex particles, latex JC, was deposited at the interface by dipping a glass rod, which had been coated with freeze-dried latex, in and out of the liquid surface. Bubbles were formed at the tip of the capillary by turning the Agla micrometer syringe mounting.

A bubble was formed and allowed to age for five minutes before the syringe was adjusted to release the bubble; thus causing it to float to the surface. The stirrer was stopped each time during the actual measurement of coalescence. The time from releasing the bubble to its bursting was recorded. Forty bubbles were timed for each salt solution.

The room temperature was recorded for each run and was found to be $23 \pm 2^{o}C$.

2. Results

A distribution of lifetimes was obtained for each run, figure 2. An explanation for this distribution has been given for droplet coalescence[149]. The statistical half-life, $\tau_{\frac{1}{2}}$, can be derived as the time after which half the bubbles had burst.

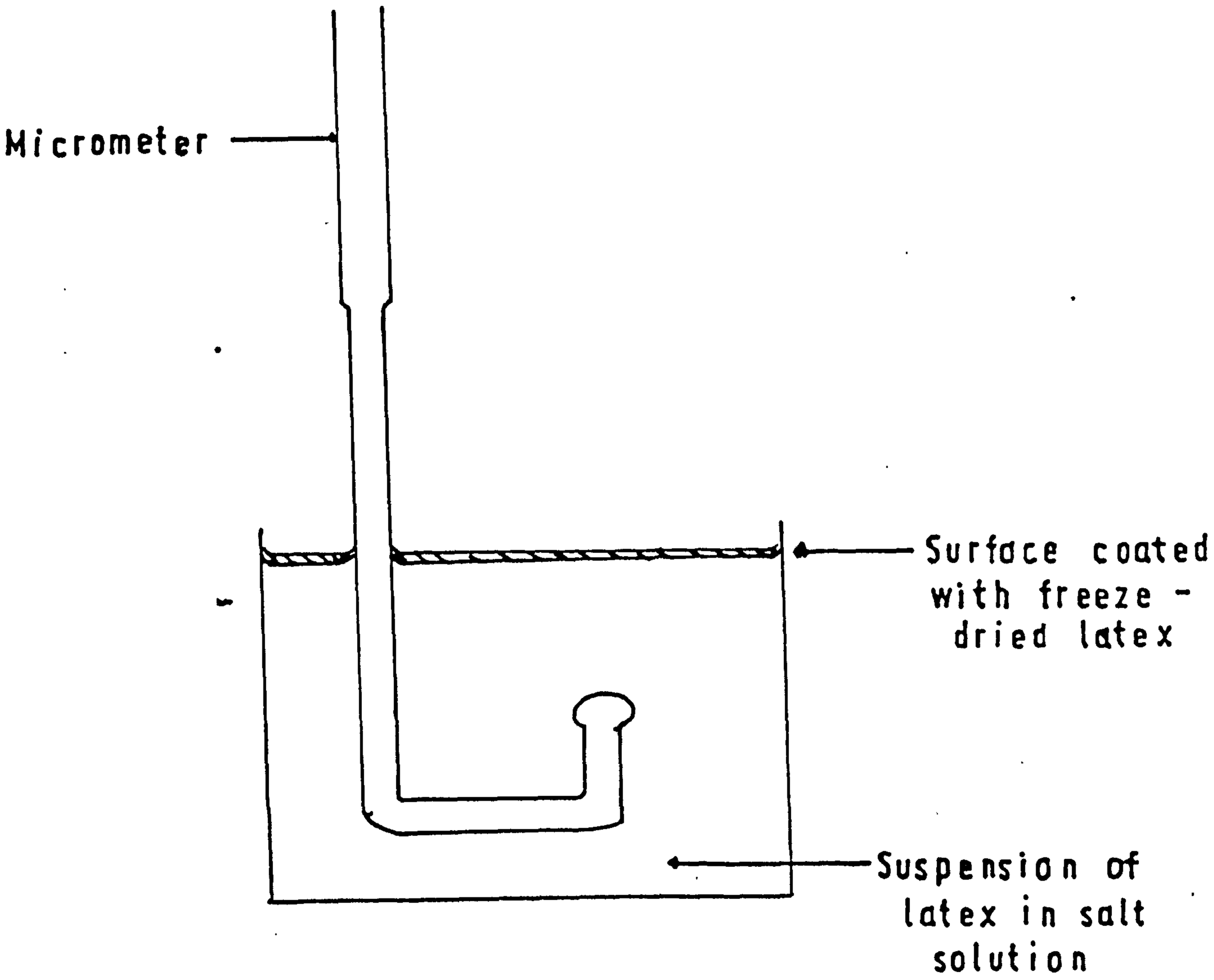

Figure 1 : Apparatus used for Bubble Coalescence Experiments

Figure 2: Determination of the Half-life of Bubbles at an Air/Solid Latex Interface

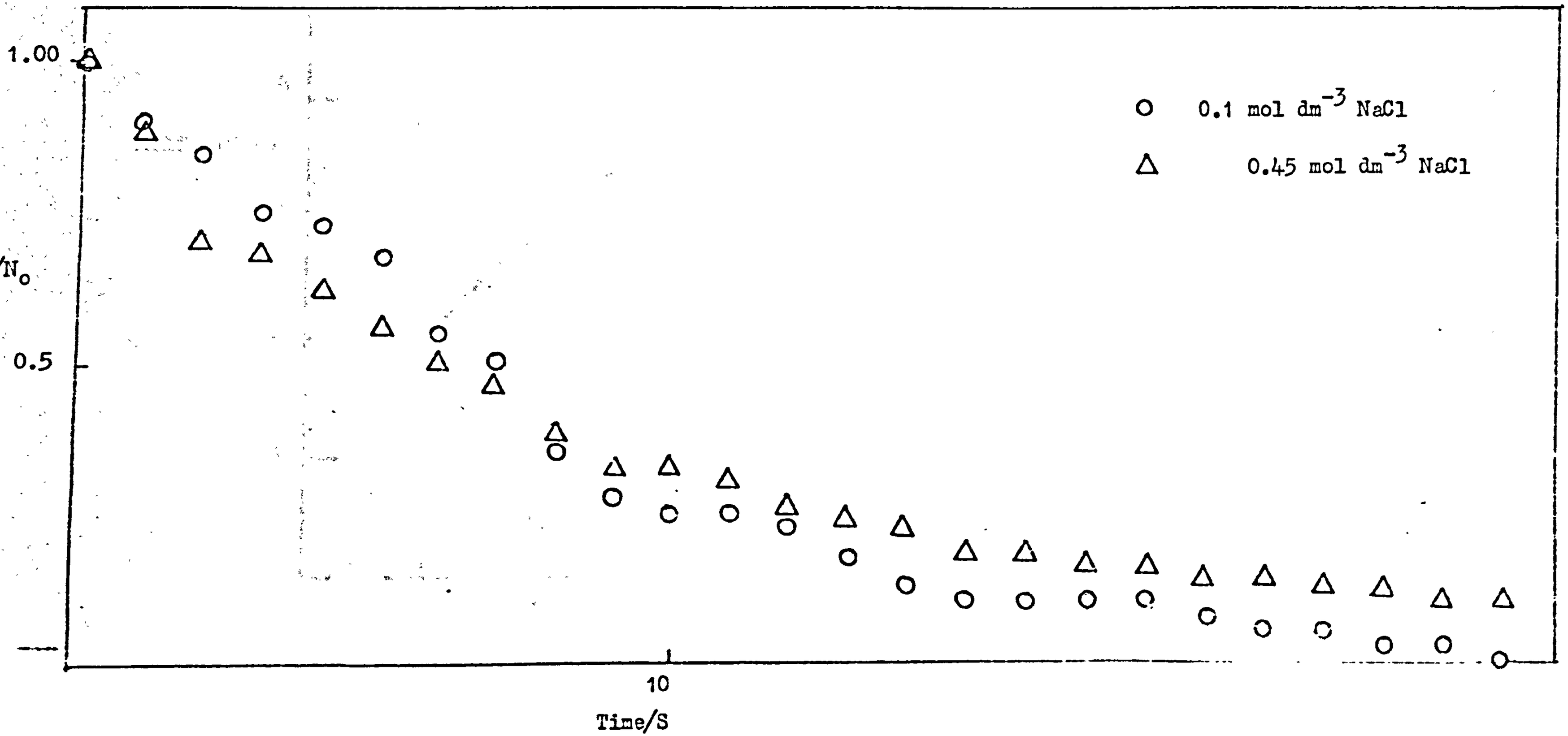

Figure 3 : Variation of Half-life with Salt Concentration

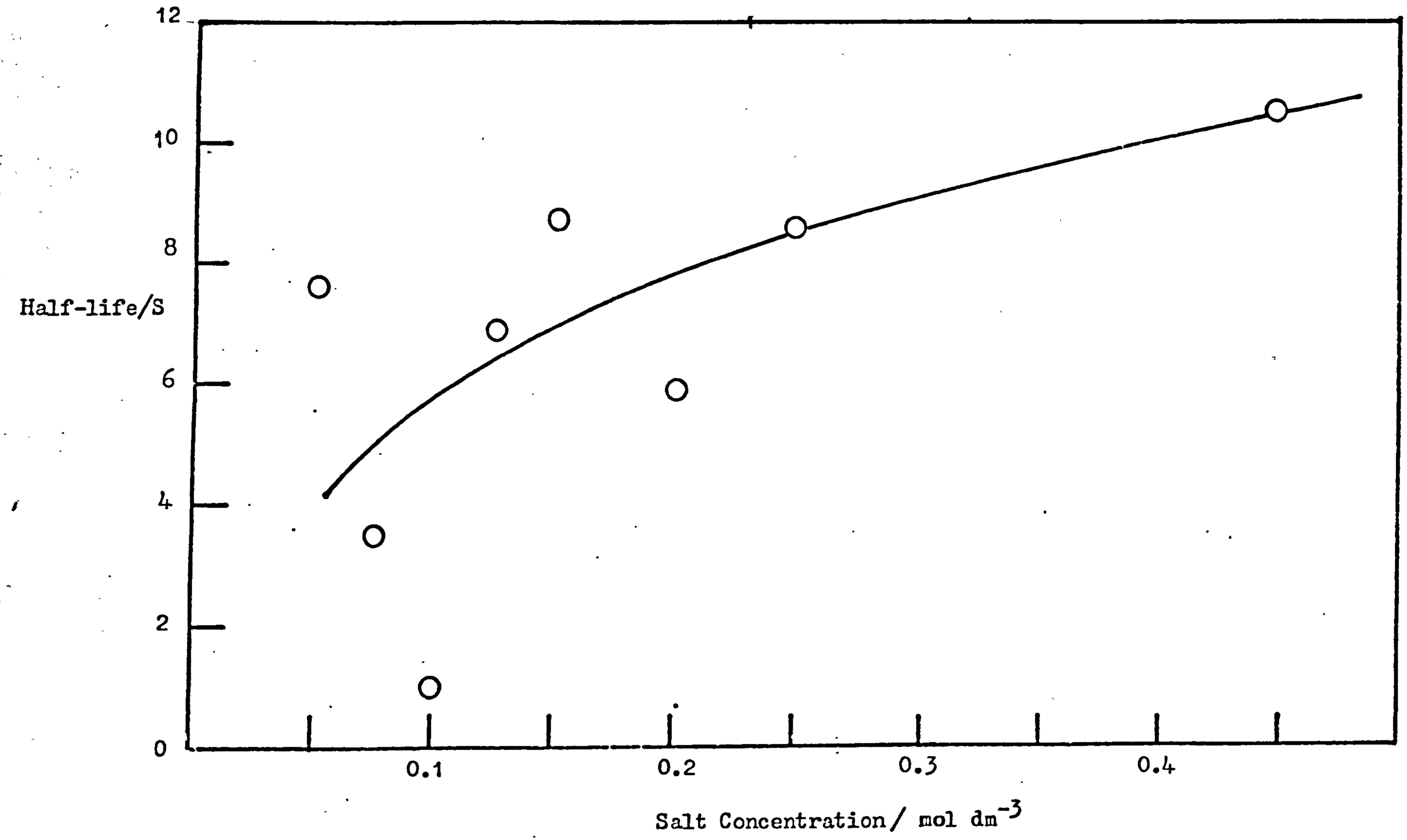

If N_o is the total number of bubbles and N the number of bubbles coalesced after time, t, then

$$\frac{N}{N_o} = 0.5$$

when $t = \mathcal{T}_{\frac{1}{2}}$

Figure 3 shows the half-life for the salt solutions, 0.05 to 0.45 mol dm^{-3} sodium chloride. Within experimental error, which is largely due to the fact that there was no temperature control and also that the stirrer probably disturbed the interface, there is a general increase in half-life with salt concentration.

3. Conclusion

The stability of the foam increases within the foaming range, 0.05 to 0.45 mol dm^{-3} sodium chloride for latex JC. A ceiling is reached in this stability at the higher salt concentrations. These concentrations correspond to the salt concentrations where bulk coagulation occurs.

Appendix III

```
10 REM CALCULATION OF POTENTIAL ENERGY OF REPULSION
20 REM DISTANCE H AND RADIUS IN CMS
30 REM POTENTIAL P IN VOLTS
40 INPUT E,R,P,K,A,H1,H2,H3
50 PRINT "VALUE OF DIELECTRIC CONSTANT = ";E
60 PRINT "VALUE OF RADIUS = ";R
70 PRINT "VALUE OF SURFACE POTENTIAL = ";P
80 PRINT "VALUE OF KAPPA = ";K
90 PRINT "VALUE OF HAMAKER CONSTANT = ";A
100 B=1.349E-08*E*R*P*P
110 C=A/(12*4.117E-14)
120 PRINT " DISTANCE     P.E.REP      P.E.ATT     TOT.P.E."
130 FORMAT E10.3,2X,E10.3,2X,E10.3,2X,E10.3
140 FOR H=H1 TO H3 STEP H2
150 D=K*H
160 D1=EXP(-D)
170 D2=1+D1
180 D3=LOG(D2)
190 V1=B*D3
200 X=H/(2*R)
210 X1=X*X+2*X
220 X2=X*X+2*X+1
230 D3=C*(1/X1+1/X2+2*LOG(X1/X2))
240 V3=V1-V2
250 WRITE (15,130)H,V1,V2,V3
260 NEXT H
270 GOTO 40
280 END
```

Appendix IV

```
10 REM TAPE NO 4; FILE NO 23
15 REM CLARES PROGRAMME
20 REM CALCULATION OF POTENTIAL ENERGY OF REPULSION
30 REM DISTANCE H AND RADIUS IN CMS
40 REM POTENTIAL P IN VOLTS
42 SCALE 0,1E-06,-750,500
44 XAXIS 0,1E-07
46 YAXIS 0,250
50 INPUT E,A,T,Z1,Z2,H1
60 INPUT R,P,C,H1,H2,H3
70 B=1.3803E-16*T
80 Z3=Z1^2
90 Z4=Z2^2
100 D6=E*B1
110 Z5=1.7456E+03/D6
120 Z6=SQR(Z5)
130 E1=C*Z2*Z3+C*Z1*Z4
140 S1=SQR(E1)
150 K=Z6*S1
160 PRINT "VALUE OF DIELECTRIC CONSTANT = ";E
170 PRINT "VALUE OF RADIUS = ";R
180 PRINT "VALUE OF SURFACE POTENTIAL = ";P
190 PRINT " ELECTROLYTE CONCENTRATION = ";C
200 PRINT "VALUE OF KAPPA = ";K
210 PRINT "VALUE OF HAMAKER CONSTANT = ";A
220 F=1.349E+08*E*R*P*P
230 C=A/(12*4.117E-14)
240 C1=A1/(12*4.117E-14)
250 PRINT " DISTANCE    P.E.REP      P.E.ATT    TOT.P.E."
260 FORMAT E10.3,2X,E10.3,2X,E10.3,2X,E10.3
270 FOR H=H1 TO H3 STEP H2
280 U=K*H
290 D1=EXP(-U)
300 D2=1+D1
310 D3=LOG(D2)
320 V1=B*D3/2
330 X=H/(2*R)
340 X1=X*X+2*X
345 X2=X*X+2*X+1
350 V2=C*(1/X1+1/X2+2*LOG(X1/X2))/2
355 V4=C1*(1/X1+1/X2+2*LOG(X1/X2))/2
360 V3=V1-V2-V4
370 WRITE (15,250)H,V1,V2,V3
375 PLOT H,V3
376 PEN
380 NEXT H
390 GOTO 60
400 END
```